DOCTOR OF VETERINARY SCIENCES

Do specific magnetic resonance and contrast enhanced computed tomography imaging provide early detection of cartilage changes after mechanical or chemical stimulation of the subchondral bone in an ovine model?

Hontoir, Fanny

Award date:
2018

Awarding institution:
University of Namur
Namur Research Institute for Life Sciences
Omnibus Animalibus Studia Sanitatis

University of Namur
Faculty of Sciences
Department of veterinary medicine

Do specific magnetic resonance and contrast enhanced computed tomography imaging provide early detection of cartilage changes after mechanical or chemical stimulation of the subchondral bone in an ovine model ?

A dissertation submitted by Fanny HONTOIR
in partial fulfilment of the requirements
for the degree of PhD in Veterinary Sciences

Supervisors:
Prof. Jean-Michel Vandeweerd
Prof. Peter Clegg

Jury: Dr. Mandy Peffers (University of Liverpool)
Dr. Sarah Taylor (University of Edinburgh)
Dr. Simon Tew (University of Liverpool)
Prof. P. René van Weeren (Universiteit Utrecht)

President of the jury: Prof. Charles Nicaise (University of Namur)

This thesis was produced in the OASIS (Omnibus Animalibus Studia sanitatIS) section of NARILIS institute.

Table of content

Abstract and list of publications

Abstract

Musculoskeletal diseases, and particularly osteoarthritis (OA), are a concern in human and veterinary medicine. In OA, the progressive alteration of the joint components (i.e. cartilage, subchondral bone, synovium) is responsible for reduced joint function, quality-of-life, or performance.

OA induces progressive changes in three main components of cartilage: increase in water content and loss of type-II collagen and proteoglycans. These biochemical changes are associated with destruction of the zonal organization of collagen, with in fine cartilage defects and exposure of the subchondral bone (SB). SB is also subject to changes in composition (synthesis of abnormal type-I collagen and decrease in minerals deposition) and microarchitecture (increase in the number and thickness of the trabeculae, disorganization of the trabeculae), due to increased remodelling. These changes are responsible for inadequate biomechanical function of the bone, which detrimental for the cartilage.

Several causes can lead to OA such as ageing, joint instability or metabolic conditions. Inflammation is nowadays considered as the common feature of OA-leading mechanisms. Moreover, interplay between joint components may occur. The crosstalk between cartilage and SB has been increasingly studied during the last decade. Chondrocytes are able to increase bone remodelling, bone turn over and to induce a decrease in density of SB. Osteoblasts can modify chondrocyte synthesis and stimulate synthesis of matrix metalloproteinase (i.e. MMP-3, MMP-13); a decrease of cartilage-constitutive molecules (i.e. aggrecan and type-II collagen) is observed. Both articular cartilage and SB changes can be present early after OA induction. The modification of bone biology in animal models has been proved to limit or stop OA initiation and further cartilage damages, suggesting an important role of SB in OA initiation.

Importantly, cartilage has limited ability to self-repair adequately, mainly because of the avascularity of cartilage, with poor access for regenerative cells or for migration of chondrocyte to the damaged area. It is therefore important to provide an early detection of structural and compositional changes associated with OA. The spontaneous healing of cartilage defect mainly leads to the filling with fibrocartilage or cartilage-like tissue, with a slight improvement of tissue organization overtime but without recovery of perfect HC organization. Finally, the tissue produced by naturally occurring repair of cartilage is most of time unable to integrate with the adjacent cartilage leading to inhomogeneities of cartilage surface, to micro-motion and potential damages to the repair tissue itself.

Due to the limited ability of appropriate self-repair of joint tissue, to the multiple structural and compositional changes that can occur, and the complexity of the OA process, it is important to better understand the early pathological processes and to better detect early structural and compositional changes that are associated to the disease. In addition, the validation of *in vivo* early diagnostic techniques is essential to promote the development of treatments and test them *in vivo*. Gold standards methods (histology or biochemistry) are invasive and most of time detrimental for the targeted tissue, inducing lesion because of the

sampling method (i.e., excision of cartilage sample). Furthermore, in longitudinal studies testing the effect of a treatment, we should ideally be able to assess the structure and composition of cartilage at baseline noninvasively, to optimally identify the changes induced by the treatment itself.

In this context, this thesis aimed:

1/ To compare magnetic resonance imaging (MRI) and computed tomography (CT) techniques in their ability to detect subtle cartilage structural changes.

2/ To review the efficacy of MRI- and CT-based imaging techniques to identify compositional changes of cartilage.

3/ To assess the efficacy of chemical or mechanical subchondral bone stimulation in inducing cartilage compositional or structural changes in an *in vivo* ovine model

4/ To test MRI T2 mapping and compositional CT to identify the early structural or compositional changes induced by subchondral bone stimulation.

Firstly, the assessment of CT arthrography (CTA) and MRI to detect structural cartilage defect implied two models of subtle naturally occurring cartilage defects (the equine metacarpo-/metatarso-phalangeal joint and the ovine stifle). Initially, MRI and CTA were compared in their ability to detect subtle cartilage defects in a series of equine metacarpo-/metatarso-phalangeal joint collected at a slaughterhouse and without evidence of articular disease. CTA sensitivity and specificity were 82% and 96%, respectively, and were significantly higher than those of MRI (41% and 93%, respectively) to detect cartilage defects in the metacarpo-/metatarso-phalangeal joint. The intra and inter-rater agreements were 0.96 and 0.92, respectively, and 0.82 and 0.88, respectively, for CTA and MRI. As CTA was found to be an adequate tool to detect subtle cartilage defects, we implemented this technique in our animal model: the sheep. We proved that this technique is feasible ex vivo, but also *in vivo* with sheep under anaesthesia; and gives an accurate assessment of the cartilage defects in the ovine knee, with high sensitivity (81.8%) and high specificity (95.2%). This technique was therefore considered as a useful tool to assess cartilage and to select only animals with healthy cartilage at baseline for experimentation.

Secondly, a review of the literature highlighted multiple imaging techniques focusing on water, glycosaminoglycan or collagen of cartilage. CT-based imaging technique (contrast-enhanced computed tomography (CECT), or quantitative CT requires the injection of a contrast medium, in order to assess the change in cartilage X-Ray attenuation between pre- and post-contrast images. This change in attenuation is associated to the ability of the contrast medium to penetrate cartilage depending primarily on its glycosaminoglycan content. MRI-based techniques such as glycosaminoglycan chemical-exchange saturation transfer and sodium imaging have been proved to correlate to glycosaminoglycan content, but require specific device and/or high field magnets, that are seldom available. Long acquisition time are sometimes require for other imaging techniques (T1 rho imaging or diffusion weighted imaging), limiting their use in practice. The review of the literature revealed that nearly all compositional imaging technique require validation for veterinary research or clinical practice, and that delayed gadolinium-enhanced MRI of cartilage and T2 mapping appear to be the most applicable methods for compositional imaging of animal cartilage.

Thirdly, two methods of stimulation of the SB was performed to induce further cartilage changes and to describe bone and cartilage changes by histology, biochemistry, micro-computed tomography, T2 mapping and CECT. The sheep was selected as an animal model for *in vivo* experiments because of its availability, its easy handling, its similar anatomy to human, and its appropriate size to either harvest samples for multiple analysis, or use clinical medical imaging devices (MRI, CT) and to assess locomotion. The SB of the medial femoral condyle was reached by drilling a track from the medial aspect of this condyle to avoid injury to the other joint's components (ligaments, cartilage and synovium). The stimulation technique was performed either mechanically (impact with a metal rod through the drill track) or chemically (ethanol injection with a needle through the drill track) depending on group allocation (N=9/group). The sheep were clinically observed and euthanized after 2, 4, 6 and 8 weeks (N=2/time-point and 1 control sheep euthanized at day 0). Several salient findings were observed, such as: the increase in apparent bone density and in trabecular thickness at micro-computed tomography, in both stimulation groups (ethanol and impact). Two opposite histological trends were observed between both groups. Ethanol-stimulated limbs showed a progressive alteration of cartilage at histology over time (i.e. increase in OARSI scores for cartilage) that could be explained by the change in subchondral bone stiffness induced by ethanol dehydration. Impact-stimulated limbs showed the inverse trend, with an improvement of cartilage histological characteristics, as suggested by the decrease in OARSI scores for cartilage over time. This inverse trend could be associate to the healing effect previously described for drilling, osteostixis or micro-picking.

The last aim of this thesis was to test advanced imaging techniques (CECT and T2 mapping) to image the alterations of cartilage following subchondral bone stimulation. We proved that these techniques were feasible in living sheep, but we were unable to identify significant differences between groups, or to correlate imaging findings with the histological changes. This could be due to multiple factors such as: the limited changes after stimulation, the limitations in imaging modalities to detect these limited changes, the restriction in limb positioning in living animals, the requirement for reduced acquisition time (to limit anaesthesia time and associated risks) and the subsequent compromise between short acquisition time and image quality (resolution, signal-to-noise ratio, volume averaging). Most of these techniques have been previously validated on osteochondral plugs, overpassing the encountered limitations, or on joint to compare fibrous cartilage to hyaline cartilage-like tissue, suggesting a larger range of changes between conditions than what was observed after subchondral bone stimulation in the ovine model.

This PhD thesis highlighted several perspectives for research and clinical applications. We demonstrated that the detection of cartilage defects was more accurate with CTA than MRI, ex vivo in the equine metacarpo-/metatarso-phalangeal joint and *in vivo* in the ovine stifle. However, the requirement of general anaesthesia (and associated risks), size of the body region of interest and the thickness of the structure of interest (and subsequent concerns about image resolution) could sometimes limit the use of powerful MRI or CT scans in practice. In research, noninvasive baseline assessment of the joint should be part of the inclusion criteria.

Compositional imaging techniques (T2 mapping and CECT) were unable to demonstrate a correlation with the subtle changes induced by chemical or mechanical stimulation. In the future, nevertheless, compositional imaging should be continuously improved since early noninvasive identification of joint changes is important for research and development of therapies.

The subchondral bone insult model developed in this PhD thesis could be intensified. The main advantage of this model was the selective stimulation of the subchondral bone (without damages to the synovium, cartilage or ligaments), therefore limiting confusing factors such as synovitis. The optimal doses should be found for ethanol-stimulation techniques to induce significant changes. Nevertheless, the histological differences that we identified between both types of stimulation were interesting since they may be highlighted two different mechanisms, one leading to pathology and the other to repair. This deserves to be investigated further to better understand how disease develops but also how subchondral bone stimulation (like drilling, micro-picking, or other) can be useful.

List of publications associated to the thesis

The full text of each publication is provided in the addendum section, at the end of the thesis manuscript.

Hontoir F, Nisolle JF, Meurisse H, Simon V, Tallier M, Vanderstricht R, Antoine N, Piret J, Clegg P, Vandeweerd JM. 2014. A comparison of 3-T magnetic resonance imaging and computed tomography arthrography to identify structural cartilage defects of the fetlock joint in the horse. The Veterinary Journal 199(1):115-122.

Hontoir F, Clegg P, Simon V, Kirschvink N, Nisolle JF, Vandeweerd JM. 2017. Accuracy of computed tomographic arthrography for assessment of articular cartilage defects in the ovine stifle. Veterinary Radiology and Ultrasound 58 (5): 512-523.

Hontoir F, Clegg P, Nisolle JF, Tew S, Vandeweerd JM. 2015. Magnetic resonance compositional imaging of articular cartilage: what can we expect in veterinary medicine? The Veterinary Journal 205(1): 11-20.

Vandeweerd JM, **Hontoir F**, Kirschvink N, Clegg P, Nisolle JF, Antoine N, Gustin P. 2013. Prevalence of naturally occurring cartilage defects in the ovine knee. Osteoarthritis Cartilage 21 (8):1125-31.

Vandeweerd JM, Vermeylen A, Goossens M, Sternon N, **Hontoir F**, Nisolle JF, Dugdale A. 2014. Anesthésie chez le mouton de laboratoire. Sciences et Techniques de l'Animal de Laboratoire 40 (4): 15-19.

List of abbreviations

3T = 3 Tesla
AC = Articular Cartilage
ADC = Apparent Diffusion Coefficient
AGEs = Advanced Glycation End products
BML = Bone Marrow Lesions
BMP = Bone Morphogenic Protein
BS/BV = Bone Surface/ Bone Volume
BV/TV = Bone Volume:Total Volume ratio
CA = Contrast Agent
CC = Calcified Cartilage
CECT = Contrast Enhanced Computed Tomography
CF = Contrast Fluid
CGRP = Calcitonin-Gene-Related Peptide
CPON = C-flanking peptide of neuropeptide Y
CT = Computed Tomography
CTA = Computed Tomography Arthrography
CTAn = CT Analyzer
DAB = 3, 3 -diaminobenzidine
DESS = Double-Echo in the Steady-State
dGEMRIC = Delayed Gadolinium-Enhanced MR Imaging of Cartilage
DMMB = DiMethyl-Methylene Blue
DNA = DeoxyriboNucleic Acid
DW = Dry Weight
DWI = Diffusion-Weighted Imaging
ECM = ExtraCellular Matrix
EDTA = EthyleneDiamineTetraacetic Acid
EL = Extra-articular Ligament
EphB4 = Ephrin type-B receptor 4
ERK = Extracellular signal-Regulated Kinase
ET or TE = Echo Time
FCM = Medial Condyle of the Femur
FN = False Negative
FOV = Field Of View
FP = False Positives
GAG(s) = GlycosAminoGlycan(s)
gagCEST = GlycosAminoGlycan Chemical-Exchange Saturation Transfer
Gd-DTPA^{2-} = Gadolinium-DiethyleneTriamine Pentaacetic Acid
GE = Gradient Echo
HA = HyaluronAn
HC = Hyaline Cartilage
HP = HydroxylysylPyridinoline
HU = Hounsfield Unit
IA = Intra-Articular
IGF = Insulin Growth Factor

IHC = ImmunoHistoChemistry
IL = Intra-articular Ligament
IV = Intravenous
MAPK = Mitogen-Activated Protein Kinases
MCP/MTP = Metacarpo-/metatarso–phalangeal
Mean attenuation of cartilage in the post-contrast image = $AC_{Contrast}$
mean attenuation of cartilage in the pre-contrast image = AC_{Blank}
micro-CT = micro-Computed Tomography
MMPs = Matrix MetalloProtease(s)
MRA = Magnetic Resonance Arthrography
MRI = Magnetic Resonance Imaging
NA = Not Available
NF = Nuclear Factor
NPV = Negative Predictive Value
OA = Osteoarthritis
OARSI = Osteoarthritis Research Society International
P = Patella
PACS = Picture Archiving and Communication System
PAR-2 = Proteinase-Activated Receptors-2
PD = Proton Density
PG(s) = Proteoglycan(S)
PGE2 = Prostaglandine E2
PGP = Protein Gene Product
PLT = Paraligamentous Technique
POD = Palmar Osteochondral Disease
PPV = Positive Predictive Value
pQCT = peripheral Quantitative Computed Tomography
PTH = Parathyroid Hormon
qCT = quantitative CT
RA = Rheumatoid Arthritis
RAGE = Receptor of AGE
RANK(L) = Receptor Activator of Nuclear factor κ-B (Ligand)
RCI = Red Color Index
RF = Radiofrequency
RGB = Red Blue Green
RPT = RetroPatellar Technique
RT = Relaxation time
RUNX2 = Runt-related transcription factor 2
SAPK/JNKs = Stress-Activated Protein Kinases/c-Jun N-terminal Kinases
SAPLs = Surface Active Phospholipids
SAR = Specific Absorption Rate
SB = Subchondral Bone
SBP = Subchondral Bone Plate
Sen = Sensitivity
SF = Synovial Fluid
SPACE = Sampling Perfection with Application-optimized Contrast using different flip-angle Evolutions
Spe = Specificity

STB = Subchondral Trabecular Bone
STT = Subtendinous Technique
T1ρ = T1rho
T2-W = T2-weighted
TbTh = Thickness of the trabeculae or trabecular bone thickness
TCM = Medial Condyle of the Tibia
TE = Echo Time
TGF = Transforming Growth Factor
TN = True Negatives
TP = True Positives
TR = Repetition Time
TRAP = Tartrate-Resistant Alkaline Phosphatase
TUNEL = Terminal deoxynucleotidyl transferase dUTP Nick End Labeling
UTE = Ultra-short (Time of) Echo
US = Ultrasonography
VEGF = Vascular Endothelial Growth Factor
WNT = Wingless-Type
WW = Wet Weight

1. General introduction

1. General introduction

1.1 Osteoarthritis, a very prevalent disease

Musculoskeletal diseases are a concern in human and veterinary medicine. In particular, osteoarthritis (OA) is a major problem. OA is a degenerative process of the diarthrodial (synovial) joint characterized by progressive degeneration of the articular cartilage, combined with subchondral bone (SB) sclerosis and osteophyte formation, leading to reduced joint function (Grynpas et al., 1991; McIlwraith, 1996). OA is associated with pain, physical dysfunction (Verbrugge, 1995; Ogino et al., 2009), and quality-of-life score being inferior to (and therefore worse than) chronic respiratory diseases and cardiovascular conditions (Reginster, 2002).

Nearly 27 million (12%) of US adults aged between 25 to 74 years have clinical OA and approximately 37% of elderly adults (> 60 years) have knee OA (Lawrence et al., 2008). The prevalence of the disease in the European Union has been estimated around 100 million (Altman et al., 2006). About 30% of elderly people suffer from OA in Spain (Carmona et al., 2001). The estimated direct cost of the disease in France in 2002 was 1.6 billion Euros, including hospital admission, physician visits and medications (Le Pen et al., 2005). Associated costs include time off at work, adaptive aids and devices (Maetzel et al., 2004).

In man, OA primarily affects the knee, the hip or the hand (Oliveira et al., 1995; Lawrence et al., 2008). Knee OA is up to three time more prevalent than hip or hand OA (Oliveria et al., 1995; Andrianakos et al., 2006). This partially explains the large interest for knee in OA, and the use of the knee as a joint of interest in animal models.

In animals, OA is also a leading cause of morbidity. Sixty-one percent of old adult cats (aged > 6 years) showed clinical OA in one joint or more (Slingerland et al., 2011), and 80 - 90% of elderly cats (>12 years) had radiographic OA in at least one joint (Hardie et al., 2002; Slingerland et al., 2011). The disease results in changes in behaviour (Slingerland et al., 2011) and decreased mobility (Lascelles, 2010). In horses, OA is involved in up to 60% of lameness cases (Caron & Genovese, 2003). One third of young (two- and three-year-old) thoroughbred racehorses show macroscopic cartilage lesions and OA of the metacarpophalangeal joint (Neundorf et al., 2010). This can lead to lameness, loss of training day, failure to race, and loss of income (Jeffcott & Kold, 1982; Santschi, 2008). As the value of the athletic horse is associated to its soundness, the high prevalence of OA challenges the equine industry (Schlueter & Orth, 2004).

1.2 Osteoarthritis, a disease of the diarthrodial joint

The diarthrodial joint unit comprises multiple structures (Dyce & Wensing, 2010). Each tissue has a proper function, with its own biology and anatomy (Goldring & Goldring, 2010). (Figure 1).

Cartilage

Articular cartilage covers bones' end. It is composed of a layer of hyaline cartilage (HC) and a deeper layer of calcified cartilage (CC). Both layers are separated by the tidemark (Meachim & Allibone, 1984; Oegema et al., 1997; Burr, 2004). The tidemark originates from chondrocytes' activity, between CC and non-calcified layers of HC. It appears with skeletal maturation (Havelak et al., 1984) and shows waviness (Oegema et al., 1997; Lyons et al., 2005 & 2006). Multiple tidemarks can be observed in normal joints (Oegema et al., 1997). The interface between CC and SB is featured by an anchorage cement line (Poole, 1997). This osteochondral junction is irregular (wavy) and does not shows fibres crossing from the SB to HC. It seems that the osteochondral junction is only maintained by interdigitations (waviness) of the SB in the CC (Clark & Huber, 1990; Oegema et al., 1997).

Articular cartilage has biomechanical properties that are attributable to its extracellular matrix (ECM) mainly composed of collagen (15-20%), proteoglycans (PGs) (5-10%), hyaluronan (HA) and water (60-80%) (Maroudas et al., 1969; Buckwalter & Mankin, 1997; Williamson et al., 2001; Goodwin et al., 2001; Kiani, 2002; Klein et al., 2007).

Water content decreases from surface (74%) to depth (67%) (Venn & Maroudas, 1977). Water exists in three forms: free water (with dissolved ions), water linked to collagen and water linked to PGs (Maroudas, 1976). The flow of water through cartilage provides chondrocytes with nutriments (Maroudas et al., 1968; Fox et al., 2009).

The second major component of cartilage is the fibrillar, type II collagen (Carney & Muir 1988; Wancket et al., 2005; Mobasheri & Henrotin 2010; Goldring & Goldring, 2010; van Turnhout et al., 2010). Collagen fibres are thin and densely packed in the pericellular area, being larger and radially organized in the interterritorial area (Meachim & Stockwell, 1979; Poole, 1997; Poole et al., 1984). The turnover of collagen is very low in normal tissue, with an estimated half-life of 117 years (Verzijl et al., 2000). Other types of collagens are also present (type I, III, X, and a small amount of type V, VI, IX and XI). They are associated to type-II collagen and regulate the fibril diameter, or allow association between type-II collagen and other components of the ECM, such as PGs (Eyre, 1987; Mendler, 1989; Aigner et al., 1993; Wotton & Duance, 1994; Dudhia, 2005; Goldring & Goldring, 2010).

PGs are composed of a central protein linked to hundreds of negatively charged polysaccharide chains called glycosaminoglycans (GAGs) and to HA (Figure 1). The principal cartilage PG is aggrecan (Venkatesan et al., 2009), and its major GAGs are chondroitin sulphate and keratan sulphate (Garvican et al., 2010). HA is a non-sulphated GAG. It is non-covalently linked to aggrecan and therefore never found in a proteoglycan form (Frazier et al., 2008; Ling et al., 2008; Watanabe et al., 2010).

Behind its biochemical composition, cartilage shows a particular organization with different zones from surface to depth (Muir et al., 1970; Franzen et al., 1981): the superficial zone, the transitional zone and the radial zone. In the radial zone, collagen fibres are perpendicular to the articular surface, forming rows with rounded-shaped chondrocytes in between. In the transitional zone, they overlap as thin lamellae. In the superficial zone, they are tangential to the articular surface, with flattened chondrocytes (Poole, 1997).

All ECM components are secreted by cells, called chondrocytes. Chondrocytes maintain a homeostatic balance between production and degradation of ECM (Urban, 1994; Muir, 1995; Poole, 1997; Young et al., 2005; Goldring & Marcu, 2009).

In addition, the surface of cartilage is covered by a microscopic lubricating layer composed of surface active phospholipids (Guerra et al., 1996; Pickard et al., 1998; Schwarz and Hills, 1998; Vecchio et al., 1999) and lubricin (or superficial zone protein or proteoglycan-4) (Goldring & Goldring, 2010; Neu et al., 2010; Goldring & Berenbaum, 2015).

Biomechanically, cartilage is represented by a solid phase (collagen and PGs), a fluid phase (water) and ions (Mow et al., 1980; Lai et al., 1991; Pearle et al., 2005). When the joint is in load, water can move through ECM (Mow et al., 1980). However, the PGs of the solid phase infer an osmotic pressure and limit the water flow, providing to cartilage, together with the collagen network, its compressive stiffness and its resistance to loading forces (Kempson et al., 1982; Carney & Muir, 1988; Kiani, 2002). Collagen limits the water flow by mean of frictional forces, leading to increase of water pressure (Lai et al., 1991; Lu & Mow, 2008). The collagen network also provides tensile strength, which ensures resistance to shearing forces (Bassleer et al., 1992; Bayliss et al., 1983; Bank et al., 1998; Cremer et al., 1998; Williamson et al., 2003; Graindorge et al., 2006; Koulouris, 2006; Crockett et al., 2007; Katta et al., 2008; Venkatesan et al., 2009; Watanabe et al., 2010).

Healthy articular cartilage is also featured by absence of vascularization and innervation. This feature relates to the ability of chondrocyte to produce chondromodulin, semaphorins, TIMP-1 and -2 (Tissue Inhibitors of metalloproteinase-1 and -2) and PGs (such as decorin). These substances have been proved to inhibit neuronal and endothelial cell migration *in vitro* (Moses et al., 1999; Pfander et al., 2000; Bara et al., 2012; Binch et al., 2014). The avascularity of cartilage limits its ability to repair (Henn et al., 2011; Bijlsma et al., 2011).

Bone

The underlying SB is composed of a compact layer of bone (the subchondral plate) underlined by the more porous trabecular SB. Like CC, the SB plate and the trabecular SB are mineralized tissues (Duncan et al., 1987; Müller-Gerbl, 1998; Burr, 2004; Madry et al., 2010). No collagen fibres cross the cement line between CC and the subchondral plate suggesting the osteochondral junction is a weakness area (Madry et al., 2010). The subchondral plate is made of parallels collagen fibrils organized in lamellated sheets (Inoue, 1981), whereas the trabecular bone is featured by spaces separating bony walls. Morphologically, this organization is depicted by the trabecular number, the trabecular thickness, and the density of the bone (Li & Aspden, 1997). It is anisotropic with trabeculae oriented in various axes, allowing resistance to stress in multiple planes (Choi et al., 1990; Mente & Lewis, 1994). Compared to HC, the biochemical composition of SB is characterized by a definitely low content of GAG (0.17% in dry weight) and a high content in minerals (65% in dry weight (van der Harst et al., 2004; Granke et al., 2015). Water content of bone is around 15-25% (Granke et al., 2015).

Collagen I (35-45% wet weight (WW)) is one of the major components of bone (Granke et al., 2015). Collagen and mineral contents provide mechanical properties to SB (Evans et al., 1992; Knott et al., 1995). The collagen cross-links level is higher for subchondral plate than for subchondral trabecular bone (van der Harst et al., 2004), while the mineral content (Ca, Mg, P and ash content) is higher in trabecular bone than in SB. The mineral content is responsible for the stiffness of the bone. However, it should be noted that the mechanical properties of bone are not only driven by its content but also by its architecture and its microarchitecture. Therefore, the higher mineral content of the trabecular SB does not lead

to a stiffer bone, as the trabecular bone has a honeycombs-like architecture (van der Harst et al., 2004).

The SB absorbs most of the loads (Radin & Paul, 1970; Radin & Rose, 1986; Pugh et al., 1973; Layton et al., 1988; Imhof et al., 2000) and provides a mechanical support for cartilage (Imhof et al., 2000).

Bone is vascularized and innervated, including sensory (Calcitonin-Gene-Related Peptide (CGRP) reactive) and nociceptive (substance P reactive) fibres (Wojtys et al., 1990; Buma et al., 1992; Nixon & Cummings, 1994; Suri et al., 2007). SB lesions are therefore known to be painful. The SB is also partially responsible for nutrients supply to cartilage, through diffusion (Malinin & Ouellette, 2000; Imhof et al., 2000; Castaneda et al., 2012). However, it seems that this route of nutrition is not dominant. The comparison between osteochondral units, whom nutrition had been selectively blocked, showed that the deterioration of cartilage was higher when the nutrition was only driven by SB compared to cartilage supplied only by synovial fluid (Wang et al., 2013).

Ligaments, capsule and synovium

Ligaments are specialized dense connective tissues involved in joint stability. They are mainly composed of collagen I, associated to a proteoglycan matrix (Frank et al., 2004).

The capsule is a fibrous connective tissue sealing the joint cavity. It is involved in limitation of joint movements by its fibrous nature and the presence of local thickenings (called capsular ligaments) (Ralphs & Benjamin, 1994). The presence of proprioceptive nerves suggests its active implication in joint stability and motion (Ralphs & Benjamin, 1994). The inner part of the capsule comprises the synovium (stratum synoviale). The outer part is made of fibrous tissue (stratum fibrosum) and is featured by multiple nervous structures (proprioceptive, mechanoreceptive, or blood-vessels associated) (Halata, 1977; Witherspoon et al., 2014).

The synovium is involved in synovial fluid secretion. The inner part of synovium (facing joint cavity) is mainly composed of type-B synoviocytes (fibroblast-like synoviocytes) and type-A synoviocytes (macrophage-like synoviocytes), overlying the innervated and vascularized subintima. Synoviocytes are responsible for secretion of hyaluronic acid and lubricin in the synovial fluid and collagen in the synovium matrix (Swann et al., 1977; Iwanaga et al., 2000; Jay et al., 2000; Smith, 2011). Lubricin is responsible for the lubrication properties of the synovial fluid whereas HA is responsible for viscosity properties (Jay et al., 2001). Synovial fluid can be considered as a mix between an ultra-filtrate of blood plasma and an active secretion by synoviocytes. This yellowish viscous fluid is present in small amount in the joint and contains a limited number of cells (Ropes et al., 1939; Pacchiana et al., 2004). Synovial fluid is involved in cartilage lubrication and nutrition (Schmidt et al., 2007).

Figure 1. Schematic representation of the component of a diarthrodial joint: the knee.

A. Bone's extremities are covered by articular cartilage (AC) and joined by ligaments: either intra-articular ligament (IL) or extra-articular ligament (EL). To increase congruence between bones' articular surfaces, complementary structures are present, the menisci (M). Synovial fluid (SF) fills the cavity. It is produced by the synovium (orange line). The detailed representation shows from surface to depth: layer of surface active phospholipids (SAPLs – green line), cartilage and subchondral bone (SB). The cartilage can be further divided in non-calcified hyaline cartilage (HC) (light green) and calcified cartilage (CC) (dark blue). The SB layer is made of subchondral bone plate (SBP) (compact bone) and subchondral trabecular bone (STB). Separation lines are seen between HC and CC (the tidemark – white line) and between CC and the SBP (the cement line – black dotted line).

B. Histological slice of an ovine femoral condyle after Safranin-O Fast Green staining and schematic representation of cartilage composition. This section shows the two layers of SB (blue): SBP and STB. The SBP is a dense bony area, with a laminated appearance, while the STB is characterized by trabeculae (walls), separated by trabecular spaces (holes; asterisks). SBP is covered by the CC (light red) and the HC (red), separated by tidemark(s) (arrows). HC can be further divided in three areas according to collagen organization. The shape and organisation of chondrocytes (grey ellipses) also vary. In the radial zone (RZ), the collagen fibres are perpendicular to the articular surface, forming rows with column-organized and rounded-shaped chondrocytes in-between (plain arrow heads, in the enlargement of the RZ). In the transitional zone (TZ), they overlap as thin lamellae. The chondrocytes are still rounded but they do not show columnar alignment (plain arrow heads, in the enlargement of the TZ). In the superficial zone (SZ), the collagen fibres are tangential to the articular surface, with flattened chondrocytes (plain arrow heads, in the enlargement of the SZ).

C. Detailed representation of cartilage composition shows that collagen fibres are formed by aggregates of tropocollagen subunits. These are composed of a triple helix of polypeptide chains. Although neutral overall, these chains bear a negative (plain arrow) and a positive (dotted arrow) charge. A hydrated gel expands through the collagen network, made of sulphated glycosaminoglycans (GAGs; black pins) linked to a core protein (brown line) to form a proteoglycan (PG). Each PG is connected to HA (woven blue line) by a link protein (orange circle). GAGs are composed of hundreds of negatively charged units, counterbalanced by sodium. Therefore, water exists in three forms: molecular water (linked to the negative [plain arrow] or positive [dotted arrow] charges of collagen and GAG) and free water (attracted by the sodium osmotic pressure; not shown in this figure).

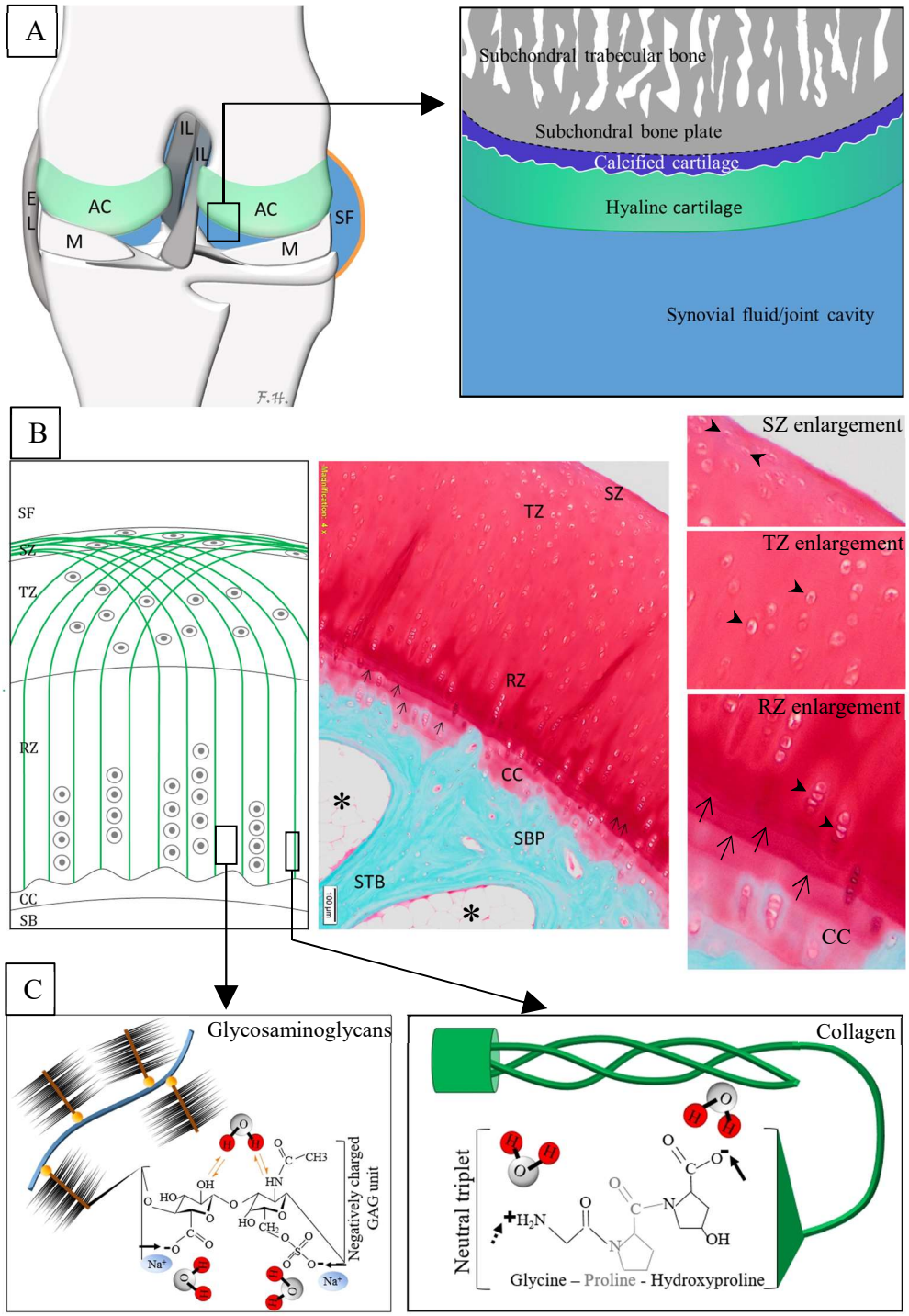
A
IL
IL
E
L
AC
AC
SF
M
M
F.H.
Subchondral trabecular bone
Subchondral bone plate
Calcified cartilage
Hyaline cartilage
Synovial fluid/joint cavity
B
SF
SZ
TZ
RZ
CC
SB
SZ
TZ
RZ
CC
SBP
STB
SZ enlargement
TZ enlargement
RZ enlargement
CC
C
Glycosaminoglycans
Negatively charged GAG unit
Collagen
Neutral triplet
Glycine – Proline - Hydroxyproline

1.3 Osteoarthritis, an inflammatory disease

OA is a condition that can be promoted by a wide range of causes. The primum movens can occur in the different tissues of the joint. (Goldring & Goldring, 2010). Different mechanisms have been proposed.

Mechanical stress can be responsible for OA. For instance, in man, anterior (cranial) cruciate ligament injuries are known to promote OA in the affected joint (Meuffels et al., 2009; Neuman et al., 2009; Holm et al., 2012; Janssen et al., 2013; Struewer at al., 2013; Sward et al., 2013; Bjorkman et al., 2015; Alazzawi et al., 2016). Ligament injuries cause instability of the knee leading to meniscal tears and cartilage defects, promoting OA (Alazzawi et al., 2016; Johnson et al., 2016). Overweight is also a source of increased chronic mechanical stress and is one of the main risk factor for OA (Felson et al., 1988; Coggon et al., 2001).

OA is also known to be an ageing disease. It can develop in stable joints (without ligament injury), following cartilage degeneration. Chondrocyte senescence is featured by a decrease in proliferative and synthetic ability (Loeser et al., 2000; Messai et al., 2000; Schinhan et al., 2012). For example, the equine ageing chondrocytes show a smaller response to growth factor (Iqbal et al., 2000). It has also been proved that the ECM produced by scenescent chondrocytes is characterized by a decreased amount of collagen and GAGs, and a reduction in tensile stiffness (Tran-Khanh et al., 2005).

Metabolic abnormalities also seem to be involved in OA. The increased risk of OA in obese patients is not limited to load-bearing joints and can expand to non-weight bearing joints such as the hand (Carman et al., 1994; Felson, 1996; Yusuf et al., 2010; Dahaghin et al., 2007; Balgojevic et al., 2010). Systemic factors (like adiponectin) have been suggested to be responsible for the increased risk for OA in non-weight bearing joint (Felson et al., 1988; Felson, 1996; Zhuo et al., 2012; Berenbaum et al., 2013; Sellam & Berenbaum, 2013). It has been proven that adiponectin is able to induce pro-inflammatory response in chondrocytes, with increase in matrix metalloprotease (MMP) synthesis (Lago et al., 2008; Kang et al., 2010; Tong et al., 2011).

In the last decades, OA has been more and more considered as an inflammatory disease (Goldring & Otero, 2011; Goldring et al., 2011; Loeser et al., 2012; Wang et al., 2011; Berenbaum, 2013). The production of inflammatory mediators by the different tissues of the joint (bone, cartilage and synovium) is a key to understand development and progression of the disease. Most of risk factors or initial events of OA can be associated with inflammation. For example, pro-inflammatory mediators, together with catabolic molecules are produced by chondrocytes and osteoblasts in response to mechanical stimuli (Goldring & Otero, 2011; Loeser et al., 2012; Berenbaum, 2013). Ageing is also related to inflammation: the accumulation of advanced glycation products (AGEs) has been proved to promote inflammation by the activation of the receptor of AGE (RAGE) (Hofmann et al., 1999; Goldring & Otero, 2011; Rasheed et al., 2011). The synovium is also able to produce pro-inflammatory mediators, in response to systemic condition or local condition (release of matrix fragments in the synovial cavity) (Goldring & Otero, 2011; Loeser et al., 2012; Berenbaum, 2013).

The synovium plays an important role of promotor or catalyser of OA. Fibroblast-like synoviocytes (type B synoviocytes) can produce pro-inflammatory mediators (Il-6, and MMPs) responsible for further cartilage damages either by direct activity on the cartilage components or by activation of catabolic activity of chondrocytes (Clegg et al., 1997; Pretzel

et al., 2009; Sutton et al., 2009; Sokolove & Lepus 2013; Larsson et al., 2015). Synoviocytes can be stimulated either by other component of the joint (i.e. release of collagen debris by meniscus) or by systemic conditions (such as the adiponectin in obese patients) (Sutton et al., 2009; McNulty et al., 2011). Synovitis has also been associated with progression of OA-associated damages (Damman et al., 2017; Mathiessen et al., 2016). Moreover, the synthesis of pro-inflammatory and catabolic factors by synoviocytes has been correlated to lower content of lubricin in the synovial fluid (Elsaid et al., 2008); this suggests that synovitis would alter biomechanics of the joint by modification of boundary lubrication properties of the synovial fluid.

In fact, a complex process leads to deterioration of the components of the diarthrodial joint, combining an interplay with molecule flow through the osteochondral junction, multiple pathways of cell stimulation and the involvement of the synovium as an initiator or a catalyser of osteo-chondral alterations (Figure 2). OA is nowadays considered as an organ disease. Another important interplay in the process of OA is the one that occurs between bone and cartilage.

Figure 2. Molecular events in OA. The primum movens of OA can occur in any of the component of the joint (ligaments, cartilage, menisci, synovium or bone). Cell senescence, mechanical injury (rupture, tear), or mechanical strain (compression, excessive load) can be responsible for degradation of the extracellular matrix and specific pathways activation with further associated changes in tissues (i.e. activation of ERK by mechanical strain in the SB, leading to secretion of matrix metalloproteinases (MMP) by osteoblasts). Metabolic condition such as obesity can also be responsible for stimulation of joint cells, such as synoviocytes and promote the secretion of pro-inflammatory mediators that causes matrix degradation either directly or by stimulating MMPs or aggrecanase production by chondrocytes. The interplay between cartilage and bone is modulated by multiple cytokines such as IL-1, IGF, TGF, and can be increased by neovascularisation (stimulated by cartilage and bone cells) or increase in bone porosity (following osteoclast activity).
Multiple signalling pathways are involved: WNT (Wingless-type), TGF-β/BMP signalling, MAPKs signalling (including extracellular signal-regulated kinases (ERKs – MAPK P44/42), stress-activated protein kinases/c-Jun N-terminal kinases (SAPK/JNKs) and p38 kinases). The WNT signalling pathway can be responsible for chondrocyte apoptosis, expression of catabolic factors by chondrocytes, but also induction of bone sclerosis (Jenkins et al., 2009).

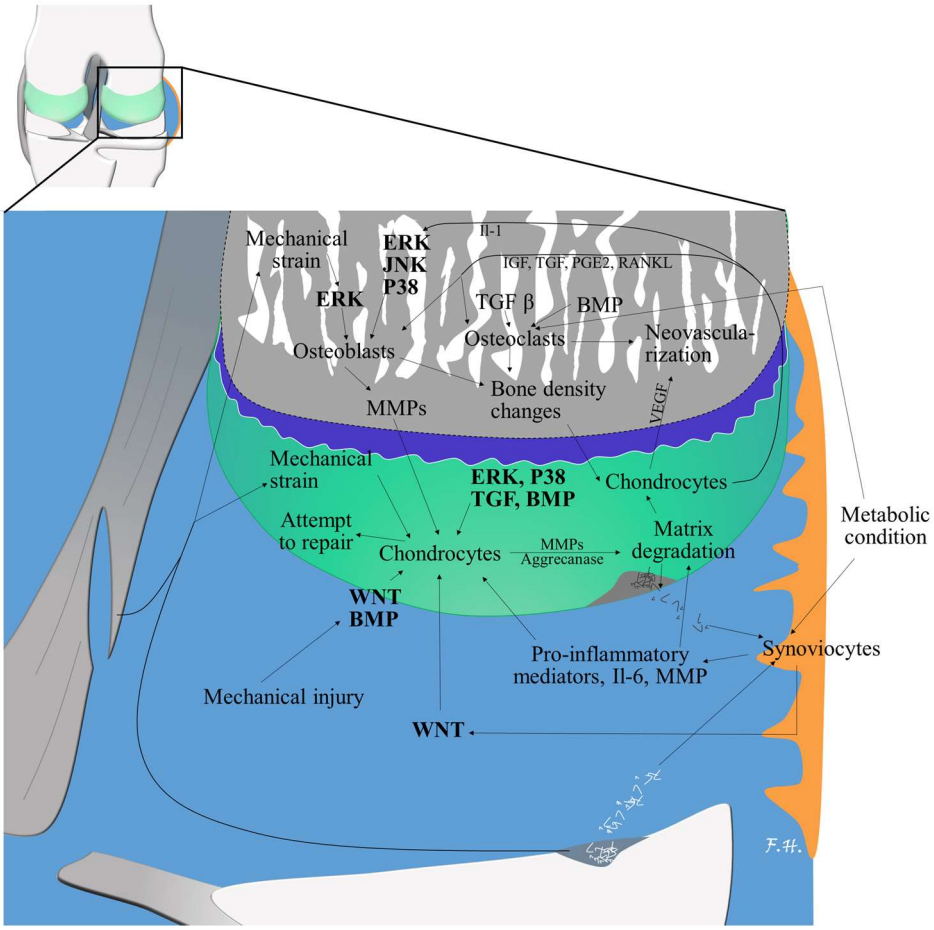

1.4 Osteoarthritis, an organ disease where bone plays a major role

The interplay between AC and SB may play a role in the process of OA. Cartilage cells (chondrocytes) and SB cells (osteoblasts, osteoclasts) are able to communicate thanks to CC and SB permeability (Lajeunesse & Reboul, 2003; Pan et al., 2009; Li et al., 2013). It seems that the tidemark is not a pure separation between HC and CC. The contact between hyaline cartilage and SB is likely made of thin digitations/prolongations of the non-calcified cartilage crossing the tidemark and the CC, and reaching the SB (Lyons et al., 2006). Moreover, vascular canals are connecting the SB together with the CC (Clark, 1990; Clark & Huber, 1990) and allow diffusion of molecules (Pan et al., 2009).

The crosstalk between SB and cartilage relies upon molecules involved in the homeostasis of cartilage. There are multiple pathways involved in the stimulation of joint cells, providing homeostasis (Sharma et al., 2013): the Wingless-Type signalling pathway (WNT), the Transforming Growth Factor β/ Bone Morphogenic Protein (TGF-β/ BMP) signalling, Mitogen-activated protein kinases (MAPKs) (Lajeunesse et al., 2004) and the Proteinase-Activated Receptors-2 (PAR-2).

The crosstalk between SB and cartilage can also occur during OA, and is probably enhanced in OA. Indeed, the fluid flow through the osteochondral unit has been proved to increase in OA samples compared to intact samples, suggesting a concomitant flow of factors. (Hwang et al., 2008).

Molecules released from chondrocytes are able to increase bone remodelling and SB changes (Henrotin et al., 2012). Osteoarthritic cartilage promotes the phenotypic change from quiescent to hypertrophic chondrocytes, in an attempt to repair cartilage damages. This phenotype is associated with expression of vascular endothelial growth factor (VEGF), Runt-related transcription factor 2 (RUNX2), MMP-13, interleukins (Il-1β; Il-6), insulin and transforming growth factor β (IGF and TGF-β), prostaglandin E2 (PGE2) or Receptor activator of nuclear factor (NF) κ-B ligand (RANKL).

VEGF promotes vascularization of the AC depth, increasing the molecular communication within the osteochondral unit. Il-1β and Il-6 promote the sclerotic phenotype of osteoblasts (Sharma et al., 2013). Increase production of IGF, TGF-β, PGE2 or RANKL are also known to enhance bone turn over and remodelling, leading to decrease in SB density (Upton et al., 2012; Martinez-Calatrava et al., 2012; Sharma et al., 2013).

In addition, changes in bone biology such as increase in TGFβ-1 or EphB4 promotes destruction of the underlying cartilage (Zhen et al., 2013). This influence of bone biology on cartilage has been demonstrated *in vitro* with either supernatant of OA osteoblasts (Webb et al., 1998) or co-culture of OA osteoblasts with normal cartilage (Sanchez et al., 2005A). The chondrocytes exposed to osteoblasts from sclerotic bone showed an increase in MMP-3 and MMP-13 expression, a decrease in production of aggrecan (Sanchez et al., 2005A), type-II collagen and GAG (Sanchez et al., 2005B), resulting in destruction of PG and collagen (Westacott et al., 1997; Neuhold et al., 2001) and destruction of cartilage.

Biomechanical stimuli to the bone can also trigger molecular events. *In vitro* cyclic compression induced the secretion of specific mediators by osteoblasts, resulting in increased

expression of proteases (MMP-3 and MMP-13) and decrease in aggrecan production by chondrocytes (Priam et al., 2013). All these *in vitro* experiments suggest that osteoblasts are able to modulate chondrocytes metabolism. An increase in CC thickness and an increase SB bone remodelling were shown to precede cartilage changes in OA-induced model of impulsive loading in rabbit knee (Radin et al., 1984; Farkas et al., 1987; Radin et al., 1995).

1.5 Osteoarthritis, an organ disease where bone initiates the disease

The interconnections between AC and SB make the determination of the initial alteration uneasy (Kawcak et al., 2001). Both AC and SB changes can be present early after OA induction, as seen in meniscectomized guinea pig (Pastoureau et al., 1999). However, the role of the SB in the development of OA has been increasingly proposed in recent years.

Mechanical properties of the SB are responsible for the cartilage integrity (Radin & Rose, 1986). Bone marrow lesions are known to be located within the area of most severe cartilage defect (Taljanovic et al., 2008). An increase in tibial SB thickness and density has been associated to cartilage damages (Yamada et al., 2002). Alterations of SB properties, induced by mutation of type-I collagen, are responsible for OA initiation and OA-specific cartilage damages (Blair-Levy et al., 2008). Bony changes have been described to occur before cartilage degeneration in spontaneous model of OA in guinea pigs, showing increase in SBP thickness before any histological changes in cartilage (Muraoka et al., 2007; Zamli et al., 2016). In a canine model of induced OA, damage of the SB preceded articular cartilage damages (Mrosek et al., 2006).

Bone microcracks are known to play a crucial role in OA initiation. They can occur in the different mineralized tissues e.g. CC, subchondral plate (SBP) and subchondral trabecular bone (STB) (Burr & Radin, 2003). These microcracks can be induced by overloading (Vener et al., 1992), by fatigue (Verborgt et al., 2000) or by acute impacts. For example, trans-articular impacts in dogs' knee induced subchondral trabecular microfractures without immediate macroscopic cartilage damage (Lahm et al., 2005; Thompson et al., 1991). Further changes included degeneration of AC collagen fibril network combined with PG loss, and cartilage loss within 6 months after the impact. In this model, SB microfractures were responsible for the onset of cartilage degeneration (Mrosek et al., 2006). In the fetlock of racehorses, the chronic repetitive overload induced micro-damages with bone response (Riggs et al., 1999; Santschi, 2008; Kawcak et al., 2001). The bone reaction is not able to cope with the damages that are accumulating overtime (Riggs et al., 1999; Santschi, 2008) because of the delay between bone removal and formation of bone (Stoveret al., 2003), and the lack of mineralization of the newly formed bone. The full mineralization of new bone, and the subsequent maximal density and stiffness, can require from 6 months to 1 year (Meunier & Boivin, 1997; Boivin et al., 2000), and may, therefore, not be achieved before new damages are encountered. This is an explanation of the accumulation of SB damages overtime, and the development of microcracks.

The microcracks trigger an increase in bone metabolism following osteocyte damages (Verborgt et al., 2000; Burr, 2004; Herman et al., 2010), enhance communication between bone and cartilage, easing the flow of molecules through the osteochondral unit (Westacott et al., 1997; Burr and Gallant, 2012) and promote vascular invasion of cartilage depth (Burr & Gallant, 2012). These changes can modify SB density and stiffness and induce consequent cartilage damages (Radin & Rose, 1986). It has also been shown that modifying bone biology in animal models attenuates or blocks OA initiation, and subsequent cartilage damages, after surgical destabilization of the joint (Kadri et al., 2008; Cui et al., 2015; Findlay & Kulibawa, 2016; Xie et al., 2016).

Another support to role of SB in the initiation of OA is the change in DNA methylation (Zhang et al., 2016). DNA methylation is responsible for modulating genes expression. In SB, the methylation of particular regions of RANKL or OPG (osteoprotegerin) gene has been described to lower their expression (Delgado-Calle et al., 2012). The comparison of methylation profiles has been performed between early, intermediate and late stages of OA (Zhang et al., 2016). This last paper, interestingly, indicated that DNA methylation changes occurred earlier in SB than in cartilage, suggesting that early events in the SB lead to OA.

1.6 Osteoarthritis, a disease with numerous structural and compositional changes

In cartilage

In very early OA, clusters of chondrocytes form in the damaged area in an attempt to repair cartilage (Goldring, 2000; Aurich et al., 2005; Bijlsma et al., 2011). This clustering is a result of increased cell proliferation and increased synthesis (Goldring & Goldring, 2010). Chondrocytes increase their collagenesis by 10 or 20 fold to cope for the loss of collagen. (Eyre, 1980; Adams & Brandt, 1991). As they switch to hypertrophic form, chondrocytes of the fibrillated cartilage synthesize type X collagen (Von Der Mark, 1992). This hypertrophic phase takes place in very early phase of OA (Adams & Brandt, 1991).

With progression of the disease, chondrocytes synthesis is insufficient to compensate the degradation of ECM. The release of collagen fragment activates inflammatory response (called microinflammation, a chronic low grade inflammation) and leads to a disruption of homeostasis and a catabolic state (Goldring & Marcu, 2009; Kapoor et al., 2010) with biochemical changes such as decrease of PGs content due to aggrecanase-mediated cleavage of PG (Hjertquist and Lemperg, 1972; Panagides & Tao, 1978; Guilak et al., 1994; Sandy & Verscharen, 2001) and degradation of collagen (Panagides & Tao, 1978; Hardingham et al., 1994; Guilak et al., 1994; Wiliams 2003; Van Den Boom et al., 2005; Bijlsma et al., 2011; Stubendorff et al., 2012). The destruction of type IX collagen by the stromelysin (MMP) is featured by modification of type II collagen fibrils leading to cartilage swelling (Eyre, 1991).

Initially, the water content increases (Sandy & Verscharen, 2001; Stubendorff et al., 2012). In cartilage, the high fluid pressure (due to the high fixed charge density and the high counter-ion content) is strengthened by the collagen network. The alteration of the collagen network is therefore a prerequisite for the increase of water content (Maroudas, 1976; Brown & Byers, 1989; Guilak et al., 1994). The increased looseness of the collagen network, together with

the increase in water content modify the cartilage properties (i.e. softening, swelling) and its dynamic behaviour (Franz et al., 2001; Pearle et al., 2005; Bhosale & Richardson, 2008). The initial swelling of cartilage is proportional to the amount of damaged collagen (Bank et al., 1997; Bank et al., 2000). Unlike PG loss, the erosion of collagen seems to be irreversible (Goldring & Berenbaum, 2015; Neu et al., 2010). This irreversibility has been associated with the type of enzyme that mediates cartilage degradation. Aggrecanases-mediated damages (PG loss) has been proved to be reversible *in vitro* (Karsdal et al., 2008) and *in vivo* (van Meurs et al., 1999), whereas subsequent MMP-mediated damages (namely collagen and PG loss) were associated to loss of repair capacity, seen as weak anabolic activity of chondrocytes (Karsdal et al., 2008).

The progression of collagen degradation together with loss of PG subsequently induces loss of water, resulting in changes of biomechanical properties such as decrease in tensile stiffness (Guilak et al., 1994; Stolz et al., 2009; Ryd et al., 2015) and in macroscopic changes such as superficial fibrillation (Madry et al., 2012). These alterations modify the biomechanical properties of cartilage (Bhosale & Richardson, 2008).

The collagen degradation and PG loss is therefore a relevant biochemical feature since it reflects the inability for chondrocytes to repair damages to the collagen framework (Heathfield et al., 2004; Hosseininia et al., 2013). These can be assessed by histology and are linked to chondrocyte apoptosis. The chondrocyte apoptosis occurs largely in the deep zone of articular cartilage in spontaneous OA (Matsuo et al., 2001; Zamli et al., 2013), but preferentially in the superficial and transitional zone in induced OA models (Hashimoto et al., 1998; Pelletier et al., 2000; Thomas et al., 2007; Almonte-Becerril et al., 2010; Turunen et al., 2012; Zamli et al., 2013).

Moreover, there is also an alteration of synthesis of superficial zone proteins (lubricin) leading to decrease in boundary lubrication (Neu et al., 2010; Desrochers et al., 2013; Goldring & Berenbaum, 2015).

Deep to HC, the CC shows some changes during OA. In dogs, the thickness of CC was significantly increased in animals with moderate and severe OA compared to healthy ones (Daubs et al., 2006). In OA, vascular invasion and tidemark duplication and advancement, are reported (Bonde et al., 2005; Hulth, 1993; Suri et al., 2007). The vascular invasion getting through the tidemark comes from the SB and is associated with nerve fibres immunoreactive to sensory nerves pattern (Protein Gene Product or PGP 9.5, substance P, CGRP) and sympathic nerves pattern (CPON or C-flanking peptide of neuropeptide Y) (Suri et al., 2007). The endochondral ossification taking place at the tidemark seems to induce biomechanical changes responsible for overlying AC damages (Bullough, 1981).

All these biochemical changes are known to precede changes in mechanical properties (Setton 1993). They lead to reduction of cartilage resilience to compressive loads (Hardingham et al., 1994; Van Den Boom et al., 2005, Wiliams 2003; Bijlsma et al., 2011), with decrease indentation modulus up to six-times in OA-induced models (Desrochers et al., 2012).

In later stages of OA, cartilage degradation leads to partial and full-thickness erosion, and wear lines (McIlwraith, 1996). In man, cartilage defects can only worsen over time. (Henn & Gomoll, 2011).

In subchondral bone

The main feature of OA in SB is its remodelling (Lane et al., 1977; Smith et al., 1992; Burr and Schaffler, 1997; Burr, 2005; Intema et al., 2010). It is associated with changes in density, thickness, architecture and composition (Radin and Rose, 1986; De bri et al., 1995; Bobinac et al., 2003; Burr, 2004; Hayami et al., 2006).

The bone remodelling involves osteoblasts and osteoclasts, in charge of anabolic and catabolic activities, respectively. The osteoclasts resorb the bone matrix whereas the osteoblasts perform collagen deposition (Redlich et al., 2002; Neve et al., 2011). The regulation of remodelling is achieved with osteoprotegerin/ receptor activator of NF-κB (RANK)/RANK Ligand (OPG/RANK/RANKL) signalling pathway (Simonet et al., 1997; Lacey et al., 1998; Komuro et al., 2001; Bellido et al., 2010). Expression of RANKL by osteoblasts activates bone resorption by osteoclasts (Neve et al., 2011). Very early OA is therefore featured by temporary subchondral loss with thinning and decreased density (increased porosity) of the SBP (Intema et al., 2010).

The increase in SB remodelling activity is characterized by increase in matrix resorption, vascular invasion and replacement of lamellar bone (Nordinn et al., 1999). The vessels invasion is associated with tidemark advancement (Bullough & Jagannath, 1983; Oegema et al., 1997) and is attributed to the osteoclastic activity (Walsh et al., 2010; Botter et al., 2011).

In case of increased remodelling (i.e. associated with microdamages), mineralization is not able to cope with the rate of turnover and does not compensate the loss of fully mineralized bone. Moreover, it is known that in OA, the newly formed collagen is not similar to the normal bone collagen, with high level of homotrimer [(α1)3], increased hydroxylation (Bailey et al., 2002) and thinner fibres (Bailey et al., 2004). The homotrimer collagen has less affinity for the calcium than the normal heterotrimer collagen (Mansell & Bailey, 1998; Couchourel et al., 2009). This leads to decrease in level of bone mineralization and abnormal collagen deposition, and consequent reduction in biomechanical properties (Grynpas et al., 1991; Li and Aspen, 1997; Mansell & Bailey, 1998; Day et al., 2001; Banse et al., 2002; Bailey et al., 2004; Kim et al., 2015) such as decrease in bone stiffness (Li & Aspen, 1997). The initial decrease of bone mineral density (BMD) is probably due to bone resorption whereas the later increase could be the expression of the bone sclerosis observed in advanced OA (Watson et al., 1996). This reveals the important changes in bone metabolism during OA progression (Pastoureau et al., 1999).

Inadequate bone mineral density, either decreased (Bellido et al., 2011; Chiba et al., 2011) or in excess (Burr, 2004; van der Harst et al., 2005), is detrimental for cartilage and can initiate cartilage damages. In combined model of osteoporosis and OA, it has been shown that boosting the bone mineral density (with parathyroid hormone administrations) limits the progression of OA-induced cartilage damages (Bellido et al., 2011). Increase in bone mineral density is due either to modelling (apposition) for the subchondral plate, or to remodelling for the trabecular bone; and is associated with increased bone stiffness (Li & Aspden, 1997; Burr, 2004; van der Harst et al., 2005). Higher stiffness of SB decreases its shock absorbing ability and leads to concurrent impact to cartilage (Radin & Rose, 1986).

The biochemical composition of SB bone changes over OA course. In early OA of the equine metacarpophalangeal joint, an increase in ash content, a lower hydroxylysine content and less hydroxylysylpyridinoline (HP) cross-links of the SBP can be observed (Van der Harst et al., 2005). The hydroxylysine content is directly associated with the degree of HP-crosslinking

(Knott & Bailey, 1998) and has been positively correlated with the thickness of collagen fibrils in skin or tendon tissues (Miles et al., 2002). The HP cross-linking is an indicator of turnover since it is a mature cross-link: the decrease of HP cross-link in OA confirms that the remodelling is higher in early OA than in non-OA joints (van der Harst et al., 2005). In OA, in the STB, the content in degraded collagen is increased (Day et al., 2003).

Later stages of OA are characterized by changes in architecture such as SB sclerosis with increased SBP thickness, increased trabecular thickness, increased apparent density, decreased trabecular separation and bone marrow spacing (Radin & Rose, 1986; De bri et al., 1995; Li & Aspen, 1997; Matsui et al., 1997; Bobinac et al., 2003; Burr, 2005; Anderson-McKenzie et al., 2005; Daubs et al., 2006; Ding, 2010; Intema et al., 2010).

Bony changes also include osteophytes formation (Menkes & Lane, 2004). They have been described as a feature of late stage of OA. However, osteophytes can occur without cartilage damage (van der Kraan & van de Berg, 2007). They are age-associated and are asymptomatic provided absence of nerve compression or mechanical disabling (Lamer, 1999; van der Kraan & van de Berg, 2007). It seems that they are involved in force redistribution and joint stability (Pottenger et al., 1990; Oni et al., 1998; Moskowitz, 1999; van der Kraan & van de Berg, 2007).

Besides bone remodelling and its consequences, bone marrow lesions (BML) have also been associated with OA and progression of cartilage damages or loss (Felson et al., 2003; Hunter et al., 2006; Neogi et al., 2009; Roemer et al., 2009; Davies-Tuck et al., 2010). These lesions are prone to develop in high mechanical loading area, i.e. malalignment (Felson et al., 2003; Hunter et al., 2006) and are associated with pain (Bergman et al., 1994; Torres et al., 2006; Felson et al., 2007), and trabecular bone remodelling and thickening (Bergman et al., 1994). The bone marrow lesions used to be called “bone marrow edema” (Felson et al., 2003; Hunter et al., 2006; McQueen, 2007; Hunter et al., 2008). They are representing an ill-defined non-cystic subchondral lesion with particular MRI signal (Roemer et al., 2009; Xu et al., 2012). They are seen as an increased signal in T2W images (Mink and Deutsch, 1989; Vellet et al., 1991). Their histological appearance is variable, including normal tissue invaded by areas of fibrosis, necrosis (Bergman et al., 1994; Zanetti et al., 2000; Garnero et al., 2005; McQueen, 2007) or hypomineralized sclerotic tissue (Hunter et al., 2009), with an increase in bone remodelling (Saadat et al., 2008). At micro-CT, they appear sclerotic with increased bone volume fraction, trabecular thickness and decrease in structural model index (Hunter et al., 2009).

SB can also show cystic lesions. The origin of SB cysts is unclear (Goldring & Goldring, 2007). They can be formed after a microfracture of the SB reaching the joint surface has allowed synovial fluid to invade the SB area and create a pseudo cyst (Madry et al., 2010). In guinea pigs, they may develop early in OA progression (Zamli et al., 2016).

In synovium

OA is also featured by changes in the synovial membrane and fluid. Synovium can show, before cartilage damages occur, inflammation, with cells infiltration (lymphocytes and plasma cells), synovial thickening and increased angiogenesis (Krenn et al., 2006; Haywood et al., 2003; Scanzello & Goldring, 2012; Mathiessen & Conoghan, 2017).

With inflammation, the volume and the composition of synovial fluid are modified due to alteration of synoviocyte function, releasing of tissue debris, and change in filtration of plasma. For example, lubricin concentration decreases after joint injury, whereas cytokines and growth factor content increases (Dahlberg et al., 1994; Elsaid et al., 2008). However, these changes can also be attributed to chondrocyte activity (Ishiguro et al., 1999; Jay et al., 2001; Tchetverikov et al., 2005; Hui et al., 2012). Moreover, the properties of the synovial fluid are altered, with lower viscosity, increase friction coefficient (Elsaid et al., 2005; Teeple et al., 2007) leading to a change in mechanical strain at cartilage surface.

Macroscopically, clinical signs of synovitis are swelling of the joint and, pain. The clinical swelling is palpable and indicates thickening of the synovium and/or synovial effusion. When related to pain, it is associated to limitation of motion (Sutton et al., 2009; Sellam and Berenbaum, 2010; de Lange-Brokaar et al., 2015).

1.7 Osteoarthritis, a disease with limited repair capacity

Obviously, many of those changes are advanced and difficult to repair. In particular, repair ability of cartilage is mainly limited by the avascularity of cartilage, with poor access for regenerative cells or for migration of chondrocyte to the damaged area (Goldring et al., 2017). Spontaneous cartilage repair can occur and depends on different factors, such as the location or the size of the defect. For example, 6-mm diameter cartilage defects in the goat do not heal spontaneously and lead to further damages of the surrounding cartilage and bone (Jackson et al., 2001). In the rabbit, 4-mm chondral defects of the patella showed a higher percentage of filling (32-49%) than the same sized defects on the femoral condyle (6-21%), when assessed 12 to 36 weeks after cartilage defect creation (Heir et al., 2010) suggesting that there is a critical size for possibility to repair and that spontaneous repair of cartilage is not homogeneous along the articular surface.

The repair tissue can be produced by local chondrocytes (along the cleft), and by cells migrating from the SB (Shapiro et al., 1993; Cokelaere et al., 2016). Cells from the synovium could migrate to the articular defects under particular conditions, i.e. decrease of PGs in the surrounding cartilage, associated with the presence of a clot in the defect area (Hunziker & Rosenberg, 1996).

The spontaneous healing of cartilage defect mainly leads to the filling with fibrocartilage or cartilage-like tissue, with a slight improvement of tissue organization overtime but without recovery of perfect HC organization (Terajima et al., 2012; Yanagisawa et al., 2012; O'Brien, et al., 2015).

Finally, the tissue produced by naturally occurring repair of cartilage is most of time unable to integrate with the adjacent cartilage leading to inhomogeneities of cartilage surface, to micro-motion and potential damages to the repair tissue itself (Shapiro et al., 1993).

2. Research question – Aim of the thesis

2. Research question – Aim of the thesis

Due to the limited ability of appropriate self-repair of joint tissue, due to the multiple structural and compositional changes that can occur, and due to the complexity of the OA process, it is important to better understand the early pathological processes and to better detect early structural and compositional changes that are associated to the disease.

In addition, the validation of *in vivo* early diagnostic techniques with fundamental techniques (i.e. biochemistry, histology) is essential to promote the development of treatments and test them *in vivo*. Gold standards methods (histology or biochemistry) are invasive and most of time detrimental for the targeted tissue, inducing lesions because of the sampling method (i.e. excision of cartilage sample).

Furthermore, in longitudinal studies testing the effect of a treatment, we should ideally be able to assess the structure and composition of cartilage at baseline noninvasively, to optimally identify the changes induced by the treatment itself.

The development and the validation of noninvasive tools to assess structural and compositional changes of articular tissues is therefore crucial both for clinical applications and for research.

The first objective of this thesis was to review and assess CT (computed tomography) and MRI (magnetic resonance imaging) techniques in their ability to detect cartilage structural and compositional changes associated with OA.

In particular, the following questions were answered:

1/Can we use MRI and CT to detect subtle structural defects of the cartilage, and what is the best technique? This question was answered in two papers:

- **Hontoir F,** Nisolle JF, Meurisse H, Simon V, Tallier M, Vanderstricht R, Antoine N, Piret J, Clegg P, Vandeweerd JM. 2014. A comparison of 3-T magnetic resonance imaging and computed tomography arthrography to identify structural cartilage defects of the fetlock joint in the horse. The Veterinary Journal 199(1):115-122.
- **Hontoir F**, Clegg P, Simon V, Kirschvink N, Nisolle JF, Vandeweerd JM. 2017. Accuracy of computed tomographic arthrography for assessment of articular cartilage defects in the ovine stifle. Veterinary Radiology and Ultrasound 58 (5): 512-523.

2/ What can we expect from MRI and CT compositional imaging?

This question was answered in one paper:

- **Hontoir F,** Clegg P, Nisolle JF, Tew S, Vandeweerd JM. 2015. Magnetic resonance compositional imaging of articular cartilage: what can we expect in veterinary medicine? The Veterinary Journal 205(1): 11-20.

Since it is now known that early changes can be induced from either the SB or the cartilage, it is useful to identify whether those changes can be detected by noninvasive imaging. We therefore hypothesized that insults of the SB would induce early bone and cartilage changes similar to those identified in OA that would be visible by histological, biochemical and high definition imaging techniques but also possibly by MRI and CT compositional imaging. This hypothesis was tested *in vivo* in an ovine model.

In particular, the following questions were answered in the current manuscript:

3/ Is it possible to induce structural or compositional changes of the cartilage by mechanical or chemical insult of the SB in an *in vivo* ovine model?

4/ Can MRI T2 mapping and compositional CT be used to identify those early structural or compositional changes?

3. The *in vivo* animal model – The sheep

3. The *in vivo* animal model – The sheep

3.1 Animal model

In this thesis, the sheep was selected as an animal model for the *in vivo* experiments. The sheep has been widely used as an animal model for research on musculoskeletal conditions, such as bone fracture management, tendon injuries, osteoporosis, OA, intervertebral disc degenerative diseases (Seibold et al., 1989; Hurtig et al., 1995; Zaruby et al., 1995; Bruce et al., 2002; Lill et al., 2003; Burger et al., 2007; Kaplan et al., 2009; McCoy, 2015). The sheep has been used for years to assess treatment for articular diseases (Huang et al., 2004; Hoeman et al., 2005; Kelly et al., 2006; Kleeman et al., 2007; Dattena et al., 2009; Zscharnak et al., 2010).

The use of small laboratory animals (mouse, rat, guinea pig) is frequent in research and has led to the development of particular strains (for example, either resistant or sensitive to OA development) and also knock-out lineages, allowing the assessment of particular pathways (Bendele and Hulman, 1988; Stanescu et al., 1993; Watson et al., 1996; Zamli et al., 2016). However, the small size of those animals is associated with several limitations such as difficulties for sampling tissues, difficulty to perform surgery and to assess locomotion, and limited use of clinical *in vivo* imaging techniques (Little and Smith, 2008). Larger laboratory animals such as dog or horses can overpass the limitations of small laboratory animals, allowing larger sampling, lameness assessment and scoring, motion analysis with force plate (Smith et al., 2005; Little and Smith, 2008; Marshall et al., 2010). However, the use of these species has some drawbacks such as emotional attachment, ethical controversial, and the need for dedicated large housing facilities (Little and Smith, 2008; McIlwraith et al., 2011). Furthermore, imaging studies are not always easy to perform with horses due to the size of the animal and the necessity or general anaesthesia.

The main advantages of sheep as an animal model are the large size of the joint (compared to mice or rabbits), the availability and the manoeuvrability (Burger et al., 2007; Little and Smith, 2008; Kaplan et al., 2009). Sheep size is adapted to human clinical imaging devices and the animal can be easily anesthetized (Vandeweerd et al., 2014; Joscht et al., 2016; Hontoir et al., 2017).

Using the sheep as an animal model requires, however, a good knowledge of the research population that is available, of the anatomy and the imaging anatomy of the region of interest (the knee), but also of imaging and anaesthetic techniques.

3.2 The ovine knee (stifle)

The ovine knee has similarities with the human knee. The main differences between sheep and human knee are the presence of the extensor digitorum longus tendon on the lateral aspect of the knee, the lack of “full extension” (as the sheep knee does not reach the same degree extension even fully extended), and the tripartition of the femoral articular surface, meaning that the lateral condyle, the medial condyle and the trochlea articular surfaces are not in large

continuity as in human being. The other major difference is the quadrupedality and unguligrady of sheep. However, it is assumed that: “the general design of both species' knees is very similar” (Bellenger and Pickles, 1993; Allen et al., 1998; Osterhoff et al., 2011).

At the University of Namur, our research population is composed of ewes (mainly Texel crossed and Ile de France) that have been reformed for reasons unrelated to orthopaedic diseases, usually mastitis or loss of fertility. The prevalence of naturally occurring cartilage degenerative changes is known within that population. Over a population of 65 sheep, most frequent location of the cartilage defects were the axial part of the middle third of the medial tibial condyle (TCM2Ax) and the middle third of the medial femoral condyle (FCM2) (figure 3) (Vandeweerd et al., 2013). This is consistent with what is found in man (Neogi et al., 2009).

In this thesis, the *in vivo* experiments required clinically healthy sheep with intact cartilage surfaces. It was therefore essential to be able to noninvasively assess the joint status of each sheep enrolled in the project.

Figure 3. Distribution of localization of cartilage defects in a population of 65 sheep assessed by gross anatomy. The most frequent location of cartilage defects (black arrow) was the axial part of the middle third of the medial tibial condyle (TCM2Ax) and the middle third of the medial femoral condyle (FCM2).

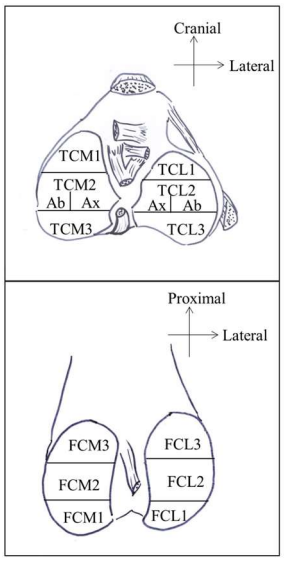

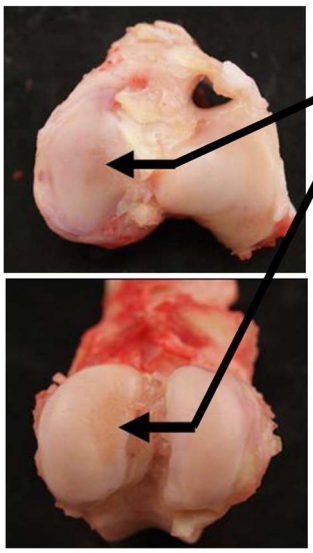

Localization	% of *n* total
TCM2Ax	32.7%
FCM2	29.4%
P2	9.8%
TCL2Ax	9.8%
G2	5.2%
FCM3	3.3%
FCL2	3.3%
G1	2.0%
TL2	1.4%
FCL1	1.3%
TCM2Ab	0.7%
P1	0.7%
P3	0.7%
Total	100.0%

4. Can we use MRI and CT to detect subtle structural defects of the cartilage ? What is the best technique ?

Adapted from:

1. **Hontoir F,** Nisolle JF, Meurisse H, Simon V, Tallier M, Vanderstricht R, Antoine N, Piret J, Clegg P, Vandeweerd JM. 2014. A comparison of 3-T magnetic resonance imaging and computed tomography arthrography to identify structural cartilage defects of the fetlock joint in the horse. The Veterinary Journal 199(1):115-122.
2. **Hontoir F**, Clegg P, Simon V, Kirschvink N, Nisolle JF, Vandeweerd JM. 2017. Accuracy of computed tomographic arthrography for assessment of articular cartilage defects in the ovine stifle. Veterinary Radiology and Ultrasound 58 (5): 512-523.
3. Vandeweerd JM, Vermeylen A, Goossens M, Sternon N, **Hontoir F**, Nisolle JF, Dugdale A. 2014. Anesthésie chez le mouton de laboratoire. Sciences et Techniques de l'Animal de Laboratoire 40 (4): 15-19.

4. Can we use MRI and CT to detect subtle structural defects of the cartilage ? What is the best technique ?

Imaging techniques for musculoskeletal diseases include X-ray, arthroscopy, ultrasonography, and advanced imaging techniques such as computed tomography (CT) and magnetic resonance imaging (MRI). All these techniques are able to provide useful information about joint tissues.

Noninvasive techniques such as radiography or ultrasonography can depict joint status by mainly focusing on bony structure and soft tissues, respectively. Radiography is an accessible technique, mainly dedicated to the assessment of bony structures and evaluation of joint space narrowing (in the weight-bearing patient) (Fife et al., 1991; Rubin and Palmer, 2005; Chan et al., 2008; Braun and Gold, 2011). Radiography is not sensitive to pure cartilage changes and to early loss bone density but is able to depict SB cysts or SB sclerosis (Altman and Gold, 2007). Ultrasonography (US) is primarily used to assess the extra-articular soft tissues (Rubin and Palmer, 2005), but may also provide details about cartilage surface, synovium or meniscal tear (Carrig, 1997). US allows dynamic imaging of joint structures (Qvistgaard et al., 2001; Naredo et al., 2005; Keen and Conaghan, 2009; Pineda et al., 2011). In knee OA, US is able to depict effusion, synovial fluid appearance, synovial hypertrophy, increase in Doppler signal correlated to increase in blood perfusion and to some extent cartilage, meniscus and ligaments lesions (Song et al., 2008; ; Pineda et al., 2011; Sarmaranova et al., 2016)

Arthroscopy is an invasive technique that can be used to assess intra-articular structures, such as cartilage (Oakley et al., 2005; McIlwraith et al., 2005; Barrett et al., 2012). It is considered as a gold standard to assess chondropathy in early OA (Oakley et al., 2005; Witschey et al., 2010). Complete arthroscopic assessment of the joint is not straightforward since some aspects of the joint could remain not visible even using multiple approaches (Martig et al., 2006; Vanderperren et al., 2009; Modesto et al., 2014). Moreover, even would a total assessment of cartilage be provided, arthroscopy does not allow assessment of the deep cartilage and bone unless there is superficial cartilage disruption or bone bruising (Nelson et al., 2018). Although having some limitations, arthroscopy provides the opportunity to perform a wide range of diagnostic or therapeutic procedure (Boening, 2002), to induce cartilage defect or cranial cruciate ligament insult in animal models (McIlwraith et al., 2011; Kuroki et al., 2011), to assess and harvest samples of synovium (Scanzello et al., 2011; Little et al., 2014), or to intervene on cartilage defects (Frisbie et al., 1999; Wilke et al., 2007).

Advanced techniques such as CT and MRI are also useful in assessment of OA-associated changes. CT allows 3D evaluation of bony structures, including osteophytes (Brooks, 1976; Kalender, 2011; Kinns & Pease, 2011). It is nevertheless inadequate to detect purely cartilaginous fragments (Moores et al., 2008) or fluid in bone (Werpy, 2012). To better visualize cartilage using CT, the intra-articular injection of a contrast medium is mandatory. This technique is named: Computed Tomography Arthrography (CTA). In CTA, the use of

contrast medium allows a good delineation of cartilage surface, increasing the contrast between radiopaque liquid (contrast medium) and radiolucent cartilage (Omoumi, 2011; Kirkland 2011). Unlike conventional CT, CTA accurately detects chondral fragment in joint (De Filippo, 2009), enables measurement of cartilage thickness (El-Khoury, 2004; Wyler, 2009, Wyler 2007) and depicts cartilage lesions (Vande Berg, 2002; Schmid et al., 2003; Lecouvet, 2007; De Filippo, 2009).

On the other side, MRI has been proved to be able to delineate cartilage when using high-field magnet and specific sequences (Gold et al., 2009; Kijowski et al., 2009, 2011; Ai et al., 2012; Crema et al., 2013). In human medicine, specific sequences provide a good cartilage-to-fluid contrast, without gap between sections to avoid misdiagnosis of subtle lesions (Recht et al., 2005; Kijowski et al., 2009; Kijowski et al., 2011; Ai et al., 2012; Crema et al., 2013). For example, the cartilage of the human knee can be assessed using fast spin echo sequences T1-, T2-, intermediate or proton density-weighted. However, those techniques developed to assess cartilage structure and thickness in man are not always applicable to other species with thinner cartilage.

In this PhD thesis, the accuracy of CTA and MRI to detect subtle cartilage defects was assessed in two models, the equine metacarpo-/metatarso-phalangeal joint and the ovine stifle.

4.1 Accuracy of CTA and MRI to detect subtle cartilage defects in the equine metacarpo-/metatarso-phalangeal joint

The metacarpo-/metatarso–phalangeal (MCP/MTP) joint of the horse is frequently involved in various equine pathologies such as palmar osteochondral disease (POD) (Barr et al., 2009) and cartilage defects (Neundorf et al., 2010). Though the severity of symptoms attributable to AC defects does not necessarily correlate with their size (Heir et al., 2010; Roemer and Guermazi, 2012), it is commonly admitted that it is essential to detect early signs of cartilage erosion to select the more appropriate treatment (Kelly et al., 2006) and to limit early pathological changes in the joints (Park et al., 2007). It is therefore useful to develop, improve and document imaging techniques that could identify cartilage defects.

In horses, conventional MRI to assess the MTP joint includes T2-turbo spin echo (TSE) sequences, proton density (PD)-TSE sequences and three-dimensional gradient echo (GE) sequences (Tucker and Sampson, 2007). In some studies, detection of cartilage defects with MRI did not show both high sensitivity and high specificity (Smith et al., 2012; Olive et al., 2010a). The cartilage defects were sometimes inferred from signal change in the SB (O'Brien et al., 2011).

In man, high field magnet and specific sequences for cartilage are recommended for the detection of cartilage defects (Gold et al., 2009; Kijowski et al., 2009; Kijowski et al., 2011; Ai et al., 2012; Crema et al., 2013); and comparison between specific MRI sequences for cartilage and CTA revealed that CTA is an accurate technique to identify cartilage defects (Daenen et al., 1998; Vande Berg et al., 2002; El-Khoury et al., 2004; Lecouvet et al., 2007; Shahabpour et al., 2008). In horses, CT and CTA have previously been used to detect cartilaginous (O'Brien et al., 2011) and non-cartilaginous changes of the MCP/MTP joint

(Olive et al., 2010b). However, CTA was not reported to improve the detection of AC defects (O'Brien et al., 2011).

The accuracy of MRI, in detecting cartilage defects, has been documented in human studies (Karvonen et al., 1990; Disler et al., 2000; McCauley & Disler, 2001; McGibbon & Trahan, 2003). The MRI sequences used in routine for the evaluation of the musculoskeletal system (for example T2W-TSE, PD) do not provide adequate assessment of articular cartilage. High-field magnets and specific sequences, providing either better resolution or cartilage-to-fluid contrast than conventional ones, are recommended for detection of cartilage defects (Gold et al., 2009; Kijowski et al., 2009; Kijowski et al., 2011; Ai et al., 2012; Crema et al., 2013). The 3.0-Tesla (3-T) systems can produce images of articular cartilage with higher spatial resolution and decreased slice thickness than 1.5-T systems (Friedrich et al., 2011). The signal to noise ratio (SNR) at 3-T is roughly twice that at 1.5-T, allowing improved image quality and spatial resolution within a similar acquisition time. Improved SNR and spatial resolution in cartilage imaging have been achieved by the 3D fast spin echo sequences (for example, the Sampling Perfection with Application-optimized Contrast using different flip-angle Evolutions (SPACE) sequence by Siemens) (Mosher, 2006). These 3D cartilage-imaging sequences can be broadly divided into dark-fluid sequences and bright-fluid sequences on the basis of the signal intensity of synovial fluid. The main disadvantage of using dark-fluid sequences, like SPGR, for clinical cartilage imaging is the low signal (dark grey to black) intensity of synovial fluid and the low contrast between articular cartilage (dark grey) and synovial fluid, which may decrease the visualisation of superficial cartilage lesions (Kijowski, 2010). The best contrast-to-noise ratio (CNR) between fluid and cartilage is achieved by the bright fluid sequences, like the Dual-Echo in the Steady-State sequence (DESS) (Mosher, 2006; Kijowski, 2010; Friedrich et al., 2011). It creates an arthrogram-like effect within the knee joint that may increase the conspicuity of superficial cartilage lesions (Kijowski, 2010).

In our study, we compared the sensitivity and the specificity of MRI sequences that are optimal for the evaluation of cartilage (i.e. DESS ans SPACE) and CTA to detect cartilage defects in 40 abattoir-derived distal limbs (20 hindlimbs and 20 forelimbs).

Material and methods

Specimens

Distal limbs (n = 40, 20 forelimbs and 20 hindlimbs) of adult horses of various ages and sizes, were collected within 12 h of euthanasia in a slaughterhouse. These were mixed breed horses but no Thoroughbreds or ponies were included in this population. Limbs were stored at -20°C and each limb was identified by a number. As required, specimens were thawed to room temperature, clipped and cleaned. No clinical data relating to those animals were known.

Imaging

MR images were acquired with a 3-T system (Magnetom Verio, Siemens) using a 15 channel-knee coil (Siemens) (Table 1). CTA was subsequently performed after injection of a 20-mL volume of ionic contrast material at 37°C (14 mL saline with 6 mL meglumine ioxaglate and sodium ioxaglate, Hexabrix 320, Guerbet) through a 21 G 1 ½ in needle placed in the dorsal recess of the MCP/MTP joint. This volume ensured throughout filling of the joint cavity.

Images were acquired with a 6-slice CT unit (Emotion 6, Siemens) following these protocol parameters: 130 kV, 80 mAs (pitch 0.4 with tube rotation time of 0.6) and collimation 0.63 mm. Time to acquire scans was recorded. The images were acquired from 2 cm above the proximal limit of the dorsal recess of MCP/MTP joint to 2 cm distal to the proximal articular surface of the proximal phalanx. The transverse resolution was 0.20 x 0.20 mm. Slices of 0.63 mm were reconstructed with an increment of 0.3 mm resulting in an overlap between the different slices and a resultant longitudinal resolution of 0.3 mm without gap. Voxel dimensions were 0.20 x 0.20 x 0.30 mm.

Table 1. Parameters of the magnetic resonance imaging (MRI) sequences used in this study. The Sampling Perfection with Application-optimized Contrast using different flip-angle Evolutions (SPACE) sequence was acquired in 2D (sagittal and coronal planes). The Double-echo in the steady-state (DESS) sequence was acquired in 3D.

ms= milliseconds; min= minutes; cm= centimetres; mm= millimetres

	DESS (isotropic – 3D)	SPACE 2D	SPACE 2D
TE (echo time) (ms)	5.04	48	48
TR (repetition time) (ms)	14.84	2800	2800
Acquisition time (min)	7'08	5'52	5'52
Acquisition plane	Sagittal	Sagittal	Coronal
FOV (field of view) (cm)	14	10	10
Pixel size (mm)	0.6 x 0.6	0.4 x 0.4	0.4 x 0.4
Slice thickness (mm)	0.6	0.8	0.8
Matrix	256 x 256	256 x 256	256 x 256
Flip angle	25	120	120

Macroscopic observation

After imaging, the distal limbs were dissected: the periarticular tissues were removed and the joint capsule was opened. The articular surfaces of the metacarpus or metatarsus III (MC/MT3), proximal phalanx and proximal sesamoid bones were examined by gross observation. The abnormalities of the articular cartilage were scored following OARSI recommendations for macroscopic scoring of cartilage defects (McIlwraith et al., 2010) (Table 2). Scoring of articular surfaces was performed by macroscopic examination in 16 anatomic regions of each MCP/MTP joint (Figure 4). The most severe defect was used to score the articular surface of one region. Joint surfaces were digitally photographed for records, with standardised lighting conditions.

Table 2. Correspondence between scores for gross anatomy (McIlwraith et al., 2010), computed tomography arthrography (CTA), magnetic resonance imaging (MRI), and cartilage structure at histology (adapted from Olive et al., 2010a).

Score	Gross anatomy	CTA	MRI	Histology (cartilage structure)
0	intact cartilage surface	sharp line of contrast material identified on the cartilage surface, without substance loss	signal intensity of the hyaline cartilage homogeneous and intermediate	smooth and regular
1	partial-thickness defect, < 5 mm in diameter*	penetration of contrast material within at least the superficial half of the cartilage thickness and not within the SB on an area of less than 5 mm diameter	signal intensity changes involving at least the superficial half of the cartilage thickness, but not reaching the SB on an area of less than 5 mm diameter	from surface irregularities, fibrillation or clefts to defect in the upper two thirds of the hyaline cartilage
2	partial-thickness defect, > 5 mm in diameter*	penetration of contrast material within at least the superficial half of the cartilage thickness and not within the SB on an area of more than 5 mm diameter	signal intensity changes involving at least the superficial half of the cartilage thickness, but not reaching the SB on an area of more than 5 mm diameter	
3	full-thickness defect, visualization of SB	contrast reaching or penetrating the SB	signal intensity changes involving the whole thickness of the cartilage	defect of the whole thickness of hyaline cartilage, ulceration to SB

* The articular cartilage defect diameter was derived from measurement of abnormal cartilage surface by applying a piece of clear flexible plastic film on the joint surface. A water-resistant black pen was used to outline the perimeter of each lesion. The resulting plastic film outlines were digitized, and morphometry software (Image J, National Institutes of Health) was used to measure the diameter of the ink-stained area. For oblong defects, the higher diameter was taken into account to distinguish a score-1 from a score-2 defect.

SB= subchondral bone.

Figure 4. Anatomic regions assessed for articular cartilage abnormalities. The joint was divided in 16 regions. Seven regions for the metacarpus/metatarsus III: dorsal (1), middle (2) and palmar/plantar (3) area of the lateral part of the condyle; dorsal (4), middle (5) and palmar/plantar (6) area of the medial part of the condyle and the sagittal ridge (7). Seven regions for the proximal phalanx: dorsal (8), middle (9) and palmar/plantar (10) area of the lateral fovea; dorsal (11), middle (12) and palmar/plantar (13) area of the lateral fovea and the sagittal groove (14). One region per proximal sesamoid bone: medial (15) and lateral (16).

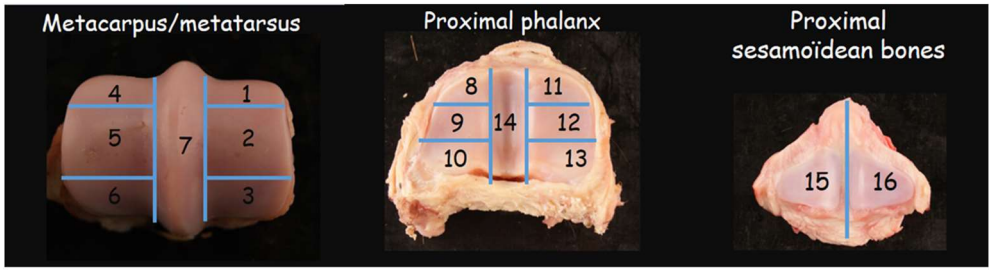

Histology of cartilage

To evaluate the accuracy of investigators in scoring defects, histological analysis was performed on randomly selected defects (20% of the total, i.e. twenty-four) and twelve control normal samples. Samples were fixed in 10% (v/v) neutral buffered formalin for 48 h. Following fixation, they were transferred to 70% (v/v) ethanol for storage or further processing. They were decalcified in chlorhydric acid and EDTA (DC3, Labonord) for 2 days and embedded in paraffin. Four-micron sections were cut. Sections were de-paraffinised with xylene and graded ethanol, and then stained with Toluidine blue. After a 2-months delay, two investigators read the sections, unaware of the identities of the sections. Histological scores used to assess cartilage structure are described in Table 2 and are illustrated in Figure 5.

Histological cartilage score was compared to macroscopic defects to evaluate the accuracy of investigators in scoring defects (for example, to confirm that a score 1 or 2 defect assessed macroscopically was a partial defect (fibrillation, fissures) not involving the SB at microscopy, while a score 3 defect was a full thickness defect). In addition, the SB plate was assessed for abnormalities (enlarged bone spaces, vessels penetrating calcified cartilage).

Images analysis

CTA and MR images were reviewed separately by a musculoskeletal radiologist and a veterinarian, using a diagnostic workstation (Telemis HE Viewer 4.3). Both observers were blinded to the identity of the specimens. CTA and DESS images were analyzed in the three different planes, while 2D SPACE images were only assessed in their planes of acquisition (coronal and sagittal). Sixteen anatomic regions were defined for each MCP/ MTP joint and were identical to those evaluated in the macroscopic analysis. The most severe defect observed in any section of each of the sixteen anatomic regions was used to score the articular surface of that region. For MRI, the most severe defect observed in one of the sequences was used for scoring. Scores are defined in Table 2. When scores differed between the imaging planes, the most severe score was reported. The radiologist repeated the blinded retrospective

interpretation of all examinations one month after the first assessment to determine intra-observer reproducibility.

Figure 5. Examples of cartilage defects of score 1 (A and C) and score 3 (B and D) assessed macroscopically (A and B) or histologically (C and D). Fibrillation and defect in the upper part of the hyaline cartilage (HC) are visible in C while a defect of AC extending to the calcified cartilage (CC) and the subchondral bone (SB) can be seen in D.

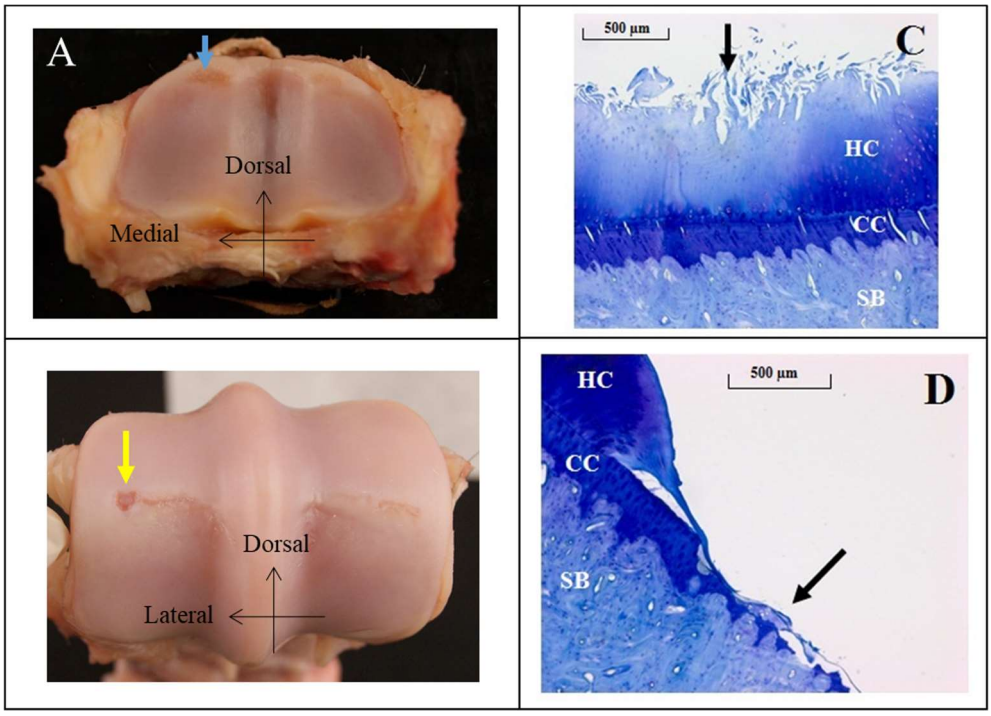

Statistical analysis

Kolmogorov-Smirnov and Shapiro-Wilk tests were used to examine the normality of data. Due to the non-normality of data, discriminant analysis was conducted using non-parametric statistics (Pearce & Frisbie, 2010). Correlation between macroscopic and histological scorings was assessed using the Spearman's rank order test. True positives (TP), true negatives (TN), false positives (FP), false negatives (FN), sensitivity (Sen), specificity (Spe), positive predictive value (PPV) and negative predictive value (NPV) were calculated by considering gross anatomic observation as the gold standard. Definitions of those outcome measures are provided in Table 3. Sensitivity and specificity differences per anatomic region were compared by using the Kruskal-Wallis test. Inter-observer and intra-observer agreement were assessed by using non-weighted Kappa statistics. A very good agreement showed a Kappa value higher than 0.80 (Breenan & Silman, 1994; Landis & Koch, 1977). Comparison between sensitivities and specificities of CTA and MRI imaging was done using the Mc-Nemar test (Dwyer, 1991; Vande Bergh et al., 2002; Liao & Lin, 2008). Correlations between

imaging (CTA and MRI) and macroscopic findings were analysed using Spearman's rank order correlation coefficient. A p-value less than 0.05 was considered to indicate a statistically significant difference.

Results

In a total of 640 regions (16 regions x 40 limbs), 123 regions showed an AC defect. In all limbs, two regions did not show any defect: the middle area of the lateral and medial fovea of the proximal phalanx. Most frequent defects were identified on the dorsal aspect of the fovea of the proximal phalanx (15%), on the middle area of the lateral part of the condyle of MC/MT3 (16%) and on the middle area of the medial part of the condyle of MC/MT3 (18%). Gross anatomy identified 89 score-1 defects (72%), 14 score-2 defects (11%) and 20 score-3 defects (16%). Gross anatomy findings were well correlated with histology (rs=0.99; P<0.0001) and failed to correctly assess the defect in 1/36 case. No SB and trabecular changes were identified by histology.

At CTA, cartilage appears as a radiolucent layer covering the high attenuating SB and underlying the radiopaque contrast medium. Using DESS sequence, cartilage and synovial fluid have a high signal intensity (bright) while SB and trabecular bone have a low signal intensity (dark). With the SPACE sequence, cartilage and SB are dark whereas synovial fluid and trabecular bone are bright (Figure 6).

Figure 6. Appearance of cartilage assessed by the different imaging techniques. At Computed tomography arthrography (CTA), the cartilage appears as a black line underlying radiopaque contrast medium. Using the dual-echo in steady state sequence (DESS) cartilage appears as a dark grey line covered by light grey synovial fluid. Using the sampling perfection with application-optimized contrast using different flip-angle evolutions sequence (SPACE), cartilage appears also as a dark grey line covered by light grey synovial fluid.

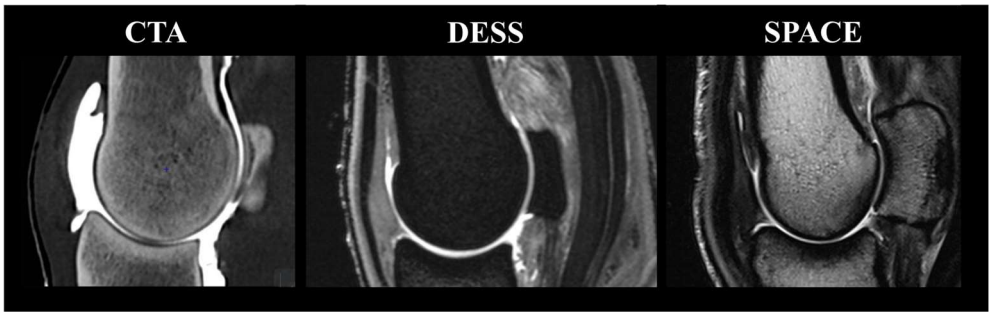

Mean acquisition time (not including preparation of limbs and injection of contrast), for CTA and MRI was respectively 2 and 26 min.

Sensitivity, Specificity, positive predictive value and negative predictive value for identification of cartilage defects for the different observers and both imaging techniques are reported in Table 3. Mean CTA Sen and Spe were respectively 0.82+/-0.03 (mean +/- standard error) and 0.96+/-0.02. Those values taken together were significantly higher than those of MRI (0.41+/-0.01 and 0.93+/-0.01) with the Mc Nemar test (P <0,001).

Table 3. Comparison of computed tomography anatomy (CTA) and magnetic resonance imaging (MRI) performances. Results are provided for each observer. For observer 1, two observations are reported as he repeated the analysis of the images one month after the first assessment to determine intra-observer reproducibility.

	CTA	MRI
Sensitivity measures the proportion of positives (macroscopically eroded cartilage) which are correctly identified as such. Sen = TP/TP + FN		
Sen (observer 1/observation 1)	85%	42%
Sen (observer 1/observation 2)	84%	40%
Sen (observer 2)	75%	41%
Mean Sen (±standard error)	82% ± 3*	41% ± 1*
Specificity measures the proportion of negatives (macroscopic score 0) which are correctly identified by the imaging technique. Spe = TN/TN + FP		
Spe (observer 1/observation 1)	98%	94%
Spe (observer 1/observation 2)	97%	93%
Spe (observer 2)	93%	94%
Mean Spe (±standard error)	96% ± 2*	93% ± 1*
Positive predictive value is the probability that a positive result at CTA or MRI (score1, 2 or 3 defect) is truly a defect. PPV = TP/TP + FP		
PPV (observer 1/observation 1)	90%	58%
PPV (observer 1/observation 2)	85%	53%
PPV (observer 2)	67%	59%
Mean PPV (±standard error)	82% ± 6	57% ± 2
Negative predictive value is the probability that a negative result at CTA or MRI (score 0) is truly erosion-free. NPV = TN/TN + FN		
NPV (observer 1/observation 1)	97%	88%
NPV (observer 1/observation 2)	97%	88%
NPV (observer 2)	95%	88%
Mean NPV (±standard error)	97% ± 1	88%

TP = true positives; TN = true negatives. FP = false positives. FN = false negatives. Sen = Sensitivity. Spe = specificity. PPV = Positive predictive value. NPV = Negative predictive value.

***** CTA sensitivity and specificity values taken together were significantly higher than those of MRI with the Mc Nemar test (P<0,001).

Correlation between CTA and macroscopic scores was 0.99 (P<0,0001), while correlation between MRI and macroscopic scores was 0.58 (P<0.05). Sensitivities and specificities to detect defects did not significantly differ between anatomical regions. At CTA and MRI, inter-observer agreement was very good for scoring the different regions (κ= 0.82 and 0.88, respectively). Intra-observer agreement was very good for CTA and for MRI (κ= 0.96 and 0.92, respectively).

Out of the 123 defects, CTA detected 90.3 +/- 2.96 defects and adequately classified 52 +/- 3.06 score-1 defects, 6 +/- 0.58 score-2 defects and 14.0 +/-0.0 score-3 defects.

MRI was able to detect 52.33 +/- 2.33 defects and adequately classified 35.0 +/-2.08 score-1 defects, 1.7 +/- 1.2 score-2 defects and 4.67 +/-2.33 score-3 defects.

Combining both techniques helped to detect 3+/-0.58 additional score-1 defects. Examples of defects are illustrated in figure 7.

Figure 7. Examples of cartilage defects. This figure illustrates the difficulty to detect subtle articular cartilage defects with magnetic resonance imaging (MRI). The appearance of three different types of defect (score 1, 2 and 3) is illustrated for computed tomography arthrography (CTA), dual-echo in steady state sequence (DESS), and sampling perfection with application-optimized contrast using different flip-angle evolutions sequence (SPACE). Figures of line 1 refer to a partial-thickness defect < 5 mm in diameter (score-1 cartilage defect) on the middle area of the medial part of the condyle of the third metacarpus (red arrow). Figures of line 2 refer to a partial-thickness defect > 5 mm in diameter (score-2 cartilage defect) in the dorsal portion of proximal phalanx detected. Line 3 refers to a full cartilage defect (score 3) on the middle area of the medial part of the condyle of the third metacarpus (yellow arrow).

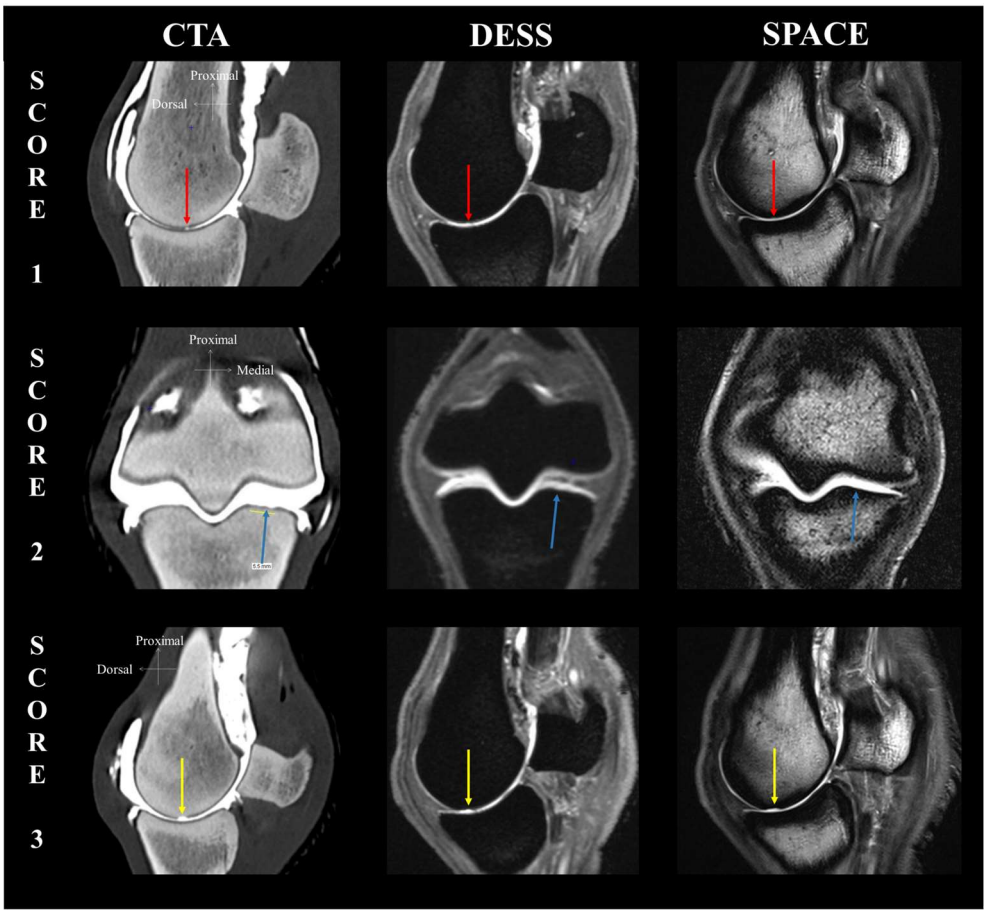

Discussion

Prevalence and significance of AC defects

The AC defects were frequently identified in the middle area of the MC/MT3 condyles (16 and 17% for lateral and medial parts of the condyle respectively) and the dorsal aspect of the proximal phalanx (15%), consistent with previous studies (Brommer et al., 2003; Neundorf et al., 2010). Wear lines, described in Thoroughbred horses (Barr et al., 2009; Neundorf et al., 2010), were rarely observed by macroscopic evaluation in this study. In this series of horses, the AC defects were of lower macroscopic score than those in other studies evaluating the accuracy of MRI to identify AC defects (O'Brien et al., 2011; Olive et al., 2010a; Smith et al., 2012). This is likely due to the non-Thoroughbred horse population examined. Longitudinal studies will be necessary to determine the clinical relevance, and any progression, of such superficial cartilage defects in the MCP/MTP joint of horses. The impact of small cartilage defects has been described in humans: prevalent focal cartilage defects were considered as a risk factor for future cartilage loss in the same sub-region (Roemer et al., 2011).

Comparison of CTA and MRI

This study demonstrated that CTA of the MCP/MTP joint enabled accurate assessment of AC defects. Our results contradict those of a previous study concluding that CTA did not improve the detection of AC defects of the distal metacarpal bone (O'Brien et al., 2011). The authors suggested, however, that, in their study, horses had sustained catastrophic injuries and repair tissue was filling chronic defects, which might have prevented movement of contrast from the joint space into the cartilage. In our study, defects were mainly small and were not associated with any obvious healing response or fibrocartilage production.

The lower sensitivity and specificity of MRI compared to CTA is in agreement with previous human studies using joints with thin cartilage such as hip or ankle (El-Khoury et al., 2004; Llopis et al., 2012). The poor correlation between MRI and macroscopic evaluation is consistent with previous human (von Engelhardt et al., 2010) and equine (Olive et al., 2010a; Smith et al., 2012) studies. Our study, in addition, demonstrates that MRI is less reliable than CTA, even when specific sequences and a high-field magnet (3-T) are used. Recently, a study assessing the detection rate, by MRI and CT, of induced cartilage defects in another thin cartilage joint, namely the equine carpus, revealed that the sensitivity of CTA was higher than the sensitivity of MRI, MRA (Magnetic Resonance Arthrography) and CT (Sanchez-Andrade et al., 2018).

The superiority of CTA to detect AC defects and the lack of accuracy of MRI can be explained by several factors: resolution, artefacts and acquisition time.

Contrast resolution is the ability of the imaging technique to visualize distinctly two structures with different attenuation coefficient (CT) or signal (MRI) (for example, bone and cartilage), while the in-plane resolution reflects the ability to generate an image that accurately represents the delineation between those two structures from the sample of pixels initially generated. Basically, both resolutions must be considered together when comparing imaging techniques. Contrast resolution of tissues is favoured by the MRI technique (and its

range of sequences and acquisition parameters) in comparison with conventional CT, though, in the latter, satisfactory delineation of cartilage surface can be obtained if contrast medium is used by techniques such as CTA (Holland et al., 1994; Tivers et al., 2008). However, this difference is counter balanced by the better in-plane resolution of CT. The CT scan system in this study had an in-plane resolution with pixels of 0.2 x 0.2 mm. The best in-plane resolution that we could obtain for MRI was 0.4 x 0.4 mm with the SPACE sequence, provided 2D acquisition to keep a clinically acceptable acquisition time. For the same reason of time constraints, the 3D isotropic DESS sequence remained unsatisfactory in our study (0.6 x 0.6 x 0.6 mm). Moreover, 2D acquisition, such as the SPACE sequence in this study, means relatively thick sections and gaps between sections which may lead to misdiagnosis of defects (Kijowski et al., 2009; Ai et al., 2012; Crema et al., 2013), while nearly isotropic (0.2 x 0.2 x 0.3 mm) CT-reconstruction enabled a complete assessment of the articular surface, in multiple planes and without gaps. However, it should be taken into account that the CT-reconstruction (slices of 0.63mm) will lead to volume averaging.

Several artefacts may explain the low PPV of MRI (Little & Schramme, 2007; Murray & Dyson, 2011; Smith et al., 2012). Partial volume artefacts may occur when a mixture of tissues with different attenuation coefficients (CT) or signals (MRI) are found within any given voxel which therefore possesses an attenuation or signal average of the different tissues. For example, it is the case at the transition between the condyle and the sagittal ridge of distal MC/MT3 in sagittal slices. This artefact can be limited by reducing the slice thickness. The risk of such an artefact is lower with CT where the slice thickness was only 0.3mm, while it was respectively 0.6mm and 0.8mm with the DESS and the SPACE MRI sequences in this study. The magic angle artefact refers to the increased signal in MR images seen in tissues with well-ordered collagen fibres in one direction (like in the articular hyaline cartilage) that occurs when the angle such fibres make with the magnetic field is equal to 54.7°. A potential increase of the cartilage signal intensity could therefore be confused with a superficial defect.

Acquisition time is also an important concern. Indeed, motion artefact is more likely to happen as scanning time increases and resolution is limited by the scanning time (Gold et al., 2009). In our study, the best compromise between resolution and scanning time was obtained with the CTA: it was less than 1 minute for the MCP/MTP joint, keeping a high spatial resolution (0.2 x 0.2 x 0.3 mm). The issue of scanning time is an important clinical consideration as the techniques described in this study would necessitate general anaesthesia in living animals.

Limitations of this study

Our limbs were mostly from horses with limited AC defects. Evaluation of limbs with more extended pathology could have given different results. However, the objective of our study was precisely to compare the imaging techniques in their accuracy to detect subtle AC changes without the risk that detection was inferred from other more obvious abnormalities.

Histological samples were obtained in limited number because they were conducted only to validate the investigator's ability to detect accurately the defects, and not the macroscopic technique itself. The correlation between macroscopic evaluation and histology was particularly good (r_s=0,99 ; $P<0.0001$) on the 20 % of defects and on the controls that were

assessed and we estimated that it was sufficient to conclude that gross anatomy assessment was accurate.

Finally, we could have compared CTA to contrast enhanced MRI. With MRA, the contrast is injected directly into the joint. Unlike what happens in CTA, the contrast medium is not visible itself, it only modifies the T1 relaxation time of the tissue. Therefore, this technique is not suitable to detect cartilage defects *in vivo* since it would require a fluid-sensitive sequence (i.e. a Fat-suppressed T1-weighted images) to maximize the signal intensity of the constrast medium (Kalke et al., 2012), but with a low resolution. Increasing the resolution would lead to long acquisition time and thus motion artefact (Waldt et al., 2005).

Conclusions

This study suggests that CTA is a potentially valuable tool to assess superficial cartilage defects in the MCP/MTP joint. It is superior to MRI with regard to its short acquisition time, its good correlation to macroscopic evaluation, its specificity and its sensitivity, in the detection of subtle cartilage defects. Thanks to the contrast medium providing a good contrast resolution and to the high spatial resolution (0.2 x 0.2 x 0.3 mm), CTA allows the assessment of the entire cartilage surface without any loss of data. Though MRI is a useful technique for joint evaluation, as it detects important abnormalities such as synovitis and bone marrow that have been associated with pain in OA, clinicians need to be aware of its limitations. Even with a high-field magnet and using specific sequences designed for cartilage assessment, in comparison to CTA, MRI was less effective in subtle cartilage defects detection. CTA is therefore suggested as an interesting tool to investigate the presence of cartilage defects in longitudinal studies before enrolling an animal in a research project.

4.2 Accuracy of CTA to detect subtle cartilage defects in the ovine knee, *ex vivo* and *in vivo*

CTA is a potentially valuable tool to assess superficial cartilage defects, with both high sensitivity and specificity (Hontoir et al., 2014). It has been proved that fibrillation and fissures not involving the SB, as well as erosions down to SB, were present in 43% of a population of cross-bred Texel ewes used for research and were more commonly identified in specific anatomical regions such as the middle part of the medial femoral condyle, the medial tibial condyle and the patella (Vandeweerd et al., 2013). It is important to detect cartilage defects at baseline before including a sheep in a longitudinal research study and to do it noninvasively, for example by CTA.

The current experimental study aimed to assess the accuracy of CTA for detecting cartilage defects in a common animal model used for OA research, the ovine stifle (knee, femoropatellar/femorotibial) joint.

This study included an *ex vivo* experiment (on cadaver limbs) and an *in vivo* experiment, to test the feasibility of the technique in living anesthetized animals. Because imaging of living animal is prone to motion artefact, a safe and efficient anaesthesia protocol is mandatory. Short acquisition time limits the risk of motion artefact (Gold et al., 2009) but will affect the image quality, with decreased spatial resolution (McRobbie et al., 2006). The use of physical and chemical contention is therefore preferred when feasible. A specific anaesthetic technique was developed and tested at the initiation of the current study.

Material and methods

Ex vivo study - Animals

The experimental protocol (reference: VA10 150) was approved by the local ethics committee for animal welfare. Paired hind limbs were collected from Texel crossbred ewes (aged from 2 to 11 years) euthanized for reasons not related to musculoskeletal disease (mastitis, loss of fertility) and used for teaching (anatomical dissection). The sheep weighed between 45 and 80 kg. They came from the Ovine Research Centre of the University of Namur. Animals were euthanized by an intravenous (IV) injection of embutramide (20mg/kg). The limbs were collected within 6 hours of euthanasia and disarticulated at the level of the coxofemoral joint. They were stored frozen (-20°C) and thawed to room temperature before CTA assessment.

Ex vivo study - Study design

CTA, macroscopic, and histologic scoring of articular surfaces were performed in 26 anatomic regions (Figure 8) for every stifle (Vandeweerd et al., 2013). Sensitivity and specificity of CTA for detecting cartilage defects were calculated by comparison of CTA assessments of articular cartilage sites (one anatomic region in one stifle in a specific sheep was defined as one "site") to the combined gross anatomic and histological observation of those sites considered as the gold standard. This meant that only articular cartilage sites where lesions (cases) or absence of lesion (controls) was corroborated by histological assessment were used to assess sensitivity and specificity.

The anatomical site was considered the unit of observation for several reasons. First, the objective of the study was to evaluate CTA as a tool to identify defects in the anatomic sites that are either commonly affected at baseline or sampled for analysis (Vandeweerd et al., 2013) (and not the other sites), or to follow-up a lesion surgically induced in a specific anatomic site such as the medial femoral condyle that is commonly used in research on regenerative and graft therapies (Schinhan et al., 2012). Then, considering the joint as the unit of observation would require assessing the whole articular surface histologically, which is not feasible technically. Finally, a previous prevalence study has shown that higher scores in one site (the axial part of the middle part of the tibial condyle, e.g.) do not necessarily imply that higher scores would also be identified in other sites of the joint (i.e. the axial part of the middle part of the femoral condyle) (Vandeweerd et al., 2013).

Figure 8. Twenty-six anatomic sub-regions macroscopically assessed for abnormalities of the articular cartilage. (A) cranial, middle, and caudal thirds of the articular surface of the medial and lateral tibial condyles, where each middle third was divided into axial and abaxial aspects (TCM1, TCM2Ax, TCM2Ab, TCM3, TCL1, TCL2Ax, TCL2Ab, TCL3); (B) proximal, middle, and distal thirds of the articular surface of the patella (P1, P2, P3); (C) cranial, middle, and caudal thirds of the articular surface of the medial and lateral femoral condyles (FCM1, FCM2, FCM3, FCL1, FCL2, FCL3); (D) proximal, middle, and distal thirds of the articular surface of the medial ridge, groove, and lateral ridge of the trochlea of the femur (TM1, TM2, TM3, G1, G2, G3, TL1, TL2, TL3). Region of interest (blue) that were systematically collected from each ovine knee (induced, control or sham operated) were P2, TCM2, TCL2, FCM2 FCL2.

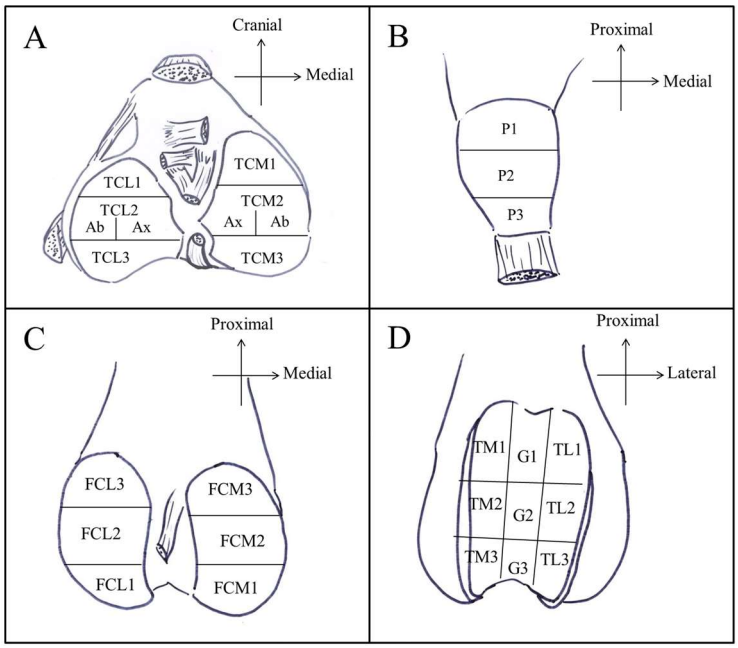

Ex vivo study -Sample size determination

The total number of sites (sample size, N_{total}), and the number of cases (N_{cases}) and controls ($N_{controls}$), that were necessary to assess to ensure the reliability of the sensitivity and specificity analysis, were calculated using the following equation: (Hajian-Tilaki, 2014)

$$N_{total} = \frac{Z_{\alpha/2} \times Sen\ (1 - Sen)}{d^2 \times \text{Prev}}$$

where $Z_{\alpha/2}$ was 1.96 for alpha = 0.05,

Sen = predetermined value of sensitivity, estimated from previous published studies (it was set to 0.80 in comparison to values for detection of cartilage defects in the human knee (Vande Berg et al., 2002), ankle (Schmid et al., 2003), and elbow (Waldt et al., 2005) and the equine MCP/MTP joint (Hontoir et al., 2014),

d = precision of estimate, i.e. the maximum difference between estimated sensitivity (or specificity) and the true value was set to 0.10 (Hajian-Tilaki, 2014),

Prev = prevalence of disease (cartilage defects for sheep) and was set to 0.66 according to published studies (Vandeweerd et al., 2013).

With these settings, the sample size calculation was 93.1. This meant that 94 comparisons between gold standard and CTA assessment were required to ensure a reliable accuracy study for detection of cartilage defects in the ovine stifle with CTA.

N_{cases} and $N_{controls}$ were calculated using the following equations:

$$N_{controls} = N_{total} \times (1 - \text{Prev})$$
$$N_{cases} = N_{total} \times \text{Prev}$$

A total 62 cases were therefore required and 32 controls were necessary. These were randomly selected in the cadaveric limbs. Sheep were enrolled until those numbers were achieved. Paired hind limbs (n = 42) from 21 ewes were collected to reach the adequate sample size of "sites."

Ex vivo study - CTA technique

To perform CTA, the joint was injected with 6-ml volume of ionic contrast material (iodine 320 mg/ml, at 37°C; meglumine ioxaglate and sodium ioxaglate; Hexabrix 320, Guerbet, Aulnay-Sous-Bois, France) mixed with 14 mL saline was injected through a 21G 1 1/2 needle (Terumo, Belgium) (Vandeweerd et al., 2012; Hontoir et al., 2017). A paraligamentous technique was used (Figure 9): the needle was inserted along the medial aspect of the patellar ligament at mid-distance between its distal and proximal insertions (Vandeweerd et al., 2012). The injected stifles were then flexed and extended 100 times to allow homogeneous coating of the articular surfaces.

The injection of the ovine knee requires a single injection since the femoropatellar compartment and the medial and lateral femorotibial compartment communicate together (Vandeweerd et al., 2012). Three different approaches have been described (Figure 9):

- The retropatellar technique (RPT): the needle is inserted horizontally under the lateral aspect of the patella, which is manually displaced laterally at mid-distance between its base and apex.
- The subtendinous technique (STT): the needle is orientated proximo-caudally and penetrates the synovial cavity, along the common tendon of peroneus tertius–extensor longus digitorum–extensor digiti III proprius, in the extensor groove, 2 cm below the level of the tibial plateau.
- The paraligamentous technique (PLT): the needle is inserted along the medial aspect of the patellar ligament at mid-distance between its distal and proximal insertions.

Figure 9. Injection techniques: (1) paraligamentous techniques (PLT); (2) subtendinous techniques (STT); (3) retropatellar technique (RPT). (Vandeweerd et al., 2012)

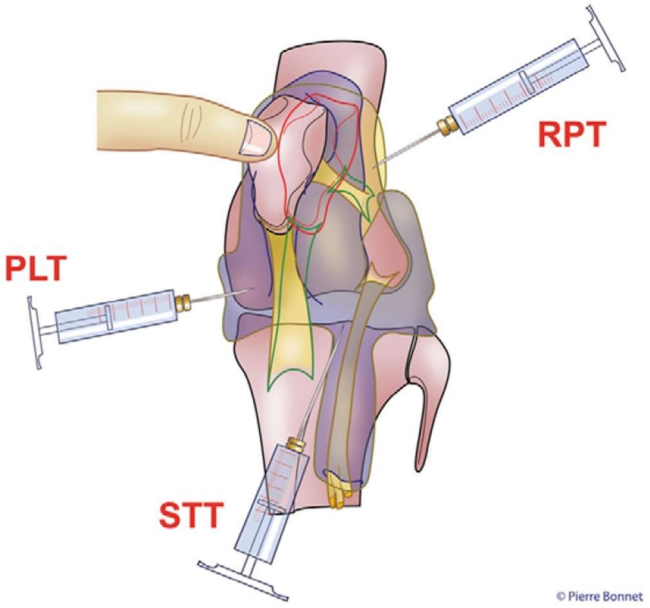

The limbs were examined with a multi-slice CT scanner (Emotion 6, 6-slice detector, Siemens, Erlangen, Germany). The image acquisition protocol was as follows: 130 kV, 140 mAs, pitch 0.4 (helical acquisition), collimation 0.63 mm, and tube rotation time 0.6 s. Images of 0.63 mm were reconstructed with an increment of 0.3 mm. From this isotropic volume of images, dorsal (coronal), sagittal, and transverse planar reformatted images were generated (1mm thickness and 1mm space between slices). The field of view extended from the base of the patella to 6 cm distal to the tibial plateau. Images were reconstructed on a 512-512 matrix, and in-plane resolution was 0.2 mm. Acquisition time was 2 min on average. The dose-length product, reflecting the radiation output from the CT scan and its extent (Mayo-Smith et al., 2014), was 143 mGray·cm. Images were then transferred on a medical digital imaging system (PACS, Télémis, Louvain-La-Neuve, Belgium). All reconstructed images were prospectively stored for assessment of cartilage. Images were reconstructed using bone

algorithm (B70, Siemens). The window centre and width were 800 HU and 2000 HU, respectively.

Ex vivo study - Macroscopic assessment of articular cartilage

Soft tissue was removed from the detached limbs and the joint was carefully disarticulated. The cartilage was kept moist by covering the joint surface with gauze sponges soaked in lactated Ringer's solution. The distal articular surface of the femur, proximal articular surface of the tibia, and articular surface of the patella were examined by gross observation by one investigator (FH). Joint surfaces were digitally photographed (Sony Alpha DSLR-A230 digital camera) with standardized lighting conditions for records (two Sony Illustar SM-300 lighting).

The abnormalities of the articular cartilage were scored by using Osteoarthritis Research Society International (OARSI) recommendations for macroscopic scoring of cartilage in sheep: score 0 for intact cartilage surface; score 1 for surface roughening; score 2 for deeper defects (fibrillation, fissures) not involving the SB; score 3 for erosions down to SB, smaller than 5-mm in diameter; score 4 for erosions down to SB, larger than 5-mm diameter (Little et al., 2010).

Ex vivo study - Microscopic assessment of articular cartilage

Sets of 3- to 4-mm-thick osteochondral slabs were obtained centered either on the articular surface defect visualized grossly, or on the centre of healthy anatomic regions. Samples were fixed in 10% (v/v) neutral buffered formalin for 48 h. Following fixation, samples were transferred to 70% (v/v) ethanol for storage or further processing.

They were decalcified in DC3 (non-ionic surfactants, hydrochloric acid, EDTA, VWR International, Leuven, Belgium) for 2 days and embedded in paraffin, and then 4-μm sections were cut. Sections were deparaffinised with xylene and graded ethanol, and then stained with Toluidine blue. Each slice was examined by two investigators (FH, JMV) working in consensus and cartilage structure was scored using the OARSI recommendations for histological evaluation of articular cartilage in sheep (Table 5).

In vivo study - Animals

All procedures complied with the Royal Decree on the Protection of Experimental Animals in concordance with European Directive 2010/73. Thirteen unpaired hind limbs (n = 13) from 13 other animals (aged from 2 to 11 years), enrolled in a research study on OA (experimental protocol OsteoOvin KI 12 181 approved by the local ethical committee for animal welfare), were used to assess the technique in living animals under general anaesthesia. After the procedure, they were euthanized and limbs were collected. The sheep weighed between 45 and 80 kg. They came from the Ovine Research Centre of the University of Namur.

In vivo study - Anaesthesia technique

In living animals, physical examination was performed to confirm their good health. Animals were fasted for 12 hours, with ad-lib access to water. Before anaesthesia, forearms were

clipped and the right cephalic vein was catheterized with a 20 G 1 ¼'' catheter (Terumo, Belgium). Xylazine (150µg /kg IV) and diazepam (150µg /kg IV) were used for premedication (Vandeweerd et al., 2014). After induction with pentobarbital (3 mg/kg), the animal was initially placed in sternal position and the neck was extended. A laryngoscope (Kawe, Germany) was used to visualize the glottis, and a cuffed 8.0 endotracheal tube was inserted, inflated with 15ml air, and secured. It was connected to an ambu-bag and 100 % oxygen was administered. Anaesthesia was maintained by IV infusion of pentobarbital in 0.9% NaCl (10 mg/kg/h).

This protocol is the result of a previous study by our team. Existing protocols include the use of propofol and/or inhalation anaesthesia for maintenance (Giavaresi et al., 2001; Hette et al., 2008; Orth et al., 2012; Moya-Angeler et al., 2016). Our research team compared a propofol-based and a pentobarbital-based protocol for sheep anaesthesia (Vandeweerd et al., 2014). Sheep were randomly allocated to one protocol (propofol-based or pentobarbital-based), and after a one-week wash out, they were submitted to the other protocol (pentobarbital-based or propofol-based). The study compared anaesthesia quality, heart rate, respiratory rate and movements, rectal temperature and SpO_2.When anesthetized following the propofol-based protocol, the sheep showed an increase in heart rate and respiratory rate, associated to a decrease of anaesthesia depth. An increase in maintenance dose (from 20 to 30 mg/kg/h) was therefore necessary to keep an adequate anaesthesia depth. Respiratory movements were more fluent and calm with the pentobarbital-based protocol, in opposition to the wide and halting movements during the propofol-based anaesthesia. The recovering period was shorter for the propofol-based protocol than for the pentobarbital-based protocol, as expected from the pharmacologic properties of the molecules. Thus, the pentobarbital-based protocol was the protocol used in our research lab to perform safe anaesthesia in the sheep when motion artefact has to be reduced significantly and stability of long-lasting anaesthesia is required.

In vivo study - Computed tomographic arthrography technique

Animals were placed in lateral recumbence and the stifle region was clipped and scrubbed with povidone iodine (Poviderm scrub, povidone iodinum 7.5%, Audevard, France; Poviderm dermicum, povidone iodinum 10%, Ecuphar, Belgium). The stifle was injected with the same technique as for the cadaver limbs. When the needle was inserted, synovial fluid was collected to confirm intra-articular position of the needle.

Animals were kept in lateral recumbence during the scanning period, with the head in a lowered position in a styrofoam box to collect saliva (Figure 10). Urinary catheterization (Foley catheter 14, Rusch Gold, Germany; connected to a 2.0L-secretion bag, Sarstedt, Germany) was performed to ensure collection of urine and to avoid contamination of the equipment and environment. Digital extremities were covered with latex gloves. To perform CT scan, the targeted limb was extended caudally and maintained with a 5-kg load, while the other limb was extended cranially and maintained with a roller bandage. The limbs were examined with the same scanner as that used for the ex-vivo study (Emotion 6, 6-slice detector, Siemens, Erlangen, Germany). The acquisition protocol was also similar to the *ex vivo* study except that scans were performed at 200 mAs. The dose-length product was 258 mGray.cm. The duration of the whole procedure (anaesthesia and CTA) was measured.

Figure 10. Sheep positioning for computed tomography arthrography procedure. (A) The sheep was placed in lateral recumbence with the targeted limb extended caudally and the contralateral limb pulled cranially and tied around the trunk with a roller bandage. Digital extremities were covered with latex gloves. (B) Oxygen supply was provided by an endotracheal tube connected to an ambu-bag (VTrade, Noville-Les-Bois, Belgium) and an oxygen tank. Saliva was collected in a stir foam box. (C) Urine was collected by bladder catheterization to avoid contamination of the equipment and environment. (D) Schematic view of limb positioning for a cadaver stifle and (E) for living animal. In living animal, despite the forced extension of the limb, the pelvis remained in the acquisition field; this affected the quality of the image since the pelvis (dotted circle), soft tissues, and stifle (plain circle) attenuated the X-rays before they reached the detectors. (F) CTA images of cadaver stifle and (G) stifle of living animal.

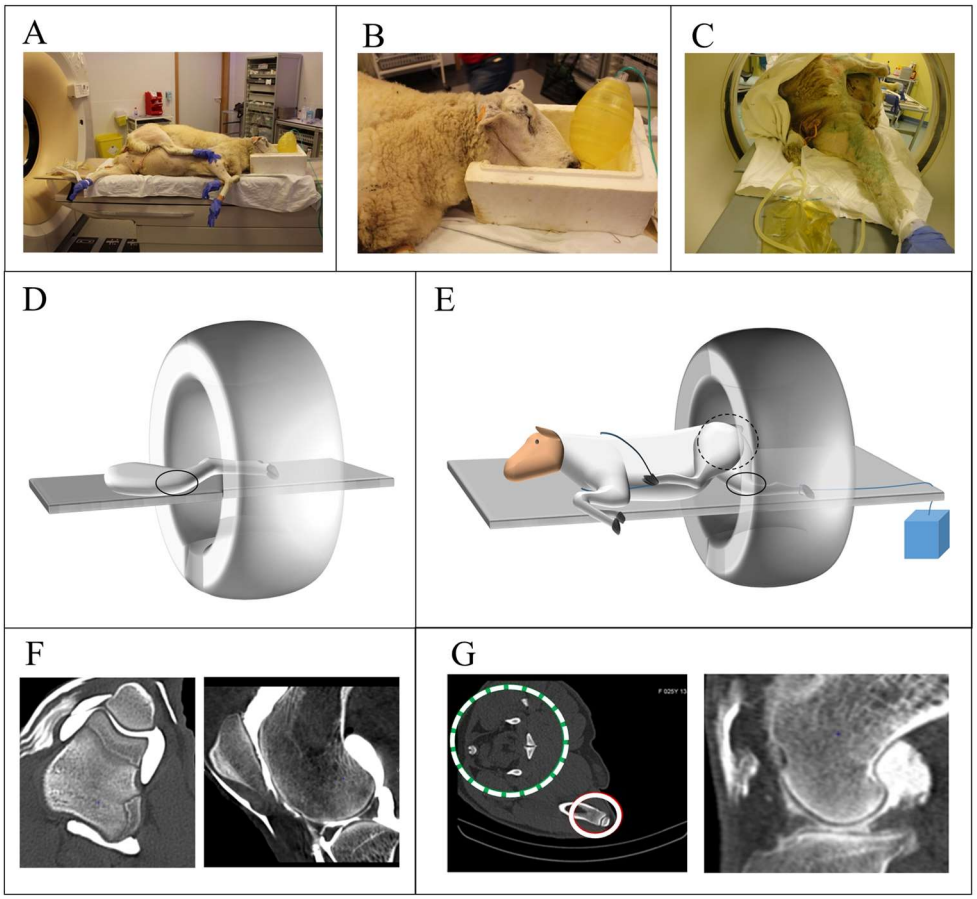

In vivo study - Macroscopic and microscopic assessment of articular cartilage

After imaging, animals were euthanized by an IV injection of embutramide (20mg/kg). The limbs were collected within 6 hours of euthanasia and disarticulated at the level of the coxofemoral joint. Soft tissue was removed from the detached limbs, and the joint was carefully disarticulated. The experimental protocol for living sheep included systematic assessment of five anatomic regions in every limb: middle third of the articular surface of the medial and lateral femoral condyles, middle third of the articular surface of the patella), axial aspect of the middle third of the articular surface of the medial and lateral tibial condyles. Gross anatomy and histology were performed as in the in-vitro study using the previously described scoring protocol.

Image analysis

Two months after performing CTA, one musculoskeletal radiologist (JFN) and one veterinarian (FH) separately retrieved and analysed the archived CTA images. Transverse, dorsal, and sagittal images were viewed simultaneously. Both observers were blinded to the identity of the specimens. The 26 anatomic regions were observed in each stifle. The CTA scoring criteria are described in Table 4. Normal cartilage was defined as a radiolucent layer covering the high attenuating SB and bordered by the radiopaque contrast medium. Lesions associated with OA (osteophytes, SB changes) were also recorded as present or absent. Scores from 0 to 4 were used for CTA and corresponded to the scores used for macroscopic examinations (Table 4). When surface scoring differed between the imaging planes of CT, the most severe score was reported. The most severe lesion observed in any section of each of the 26 anatomic regions was used to score the articular cartilage surface of that region. After a 1-month delay, one investigator (JFN) repeated the blinded retrospective interpretation of all examinations to determine intra-observer reproducibility.

Table 4. Macroscopic and computed tomographic arthrography scoring scales. (SB = subchondral bone, CTA= computed tomography arthrography, mm = millimetre)

Score	Macroscopic scoring	CTA scoring
Score 0	Intact cartilage surface	A sharp line of contrast material is identified on the cartilage surface without substance loss
Score 1	Surface roughening	Loss of the sharp and smooth contour of the cartilage surface
Score 2	Deeper defects (fibrillation, fissures) not involving the SB	Penetration of contrast material within at least the superficial half of the cartilage thickness but not down to the SB
Score 3	Erosion down to SB, <5 mm diameter	Penetration of contrast material down to SB, <5 mm diameter
Score 4	Erosion down to SB, >5 mm diameter	Penetration of contrast material down to SB, >5 mm diameter

Statistical analysis

The prevalence (number of defects/number of observed limbs) and anatomical distribution of (number of defects per region/total number of lesions) of defects were assessed for both cadaver limbs and limbs from living sheep. Statistical analyses were performed by the first

author (FH) using a computer software system (Stats Direct, Medical Statistics Software, Cheshire, UK). Kolmogorov–Smirnov and Shapiro–Wilk tests were used to examine the normality of data. Due to positive skewness and kurtosis of the macroscopic, histologic and imaging scores distribution, nonparametric statistics were conducted (Pearce & Frisbie, 2010).

According to the requirements of the sensitivity–specificity analysis, data were used for analysis only if macroscopic scores were confirmed by histology; this means that macroscopic scores of 1, 2, 3, and 4 corresponded, respectively, to histological (1) surface irregularities from moderate to severe but where disruption, fissuring, and fibrillation do not reach more than 10% of articular cartilage depth (OARSI scores 2 and 3; Table 5); (2) fissures, erosions, or fibrillations that do not go deeper than the calcified layer (OARSI scores 4–9; Table 5); (3 and 4) erosion or severe fibrillation to SB (OARSI score 10; Table 5).

Using the Spearman rank coefficient assessed correlation between macroscopic scoring and histological scoring. Inter-observer and intra-observer agreement were tested by using Kappa statistics. Kappa values less than 0 were considered to be poor agreement; between 0 and 0.2, slight agreement; between 0.21 and 0.40, fair agreement; between 0.41 and 0.60, moderate agreement; between 0.61 and 0.80, substantial agreement; and between 0.81 and 1.00, almost perfect agreement.[29] Sensitivity, specificity, positive predictive value, and negative predictive value were calculated separately for cadaver limbs and living animals. Pooled estimated sensitivity, specificity, positive predictive value, and negative predictive value were calculated after consensus between observers was reached. Pooled estimated parameters for cadaver limbs and living animals were then compared using chi-square test (and Fischer's exact test when required). A P-value < 0.05 was considered to indicate a statistically significant difference.

Table 5. Osteoarthritis research society international (OARSI) recommendations for histological assessment of cartilage structure (Little et al., 2010)

Score	Definition
0	Normal
1	Slight surface irregularities (surface barely disturbed)
2	Moderate surface irregularities (surface roughened)
3	Severe surface irregularities (disruption, fissuring/fibrillation to <10% depth)
4	Fissures to transitional zone (1/3 depth)
5	Fissures to radial zone (2/3 depth)
6	Fissures to calcified zone (full depth)
7	Erosion or severe fibrillation to mid-zone (1/3 depth)
8	Erosion or severe fibrillation to deep zone (2/3 depth)
9	Erosion or severe fibrillation to calcified zone (full depth)
10	Erosion or severe fibrillation to subchondral bone

Results

Descriptive statistics

The CTA duration was 2 minutes. The whole procedure (anaesthesia and CTA) had a mean duration of 40 minutes. No complications occurred in the living animals.

Figure 11 illustrates the appearance of articular cartilage at CTA and examples of score-2 and -3 defects.

A total of 115 osteochondral samples were assessed, including 99 that had their macroscopic scoring confirmed by histology and were used for sensitivity-specificity analysis. Prevalence and anatomical distribution are described in the flow chart in Figure 12. Lesions were primarily score-2 defects (71.0%). Score-1 defects, score-3 defects and score-4 defects accounted for 24.2%, 1.6% and 3.2% respectively. Most frequent affected anatomic regions were: middle third of the articular surface of the medial tibial condyle) (50.0%) and middle third of the articular surface of the medial femoral condyle (27.4%). No signs of OA (such as osteophytes and SB changes) were identified by CTA either in the cadaver limbs or in living animals.

Figure 11. Appearance of cartilage in CTA images. (A) Intact cartilage appears as a sharp radiolucent layer (plain arrows) underlined by the radiopaque contrast medium (dotted arrow). (B and C) Examples of cartilage defects. (B) A score-2 defect on the medial femoral condyle; (C) a score-3 defect on the axial aspect of the medial tibial condyle.

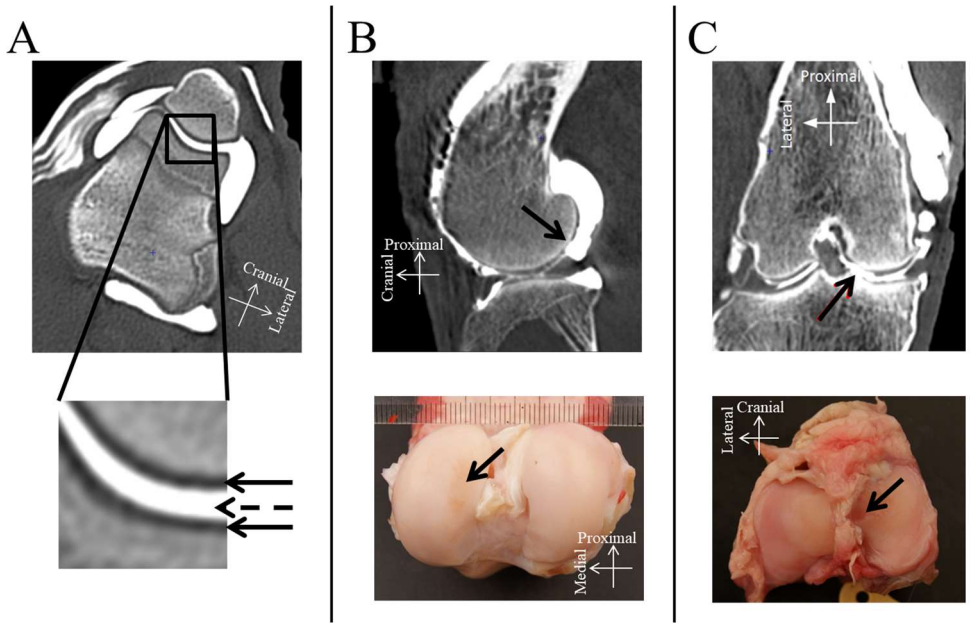

Figure 12. Flow chart of limbs and samples, mean performances of CTA, distribution of lesions, and prevalence of lesions

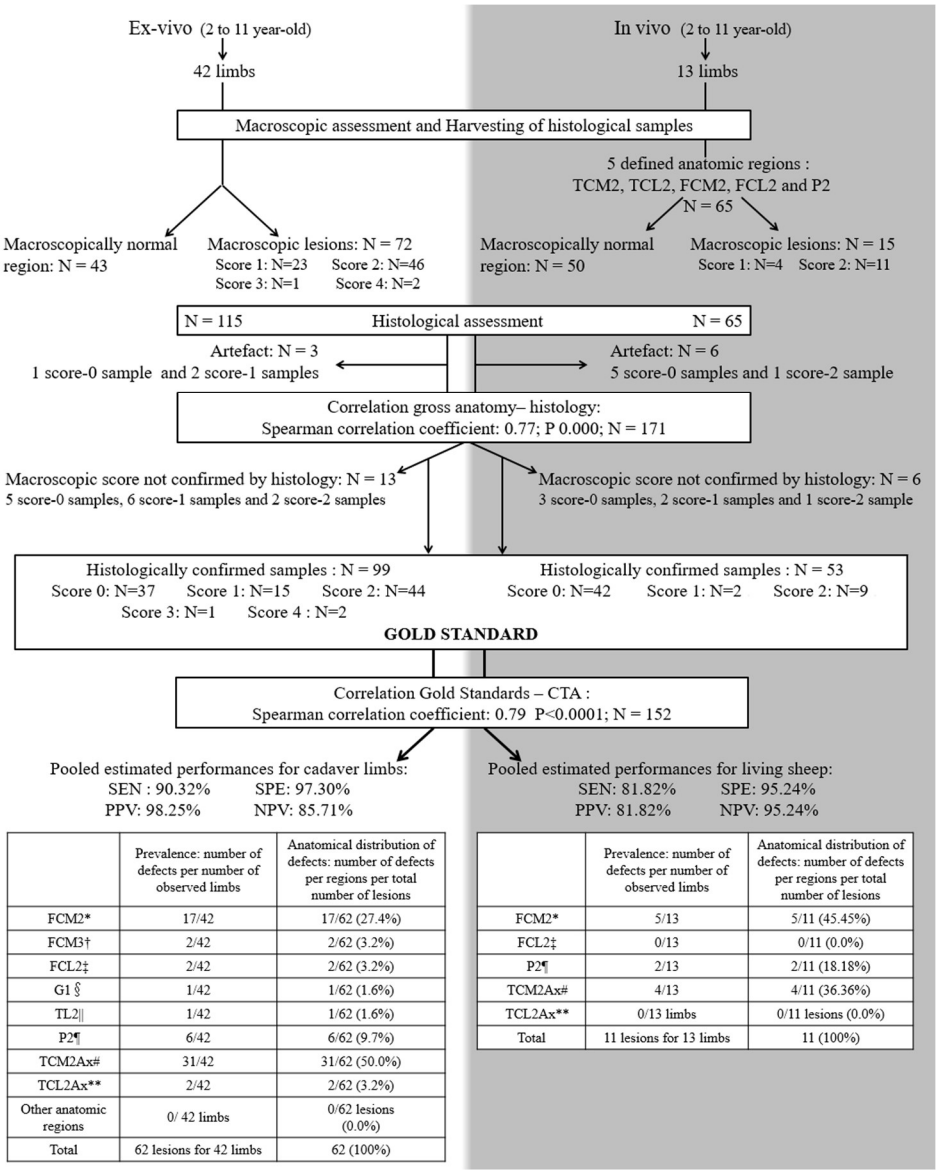

	Prevalence: number of defects per number of observed limbs	Anatomical distribution of defects: number of defects per regions per total number of lesions
FCM2*	17/42	17/62 (27.4%)
FCM3†	2/42	2/62 (3.2%)
FCL2‡	2/42	2/62 (3.2%)
G1 §	1/42	1/62 (1.6%)
TL2‖	1/42	1/62 (1.6%)
P2¶	6/42	6/62 (9.7%)
TCM2Ax#	31/42	31/62 (50.0%)
TCL2Ax**	2/42	2/62 (3.2%)
Other anatomic regions	0/ 42 limbs	0/62 lesions (0.0%)
Total	62 lesions for 42 limbs	62 (100%)

	Prevalence: number of defects per number of observed limbs	Anatomical distribution of defects: number of defects per regions per total number of lesions
FCM2*	5/13	5/11 (45.45%)
FCL2‡	0/13	0/11 (0.0%)
P2¶	2/13	2/11 (18.18%)
TCM2Ax#	4/13	4/11 (36.36%)
TCL2Ax**	0/13 limbs	0/11 lesions (0.0%)
Total	11 lesions for 13 limbs	11 (100%)

*FCM2: middle third of the articular surface of the medial femoral condyle
†FCM3: caudal third of the articular surface of the medial femoral condyle.
‡FCL2: middle third of the articular surface of the lateral femoral condyle.
§G1: proximal third of the articular surface of the groove of the trochlea of the femur.
‖TL2: middle third of the articular surface of the lateral femoral trochlear ridge.
¶P2: middle third of the articular surface of the patella.
#TCM2Ax: axial aspect of the middle third of the articular surface of the medial tibial condyle.
**TCL2Ax: axial aspect of the middle third of the articular surface of the lateral tibial condyle.

Sensitivity/specificity analysis

Including all slides (even those where histological scores were not similar to macroscopic scores), gross anatomy findings were significantly correlated with histology (Spearman correlation coefficient 0.77; P 0.000). Considering only sites where macroscopic scores were corroborated by histology, there was substantial agreement between those scores and those at CTA (Spearman correlation coefficient: 0.76 (observer 1 - assessment 1), 0.81 (observer 1 – assessment 2), 0.79 (observer 2); $P<0.0001$).

The sensitivity, specificity, positive predictive value and negative predictive value of CTA for detecting cartilage defects are reported in Table 6, both for observer 1 and 2. In cadaver limbs, CTA was able to adequately classify on average (pooled estimated of the three assessments) 36 of 37 score-0 area, 14 of 15 score-1 defects, 39 of 44 score-2 defects, 1 of 1 score-3 defects and 2 of 2 score-4 defects. In living animals, CTA was able to adequately classify on average (pooled estimated of the three assessment) 43 of 45 score-0 areas, 1 of 2 score-1 defects, 8 of 9 score-2 defects. The k-values observed for inter- and intra-observer reproducibility were 0.76 and 0.94, respectively. The negative predictive value of CTA for detecting defects in cadaver limbs was significantly lower than the negative predictive value in living animals while the positive predictive value in cadaver limbs was significantly higher than the positive predictive value in living animals ($P<0.05$). The sensitivity and specificity of CTA for detecting defects in living animals did not significantly differ from values in cadaver limbs.

Table 6. Performance parameters of computed tomography arthrography to detect cartilage defects.

	Cadaver Limbs (N = 99 histological samples)[a] Estimate in % (95% confidence interval)	Living sheep under anesthesia (N= 53 histological samples)[b] Estimate in % (95% confidence interval)
SEN [c]		
Observer 1/ assessment 1[h]	80.65 (69.1 to 88.6)	81.82 (52.3 to 94.9)
Observer 1/ assessment 2 [h]	87.80 (74.5 to 94.7)	88.89 (56.5 to 98.0)
Observer 2	79.03 (67.4 to 87.3)	81.82 (52.3 to 94.9)
Pooled estimated SEN	**90.32 (80.2 to 95.4)**	**81.82 (52.3 to 94.9)**
SPE [e]		
Observer 1/ assessment 1[h]	97.30 (86.2 to 99.5)	92.86 (81.0 to 97.5)
Observer 1/ assessment 2 [h]	93.75 (71.7 to 98.9)	100.00 (71.0 to 100.0)
Observer 2	97.30 (86.2 to 99.5)	95.24 (84.2 to 98.7)
Pooled estimated SPE	**97.30 (86.5 to 99.5)**	**95.24 (84.2 to 98.7)**
PPV [f]		
Observer 1/ assessment 1[h]	98.04 (89.7 to 99.7)	75.00 (46.8 to 91.1)
Observer 1/ assessment 2 [h]	97.30 (86.2 to 99.5)	100.00 (66.2 to100.0)
Observer 2	98.00 (89.5 to 99.6)	81.82 (52.3 to 94.9)
Pooled estimated PPV	**98.25 (90.6 to 99.7)**	**81.82 (52.3 to 94.9)**
NPV [g]		
Observer 1/ assessment 1[h]	75.00 [d] (61.2 to 85.1)	95.12 [d] (83.9 to 98.7)
Observer 1/ assessment 2 [h]	75.00 [d] (53.1 to 88.8)	90.91 [d] (62.3 to 98.4)
Observer 2	73.47 [d] (59.7 to 83.8)	95.24 [d] (84.2 to 98.7)
Pooled estimated NPV	**85.71** [d] **(72.7 to 93.4)**	**95.24** [d] **(84.2 to 98.7)**

Notes. Pooled estimated values (SEN, SPE, PPV, NPV) are highlighted in **bold letter** to distinguish them from the assessments of observer 1 and 2.
a From these 99 histological samples, 37 were control samples and 62 were case samples.
b From these 53 histological samples, 42 were control samples and 11 were case samples.
c Sensitivity (SEN) measures the proportion of positives (macroscopically eroded cartilage) that are correctly identified as such. Sen = TP / (TP + FN). TP =true positive; TN = true negative; FP = false positive; FN = false negative.
d Significantly different ($P < 0.05$).
e Specificity (SPE) measures the proportion of negatives (macroscopic score 0) that are correctly identified by the imaging technique. SPE = TN / (TN + FP).
f Positive predictive value (PPV) is the probability that a positive result at CTA (score 1, 2, or 3 defect) is truly a defect. PPV = TP / (TP + FP).
g Negative predictive value (NPV) is the probability that a negative result at CTA (score 0) is truly erosion-free. NPV = TN / (TN + FN).
h The two observers (Observer 1 and Observer 2) separately analyzed the CT images. After a 1-month delay, Observer 1 repeated the blinded retrospective interpretation (Observer 1/ assessment 2) to determine intra-observer reproducibility.

Discussion

This study demonstrated that CTA can detect articular cartilage in cadaver sheep stifle joints with acceptable sensitivity (90%) and specificity (97%). This technique is also feasible in living sheep with acceptable sensitivity (82%) and specificity (95%). The study also showed that naturally occurring articular cartilage defects were highly prevalent in this population of sheep, with 73 lesions being identified in 55 cadaver limbs. The most frequent locations of lesions were the axial aspect of the middle third of the articular surface of the medial tibial condyle, the middle third of the articular surface of the medial femoral condyle, and the middle third of the articular surface of the patella. This is in accordance with a previous study by the authors that demonstrated that these three regions were the most frequent affected anatomic regions (Vandeweerd et al., 2012). In ovines, as well as in humans, the medial femorotibial compartment shows higher prevalence of cartilage defects (Vandeweerd et al., 2011) and bears a larger part of the total load than the lateral compartment (Taylor et al., 2011). In man, medial femoral condyle and patellar defects are more prevalent than lateral femoral condyle defects or trochlear defects (Arøen et al., 2004; Flanigan et al., 2010). The higher prevalence of defects in the medial compartment may be associated to the asymmetry of forces distribution in the stifle (Thomas et al., 1975; Baliunas et al., 2002).

The current study confirmed that cartilage defects can be present in a population of research sheep without clinical signs and radiographic changes associated with OA. This is important since animal studies rarely assess cartilage at baseline in clinical trials (Vandeweerd et al., 2015). At best, radiography is used to confirm the initial healthiness of joints (Simmons et al., 1999; Frisbie et al., 2002), though it is known that radiographic assessment has methodological flaws and may not accurately identify cartilage changes associated with OA (Altman, 2004). Biopsy is not used to assess histological characteristics and biochemical contents of cartilage since it would create defects in articular cartilage. Therefore, caution should be used when generalizing conclusions based on those experimental outcomes, and CTA might be a useful technique to detect articular cartilage defects present at baseline. Detection of cartilage defects of various depths may be also useful for clinical cases. Though

the size of the defect does not correlate with clinical signs (Heir et al., 2010; Roemer & Guermazi, 2012), early detection allows selection of more appropriate treatments to help limit early pathological changes in the joints (Kelly et al., 2006; Park et al., 2007).

The good performance of CTA in the current study was expected since it is known to be a useful technique to define the cartilage surface. With CTA, the entire articular surface can be assessed in multiple planes because of the isotropic reconstruction of the joint and the delineation of the cartilage defects by the contrast medium (Holland et al., 1994; Tivers et al., 2008). In the human knee, e.g., CTA revealed articular cartilage defects in radiographically healthy joints and articular cartilage defects that were not identified by MRI (Vande Berg et al., 2002b; Vande Berg et al., 2002). In one of these studies, CTA accuracy was higher for the detection of knee cartilage defects (with sensitivity ranging from 80% to 94% and specificity ranging from 86% to 94%) than MRI (Vande Berg et al., 2002b). In another human study, CTA was more accurate to detect cartilage loss even in comparison to MR arthrography (Omoumi et al., 2015).

In the horse, MRI was significantly less sensitive and less specific than CTA to identify articular cartilage defects in the metacarpo-/metatarso-phalangeal joint, even with specific sequences and a high-field magnet (3-T) (Hontoir et al., 2014). The high accuracy of CTA is related to the resolution and short acquisition time. Short acquisition time limits the risk of motion artefacts (Gold et al., 2009). For example, to assess the articular cartilage in the equine metacarpo-/metatarso-phalangeal joint, several cartilage-specific MRI sequences (DESS, SPACE) of 5 to 8 minutes were necessary in comparison to a single 2-minutes acquisition with CTA (Hontoir et al., 2014). Resolution is also a concern when imaging such thin structures as cartilage. Cartilage thickness of the stifle in sheep ranges from 0.3 mm to 1.23mm +/- 0.29 depending on the anatomical region (Appleyard et al., 2003; Frisbie et al., 2006). If the voxel size is not small enough (i.e. 2mm) and encompasses the signal of tissues with different attenuation coefficients (i.e. SB and/or contrast medium), partial volume averaging occurs and the cartilage delineation is indistinct, leading to a misinterpretation of the CT images (Barrett & Keat, 2004). In our study, the voxel size was 0.2 mm; this allowed accurate imaging of the sheep cartilage limiting the partial volume averaging and related misinterpretation.

In CTA, the cartilage is delineated by the contrast medium. It is therefore essential that this contrast medium reaches all parts of the synovial cavity. In the human knee and the ovine stifle, the meniscus, covering the tibial plateau and partially covering the femoral condyles, could prevent contrast to fully outline the cartilage. Passive mobilization of the joint and warming of the contrast medium (to enhance fluidity) are helpful to avoid this issue (Halsell, 1987; Hughes & Bisset, 1991; Roth et al., 1991).

Interestingly, in the current study, CTA could be performed in a short time (2 minutes). Total acquisition time for one limb in a living sheep was longer because it included the following multiple steps: handling the sheep, catheterization of cephalic vein, IV induction of anaesthesia, intubation, urethral catheterization, positioning the sheep on the table and the limb on the gantry, scrubbing, injection of contrast medium, passive motion of the limb, and scanning the limb. All these steps took about 40 minutes. Lateral recumbence was preferred during scanning as it allowed the stifle to be in the centre of the gantry. This is important since CT, unlike MRI, is prone to cone beam artefact, which is a deformation artefact due to the cone-shape of the X-ray beam. This artefact is more important for outer detectors. Therefore the further the imaged structure is from the centre of the gantry, the more important

the artefact becomes (Barrett & Keat, 2004). Moreover, miscentering of the targeted structure is known to affect negatively the signal-to-noise ratio and to induce an increase in patient radiation dose to achieve the same image quality (Toth et al., 2007; Habibzadeh et al., 2012; Mayo-Smith et al., 2014). Though sternal recumbence is recommended in sheep and other ruminants for maximizing anaesthesia safety, minimizing rumen bloating, and maximizing cardio-vascular stability (Taylor, 1991), those problems were not seen with the lateral recumbence used in our study.

Another important concern regarding positioning is the presence of the pelvic cavity in the gantry, together with the stifle, even if the limb is caudally extended and maintained with a 5-kg load. This means that the X-ray beam has to penetrate the pelvis and the stifle before reaching the detectors (Figure 10 D-G, p. 60). This induces signal attenuation and degrades the image quality, as it could happen when imaging a human patient with large body mass (Yoshimura et al., 2006). In our study, the tube current-time product was increased (200 mAs) to enhance image quality. However, this increase and enhancement is limited by the CT unit specifications and the ALARA (as low as reasonably achievable) principle, commonly observed in human medicine (Mayo-Smith et al., 2014). This may explain why, in living animals, images had more artefacts than in cadaver limbs. However, the impact of these artefacts was minimal because sensitivity and specificity for detecting cartilage defects did not differ between live sheep and cadaver limbs.

The fact that positive predictive value (98%) and negative predictive value (86%) in cadaver limbs were different from positive predictive value (82%) and negative predictive value (95%) in living animals could be linked to the difference in the number of controls. Positive predictive value and negative predictive value are driven by the prevalence and its complement (1-prev), respectively (Altman and Bland, 1994). For example, in living animals, there were 42 controls, which is proportionally higher than in cadaver limbs (37 samples). Negative predictive value is therefore higher for living animals than for cadaver limbs, even if both sensitivity and specificity are high.

Conclusion

This study demonstrated that detection of cartilage defects is feasible in the ovine stifle by CTA with excellent sensitivity and specificity. A high prevalence of naturally occurring cartilage defects were identified in this sample of sheep, with no clinical signs of lameness and no CTA signs of OA. These findings supported the use of CTA for baseline screening and longitudinal assessment of cartilage in OA research studies using sheep models. Future studies are needed to further develop and assess minimally invasive techniques for assessing cartilage such as conventional CTA and MRI, MRI compositional imaging, and fluid biomarkers.

5. Advanced imaging techniques for compositional defects of cartilage: What can we expect from MRI and CT compositional imaging?

Adapted from:

- **Hontoir F,** Clegg P, Nisolle JF, Tew S, Vandeweerd JM. 2015. Magnetic resonance compositional imaging of articular cartilage: what can we expect in veterinary medicine? The Veterinary Journal 205(1): 11-20.

5. Advanced imaging techniques for compositional defects of cartilage: What can we expect from MRI and CT compositional imaging ?

Partial- or full-thickness cartilage defects are late signs of OA, resulting from accumulation of cartilage compositional changes. Preventing the breakdown of cartilage is thus believed to be of critical importance to preserve the functional integrity of the joint since cartilage has a poor self-repair capacity and is replaced by fibrocartilage when the defect is self-filled. Evaluating the joint to assess cartilage integrity is therefore essential in clinical cases but also in longitudinal research studies evaluating treatments and surgical techniques.

Some specific imaging techniques can provide information about the biochemical and physiologic status of the cartilage. They focus on one component of the cartilage (collagen network, water, GAGs) or a combination of components. They are called compositional imaging techniques.

5.1 CT-based compositional imaging technique

Compositional imaging of cartilage can be achieved by contrast enhanced computed tomography (CECT) or delayed CT (Bansal et al., 2011). This technique is also known as quantitative CT (qCT) (Nelson et al., 2018). It relies on the comparison of two acquisitions: a blank acquisition and a contrasted acquisition. In "*in vitro*" studies, after a blank CT-scanning, the cartilage is immersed in contrast agent for 6 to 12 hours to allow the contrast to penetrate the cartilage thickness. Then, another CT-scan is obtained. The X-Ray attenuation is directly proportional to the concentration of contrast in the cartilage. If a negatively charged contrast is used, the attenuation will be inversely proportional to the content in GAGs as these are negatively charged (Bansal et al., 2010). Computation of blank and contrasted scans provides an indirect measure of GAGs' content of cartilage.

The technique was first developed and tested *in vitro* with micro-computed tomography (micro-CT) on very small samples in a model of IL-1 induced cartilage degradation (Palmer et al., 2006). Since then, CECT on micro-CT has been used: (1) to assess induced PG loss in bovine trypsin-induced model (Cockman et al., 2006) or rat monoiodoaceteate-induced model (Piscaer et al., 2008); (2) to detect PG loss after mechanical injury of articular cartilage in bovine osteochondral plugs (Kokkonen, et al., 2011); (3) to assess spontaneous repair of equine cartilage in the carpus (Kulmala et al., 2012).

Later, the technique was adapted to peripheral Quantitative computed tomography (pQCT) and used for different specimens and models: visually intact osteochondral samples of bovine tibial plateaus (Aula et al., 2009), chemically-induced PG loss in bovine patellar cartilage (trypsin-induced model for Kallionemi, 2007; chondroitinase-induced model for Bansal et al., 2011), and spontaneous degenerated cartilage in human (Silvast et al., 2009A) and bovine knees (Silvast et al., 2009B).

The technique was finally applied to clinical CT systems and tested using either *ex vivo* porcine patellae (Yoo et al., 2011) or human cadaver knee joint (Siebelt et al., 2011; van Tiel et al., 2012).

Either anionic or cationic contrast agents can be used (Bansal et al., 2011). Anionic agents are Magnevist® (Gadopentetate dimeglumine) or Hexabrix® (ioxaglate dimeglumine and ioxaglate sodium) (Kallionemi, 2007). Using an anionic tri-iodinated contrast (17.2% w/v iothalamate meglumine, Cysto-Conray II, Mallinckrodt, MO, USA) agent on osteochondral plugs of bovine patella-femoral joint, the X-Ray attenuation linearly and inversely correlates to the GAG content of the cartilage ($r^2 = 0.83$; $P < 0.0001$) (Bansal et al., 2010).

Cationic contrast agent (CA) carry one (CA1+) or four (CA4+) positive charges depending on the number of amino groups. They are attracted within cartilage proportionally to GAG content. CA4+ seems to correlate better to GAG content than the anionic one ($r^2 = 0.85$ for CA4+ versus $r^2 = 0.62$ for anionic agent). When used *ex vivo*, CA4+ requires up to 6 hours contact to obtain maximal X-Ray attenuation on osteochondral plugs or rabbit knee (Bansal et al., 2011). When used *in vivo*, CA4+ has a slower diffusion kinetic than the negatively charged ioxaglate contrast (13.8 minutes versus 6.5 minutes in the rabbit knee) (Stewart et al., 2013). Using cationic contrast agent (CA4+), the CECT attenuation of cartilage has been proved to correlate to its equilibrium compressive modulus in an ex-vivo mouse (r^2=0.75) and bovine (r^2=0.90) cartilage experiment, suggesting CECT to be a non-destructive technique to evaluate biomechanical properties of mouse tibial plateau (Lakin et al., 2014; Lakin et al., 2013). Another study, using cationic contrast agent as well, found a correlation between CECT and cartilage stiffness measured with an indentation test (Nickmanesh et al., 2015). However, it should be noticed that in this study, the correlation was featured by a coefficient of variation (r) of 0.55, meaning that change in CECT values accounted for only 30.25% of the variation in stiffness ($r^2 = 0.3025$ = coefficient of determination). This suggests that the extrapolation of CECT values is a sensitive point, and that biomechanical properties does not rely on only one component of the targeted tissue, but on the interaction of the multiple tissue's components.

The concentration of contrast agent varies also with authors: high concentration such as 128 mM of anionic iodinated contrast (Palmer et al., 2006) and low concentration such as 21mM of ioxaglate (Kallionemi et al., 2007) have been described. However, diffusion of the contrast seems to be more influenced by the type of contrast than by the concentration (Silvast et al., 2013). It might be clinically important to note that hypertonic X-ray contrast agent combined with pressure might increase the risk of chondrocyte death in articular cartilage specifically in the deep zone (Turunen et al., 2012).

In human cadaver knee joints, CECT showed an excellent correlation with GAG content of the cartilage ($r^2 = 0.90$; $P < 0.0001$) (van Tiel, 2012; Siebelt et al., 2011) and required only 10 minutes delay between injection of the contrast agent (30% ioxaglate (Hexabrix 320) in phosphate buffered saline (PBS) solution) and the images acquisition (van Tiel et al., 2016). The limits in the use of CECT are the potential risk of radiation exposure due to repetitive scans and the lack of validation, so far, of its use *in vivo* (Bansal et al., 2010; Kokkonen et al., 2012).

5.2 MRI-based compositional imaging technique

Multiple sequences have been developed for cartilage composition assessment (Hontoir et al., 2015; Nelson et al., 2018).

T2 mapping

The mobility of water protons varies with tissue type; it is high when protons are in free water and low when they are immobilized in ECM. This influences the transverse (T2) relaxation time, due to spin–spin (neighbouring) interactions (Watrin et al., 2001). In MR imaging (MRI) sequences highlighting T2 (T2 weighted, W), mobile water protons (e.g. in synovial fluid or in damaged collagen networks with increased free water content) give a hypersignal (long T2), whereas water protons immobilised in ECM (short T2) give a hyposignal (David-Vaudey et al., 2004). Since T2 reflects water content and integrity, specialised T2 sequences have been created in an attempt to identify the early stages of OA. In general terms, T2 sequences can demonstrate pathology because they identify changes in water content. Signals can be plotted in a T2 decay curve, which is used to calculate a mathematical parameter called the T2 relaxation time of the tissue (Mosher et al., 2001; Xia et al., 2001; Foltz et al., 2003). T2 mapping involves multiple T2 sequences with slightly varying parameters. The differences in T2 relaxation time over all sequences are then combined and a colour map of T2 times is generated. The application of T2 mapping to cartilage assessment was initially reported in 2000 (Mosher et al., 2000) and can be performed with a 1.5 Tesla system.

T2 is highly sensitive to changes in hydration and it is able detect a temporary physiological loss of water after exercise (Liess et al., 2002; Mosher et al., 2010; Stehling et al., 2010). T2 values are higher in the radial zone of elderly people due to higher water mobility, secondary to changes in the structure of PG aggregates (Mosher et al., 2000).

T2 values are also influenced by the orientation of collagen fibrils. A lack of signal occurs when fibres are so well aligned that the amount of signal produced in a T2 weighted image is changed, a phenomenon called isotropy. This is very evident with a 9.4 T magnet, but is less apparent in clinical systems (Nissi et al., 2006). For example, imaging the same osteochondral plug placed at angles of 3°, 25°, 40° and 57° with respect to the z-axis produces T2 values which vary from 28 ms to 56 ms. In the radial zone, where collagen fibrils are highly aligned and perpendicular to the articular surface, T2 varies up to 80% with the direction of the main magnetic field. In the transitional zone, where collagen fibrils are less aligned, T2 is less influenced by plug orientation (Xia, 1998). This orientational effect seems to be less pronounced *in vivo*; it has been suggested that compression of cartilage during normal daily activity results in modifications to the orientation of the collagen fibres in the radial zone (Mosher et al., 2001). These differences should be taken into account when comparing data from *in vitro* and *in vivo* studies.

Several studies have demonstrated the utility of T2 mapping for the assessment of osteoarthritic cartilage. In human cadaver knee specimens, T2 values correlated to macroscopic, histological and mechanical assessments and increased with OA grade (David-Vaudey et al., 2004; Lammentausta et al., 2007). The orientational effect was used in clinical research to assess the structural organization of cartilage before and after treatment. T2 mapping has also been used to monitor cartilage repair over time in patients, especially to assess the development of a collagen network with zonal organisation similar to normal

cartilage (Smith et al., 2001; Kelly et al., 2006; Trattnig et al., 2007a; Welsch et al., 2008a; Domayer et al., 2010).

In veterinary medicine, several studies have investigated possible applications of T2 mapping. The accuracy of the technique to measure cartilage thickness of the distal metacarpus/metatarsus was determined in equine cadaver limbs (Carstens et al., 2013a). The authors concluded that T2 mapping was accurate for measuring thickness, except at locations where the cartilage was in direct contact with the cartilage of the proximal phalanx. This exception was explained by the fact that, when windowing images to identify the articular surface, partial volume averaging of the thin intra-articular space (often on the 1-pixel threshold) tended to determine the boundary between the articular surfaces to be halfway between them, resulting in a halving of the measured distance. It was concluded that future research could be conducted to assess whether higher resolution images could be obtained with a 3-T system, which could result in superior measurement of the thin (0.8–0.9 mm) cartilage in that anatomical region.

Another study determined the intra- and inter-observer variability of T2 mapping to assess the articular cartilage in the region of the medial coronoid process of six healthy dogs (Wucherer et al., 2012). The histology and PG content of medial coronoid process were used to confirm normal articular cartilage, but not to evaluate the accuracy of the technique to assess the biochemical composition of articular cartilage. The study demonstrated that T2 mapping was reproducible (i.e. it had low variability) and established a normal reference range of T2 values (56 ± 8 ms) for healthy cartilage of the medial coronoid process.

The utility of the technique at 1.5 T to evaluate cartilage repair has been investigated in several clinical studies in horses. It helped differentiate deep, middle and superficial cartilage in reparative fibrous tissue sites (mean T2 values 53.3, 58.6 and 54.9 ms, respectively) from normal hyaline cartilage (40.7, 53.6 and 61.6 ms, respectively) after arthroscopic osteochondral autograft transplantation and microfracture arthroplasty (White et al., 2006). The effects of those procedures were also assessed in a pony osteochondral model. While there were increasing T2 values from the deep to the superficial layer of normal hyaline cartilage (range, 40.7–61.6 ms), as expected, fibrous tissue from cartilage repair did not show the same depth-dependent variation in T2 values. There was a good agreement between T2 pattern (presence or absence of a depth-dependent organisation) and histological findings (Clark et al., 2010). The same group also used T2 mapping data as an outcome measure in a study evaluating direct delayed human adenoviral bone morphogenic protein (BMP)-2 or BMP-6 gene therapy for bone and cartilage regeneration in the pony model (Menendez et al., 2011). T2 mapping of the defect produced high T2 values, corresponding with the disorganisation of collagen repair. Another group showed that T2 values were longer in the centre of cartilage repair in an equine model where an osteochondral defect was created in the lateral trochlear ridge (Pownder et al., 2011).

T2* mapping

In T2* mapping, when the radiofrequency (RF) pulse is 90°, the longitudinal magnetisation disappears and transverse magnetisation appears. The curve that represents the time needed for the transverse magnetisation to decrease should represent T2. This would be the case if the interaction between protons (spin–spin interaction) were the only reason for the reduction in phase coherence and for increasing entropy. However, the microscopic heterogeneity of

the main field (i.e. constant heterogeneity) accelerates dephasing. Therefore, the signal decreases at a faster time (called T2*). This is why a 180° pulse must follow the 90° pulse (in a T2W sequence) if the true T2 characteristics of the tissue are to be measured (McRobbie et al., 2006; Hoa et al., 2008).

One advantage of T2* mapping is the shorter acquisition time compared to T2 mapping. In a comparative study where field of view, matrix, slice thickness, and voxel size were identical, acquisition time for T2 mapping was 5 min 11 s vs. 2 min 35 s for T2* mapping (Welsch et al., 2011). It is important to note that T2* is the inverse of the T2 signal, so the information gained from T2* images might not be the same as from T2 images, since the inhomogeneity of the signal is measured more than the true T2 signal. T2* has been tested *in vivo* in human knee (Hughes et al., 2007; Welsch et al., 2008b; Mamisch et al., 2012) and hip joints (Bittersohl et al., 2009). This technique has not yet been assessed in veterinary medicine for articular cartilage.

Ultra-short echo (UTE) – T2 mapping

Deep and calcified zones of articular cartilage, with their highly ordered collagen fibrils, limit the motion of protons. Protons are therefore more influenced by spin–spin interactions and lose phase coherence more quickly. T2 is very short, between 1 ms and 2 ms (Du et al., 2009). While standard T2 mapping uses echo times of 10 ms or more, UTE-T2 mapping uses echo times shorter than 1ms (Bae et al., 2010; Williams et al., 2010). It has the potential to visualize cartilage at the osteochondral junction, focusing on deep cartilage and CC. UTE-T2 values are most likely more sensitive to matrix disorganisation than to matrix content, as they did not seem to correlate with cartilage composition (collagen or GAG) in one study (Williams et al., 2010). UTE-T2 mapping has been performed at 3 Tesla with an acquisition time of 4–10 min (Gao et al., 2013). The technique has not been used in veterinary medicine and although it could have research applications for visualising the cartilage–bone interface, its clinical utility needs further investigation.

T1rho (ρ) mapping

In the T1ρ technique, a supplementary low amplitude RF pulse is applied for a prolonged period of time during relaxation and appropriately aligned with the transverse magnetisation (Charagundla, 2004). The pulse, called spin-locking pulse, alters the tendency of the spin components to process at their own individual frequencies, instead locking them in an orientation aligned with the spin-locking pulse (Figure 13). The magnetisation no longer relaxes according to T2, but instead relaxes according to a time called T1ρ. The prevention of dephasing slows down magnetisation decay dramatically, resulting in a T1ρ that is longer than T2.

In the T1ρ technique, due to the spin-locking pulse, a new small magnetic environment is created where energy transfer can occur. In the presence of the spin-locking pulse, transverse magnetisation can exchange energy with lattice (magnetic environment) processes occurring at the spin-locking frequency, which is directly proportional to the amplitude of the spin-locking pulse. Since there are far more processes (movements) in the lattice operating at the low spin-locking frequencies (so-called ‘slow motions’) than at the Larmor frequency, more energy can be lost and T1ρ is shorter than T1 (Charagundla, 2004).

Figure 13. T1rho(ρ). The tissue is first submitted to the main magnetic field of the MR unit, resulting in a net magnetisation along Z-axis (A). This sequence is characterized by the application of a 90° radiofrequency pulse (B) followed by a spin-locking pulse (C). The magnetisation no longer relaxes according to T2, but instead relaxes according to a time called T1ρ (D).

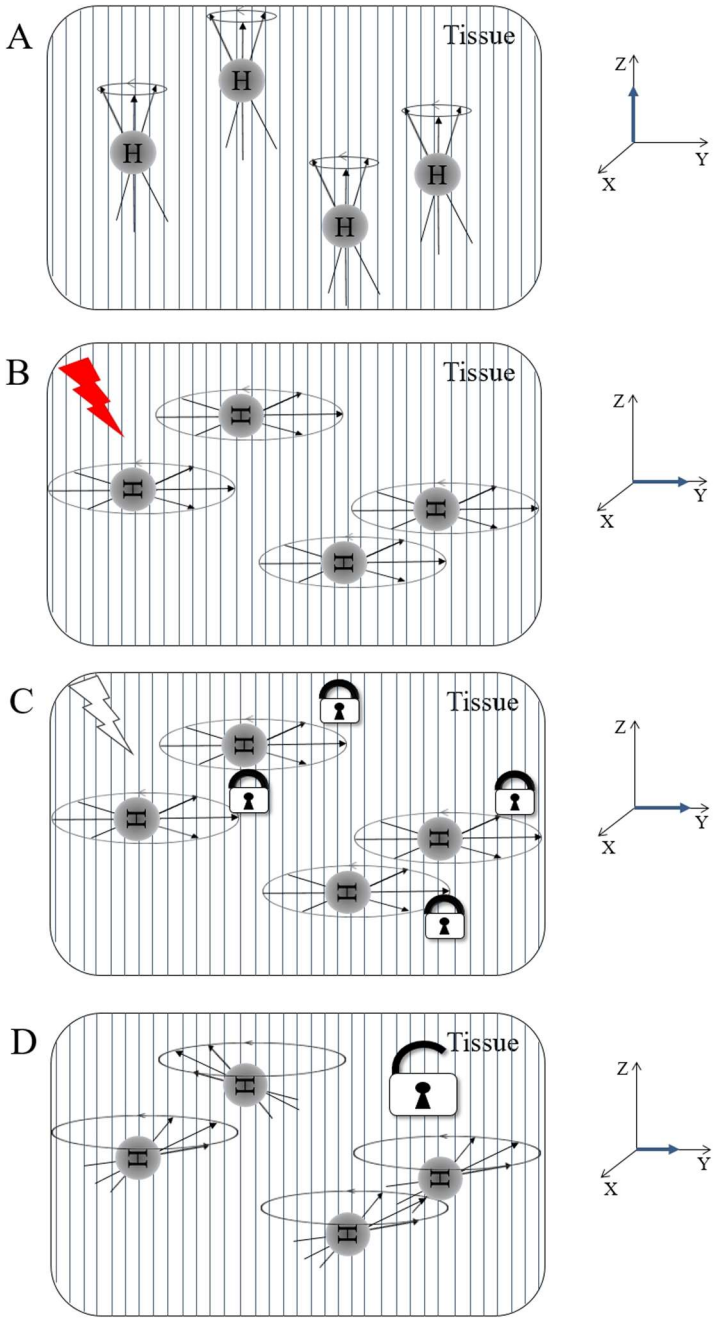

Because slow motions in the lattice are typically associated with large molecules, T1ρ is sensitive to the protein composition of tissue, and could therefore provide information about the macromolecular properties of tissue such as GAG content. Some authors have suggested that T1ρ and T2 imaging might be complementary since T1ρ seems to be a more specific indicator of PG content, while T2 is more sensitive to collagen network modification (Taylor et al., 2008). The technique can be performed with a 1.5 system (Duvvuri et al., 2001). In a study using a 3.0 Tesla MRI unit (Stahl et al., 2009), the acquisition time was approximately 13 min.

In a human cadaveric study, T1ρ moderately and variably correlated with the content of the GAG and r^2 ranged from 0.13 to 0.84, depending on the specimen (Keenan et al., 2011). In live subjects, T1ρ values were significantly higher in patients with OA compared to those that were healthy (Li et al., 2005; Regatte et al., 2006; Stahl et al., 2009).

When T1ρ imaging was tested in a live porcine model of OA, following the injection of interleukin-1β, T1ρ seemed to correlate with the induced PG loss. This study highlighted difficulties encountered in reaching adequate resolution while preserving an acceptable acquisition time (Wheaton et al., 2004). Other authors have also stressed the problem of sequence length. Due to the long-duration of the spin-locking pulse, T1ρ is sensitive to inhomogeneities (called B1 inhomogeneities) (Charagundla, 2004). Moreover, the long duration of the RF can reach the allowable specific absorption rate (SAR) of RF energy (Wheaton et al., 2004). The human SAR limits, in Europe, range from 0.08 W/kg (whole-body) to 20.0 W/kg (limb extremities) for an average duration of 6 min. SAR limits are made to limit the amount of energy absorbed by the human body and this limit can only be extrapolated to animals.

In veterinary research, T1ρ has been used in a preclinical model of equine cartilage repair. Cadaver stifle specimens showed higher T1ρ values in the centre of the cartilage repair area relative to normal cartilage, both in the superficial zone (66 ± 22 ms vs. 42 ± 5 ms) and in the deep zone (57 ± 19 ms vs. 33 ± 4 ms; Pownder et al., 2011). T1ρ values were only slightly reduced at the interface. The authors suggested this could reflect the non-uniformity of the tissue in the centre of the repair and incorporation with the native tissue at the periphery of the repair. It was acknowledged that this hypothesis needed to be confirmed by histological analysis.

Diffusion-weighted imaging (DWI)

DWI is based on the varying motion properties of water protons in different environments. Protons can move in all three directions in free water, but they are restricted by collagen or PG barriers in cartilage (Hagmann et al., 2006). In DWI, an RF pulse is applied with decreasing intensity with distance, the so-called ‘gradient pulse’. If the structure of the tissue allows diffusion (Figure 14), such as when the direction of the gradient is parallel to the collagen fibres, the gradient pulse induces motion of the water protons in the direction of the gradient pulse. Water protons also gain energy from the RF pulse in proportion to the distance.

A 180° RF pulse (spin-echo) is then applied, followed by a second gradient pulse with the same decreasing intensity as the first. Since all water protons do not move the same distance

due to the different intensities of pulse, the second gradient pulse is not able to bring all water protons do not move the same distance due to the different intensities of pulse, the second gradient pulse is not able to bring them back to their initial position. The MRI signal in the new position (and energy state) is different from that in the initial position; the system measures this difference.

If diffusion is not allowed by the structure of the tissue (Figure 14), such as when the direction of the gradient is perpendicular to the collagen fibres, motion by water protons is not allowed. After the 180° RF pulse and second gradient pulse, water protons are found in their initial position at the same level of energy. In this new setting, no loss of signal is detected.

The setting where diffusion is allowed in both directions is observed when, for example, collagen fibres have disappeared. The combination of three different directions of gradient is necessary to thoroughly capture the mobility of water and indirectly provide an image of the 3D integrity of the tissue network (Bammer, 2003).

The DWI pulsed-gradient spin-echo sequence is characterized by several parameters: the length (duration) of the gradient pulse, the time-period between both gradient pulses, and the amplitude of the gradient pulse (Bammer, 2003). The three parameters are summarised by a mathematical coefficient called the diffusion sensitising factor (b-value), which is used to calculate the apparent diffusion coefficient (ADC; Xia et al., 1995). A low ADC is associated with the restriction of water molecules by the environment, e.g. by a healthy intact collagen network in cartilage (Burstein et al., 1993). This sequence can be performed with a 1.5 Tesla system. In one study that used a 3.0 Tesla unit, acquisition time was approximately 6–7 min (Apprich et al., 2012).

ADC has been shown to correlate positively with OA in human cartilage samples (Mlynarik et al., 2003). DWI has also been used *in vivo* for the follow-up of surgical cartilage repair in human patients (Mamisch et al., 2008; Friedrich et al., 2010). Interestingly, a canine study has been reported (Xia et al., 1995). Four millimetre discs of cartilage were harvested from both humeral heads of an 8-month old, skeletally mature, disease-free Labrador retriever, and from an osteoarthritic 4-year old Labrador retriever. The observation was made that ADC was approximately 25% higher in osteoarthritic cartilage than in the surrounding cartilage. This increase was mimicked by enzymatic degradation of normal cartilage with trypsin, hyaluronidase, and collagenase, or by mechanical means, suggesting that ADC is more specific for the assessment of cartilage matrix integrity than selective GAG loss or collagen loss.

Figure 14. Diffusion weighted imaging. In this technique, a gradient pulse is applied, followed by a 180° radiofrequency pulse and a second gradient pulse. Collagen fibres (green lines) restrict the motion of water molecules (blue dots). In the cartilage radial zone, collagen fibres are aligned perpendicular to articular surface. If the pair of gradient pulses is aligned with the direction of the collagen fibres, the dephasing (blue arrow) of water by the first gradient pulse is not compensated for by the effect (shorter backward blue arrow) of the 180°RF pulse and the second gradient pulse, leading to a loss of signal. If the gradient pulse is perpendicular to the direction of the collagen fibre, no loss of signal occurs, since the water molecule is in the same position and is subject to the same pulse. The intensity of the gradient pulse is represented by the greyscale arrow and the greyscale background under the collagen fibres.

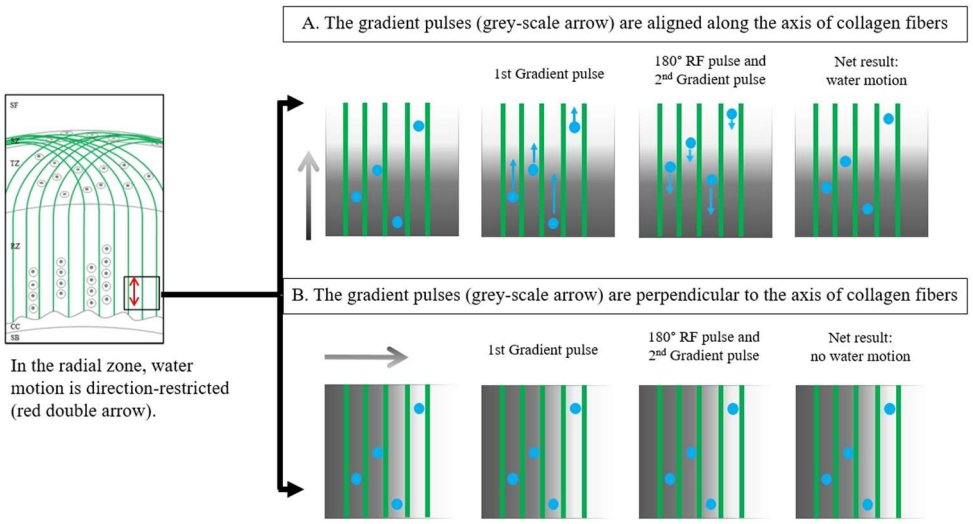

Delayed gadolinium-enhanced MR imaging of cartilage (dGEMRIC)

Gadopentetate dimeglumine (Gd-DTPA^{2-} or gadolinium-diethylenetriamine pentaacetic acid), a contrast agent, can shorten T1 relaxation; an increased signal was demonstrated in a study comparing pre- and post-contrast images after IV injection of the agent (Bashir et al., 1996). Since the contrast is negatively charged and its concentration varies inversely from the concentration of the negatively charged GAGs, T1 is shorter in GAG-depleted cartilage. T1 values are mapped and translated in a colour scale. It can also be administered intra-articularly, but requires a large dilution (Kwack et al., 2008).

The principal disadvantage of dGEMRIC is the delay needed for Gd-DTPA2− to penetrate through the cartilage (Gold et al., 2009). For example, a 90 min delay is required for the human knee cartilage (Welsch et al., 2008b; Domayer et al., 2010). The Gd-DTPA2− penetration is also influenced by mobilisation of the joint and it is increased after exercise

(Tiderius et al., 2004). Additionally, penetration is also better in thinner cartilage (Hawezi et al., 2011). The technique has been used for a number of years. *In vitro* research has demonstrated that T1 values in dGEMRIC correlate well with GAG concentration in human cartilage (Bashir et al., 1996; Miyata et al., 2006) and that dGEMRIC predicted changes in Young's modulus in plugs of bovine humeral head (Nieminen et al., 2004) and in human knee plugs (Kurkijarvi et al., 2004). Longitudinal clinical studies have also used dGEMRIC for ongoing assessment of autologous chondrocyte transplants in humans (Gillis et al., 2001; Watanabe et al., 2006; Trattnig et al., 2007b; Wiewiorski et al., 2013).

In veterinary cartilage research, dGEMRIC was first used to assess the effects of administration of human adenoviral BMP-2 or BMP-6 in experimentally created femoral condyle lesions in ponies (Menendez et al., 2011). The authors demonstrated that dGEMRIC T1 relaxation times were greater in lesions treated with Ad-BMP6 than in saline treated controls. Reference values for dGEMRIC T1 values have been obtained for normal articular cartilage near the medial coronoid process in dogs with a 3.0 T magnet (400 ± 47 ms; Wucherer et al., 2012). In that study, dogs received IV Gd-DTPA2− under general anaesthesia and passive motion of the joint was performed for 10 min. The time between IV injection and the start of the dGEMRIC sequence ranged from 47 to 82 min.

Another group assessed the dGEMRIC characteristics of the cartilage of the distal metacarpus/metatarsus after intra-articular injection of contrast in 20 cadaver specimens collected from normal Thoroughbred horses (Carstens et al., 2013a). Significant differences were observed between anatomical sites and this was attributed to differences in cartilage substrate that could have occurred as an adaptation to the varying forces applied. Since dGEMRIC T1 values at the sites with significant differences decreased to a minimum at 60–120 min post-contrast, this was proposed as the optimal time for post-contrast scans. T1 values were measured between 642 and 674 ms after 60 min post-contrast, which is longer than the 400 ms used for the canine MCP (Wucherer et al., 2012).This discrepancy could be due to the method of injection, cartilage thickness or other inherent cartilage differences between the two species and joints. There was also poor spatial resolution of the thin distal metacarpus/metatarsus. The authors suggested that dedicated surface coil, decreased field of view, or a higher field strength magnet could be used to improve resolution.

The same group also used dGEMRIC to determine the cartilage thickness of the distal metacarpus/metatarsus in equine cadaver limbs with a 1.5 T system (Carstens et al., 2013b). The conclusions were similar as those for T1ρ mapping: the technique was accurate only at locations where the cartilage of the distal metacarpus/metatarsus was not in direct contact with the proximal phalanx cartilage.

Sodium imaging

In this technique, MRI targets the sodium nucleus, which is composed of 11 protons and 12 neutrons; the unequal number of protons and neutrons confers magnetic properties to sodium. In cartilage, sodium content is proportional to PG content, since it counterbalances the negative fixed charge density of GAGs. A loss of PG induces a decrease in fixed charge density and thus a loss of sodium (Shapiro et al., 2002).

Though a better signal is obtained with high field magnets, imaging can be performed with a 1.5 T system (Hani et al., 2013). Because the spin frequency of the sodium nucleus differs from that of hydrogen, a dedicated system is required to reach resonance (Krusche-Mandl et

al., 2012; Madelin et al., 2012). The system is used mostly for research and uses long acquisition times of approximately 20–30 min (Krusche-Mandl et al., 2012; Newbould et al., 2013).

Sodium MRI was able to detect chemically-induced PG loss in animal articular cartilage (Borthakur et al., 2000; Wheaton et al., 2004). It has been tested *in vivo* at 7 T in the human knee (Wang et al., 2009) and it has been used to follow-up matrix-associated autologous chondrocyte transplantation in the human knee (Trattnig et al., 2010).

GAG chemical-exchange saturation transfer (GAG-CEST) sequence

In conventional MRI, signals are detected from the protons of components (such as water) that have sufficiently long T2 relaxation times (>10 ms). The T2 of the restricted protons (with low mobility), such as protons of the amide group (−NH) and hydroxyl groups (−OH) of GAGs, are too short (<1 ms) to be detected. An effect called 'chemical exchange saturation transfer' (CEST) refers to the induced exchange of protons between water and protons of specific molecules, such as GAGs (Figure 15). For the transfer to happen, a selective non-resonant RF pulse must be applied.

The protons of low energy in GAGs are excited in such a way that populations of the higher and lower energy levels become equal. When this occurs, further absorption of energy is not possible and there is no net magnetisation; the spin system is termed 'saturated'. Saturated protons are able to exchange with unsaturated protons of water. The selective saturation of exchangeable protons requires high field strength (3.0 or 7 T), otherwise saturation of GAG molecules and water molecules would occur at the same time and no exchange would be possible (Zhou and van Zijl, 2006; Borthakur and Reddy, 2010). This exchange (CEST effect) causes a change in magnetisation of water and a signal difference that can be recorded. This technique is also affected by pH changes, since H^+ and OH^- contribute to the overall chemical exchange. It is also temperature-dependent (Ward et al., 2000) and acquisition time is around 15 min (Krusche-Mandl et al., 2012). GAG-CEST has been tested for human knee imaging (Schmitt et al., 2011; Krusche-Mandl et al., 2012; Singh et al., 2012).

Figure 15. Glycosaminoglycan (GAG) chemical exchange saturation transfer (gag-CEST).

A. In cartilage, protons are found in the hydrogen nucleus (H) of every molecule (collagen, water, GAGs). Orange double arrows illustrate the chemical exchange saturation transfer (CEST) of protons that is possible between amide (-NH) and hydroxyl (-OH) groups.

B. Inside the magnet, the protons of water and GAGs are aligned along the main magnetic field. Most protons are in the same direction as the main magnetic field (up arrows), showing a low state of energy, while some protons are anti-sense, with a higher state of energy (down arrows). The sum of these protons gives a positive net magnetization for both pool of protons (GAGs and water). A specific radiofrequency pulse selectively activates GAG protons so that high-energy protons and low energy protons are in equal numbers. The system eventually becomes saturated; no energy transfer is possible and there is no net magnetisation. During the chemical exchange phase, the saturated protons of GAGs can exchange energy with the unsaturated protons of water. The water protons in higher state of energy are therefore antisense, so this transfer induces a decrease in water magnetisation that can be recorded.

SF = synovial fluid; SZ= superficial zone; TZ= transitional zone; RZ= radial zone of cartilage. CC= calcified cartilage; SB= subchondral bone.

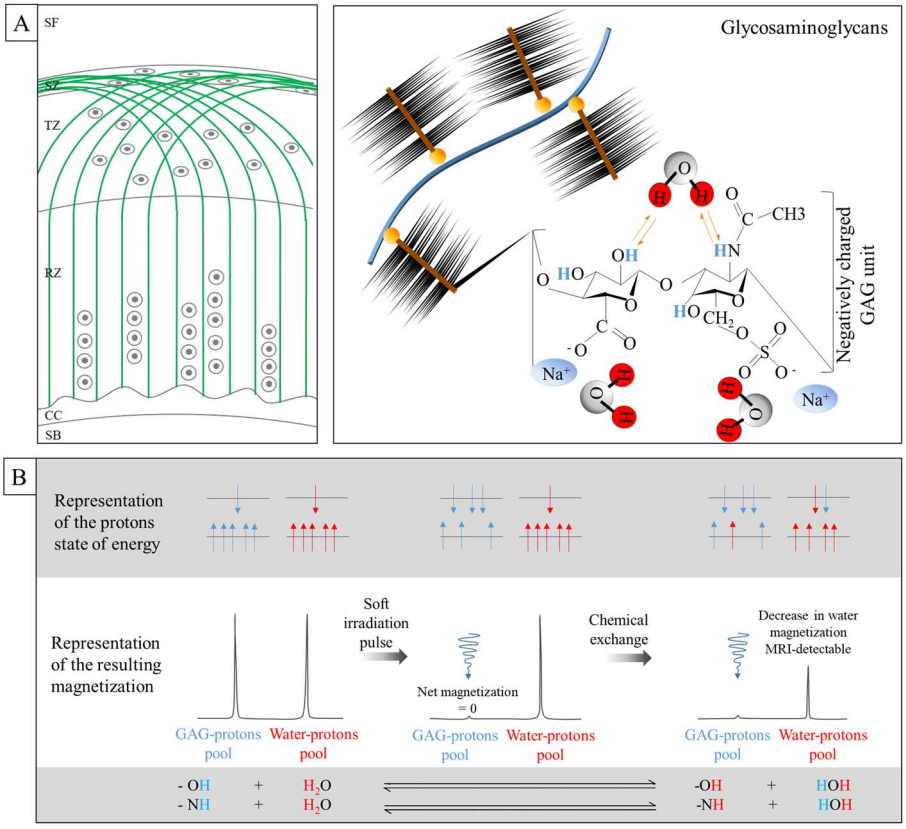

Applications in veterinary medicine

This review demonstrates that compositional imaging of cartilage in animals is primarily undertaken for research purposes, using small or large animal models. Technical concerns still limit the use of some techniques for both research and clinical use. Gag-CEST and sodium imaging necessitate high field magnets and long acquisition times (approximately 15 min and 20 min, respectively). UTET2 mapping has not been investigated in veterinary research. DWI was initially tested *in vitro* on fragments of canine cartilage in 1995 (Xia et al., 1995), but has not received much attention since. It appears that T2 mapping, T1ρ and dGEMRIC are the most applicable to clinical veterinary medicine.

T2 mapping can be performed at 1.5 T with an acceptable acquisition time (about 4 min) and is easily applicable in veterinary medicine. The intra- and inter-observer variability of T2 mapping is low (Wucherer et al., 2012) and its ability to differentiate repair cartilage from normal cartilage has been demonstrated in animal studies (White et al., 2006; Clark et al., 2010; Menendez et al., 2011; Pownder et al., 2011). However, human studies have shown that several factors can influence T2 values, such as age (Mosher et al., 2000), exercise level (Mosher et al., 2010; Stehling et al., 2010) and the orientation of the collagen fibrils to the Z-axis (Nissi et al., 2006) and therefore the anatomy and the curvature of the articular surface. In addition, this orientation effect can differ *in vivo* and *ex vivo* (Mosher et al., 2001). Validation of the technique for each species and joint to account for the aforementioned variables is required. Moreover, identical study protocols must be used to enable comparison. The use of T2* mapping could shorten acquisition time, but it remains to be determined if information from T2* images is similar to that obtained with T2 images. In addition, correlations with the biochemical composition of the cartilage have not been demonstrated in animals, so it is possible that T2 times are more reflective of the network and the state of water than the concentration in water or PG.

T1ρ is potentially complementary to T2 mapping, as it is more correlated to PG content, while T2 is an indicator of collagen network. Human T1ρ studies have demonstrated the challenge of reaching adequate resolution in a reasonable acquisition time despite the use of a 3.0 T magnet (14 min; Charagundla, 2004, Wheaton et al., 2004). Its use in veterinary medicine has been reported in just one study in cadaver specimens (Pownder et al., 2011) and the sequence is not available for all systems (e.g. Siemens).

A 1.5 T system has been used with dGEMRIC, but the resolution was suboptimal. In addition, Gd-DTPA2− penetration varies with injection technique (IV or intra-articular), time after administration, mobilisation of the joint (Tiderius et al., 2004), thickness of cartilage (Hawezi et al., 2011), or other inherent cartilage differences between species and joints (Carstens et al., 2013a, 2013b). This should be taken into account when studies are compared.

The poor spatial resolution of the thin cartilage in some animal joints is a common difficulty. The cartilage of the metacarpo-/metatarso-phalangeal joint in horses, for example, is 0.8–0.9 mm (Carstens et al., 2013b). This technical problem occurs not only with the compositional MRI techniques discussed in the current review, but also with conventional MRI, even when using high field magnets and sequences that are considered optimal for the study of cartilage (Hontoir et al., 2014). Cartilage thickness can also vary with anatomical site. In a study of twelve 7-year old purebred Merino sheep, the mean articular cartilage thickness was 0.43 mm in the abaxial part of the lateral tibial condyle, 1.10 mm in the axial part of the lateral tibial condyle, 1.17 mm in the axial part of the medial tibial condyle and 0.56 mm in the abaxial part of the medial tibial condyle (Appleyard et al., 2003). Cartilage thickness also

varies with species. In one study, cartilage was 2.2 mm thick in human medial femoral condyles, 2.0 mm in horses and 0.5 mm in sheep (Frisbie et al., 2006). Another study in crossed Texel sheep reported that the thickness of the femoral condyle cartilage varied from 1.5mm (medial condyle) to 1.0 mm (lateral condyle; Pirson et al., 2014). These studies indicate that animal cartilage thicknesses can be very different from those in humans, resulting in poor inter-species generalisability of techniques.

Higher field strength magnets can improve resolution since more protons are available and the signal is reinforced, enabling smaller pixels. It is also possible to increase the size of the matrix, but this involves increasing acquisition time. Zero filling interpolation can also be used, which is the substitution of zeroes for unmeasured data points to increase the matrix size of new data prior to Fourier transformation of MR data. This results in pixels smaller than the actual resolution of the image. To illustrate the feasibility of T2 mapping and dGEMRIC, we provide images of the ovine knee obtained by our group with a 3.0 T in crossed Texel cadavers. Interpolation was used and resolution was 0.14× 0.14× 2mm for T2 mapping (TR 900 ms; TE 16.9 ms, 33.8 ms, 50.7 ms, 67.6 ms, 84.5 ms, 101.4 ms; averages 4, bandwidth 237, acquisition time 18 min; Figure 16) and 0.2× 0.2× 1.5mm for dGEMRIC (T1 vibe 3D, TR 15 ms, TE 3.21 ms, flip angle 5, averages 3, bandwidth 289, acquisition time 20 min) after IV injection of 15 mL gadolinium (0.5 mmol/mL) 120 min before imaging (Figure 17). Those examples show that it is possible to reach high resolution, but acquisition time remains long, which is challenging in live animals.

So far, T2 mapping and dGEMRIC seem to be most applicable for compositional imaging of animal cartilage. Since the thickness of the cartilage varies with species, joints and anatomic sites in animals can be small and resolution must be optimised. The combination of T2 mapping and T1ρ might allow for the assessment of both PGs and the collagen network, respectively. Compositional imaging is currently a research tool rather than a clinical tool and it usually requires a high field magnet. Confirmation that it can detect the early stages of OA will be an important step in the justification of its clinical use. Compositional imaging has been tested in joints used as models, but its application should be improved for joints with clinical interest (e.g. the equine metacarpo-/metatarso-phalangeal joint). Because of the relative thinness of cartilage in specific joints, increased availability of powerful imaging systems is required if compositional imaging is to be made more applicable to practice.

Figure 16. Example of a T2 mapping of the medial femoral and tibial condyles of the ovine knee. The colour scale assigns a colour to each T2 relaxation time. Tissue with a long relaxation time (RT) will appear red (i.e. synovial fluid) or green. Short RT tissue will appear light blue (i.e. articular cartilage), while very short RT will appear dark blue (i.e. subchondral bone).

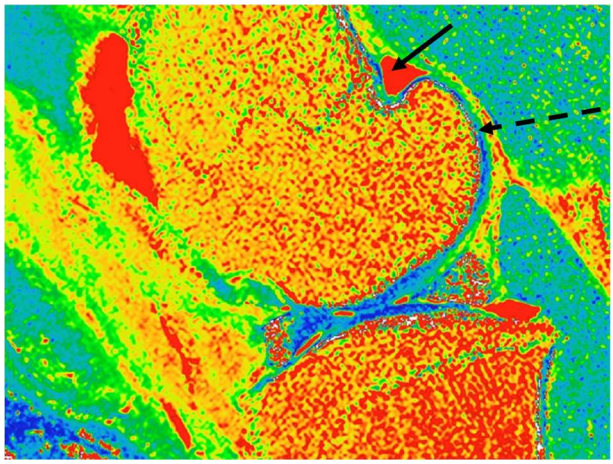

Figure 17. Example of a T1 mapping of the medial femoral and tibial condyles of the ovine knee by delayed gadolinium-enhanced MR imaging of cartilage. T1 is measured in three different regions of interest.

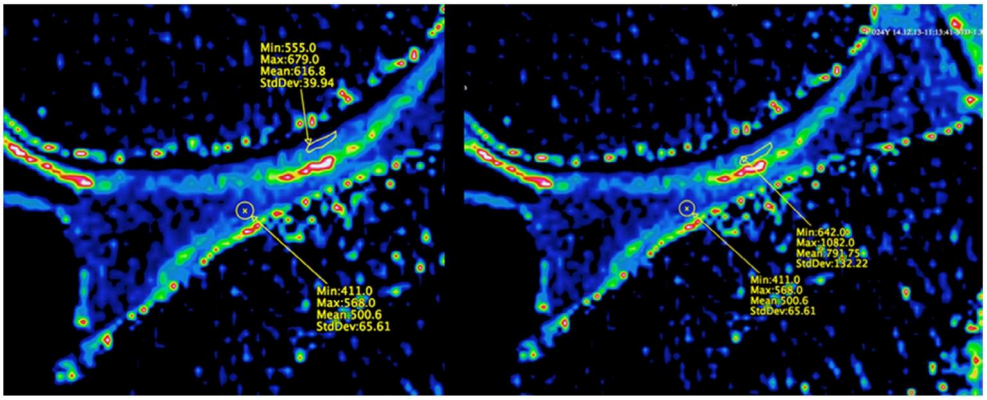

6. Is it possible to induce structural or compositional changes of the cartilage by mechanical or chemical insult of the subchondral bone in an *in vivo* ovine model ?

6. Is it possible to induce structural or compositional changes of the cartilage by mechanical or chemical insult of the subchondral bone in an *in vivo* ovine model?

The role of the SB regarding initiation of cartilage changes in OA is more and more considered (Yamada et al., 2002; Mrosek et al., 2006), and subchondral bone changes have been suggested to precede and be responsible for cartilage changes in OA (Blair-Levy et al., 2008; Zhang et al., 2016).

Therefore, we hypothesized that stimulation of the SB would induce changes in the bone itself and further changes in the cartilage. These potential changes in cartilage composition were imaged with T2 mapping and CECT and compared to gold standards of cartilage composition (biochemistry), cartilage structure (histology) and bone structure (microCT). The ovine knee was chosen as model.

6.1 The induction model: the SB stimulation

Studying this hypothesis requires to selectively induce SB changes, without concurrent stimulation of other structures of the joint (namely, the synovium, the ligament or the cartilage itself).

Most of models of induced OA imply stimulation of multiple tissues of the joint. For example, in cruciate ligament transection models or meniscectomy models (Hayami et al., 2006; Kuroki et al., 2011; Saito et al., 2012; Anetzberger et al., 2014), the joint is surgically penetrated with potential stimulation of the synovium.

Our model aimed to a selective stimulation of the SB. Initially, the medial femoral condyle was drilled to provide an extraarticular access to the SB without impairing the other structures of the joints (namely the ligaments, the cartilage or the synovium). Then, the SB stimulation was provided either by administering a chemical insult with ethanol injection or by a mechanical impact.

Chemical stimulation: ethanol injection

The chemical insult by ethanol is used in therapy of metastases and arteriovenous malformations by induction of embolization (Wright et al., 1990; Gangi et al., 1994; Ko et al., 2011). Intraosseous injection of ethanol has been used to induce the necrosis of femoral head in sheep, as a model of human osteonecrosis of the femoral head (Manggold et al., 2002). In the osteonecrosis of the femoral head model, 8 ml of purified ethanol was injected after performing a drill track to the femoral head. This 8-ml volume is a critical value corresponding to twice the volume of the ovine femoral head. This critical volume is supposed to ensure spreading of ethanol to the entire femoral head (even if reflux occurs) and leading to drastic osteonecrosis of the femoral head. The microscopic changes associated to

the alcohol-induced femoral head osteonecrosis were necrosis of the osteocytes, presence of fibrous tissues, with trabecular bone resorption, progressive new bone formation, with active osteoblasts (Manggold et al., 2002; Zhu et al., 2011).

In our sheep model, we hypothesized that induction of necrosis of the subchondral bone area would initiate cartilage alteration. Practically, the anesthetized sheep laid down in lateral recumbence. The limb of interest was extended caudally while the contralateral limb was extended cranially and maintain by a roller bandage around the trunk. The stifle region was scrubbed with povidone iodine (Poviderm scrub, povidone iodinum 7.5%, Audevard, France; Poviderm dermicum, povidone iodinum 10%, Ecuphar, Belgium). Local anaesthesia was ensured by injection of 2ml xylocaine 2% subcutaneously. The medial collateral ligament of the knee was located by palpation. The skin incision was performed caudally to the femoral insertion of the medial collateral ligament, centered at the level of this insertion and extending distally over 2 cm. The fascia of the semimembranosus and gracilis muscles was incised to reach the caudal part of the femoral condyle. The drill hole was performed with a 3.5mm-diameter stainless steel drill bit, passed through a drill sleeve, directed caudally and distally, parallel to a line joining the basis of the patella and the caudal limit of the tibial plateau and with a 45°-oblique angle to the sagittal plane (Figure 18 A-C). The drill hole was 1.5 cm long to access of the subchondral area. The depth and the direction of the drilling was established with preliminary assays on cadavers of similar size.

After the hole drill was performed, the tissue protection sleeve was left in place and a puncture needle (Jamshidi needle, Medax, San Possidonio, Italy) was inserted through the tissue protector sleeve to reach the subchondral bone (Figure 18 D1). Soft tissues around the hole were covered by gauze. A 2ml-ethanol 70% syringe was connected to the needle and ethanol was slowly injected (1ml/minute). The 2-ml volume (thus lower than the 8 mL used by Manggold et al., (2002)) was selected to ensure a limited area of stimulation, avoiding dramatic osteonecrosis of the entire medial femoral condyle.

After stimulation, the needle and the protector sleeve were withdrawn. The drill hole was filled with bone wax (Bone wax, S.M.I., St Vith, Belgium). Fascia were sutured with absorbable suture (Polygalactine 910, Surgicryl 910, USP 2/0, S.M.I., St Vith, Belgium) and the skin was closed with non-absorbable suture (Nylon, Daclon USP 2/0, S.M.I., St Vith, Belgium). Protection of the skin suture was achieved with aluminium spray (Aluspray, VMD, Arendonk, Belgium).

Figure 18. Schematic representation of the access to STB of the medial femoral condyle (A-C) and the stimulation procedure (D1-2).

A. Anatomical structures and landmarks: palpation of the femoral insertion of the medial collateral ligament of the knee (white dotted arrow) allows to perform a parallel skin incision (white dotted line), 1 cm caudally, extending over 2 cm distally. The insertion fascia of the semimembranosus and gracilis muscle (light shaded muscle) was incised to reach the femoral bone. Palpation of the basis of the patella (black plain arrow – P) and of the caudal limit of the tibial plateau (black plain arrow – T) ensure the appropriate positioning of the tissue protection sleeve before drilling.

B/C. The tissue protection sleeve was placed 1 cm caudally to the femoral insertion of the medial collateral ligament, and directed caudally and distally, parallel to a line joining the basis of the patella and the caudal limit of the tibial plateau and with a 45°-oblique angle to the sagittal plane. The drill hole was performed to reach the STB. The tissue protector sleeve was maintained and the stimulation device was placed.

D1. For the chemical stimulation, a puncture needle was inserted through the drill track and 2-ml pure ethanol was slowly injected.

D2. For impact-stimulated limbs, a metal rod was inserted through the drill track. It was subsequently connected to an air hammer and an impact was performed.

After stimulation, the devices (needle or rod, and protection sleeve) were withdrawn; soft tissues and skin were closed.

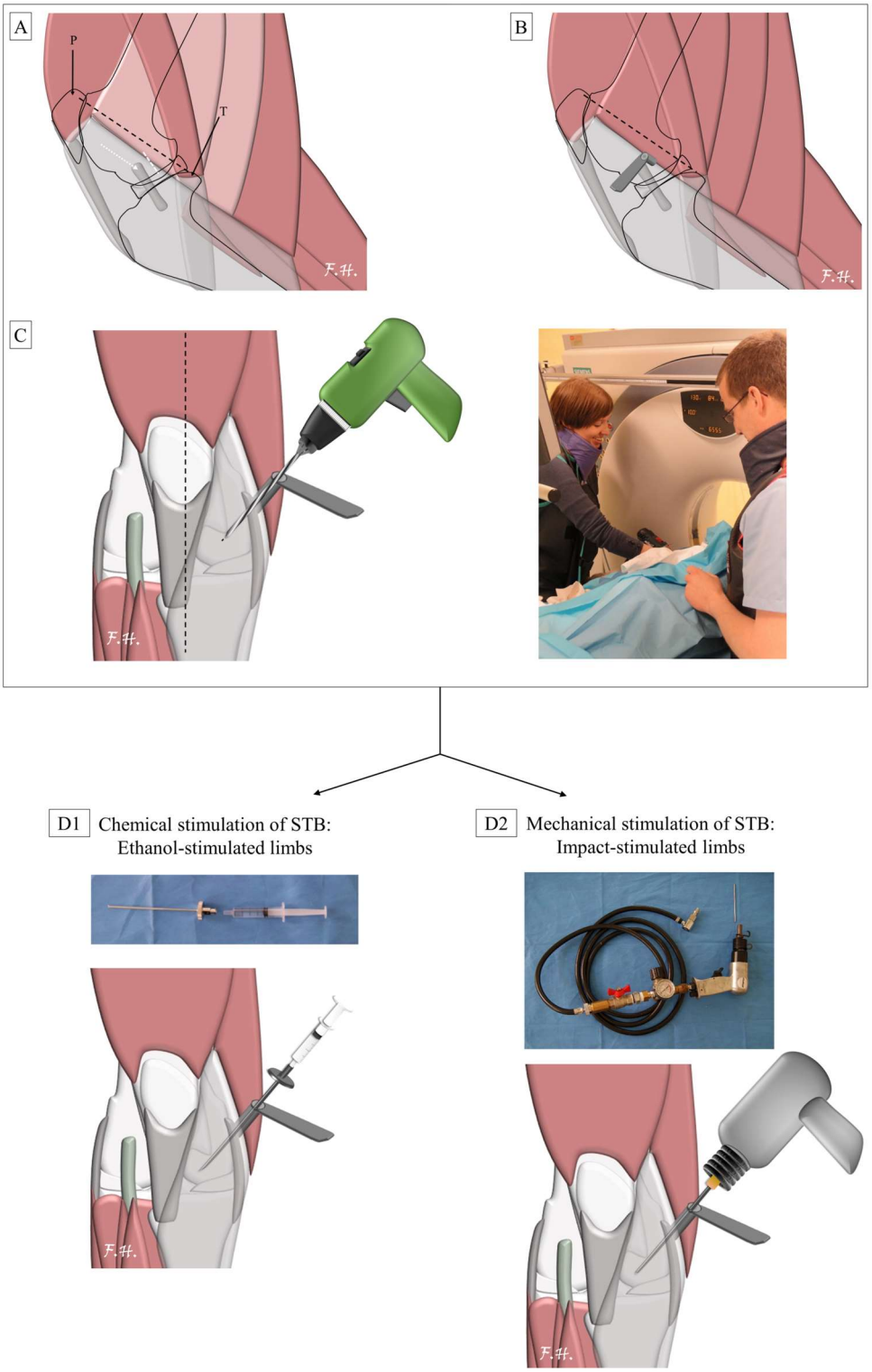
A
P
T
B
C
D1 Chemical stimulation of STB:
Ethanol-stimulated limbs
D2 Mechanical stimulation of STB:
Impact-stimulated limbs

Mechanical stimulation: impact

A mechanical insult of the SB has been previously performed trans-articularly (Lahm et al., 2004; Lahm et al., 2005; Mrosek et al., 2006). In studies in dogs, patellae were impacted with a load to produce micro-fractures of the subchondral trabeculae, without immediate macroscopic damages to the articular cartilage (Mrosek et al., 2006). This kind of trans-articular insult led to macroscopic softening of cartilage, fissures, superficial irregularities 6 months after the impact. The microscopic-associated changes included remodelling of cartilage to fibrocartilage, and loss of chondrocyte column-aligned organization in the radial zone (Mrosek et al., 2006). The SB showed an increase in trabecular bone volume and trabecular thickness as well as a decrease in the trabecular number. These changes were associated to a significant increase in the number of osteoblasts and a tendency toward increase in the number of osteoclasts (Lahm et al., 2006). The chronic negative effect of sudden impact loading has also been proved in rabbit with an increase in SB thickness and an increase in cartilage damages such as: depth and number of fissures, alteration of cartilage thickness) (Ewers et al., 1992). In this trans-articular model, cartilage was also stimulated during the impact although changes were not immediately visible.

In our sheep model, we tried to stimulate selectively the SB by extra-articular application of a high-level sudden impact. To access the SB, a drill hole was performed as previously described for the ethanol stimulation of the SB (Figure 18 A-C). After the hole drill was performed, the tissue protection sleeve was maintained. The drill was removed and a 3mm-diameter metal rod was inserted until the subchondral area. The rod was connected to an air hammer (Figure 18 D2), linked to a 10-meter long tube filled with 4-bar compressed air. One sudden stimulation was performed, resulting in 25 impacts of a maximal pressure of 3.45MPa. The rod was withdrawn and procedure was conducted similarly to the chemical stimulation with the following steps: filling of the drill hole, fascia and skin suture, and wound protection. After the end of the entire procedure, the anaesthesia maintenance was stopped and sheep was allowed to recover.

6.2 Material and methods

Animals

The experimental protocol was approved by the local ethical committee for animal welfare of the University of Namur (KI 12/181 OsteoOvin). This descriptive study enrolled 18 ewes (aged from 2 to 6 years; weight between 45 and 80 kg). The history of the ewes did not mention any musculoskeletal disease. They were reformed because of suboptimal reproductive performance, fibrotic udder related to a previously resolved mastitis or resolved lambing troubles (i.e. uterine prolapse).

The ewes came from the Ovine Research Centre of the University of Namur and were housed in the research centre during the whole research period. They were identified by ear tags. Seven days before induction of the SB stimulation, sheep were transferred from the general flock to the research flock, to ensure social adaptation and acclimation to the new environment.

Baseline assessment

Sheep were submitted to a preliminary examination (Table 7). The daily follow-up included the assessment of comfort, movement and flock behaviour with a scoring scale (Dowd et al., 1998; Shafford et al., 2004) (Table 8).

Table 7. General examination. Every sheep underwent general examination and daily assessment during one week before enrolling.

OASIS Project – Subchondral model KI 12/181 OsteoOvin Preliminary general examination			
Sheep identification			
Date of the examination (J-7) :			
Age :	Sex :	Race :	
General			
Respiratory rate		Color of the mucosa	
Heart rate		Capillary Filling Time	
Body condition		Weight	
Locomotion			
Movement score			
Limbs examination (knee palpation, digit assessment, abnormalities)			
Left fore		Right fore	
Left hind		Right hind	
Note :			

Table 8. Scoring scale for daily assessment, before and after stimulation surgery (Shafford et al., 2004). Limit point was set at 8, meaning that a sheep having a total score equal or superior to 8 would require particular treatment (analgesic administration: transdermal fentanyl patch) and potential euthanasia.

Wellness scoring scale		
Comfort score	Awake, interested in surroundings, patient recumbent or standing, chewing cud, eating	0
	Awake, standing or recumbent, not interested in surroundings, not chewing cud, reduced appetite	1
	Lethargic, depressed appearance, ears drooped, not chewing cud, not eating	2
	Head down, very lethargic, ears stay drooped when aroused, not chewing cud, bruxism (grinding teeth)	**3**
	Recumbent, no response when approached, fixed look and staring, or eyes half closed, little response when gently prodded, bruxism	**4**
Movement score	Normal ambulation, full weight-bearing, no lameness	0
	Slightly lameness on operated limb, toe-touching on all steps	1
	Lameness on operated limb, toe-touching on some, but not all steps	2
	Lameness on operated limb, not toe-touching on all steps when walking voluntarily, but will toe-touch when herded	**3**
	Lameness on operated limb, not toe-touching on all steps when walking voluntarily and when herded	**4**
Flock behavior score	Normal, moves with the rest of the flock	0
	Mild changes, lethargic or lags behind rest of the flock when flock is moved, but eventually joins them voluntarily	1
	Moderate changes, lags behind rest of flock when flock is moved, but eventually joins them if encouraged to do so	**2**
	Severe changes, no interest in rest of flock, always separated from flock	**3**
Score = Sum of 3 scores	**If > 8 : limit point reached**	0 to 11

Before induction of SB stimulation, each sheep underwent imaging assessment of each knee to ensure the absence of pre-existing joint abnormalities (Figure 19). After anaesthesia had been performed, the animal was placed in lateral recumbence, with the head in lower position in a stir foam box to collect saliva. For hygienic purpose, additional interventions were implemented: (1) a urinary catheterization to ensure collection of urine and to avoid contamination of the equipment and environment; (2) covering the digital extremities with latex gloves. The targeted limb was extended caudally and maintained with a 5-kg load, while the other limb was extended cranially and maintained with a roller bandage. This position allowed the knee to lie down in the centre of the gantry (Hontoir et al., 2017).

The pre-induction imaging included a T2 mapping, a blank-CT (CT without contrast medium) and a contrast-enhanced CT. The acquisition parameters were:

(1) For T2 mapping: Both knees (left and right) were scanned using high-field 3 Tesla (3T) MR (Verio, Siemens, Erlangen, Germany). The sheep was placed in sternal recumbence, hindlimbs were extended caudally, toward the magnet. A 15-channel-knee coil (Siemens) was used and the targeted limb was maintained in extension with a 5-kg load. The acquisition was performed in 2D, in the sagittal plane. Field

of view extended from the base of the patella to 4 cm below the tibial plateau. The sequence parameters were: repetition time: 1420 ms, average number: 2, flip angle: 180, echo number: 6, space between slices: 4.4, slice thickness: 4.0mm, pixel size was: 0.2x 0.2 mm, matrix 512 x 512. The six echo time to perform the T2 mapping were: 15.7 ms, 31.4 ms, 47.1 ms, 62.8 ms, 78.5ms 94.2 ms. The total length of the sequence was 20 minutes.

(2) For blank CT: After T2 mapping, the sheep was transferred to the CT room. Both knees (left and right) were subsequently imaged with an Emotion 6 scan (Siemens, Erlangen, Germany). The targeted limb was extended caudally and maintained with a 5-kg load, while the other limb was extended cranially and maintained with a roller bandage. This position allowed the knee to lie down in the centre of the gantry (Figure 19). Acquisition parameters were: 130 kVp, 80 mAs, helicoidal/sequential acquisition, pitch factor: 0.4, collimation of 0.63mm, revolution time: 0.6s. Field of view was similar to T2 mapping field of view. The transverse resolution was 0.20 x 0.20 mm. Slices of 0.63 mm were reconstructed with an increment of 0.3 mm resulting in an overlap between the different slices and a resultant longitudinal resolution of 0.3 mm without gap. The voxel size was 0.2x0.2x0.3mm. Images were then transferred on a medical digital imaging system (PACS, Télémis, Louvain-La-Neuve, Belgium). Images were reconstructed using bone algorithm and stored until analysis.

(3) For contrast CT: the parameters were the same as those used for blank images. The CTA injection was easily performed in the femoropatellar compartment of the stifle, after the stifle has been clipped and scrubbed with povidone iodine (Poviderm scrub, povidone iodinum 7.5%, Audevard, France; Poviderm dermicum, povidone iodinum 10%, Ecuphar, Belgium) (Hontoir et al., 2017). A 21G-38mm needle was inserted in the femoropatellar compartment, using the retropatellar technique. Synovial fluid was collected, if present. Twenty millilitres of a mixture of 6 ml contrast medium Ultravist 370 mg (Iopromide 768.86 mg/ml, equivalent iode 370 mg/ml, Bayer NV, Diegem, Belgium) and 14 ml of NaCl 0.9% (Viaflo, Baxter, Lessines, Belgium) were subsequently injected. The joint was flexed and extended 100 times to ensure a good spreading of the contrast medium. The limb was finally imaged with the same acquisition parameters as for blank CT, keeping a 10-minute delay between the injection of contrast medium and the contrast CT acquisition.

Figure 19. Sheep positioning during the scanning period for CT scan (A-D) and MRI (E-F). (A) The sheep was placed in lateral recumbence with the targeted limb caudally extended and the other limb cranially extended and tied forward with a roller bandage around the trunk. Digital extremities were covered with latex gloves. (B) Oxygen supply was ensured by endotracheal tube and an ambu-bag (VTrade, Noville-Les-Bois, Belgium). Saliva was collected in a stir foam box. (C) Urine was collected through a urinary catheterization to avoid contamination of the equipment and environment. (D) Schematic view of sheep and limb a positioning. (E) Sheep was lying down on the MR table. The sheep was in sternal recumbence. Hindlimbs were extended caudally, and the targeted limb was maintained in the coil, with a load to maintain the limb in extension. (F) Schematic representation of the limb, extended caudally, with the load to maintain the extension.

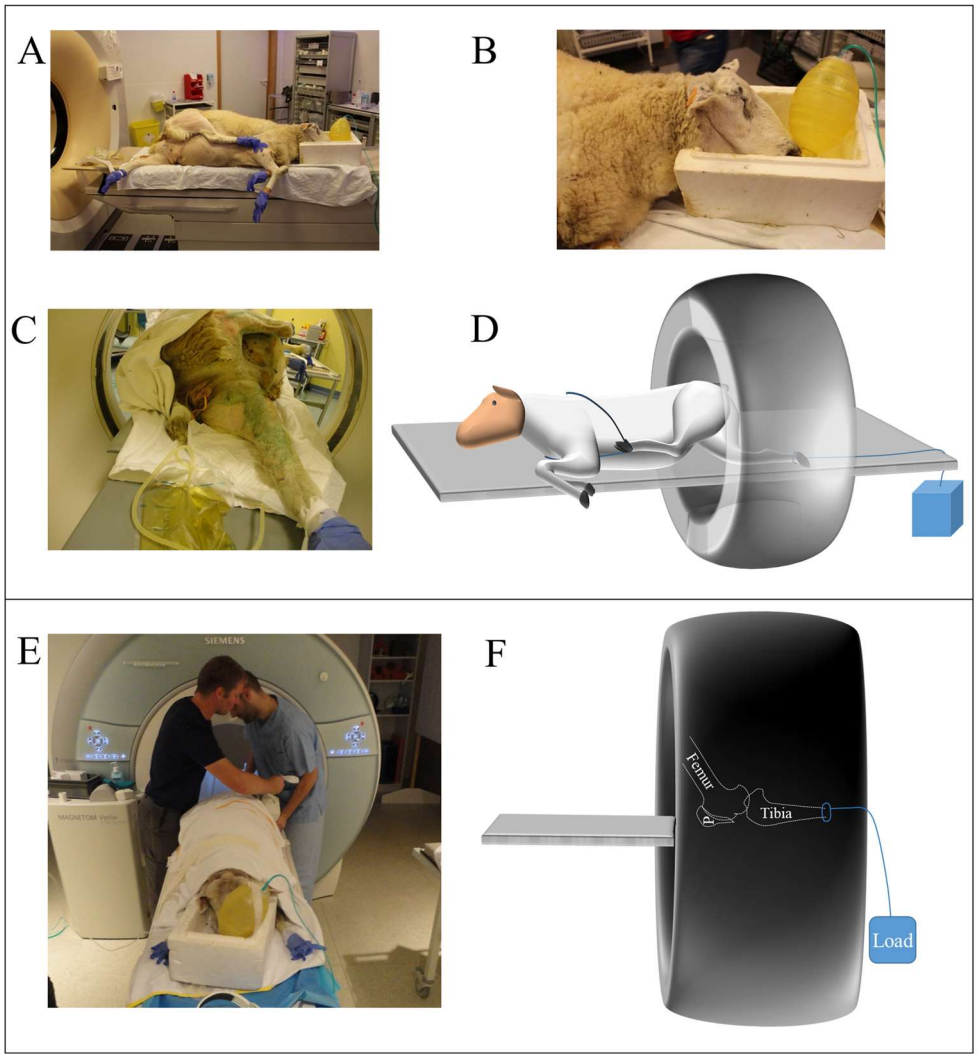

Study design

This study included five observational time-point (5 groups): T0, T2, T4, T6, T8 for 0, 2, 4, 6, 8 weeks delay between induction of SB stimulation and euthanasia, respectively. Two stimulation techniques (ethanol injection and impact) were tested at each time-point. Four sheep (2 by stimulation technique) were included in four groups (T2 (n = 2 + 2 = 4), T4 (n = 4), T6 (n = 4, T8 (n = 4)) and only two sheep were included in the T0 group (n = 2), considering the sheep would be euthanized 1 hour after the induction of the SB stimulation in this group. The flow of events and animals is described in figure 20.

Figure 20. Flow chart of the protocol. Selection of the sheep allowed to create homogeneous groups of age and weight. Sheep had no history of musculoskeletal disorders. An initial physical examination ensured the good health of animals. The sheep were excluded in case of lameness or disorder incompatible with the study design. Daily assessment was performed from the inclusion to the euthanasia. Sheep could be excluded at different time-points (red arrows). Sheep were euthanized 2, 4, 6, 8 weeks after induction of SB stimulation.

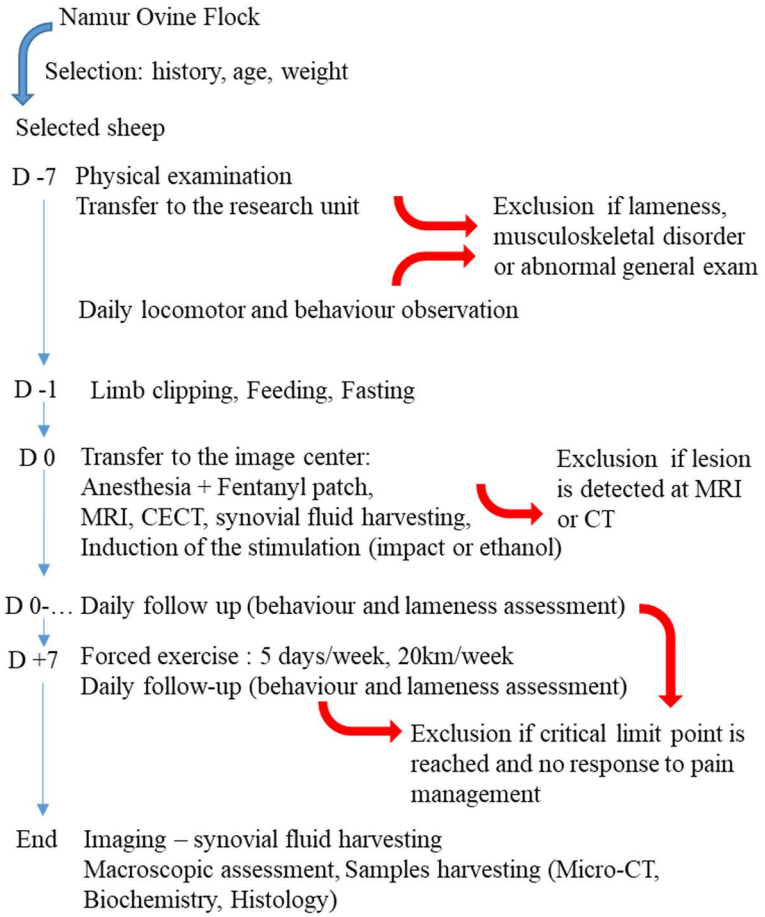

Induction technique

One limb was randomly assigned to either ethanol or impact stimulation. The contralateral limb was either a sham operated limb (tissue incision, drill but no stimulation) or control limb (no surgery, no stimulation). The detailed protocols are provided in the previous section ("The induction model: the subchondral bone stimulation"). After potentially painful orthopaedic intervention, pain management is mandatory. It has been showed that transdermal fentanyl provides an equivalent, if not higher, analgesia than oral phenylbutazone (Dowd et al., 1998). A fentanyl patch (Fentanyl Matrix Sandoz, 100 mcg/h, Sandoz, Vilvoorde, Belgium) was therefore placed on the clipped forelimb, at the level of the forearm. A dressing retention sheet (Hypafix, BSN medical, Hamburg, Germany) and a bandaging tape (Vetrap, 3M, Cergy, France) ensured a perfect contact and retention of the patch during 5 days.

Clinical follow –up

Sheep were examined twice a day. The comfort, movement and flock behaviour were assessed following a dedicated scoring scale (Dowd et al., 1998; Shafford et al., 2004) (Table 7 and 8, p. 93-94). The sheep were maintained together in sheep stalling/box. There was no restriction on animal walking.

If sheep were not lame, they were exercised one week after stimulation of the SB. Sheep were exercised 5 days a week, on a dog trainer (Dog Gym 2000, Harburg-Großsorheim, Germany), set at 26-28 cycle/min (1 cycle = 1 revolution of the conveyor belt = 3.10 m) for 50 minutes (Figure 21). The sheep were therefore walking at least 20 km/week, since they were free of motion at other times.

Figure 21. Sheep walking in a "dog trainer". The sheep entered the dog trainer by the rear door (A). A removable wall (B) was maintained in front of the sheep to avoid attempts to escape. A feeding bucket (C) was provided to stimulate the sheep to enter the dog trainer and to walk during the initial sessions. The parameters were set up (D) and the sheep was allowed to walk. At the end of the exercise session, the wall (B) was removed and the front door was opened and the sheep was allowed to come back to the research group. The dog trainer was washed with water (E) every day, at the end of all exercise sessions.

Euthanasia and imaging

The sheep were euthanized by an IV injection of 20 mg/kg embutramide. The knees were imaged using the same techniques and parameters as the pre-induction imaging protocol (T2 mapping, blank-CT and a contrast-enhanced CT).

Macroscopic assessment

Joints were dissected. Assessment of cartilage surface was performed following OARSI recommendations for scoring of cartilage in sheep: score 0 for intact cartilage surface; score 1 for surface roughening; score 2 for deeper defects (fibrillation, fissures) not involving the SB; score 3 for erosions down to SB, smaller than 5-mm in diameter; score 4 for erosions down to SB, larger than 5-mm diameter (Little et al., 2010).

The scoring was performed by partitioning the whole cartilage surface of the joint in 26 anatomic subregions (Figure 22) (Pierson et al., 2012; Vandeweerd et al., 2013; Hontoir et al., 2017). The major area of interest was the medial femoral condyle since the drill hole was performed in this condyle. Joint surfaces were digitally photographed for records, with standardised lighting conditions (two Illustar SM-300 lighting and a Sony Alpha DSLR-A230 digital camera, Sony SAL 1855 zoom lens, aperture 4.5, shutter speed 1/60, object distance 30 cm, resultant resolution: 3 872 x 2592 pixels).

Sampling

After macroscopic assessment, articular cartilage samples and osteochondral slabs were collected from the above specified area (namely the middle third of the patella (P2), of the medial (FCM2) and lateral (FCL2) femoral condyles and of the medial (TCM2) and lateral (TCL2) tibial condyles). Histological samples were harvested with a bandsaw, as 3-4 mm-thick osteochondral plugs. For the medial femoral condyle, the operator tried to centre the sample on the drill hole. Osteochondral samples were fixed in 10% (v/v) neutral buffered formalin for 48h. Following fixation, samples were transferred to 70% (v/v) ethanol for storage until further processing.

Samples were collected from the remaining cartilage of the selected area for biochemical assessment. They were kept frozen at -80°C until process for water, glycosaminoglycans, collagen and DNA content.

Synovial fluid assessment

The synovial fluid (collected before injection of contrast medium) was submitted to the pathology laboratory (Lab For Vet, Isnes, Belgium) for cells count (leukocytes and erythrocytes), cells differential count, cytology and protein content measurement. The synovial fluid assessment was planned for samples collected before the induction of the SB stimulation and at the final time-point.

Figure 22. Twenty-six anatomic sub-regions macroscopically assessed for abnormalities of the articular cartilage. (A) cranial, middle, and caudal thirds of the articular surface of the medial and lateral tibial condyles, where each middle third was divided into axial and abaxial aspects (TCM1, TCM2Ax, TCM2Ab, TCM3, TCL1, TCL2Ax, TCL2Ab, TCL3); (B) proximal, middle, and distal thirds of the articular surface of the patella (P1, P2, P3); (C) cranial, middle, and caudal thirds of the articular surface of the medial and lateral femoral condyles (FCM1, FCM2, FCM3, FCL1, FCL2, FCL3); (D) proximal, middle, and distal thirds of the articular surface of the medial ridge, groove, and lateral ridge of the trochlea of the femur (TM1, TM2, TM3, G1, G2, G3, TL1, TL2, TL3). Region of interest (blue) that were systematically collected from each ovine knee (induced, control or sham operated) were P2, TCM2, TCL2, FCM2 FCL2.

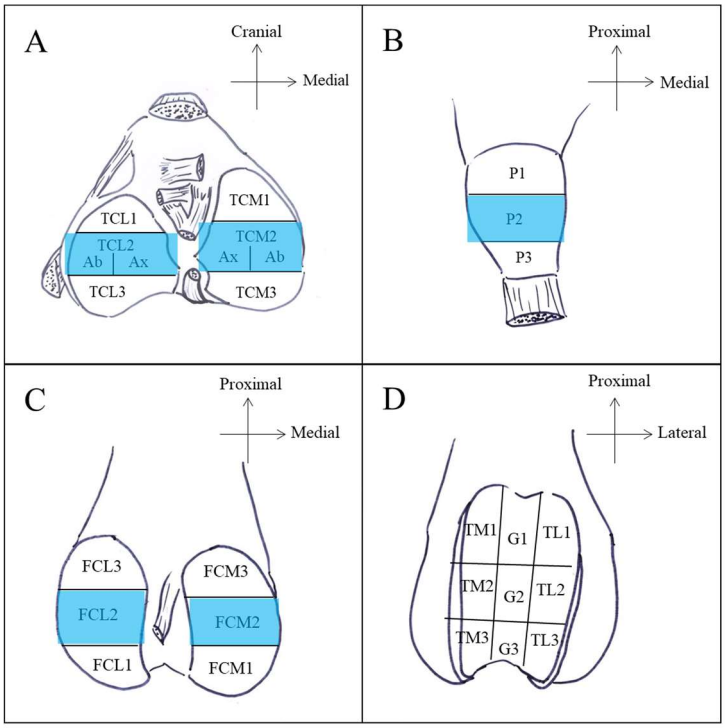

Micro-computed tomography

Microcomputed tomography (micro-CT) is an X-ray based imaging technique that allows assessment of bony alterations, such as SB plate thickening, subchondral sclerosis or trabecular remodelling. Its spatial resolution is higher than CT, reaching micro-millimetric resolution (Muller et al., 1996; Ruegsegger et al., 1996; Wachsmuth and Engelke, 2004). However, the size of the sample is limited to several centimetres (Wachsmuth and Engelke, 2004) preventing *in vivo* scanning of the entire ovine knee.

The FCM2 samples were imaged with a micro-computed tomography system before processed for histology (Skyscan 1272, Bruker, Aartselaar, Belgium) (Figure 23). The samples were taken out of 70% ethanol solution and wrapped in a sealing film (Parafilm M, Bemis, Neenah, USA) to avoid dehydration of the tissue during scanning and subsequent shrinking and blurring artefact (Wachsmuth and Engelke, 2004). The tube voltage was set at 70 kV, and the current was 142 mA. Projections were obtained at 0.3° intervals with 1600 millisecond exposure time and a combined 0.5-mm aluminium/copper filter interposed. The pixel size was set at 10 µm. The average time for scanning was 20 minutes per sample. After imaging, samples were unwrapped and brought back in 70% ethanol until histological processing.

Reconstruction was done with NRecon software (Bruker, Aartselaar, Belgium). The settings were: smoothing: 1 (Smoothing Kernel= Gaussian); beam-hardening correction: 38%; ring artefact reduction: 5. The isotropic pixel resolution was 10µm. Thresholding levels of grey values were set from 90 to 255, for segmentation of binary images.

Analysis was performed with the CTAn program (CT Analyzer, Skyscan). Volume of interest were set to 800 pixels x 800 pixels x 300 pixels. 3D analysis automatically calculates relevant values (percent bone volume or apparent bone density, intersection surface, bone and tissue surface, trabecular pattern factor, structure model index, trabecular thickness, anisotropy, trabecular number, trabecular separation). (See Table 9 for definition of the different values).

Figure 23. Preparation of the samples for micro-CT assessment. Sample were transferred from 70% ethanol (A) to be wrapped in a sealing film (B) to keep them wet. Samples were subsequently placed vertically on the micro-CT sample block (C) to proceed to loading of the samples (D) in the micro-CT system.

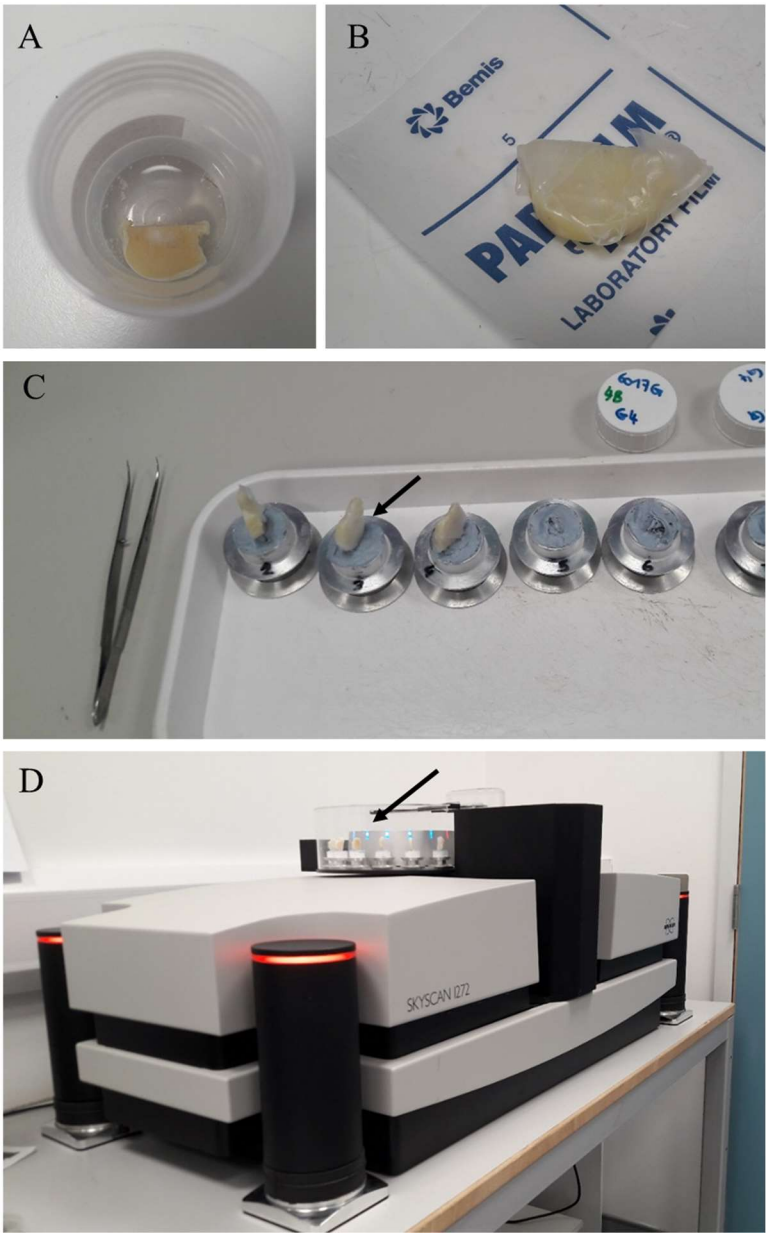

Table 9. Definition and calculation of the different values for trabecular bone assessment (Kamibayashi et al., 1995; Bouxsein et al., 2010).

Parameter	Definition	Interpretation
Percent bone volume (%)	Direct measure of the bone volume (BV) occupied in the total volume (TV) of interest (BV/TV)	= apparent bone density
Structure model index	Relative prevalence of rods and plates in the trabecular bone	Transition from plate-like to rod-like structure in osteoporosis
Trabecular thickness (µm)	Estimated mean of the trabecular thickness in the volume of interest	
Degree of anisotropy	Calculated value, expressing the presence of preferential alignment of the inner architecture	0 = total isotropy 1 = total anisotropy
Trabecular number (/mm)	Estimated number derived from the frequency with which the scanning line will intersect with a structural element of bone averaged over all directions of scanning	
Trabecular separation (µm)	Estimated index, derived from the shortest distance between trabecular plates on the assumption that they are parallel.	
Trabecular connectivity (%)	Estimated ratio of the number of trabecular intersections (nodes) to the number of individual trabeculae (struts) within the volume of interest	0% = no connectivity 100% = high connectivity

Histologic assessment of AC and SB

To assess the stage of decalcification, 5-ml decalcifying fluid was sampled on the bottom of the sample jar and was mixed with 5-ml sodium hydroxide (5%) solution and 5-ml ammonium oxalate (5%) solution. If the decalcification had reached its endpoint, the solution was still clear after 30 minutes incubation at room temperature. If any white precipitate formed after a 30-min stand, the decalcifying fluid still enclosed calcium, meaning the decalcification process was not over.

Mechanical test was performed by trying to penetrate the bone with a needle. Care was taken not to insert the needle in a bony region of interest (i.e. avoid the SB close to the articular cartilage or the SB around the drill hole). The needle should easily pass through a decalcified sample.

The decalcified samples were rinsed in 70% ethanol before being automatically impregnated in paraffin (Tissue-Tek VIP tissue processor, Sakura France, Villeneuve d'Ascq, France). The samples were subsequently embedded in paraffin using an embedding workstation (Histostar, Thermo Fisher Scientific). After cutting the exceeding paraffin, the blocks were incubated overnight in a softening solution (Mollifex Tissue softener, Merck). Seven-micron sections were cut, floated on a 42°C-distilled water bath and fixed on coated slides (Superfrost Plus slides, Thermo Fisher Scientific). The slides were allowed to drain water, vertically, overnight and were subsequently dried in a 48°C oven for 1h30, to avoid tissue loss during staining steps.

For staining, sections were de-paraffinised with toluene and graded methanol, and rehydrated in tap water. The sections were subsequently stained with Toluidine blue O-Fast Green, Hematoxylin-Eosin, Safranin O-Fast Green, Picrosirius Red following published protocols (Melrose et al., 2004; Schmitz et al., 2010; Kang et al., 2010). The detailed protocols can be found in Table 10.

Cartilage structure was scored using the OARSI recommendations for histological evaluation of AC in sheep (Table 11) (Little et al., 2010). These recommendations provide scores for: cartilage structure (0-10), chondrocyte density (0-4), cell cloning (0-4) inter-territorial Toluidine blue (0-4), tidemark (0-3) and extension of the surface area affected by structural damage greater than score 3 (0-5). Scoring was performed on Hematoxylin-Eosin sections and on Toluidine blue sections.

Proteoglycan content ratio was calculated by analysing the Safranin O-Fast Green sections. Pictures of the sections were acquired with Olympus BX63. Images were then transferred for analysis on ImageJ program (Rasband, W.S., ImageJ, U. S. National Institutes of Health, Bethesda, Maryland, USA, https://imagej.nih.gov/ij/, 1997-2016). HC was segmented on the histological slide image and then, analysis of RGB (red blue green) intensities was performed and expressed in Red Color Index (RCI= R/ (R+G+B) (Mickievicius et al., 2015).

Collagen organization was assessed under polarized light microscopy (AxioPhot, Zeiss) on Picrosirius red stained sections (Changoor et al., 2011), with a score-5 cartilage being a perfectly organized cartilage, with multiple well-proportioned birefringent zones, and a score-0 cartilage showing fibres randomly oriented in the specimen.

Table 10. Staining protocols for histomorphometry of bone and cartilage. (Adapted from: Melrose et al., 2004; Kang et al., 2010; Schmitz et al., 2010). Color indexes for pigments are Toluidine blue CI 52040, Fast Green FCF CI 42053 and Safranin CI 50240.

* mouting medium: DPX mountant for histology (Merck). min= minutes

Staining technique	Protocol	Solutions	Result
Toluidine blue O-Fast Green (Melrose et al., 2010)	Deparaffinise the sections Rehydrate in tap water (3 min) Stain in Toluidine blue (10 min) Rinse briefly in running tap water Counterstain with fast green Rinse briefly in running tap water Dehydrate in isopropanol (2x2min) Clear slides in toluol (2x2 min) Mount slides *	Toluidine blue solution: cfr Toluidine blue stain. Fast Green solution (0.1% w/v): dilute 0.2g Fast Green FCF in 200 ml distilled water.	Cartilage dark blue Calcified cartilage: blue Bone: green
Hematoxylin Eosin (Schmitz et al., 2010)	Deparaffinise the sections Rehydrate in tap water (1 min) Stain in Mayer Hematoxylin (8 min) Rinse with running tap water (10 min) Rinse with 95% ethanol (10 dips) Stain in Eosin solution (1 min) Dehydrate in isopropanol (2x2min) Clear slides with toluol (5 minutes) Mount slides *	Eosin solution: 10g eosin mixed with 200 ml distilled water and 800 ml 95% ethanol. Mayer Haematoxylin: 50g potassium aluminium sulphate, 1g Hematoxylin, 0.2g sodium iodate, 1g citric acid, 1000 ml distilled water.	Cartilage: pink (bluish) Bone: pink to red Nuclei: blue
Safranin-O Fast Green (Kang et al., 2010)	Deparaffinise the sections Rehydrate in tap water (3 min) Stain in Safranin-O (40 min) Rinse in distilled water, 3x6 dips Briefly Rinse in fresh acetic water solution (1 dip) Stain with Fast green for 30 seconds. Rinse in distilled water, 6 dips. Dehydrate in 95% then 100% ethanol, 8 dips each Clear slides in toluol (2x2 min) Mount slides *	Safranin solution (1.5% - aqueous): 1.5g Safranin CI50240) in 100 ml distilled water Fast green solution (0.02% - alcoholic): 0.02 g fast green (CI 42053) in 100 ml 95% ethanol Acetic water (1% acetic acid, always use fresh): 1ml glacial acid in 99ml distilled water	Cartilage: red Calcified cartilage: red Bone: green

Picrosirius Red (Melrose et al., 2010; Changoor et al., 2011)	Deparaffinise the sections Rehydrate in tap water (3 min) Incubate with hyaluronidase for 2h at 37°C. Color with Weigert's Hematoxylin for 8 minutes. Rinse in running tap water for 10 minutes. Stain with Picrosirius red solution for 1 h at room temperature Rinse with acetified water (2x5 min). Dehydrate in 100% ethanol (2x5min) Clear slides in toluene (2x2 min) Mount slides *	Hyaluronidase: 1 mg/ml in 0.1M Phosphate buffer solution (pH 5.0). Weigert's Hematoxylin: Solution A: 1% haematoxylin in 95% alcohol. Solution B: 4 ml of 30% ferric chloride ($FeCl_3$) anhydrous, 1 ml concentrated HCl, 95 ml distilled water. Mix equal parts of solution A and B. Filter before use. Stable for 3-4 days. Picrosirius red solution (0.1%): 0.1g Sirius Red F3B200 in 100ml aqueous saturated picric acid solution	Light microscopy: Collagen fibres: red

Table 11. Glossary for histological assessment of cartilage in the sheep. Histological examples are reproduced from the OARSI recommendations (Little et al., 2010).

Structure (0 – 10)	
0	Normal
1	Slight surface irregularities (surface barely disturbed)
2	Moderate surface irregularities (surface roughened)
3	Severe surface irregularities (disruption, fissuring/fibrillation to < 10% depth)
4	Fissures to transitional zone (1/3 depth)
5	Fissures to radial zone (2/3 depth)
6	Fissures to calcified zone (full depth)
7	Erosion or severe fibrillation to mid zone (1/3 depth)
8	Erosion or severe fibrillation to deep zone (2/3 depth)
9	Erosion or severe fibrillation to calcified zone (full depth)
10	Erosion or severe fibrillation to subchondral bone

White arrows show the irregularities, fissures, erosion or fibrillation depending on the score; black arrows highlight the depth of the lesion.

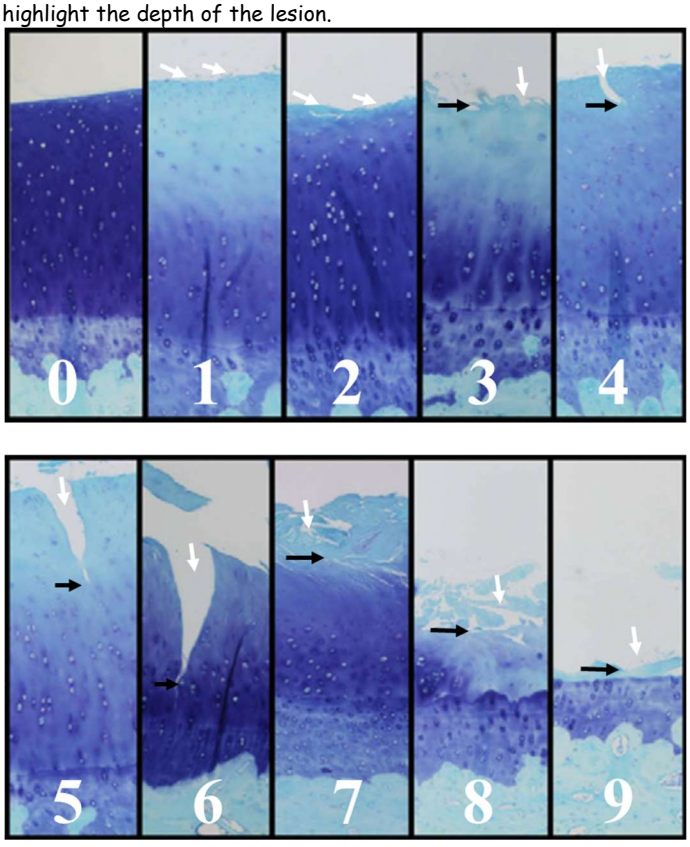

Chondrocyte density (0 – 4)	
0	Normal
1	Increase or slight decrease
2	Moderate decrease
3	Severe decrease
4	No cells

The bracket highlight the area of assessment of the chondrocyte density.

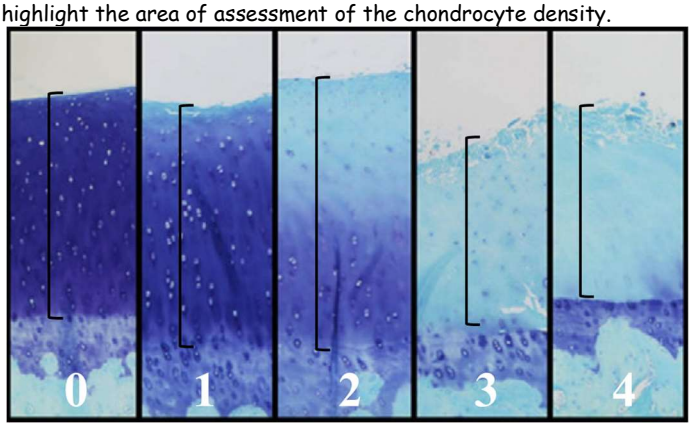

Cell cloning (0 – 4)	
0	Normal
1	Several doublets
2	Many doublets
3	Doublets and triplets
4	Multiple cell nests or no cells in section

White arrows showed cells, doublets, triplets or nests depending on the score.

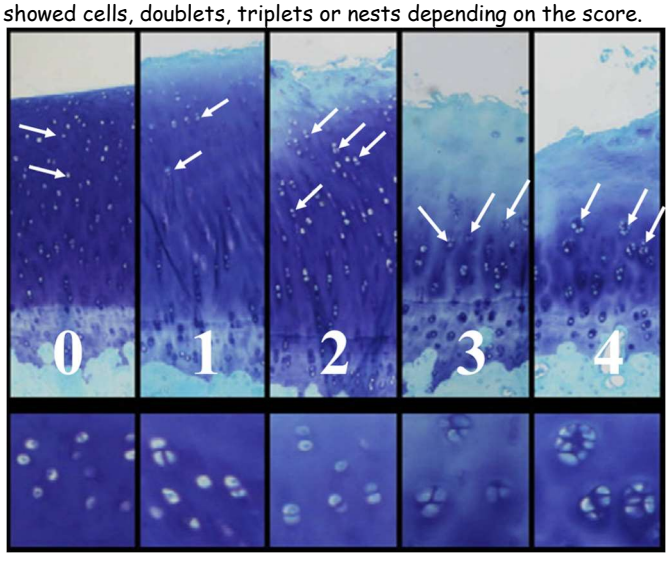

Interterritorial Toluidine Blue (0 – 4)	
0	Normal
1	Decreased staining to mid zone (1/3 depth)
2	Decreased staining to deep zone (2/3 depth)
3	Decreased staining to calcified zone (full depth)
4	No staining

The large bracket shows the plain staining (0) or the total absence of staining (4).
The white arrows show the depth of decreased staining.

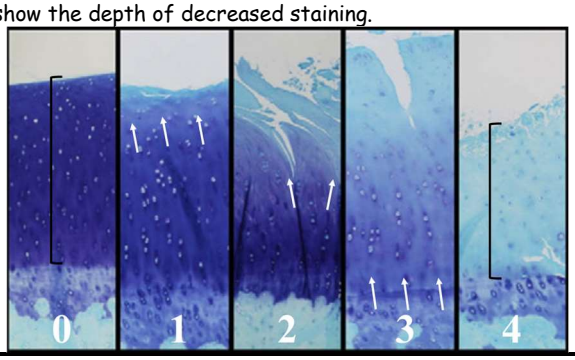

Tidemark – calcified cartilage – subchondral bone (0 – 3)	
0	Intact subchondral bone plate + single tidemark
1	Intact subchondral bone plate + duplicated tidemark
2	Blood vessels penetrate through subchondral bone plate to calcified cartilage
3	Tidemark penetrated by blood vessels

The black arrows show the tidemark; the dotted arrow highlights the blood vessel and the white arrow shows the level of penetration of the blood vessel.

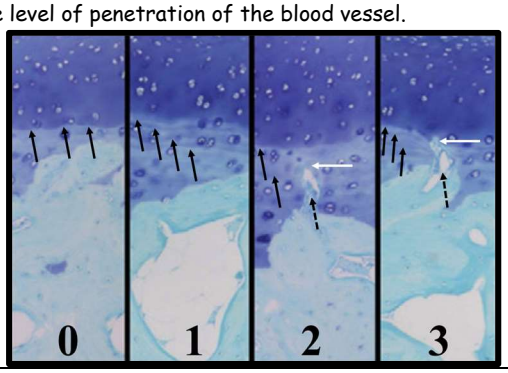

Extension of the surface area affected by structural damage greater than score 3	
0	No structural damage extending below 10% depth
1	< 10% surface area with structural damage extending below 10 % depth
2	10 - 25 % surface area with structural damage extending below 10% depth
3	26 - 50 % surface area with structural damage extending below 10% depth
4	51 – 75 % surface area with structural damage extending below 10% depth
5	> 75 % surface area with structural damage extending below 10% depth

For immunohistochemistry (IHC) of type-I collagen, type-II collagen and aggrecan, the sections were deparaffinised in toluene and graded alcohol, and rehydrated in tap water. The slices were incubated with a mild temperature retrieval solution (Uni-Trieve, Innovex Biosciences, Richmond, USA) for 30 minutes in a 55°C oven. After phosphate buffer solution (PBS) wash, the endogenous peroxidases were blocked (Bloxall blocking solution, Vector Laboratories, Peterborough, United Kingdom). The slides were subsequently washed in PBS and incubated with the provided blocking solution (2.5% horse serum, Vector Laboratories, Peterborough United Kingdom). The slides were incubated, in a humidified chamber, overnight at 4°C, with the primary antibody diluted in provided blocking solution (2.5% horse serum): 1/100 dilution for collagen II (Ab 34712 Abcam, Cambridge, UK) and for collagen I (Ab34710, Abcam, Cambridge, UK); 1/200 dilution for aggrecan (Ab3778 Abcam, Cambridge, UK). After overnight incubation, the slices were washed in PBS and incubated for 30 minutes with the provided secondary antibody (ImmPRESS reagent Anti-Mouse IgG Peroxidase kit MP 7402 and ImmPRESS reagent Anti-Rabbit IgG Peroxidase kit MP7401, Vector Laboratories, Peterborough United Kingdom). After PBS wash, the slices were incubated with the revealing solution (ImmPACT DAB kit, Vector Laboratories, Peterborough United Kingdom). The reaction was controlled under the microscope and stopped with tap water. The slides were dehydrated and clear before mounting with a resinous medium (DPX mountant for histology, Merck). Immunostained sections were analysed by assessing the intensity of staining and the location of the stain. Negative controls were similarly processed, using the provided blocking solution and omitting the primary antibody for the overnight incubation at 4°C. Ovine placenta samples were also processed using the same protocol for fixation, storage, embedding, slicing, and processing for sections. The placenta sections were processed following the same IHC protocol, to test the specificity of the antibodies and to compare the staining between decalcified (osteochondral samples of medial femoral condyle) and non-decalcified tissue, in order to ensure that decalcification would not affect the antibody binding.

Detection of apoptotic cells was performed by Terminal deoxynucleotidyl transferase dUTP nick end labelling (TUNEL) assay (Click-iT TUNEL colorimetric IHC detection kit, C10625, Invitrogen, Thermo-Fisher Scientific). The principle of this technique is to detect the 3'OH ends of fragmented DNA. The samples were incubated with an enzyme (Terminal deoxynucleotidyl transferase, TdT) that incorporate a modified deoxyuridine triphosphate (dUTP). This modified dUTP was conjugated with a detection system (biotin) that was revealed by the combination of streptavidin-peroxidase and it substrate (DAB or 3,3-diaminobenzidine). The substrate is turned into a dark brown signal where the streptavidin-peroxidase is fixed, i.e. where the dUTP-biotin has been incorporated: the 3'OH ends of fragmented DNA. The more the signal, the more DNA is fragmented.

Biochemical content of articular cartilage

Biochemical content assessment included determination of water, GAG, collagen and DNA content.

Briefly, water content was calculated from the wet weight and the dry weight of the sample. For the dry weight, the frozen samples were freeze dried for 48 hours, at -55°C and 1.2mBar. The samples were weighted (dry weight). Water content was subsequently calculated and expressed in % of the wet weight (Brama et al., 2002). One part of the sample underwent GAG and DNA assay while the other part was submitted to collagen assay.

GAG content was measured by the DMMB assay (DiMethyl-Methylene Blue assay) (Farndale et al., 1986; Hoemann, 2004). One part of the dried sample was weighted and underwent papain digestion (10UI/ml Papain from papaya latex, P3125, Sigma Aldrich; in buffer: 0.1M sodium acetate trihydrate, 2.4mM EDTA, 5mM L-cystein), at 65°C overnight. Aliquots of the solubilized samples were diluted (1/100). Triplicates (40µl) were transferred to a 96-well microplate and mixed with 250 µl of DMMB solution (16mg 1,9-DiMethyl-Methylene Blue, 2g sodium formate, 2 ml formic acid, 1 litre of distilled water). Absorbance was read immediately with a spectrophotometer (Multiskan EX, Thermo-Fisher) at 620nm. A standard curve (0, 10, 20, 30, 40, 50, 60, 70 µg/µl) of Chondroitin Sulfate sodium salt from shark cartilage (C4384, Sigma-Aldrich) was also submitted to the DMMB assay to convert the measured absorbance into GAG content. The GAG content in the diluted aliquot was then converted in GAG content per mg of cartilage dry weight.

The collagen content was measured with the Sircol® insoluble collagen assay (Biocolor, Carrickfergus, Northern Ireland, UK). The protocol followed manufacturer instructions. A standard 10.0-mg weight of freeze-dried tissue was incubated with 1.0 ml cold pepsin (0.1 mg/ml, in 0.5M acetic acid) at 4°C overnight. The tissue was then submitted to EDTA-fragmentation reagent overnight at 4.0°C, in order to convert the native insoluble collagen in to soluble denatured collagen. To ensure an adequate solubilisation of collagen, tubes were incubated at 65°C during 2 to 3 hours. Because the required volume to perform the assay is limited to 100µL, samples were diluted (1:5) to obtain a final volume of 100 µl. The collagen standards (0 to 80 µg/100µl) and the diluted samples were subsequently submitted to the assay: each one was incubated with 1.0 ml of Sircol dye reagent during 30 minutes. This allowed the collagen to complex with the dye. Further centrifugation ensured the complex to be firmly packed at the bottom of the tube. The tubes were drained to only keep the pellet. The pellet surface was drained to remove unbound dye from the surface of the pellet and the inner surface of the tube. The dye complex was finally diluted in alkali reagent. Each tube was then transferred in duplicates in a micro-well plate to allow spectrophotometer reading at 550nm (Multiskan EX, Thermo-Fisher). The collagen standard curve allowed the calculation of collagen content of each solution and subsequent calculation of collagen content in sample dry weight.

The nucleic acid quantification was performed with the Qubit™ ds DNA BR assay (Q32850, Invitrogen, Thermo-Fisher Scientific). Diluted Qubit ds DNA BR reagent (190µl) was incubated with 10 µl of standard (0 and 100 ng) or 10µl of papain digested samples for 2 minutes in the dark. The absorbance was subsequently read with the Qubit Fluorometer (ThermoFischer Scientific) (Jin et al., 2011). The system automatically calculated the concentration of DNA in the solution (µg/ml). The concentration was subsequently calculated in cartilage dry weight.

Statistics

All data were tested for normality (Shapiro-Wilk normality test and D'Agostino & Pearson normality test). Multiple comparisons among groups were performed with ANOVA, or Kruskal-Wallis test provided non-normality of the data distribution be detected. Comparisons between two groups were performed with unpaired t-test, or Mann-Whitney test provided non-normality of the data distribution was detected. Correlation between outcomes was assessed by Spearman or Pearson correlation coefficient, depending on the normality of the data. Statistical analysis was computed with GraphPad Prism 7.04 for Windows (GraphPad Software, La Jolla California USA, www.graphpad.com)

6.3 Results

Clinical follow-up

Sheep were examined twice a day. There was no sign of discomfort and no trouble in flock behaviour. The highest lameness score observed after stimulation was 1, meaning a slight lameness on operated limb, toe-touching on all steps. The average duration (median (minimum-maximum)) of the score-1 lameness was: 2 days (1-6 days) for sheep induced with ethanol injection and 3.5 days (1-9 days) for sheep with mechanical stimulation. There was no significant difference between stimulation techniques for the duration of the post-op lameness (P= 0.2913). The statistics were also performed excluding the sheep submitted, at the same time, to sham operation and stimulation; and no significant difference for lameness duration was highlighted between ethanol stimulation and impact stimulation (P=0.4458).

Synovial fluid assessment

Analysis of synovial fluid before induction of the stimulation was impossible because the harvested volume of synovial fluid was too low (< 0.2ml when present in the syringe). Collection of synovial fluid at final time-points was not sufficient to perform analysis for 18 of 36 limbs. For the other 18 limbs, red blood cells count was < 10,000/mm³ (normal range) for 12/18 limbs and < 40 000/mm³ for 6/18 limbs, meaning a blood contamination. This was confirmed by a slightly higher proteins content (2.8 to 3.4 g/dl) with normal white blood cells count (between 40 and 80 cells/µl). Proteins content did not differ significantly for all time-points or all type of intervention (control, sham operated, impact, and ethanol).

Macroscopic assessment

Macroscopic scores were not significantly different between intervention and time-points. The surface of the cartilage was preserved in all but one limb (Figure 24). In this limb, we clearly saw a surface collapse due to inadequate surgical drilling. This limb was a sham-operated limb and was simply excluded from the analysis. No osteophytes were present in any sheep.

Figure 24. Distal end of the femur of two induced limbs. (A) A correctly induced stimulation. The hole can be seen (B) The sham operated limb presenting cartilage collapse. The drill hole was too close to the subchondral plate, leading to a collapse of the structure. This was due to an inappropriate position of the drill entrance (arrow), being too distal and therefore, too close to the joint limit (dotted line).

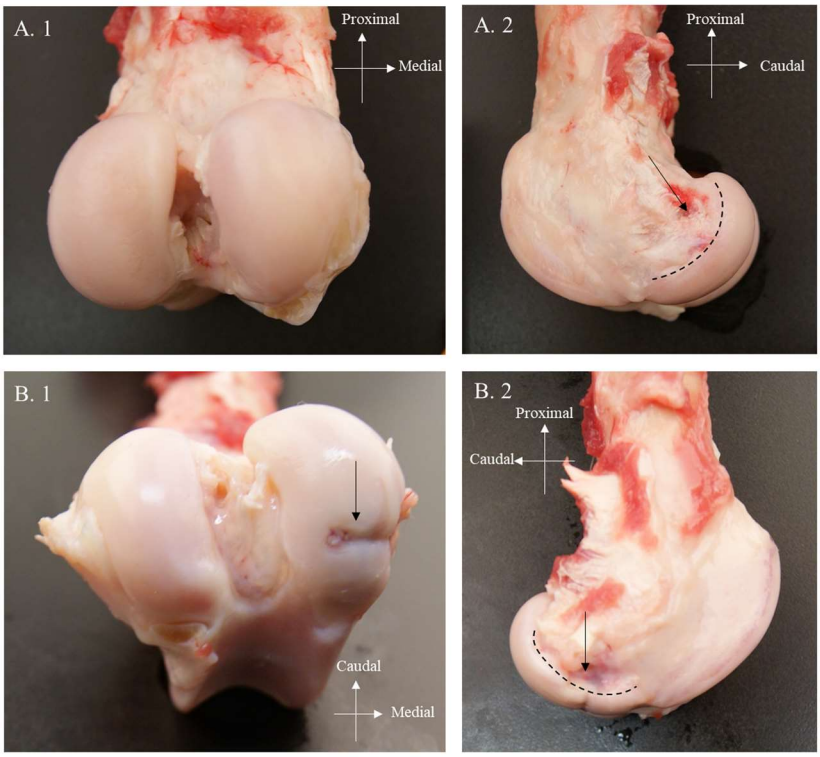

Micro-computed tomography

Four weeks after SB stimulation, the ethanol model showed an increase in apparent bone density (56.29% +/-0.51) and trabecular thickness (259.00µm +/-12.00), a decrease of trabecular separation (338.00µm +/-24.00) and a slight decrease in trabecular number (2.18+/- 0.12), compared to control (38.51% +/-2.94; 161.32µm +/-3.69; 341.01µm+/-31.01; 2.39+/-0.13, respectively). This means that the increase in apparent bone density 4 weeks after stimulation is due to an increase in trabecular thickness ("larger walls"), rather than to an increase in the number of trabeculae ("number of walls") (Figure 25). For the impact-stimulated limbs, the increase in apparent bone density (60.56% +/-1.45) was associated with a slight increase in trabecular number, suggesting another process leading to increase in bone volume.

The sample size for each intervention and time point (N=2) was too small to reach significance when performing statistical tests. However, when grouping data for general bone stimulation (i.e. combining data from ethanol time-points and impact time-points), significance was reached for the difference between 4-week time-point and day-0 time-point

for bone apparent density, trabecular thickness, specific surface of bone (BS/BV), degree of anisotropy and structure model index.

In this study, age and weight did not correlate to any micro-CT outcome. Apparent bone density correlated with trabecular thickness ($r = 0.8370$; $P < 0.000$) and negatively with BS/BV ($r = -08712$; $p < 0.000$). Trabecular space correlated with trabecular number ($r = -0.8207$; $P< 0.000$).

Figure 25. Example of trabecular bone 4 weeks after induction of subchondral stimulation (B) and a control limb (A). The SBT is made of trabeculae (light grey walls; white asterisk) separated by trabecular space (dark grey areas; yellow asterisk). In this ethanol-stimulated limb, the trabecular thickness is increased and the trabecular space is decreased, resulting in an increase in apparent bone density.

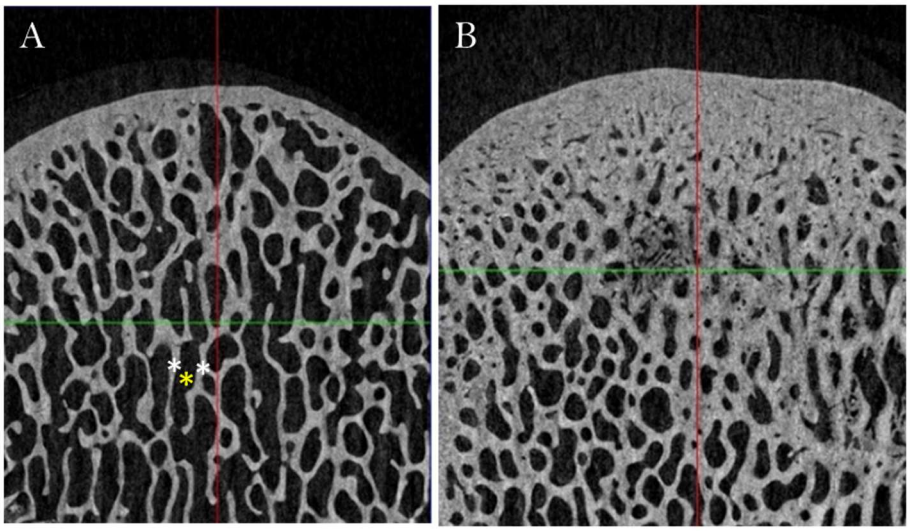

Histological assessment

Statistical analysis of histological scores (OARSI scores, Picrosirius, TUNEL) and values (Red Color Index) did not show significant differences between groups (bulk ethanol, control, sham-operated, impact), or between groups at different time-points (n=2).

However, the structure score and the total score for cartilage assessment showed slight increase overtime in the ethanol-stimulated limbs, whereas these parameters decreased in the impact-stimulated limbs. The Red Color Index and the Picrosirius score presented the opposite trend with a decrease in the ethanol-stimulated limbs over time, and an increase in the impact-stimulated limbs (Table 12, figure 26)

The area of the drill hole showed the sparse presence of fibrous tissue with giant multinucleated cells. The borders of the trabeculae were surrounded by numerous osteoblasts. A high number of osteoblasts around the trabeculae of drilled limbs was observed in 4 of 9 ethanol-stimulated limbs and in 5 of 9 impact-stimulated limbs, and only 1of 4 sham operated-limbs. The trabeculae close to the articular cartilage were also filled with fibrous tissue and numerous, aligned side-by-side, cuboid osteoblasts (Figure 27).

Observation of the SB (Figure 28) under polarized microscopy (Picrosirius red slides) also revealed a larger band of less organized tissue along the trabeculae wall, for 5 of 9 impact-stimulated and 1 of 9 ethanol-stimulated femoral condyle and 0 of 4 sham operated limbs. Finally, the TUNEL assay revealed little to no stain in bone and cartilage for ethanol-stimulated limbs. Impact-stimulated limbs showed TUNEL stain in 5 of 9 limbs for SB and only 1 of 9 for cartilage, whereas sham operated limbs only showed SB stain for 2 of 4 limbs.

Immunohistochemical staining did not provide conclusive information (Figure 29). Anti-type-II collagen antibody was cross-reacting with both type-I and type–II collagens, avoiding any interpretation. Aggrecan IHC and type-I collagen IHC did not reveal any particular pattern. Moreover, the antibody for collagen type-I showed slight cross reactivity with collagen type-II, with high staining of bone and slight staining of cartilage in all slides.

Correlation between histological outcomes revealed that cell cloning and cell density correlated (r= 0.350; P= 0.03583). Toluidine blue score correlated negatively with Red Color Index (r= -0.525; P= 0.00593) and Picrosirius scoring (r= -0.4834; P= 0.01750); and positively with OARSI total score (r= 0.5470; P= 0.00015). Histological outcomes did not show significant correlation with micro-CT outcomes.

Table 12. Detailed data for histological scores of ethanol-stimulated limbs and impact-stimulated limbs. Data are provided as median (minimum – maximum).

Technique	Ethanol-stimulated limbs				Impact-stimulated limbs			
Time-point	Week 2	Week 4	Week 6	Week 8	Week 2	Week 4	Week 6	Week 8
Total score for cartilage assessment	8.5 (8 – 9)	7 (7 – 7)	11.5 (6 – 17)	13 (13 – 13)	14 (10 – 18)	7 (4 – 10)	6.5 (4 – 9)	6.5 (6 – 7)
Red Color Index	0.47 +/-0.10	0.41 +/-0.11	0.36 +/-0.08	0.37 +/-0.02	0.35 +/-0.14	0.38 +/-0.04	0.47 +/-0.06	0.57 +/-0.08
Picrosirius red score	4 (3 – 5)	2 (1 – 3)	0.5 (0 – 1)	0.5 (0 – 1)	2 (1 – 3)	2 (2 – 2)	4 (4 – 4)	4 (4 – 4)

Figure 26. Examples of histological slides. (A) An impact-stimulated medial femoral condyle showing a regular surface, a decrease in Safranin staining in the superficial zone, associated to an intake of fast green (blue area in the superficial zone, arrows). The decrease in Safranin staining suggests a decrease in proteoglycan content. This sample had a calculated Red Color Index of 0.51. (B) A polarized-light microscopic view of an impact-stimulated medial femoral condyle stained with Picrosirius red. The cartilage shows multiple zones of birefringence with the deep zone of cartilage (RZ, radial zone) appearing here, green-blue, accounting for less than 50% of the cartilage thickness, whereas the transitional zone (TZ, light red) is large, more than 50% of the cartilage thickness. In this area, collagen fibres are crossing obliquely, with multiple orientations. The third birefringency area is occupied by the superficial zone (SZ), with collagen fibres oriented tangentially to the articular surface (dark red). (C) An ethanol-stimulated medial femoral condyle, stained with Safranin O-Fast Green. The fast-green intake was higher in the superficial zone and in some area of the transitional zone (arrows), meaning a loss of proteoglycans. This sample had a Red Color Index of 0.29. Vertical artefactual folds are visible in the deep half of cartilage. (D) A Picrosirius-stained femoral condyle observed under polarize-light microscopy. The zonal organization of cartilage is no longer visible (arrow). Birefringency suggests an oblique, non-parallel orientation of the collagen fibres.

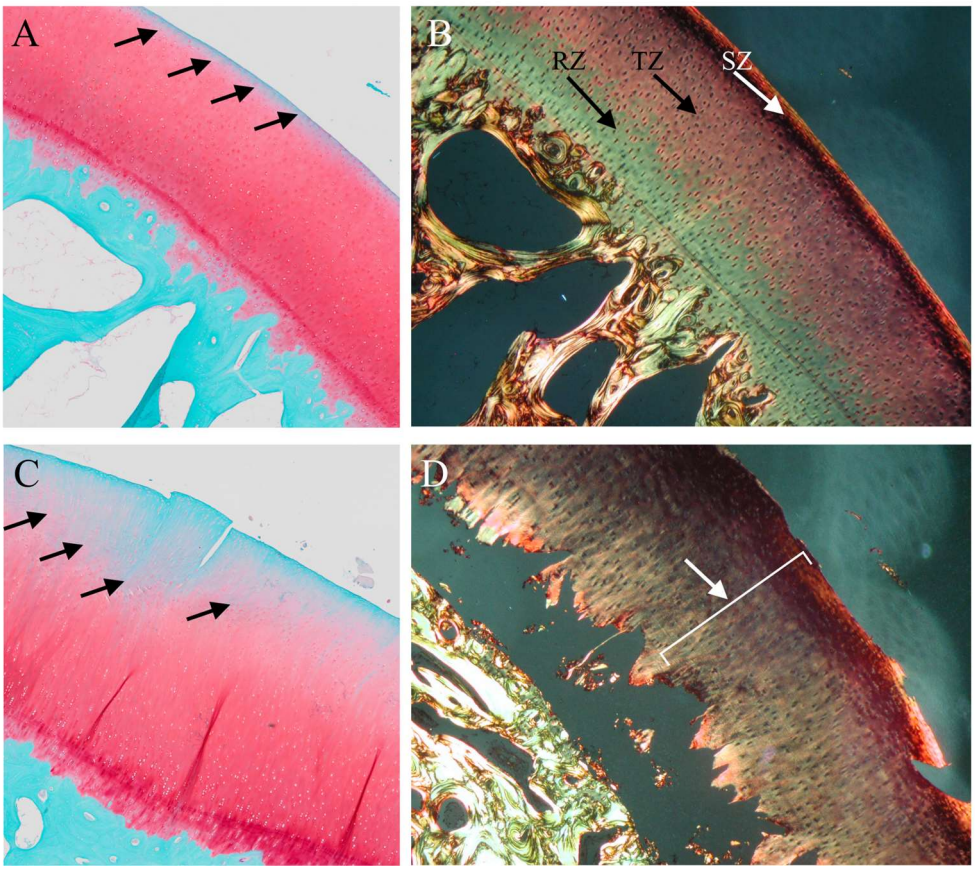

Figure 27. Repair area of the drill hole and surrounded trabecular spaces. (A) Safranin-O Fast Green section. Fibrous tissue was progressively filling the area of the drill hole. This fibrous tissue showed an increased organization overtime (4 weeks post-stimulation), with increased waviness (arrows). (B) Toluidine blue O-Fast Green section. Numerous osteoblasts were lining the border of all trabeculae, surrounding the drill hole, suggesting bone remodelling around the hole. (C) Hematoxylin-Eosin section. Multi-nucleated giant cells (arrows) were present in the fibrous tissue filling the surrounding trabeculae.

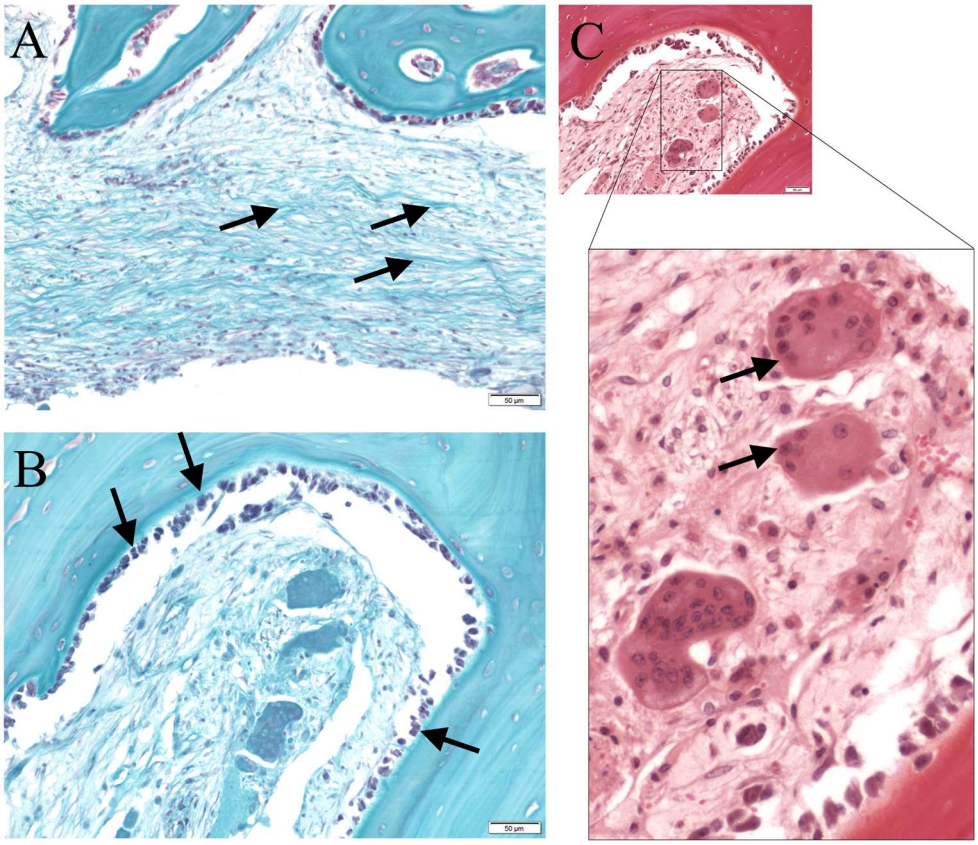

Figure 28. Subchondral bone appearance at microscopy in Picrosirius red stained sections under polarized light microscopy (A-F) and in Toluidine blue O-Fast Green sections (G-H).

(A, C, E) Trabeculae showed a similar, organized birefringence under multiple angle of observation (classical pattern of birefringency).

(B, D, F) For 5 of 9 impact-stimulated and 1 of 9 ethanol-stimulated, we clearly saw a different pattern of trabeculae, with a higher proportion of red tissue (B and D: white arrows), surrounding the trabeculae. This tissue had a similar birefringence under different angle of observation, suggesting a non-parallel organization of constitutive collagen fibres. This red SB pattern was observed around the drill hole but also extended to other part of the section, until the subchondral plate (F: white arrows).

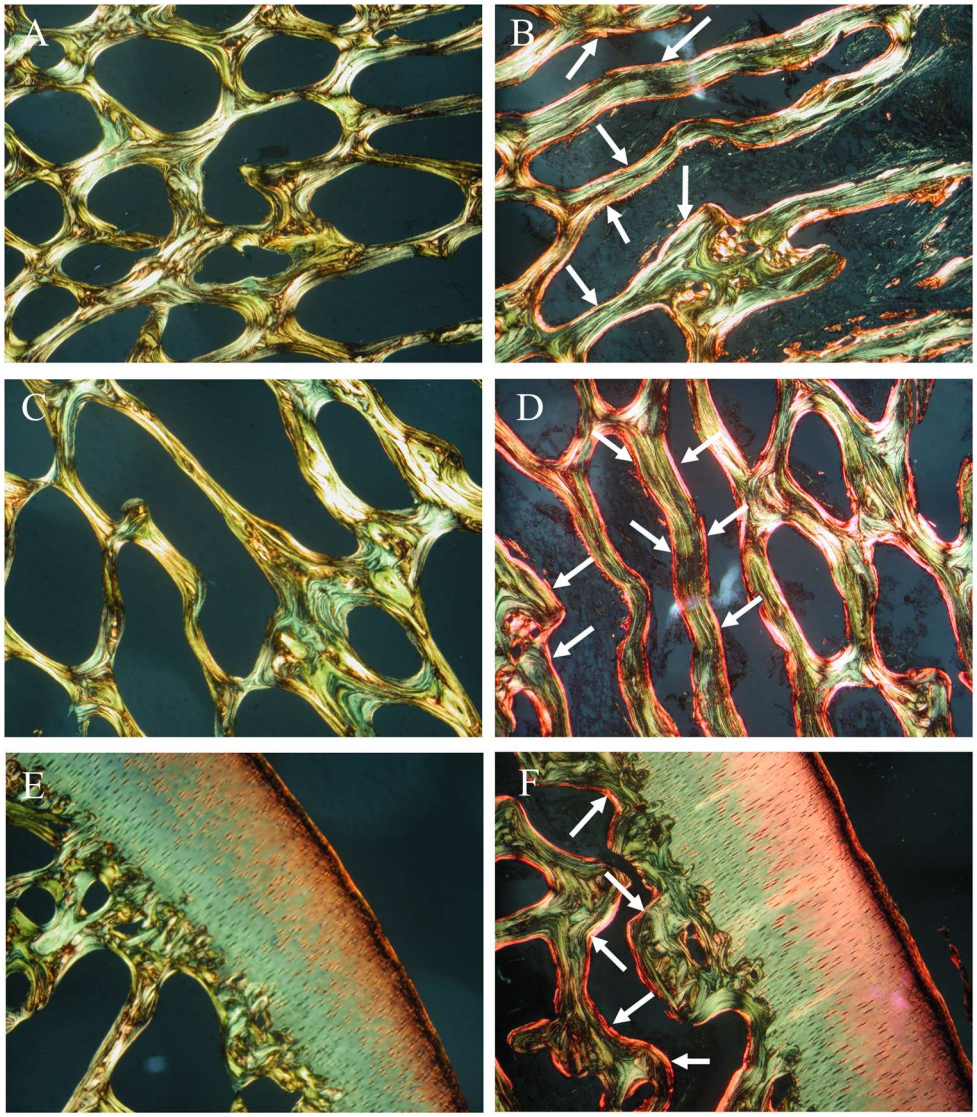

Figure 28-continue. Subchondral bone appearance at microscopy in Picrosirius red stained sections under polarized light microscopy (A-F) and in Toluidine blue O-Fast Green sections (G-H).

(G, H) These birefringency patterns (A, C, E and B, D, F) were associated with particular cellular patterns of the SB in the Toluidine blue O-Fast green sections. In the classical subchondral birefringence pattern (A, C, E), the trabecular space (G) was filled with some adipocytes (asterisk) and nuclei were flat (black arrows), suggesting small cell activity, whereas in the red SB pattern (B, D, F), the trabecular space (H) was filled with lots of osteoblasts with rounded nuclei (black arrows), suggesting higher cell activity than in the classical pattern.

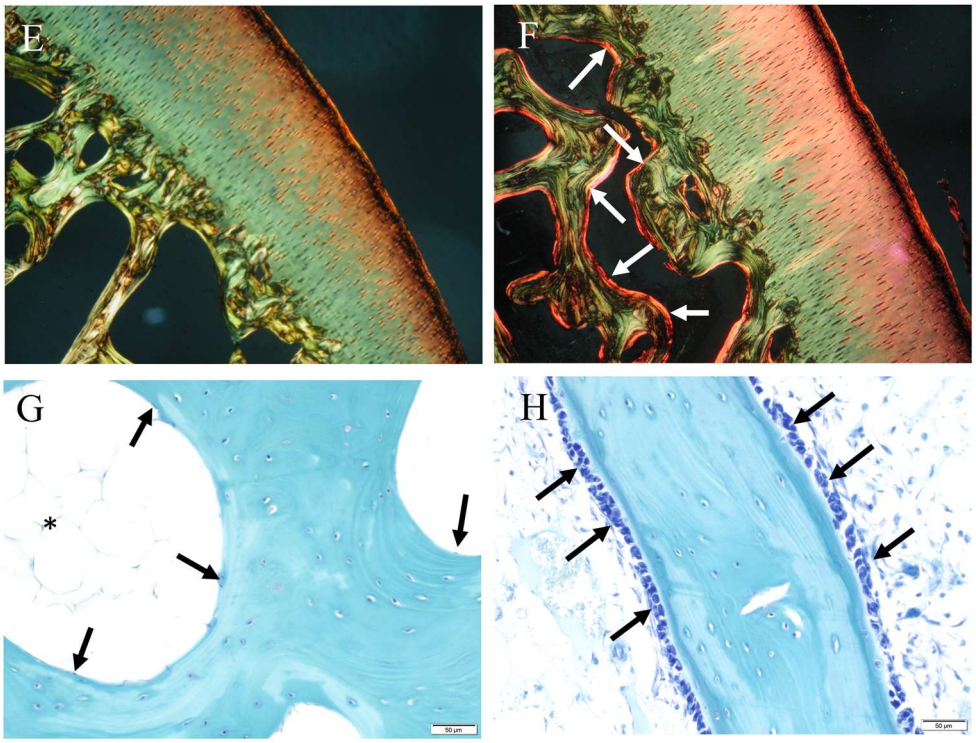

Figure 29. Immunohistochemical staining with antibodies against type II collagen (A-D), type I collagen (E-H) and aggrecan (I-L), respectively. (A-D) Anti-collagen II primary antibody was crossing with other collagens types, as seen by the staining of collagen II-rich tissues (hyaline cartilage (HC) and calcified cartilage (CC) in A), associated with the staining of collagen II-poor tissues (subchondral bone (SB) and fibrous tissue of the repair area (arrows) in B; interstitial tissue (IT) or vessel walls (V) in B). (E-H) Immunohistochemical staining of type-I collagen did not revealed any particular pattern in the bone (E, F). There was a slight cross-reaction between anti-collagen I primary antibody and type-II collagen, seen as a slight staining of the cartilage (E). The repair area (F) was stained, suggesting the presence of type-I collagen in this fibrous tissue. The immunohistochemical staining of the placenta. (I-L) Anti-aggrecan staining showed a slight staining of cartilage (I) with apparent cross-reaction with other structures as seen as staining of the SB (J), and vessels (V) and interstitial tissue (IT) of the placenta (L). Negative controls (C, G and K) for the three primary antibodies were obtained by omitting the primary antibody and allow the assessment of non-specific staining due to the IHC protocol itself (excluding the primary antibody). The negative controls were conclusive for all primary antibodies, showing very slight to no stain of the tissues.

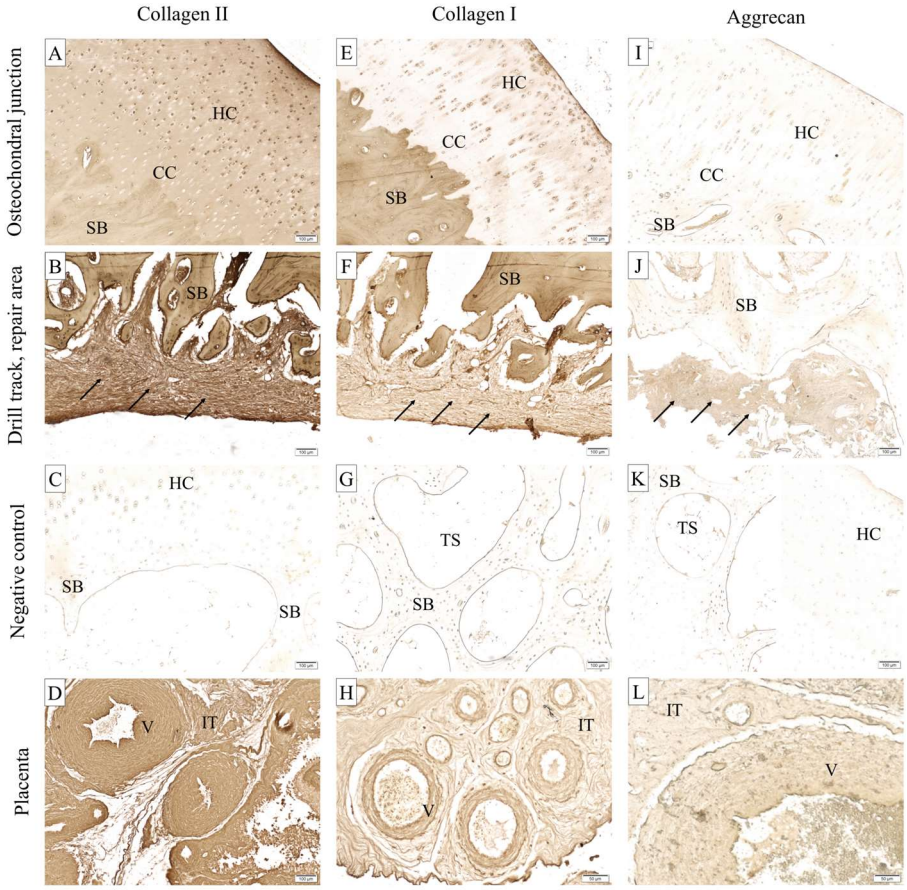

Biochemical composition of cartilage

Biochemical composition of cartilage (water, collagen, GAG, DNA) did not show significant differences between groups and between time-points. However, there was a trend toward decrease in water content overtime for both ethanol-stimulated and impact-stimulated limbs (Table 13).

Table 13. Detailed data for biochemical analysis of ethanol-stimulated and impact-stimulated limbs. Water content (% of wet weight, %WW) seemed to decrease overtime for both ethanol-stimulated and impact-stimulated limbs. GAG content (% of dry weight, %DW) showed a decrease with a minimum at 6-weeks post-stimulation for both stimulation models. Collagen content showed a decrease for ethanol-stimulated limbs overtime, whereas the collagen content for impact-stimulated limbs showed a more variable profile, as well as DNA content for both stimulation models. Because of trouble shooting with the day 0 sample of impact-stimulated limbs, DNA content for this time-point was not available (NA). Data are provided as mean +/- standard deviation.

	Ethanol-stimulated limbs					Impact-stimulated limbs				
	Day 0	Week 2	Week 4	Week 6	Week 8	Day 0	Week 2	Week 4	Week 6	Week 8
Water content (% WW)	71.5 +/- 1.5	63.5 +/-2.5	62 +/-1	63.5 +/-0.5	64 +/-7	67.5 +/- 0.5	59 +/-5	64 +/-3	58.5 +/-2.5	55.5 +/-0.5
GAG content (% DW)	18.55 +/- 2.25	13.1 +/-0.7	13.65 +/- 2.35	12.9 +/-1	16.2 +/- 2.6	10.3 +/-0	11.55 +/- 0.65	10.4 +/-0.4	8.05 +/- 3.05	10.35 +/- 3.65
Collagen content (% DW)	82.3 +/-0	84.7 +/-8.2	72.25 +/- 9.35	70.45 +/- 11.75	61.2 +/- 11.1	59.65 +/- 4.55	89.8 +/- 5.6	74.6 +/-7.3	70.5 +/-1.4	69.85 +/- 13.85
DNA content (% DW)	0.039 +/-0	0.036 +/- 0.008	0.0375 +/- 0.0065	0.0315 +/- 0.0015	0.044 +/- 0.001	NA NA	0.066 +/-0	0.034 +/- 0.009	0.069 +/- 0.025	0.0325 +/- 0.0035

6.4 Discussion

Several salient changes were identified after stimulation of the SB by chemical (ethanol) or mechanical (impact) technique: alteration of SB at micro-CT, alteration of cartilage at microscopy (OARSI scores, Red Color Index, Picrosirius red score), changes in SB activity at microscopy and slight decrease in water content of cartilage. However, these changes were not statistically significant due to the small number of sheep for each time-point and technique of stimulation. Nevertheless, our study highlighted interesting insight of the SB stimulation model.

Drill track was the site of bone repair. It was still detectable at 8 weeks post stimulation. This is consistent with previous observations made by authors performing drill hole for injection of ethanol, who still see the drill track at X-Ray 12 weeks after stimulation (Manggold et al., 2002). The drill track was partially filled with fibrous tissue, with multinucleated giant cells. These cells have not been described in the repair tissue of previous studies (Manggold et al., 2002; Zhu et al., 2011). The multinucleated giant cells have been recently described in the SB and the synovium, surrounding fat cells, in patients suffering from OA and rheumatoid arthritis (Prieto-Potin et al., 2015). This suggests that the stimulation of SB, by either mechanical or chemical stress, is associated to presence of cells, associated with OA or rheumatoid arthritis condition. The further characterization of these cells would require TRAP (Tartrate-resistant alkaline phosphatase), RANK (receptor activator of NF-κB) and OPG (osteoprotegerin) immunostain to further describe their function. Theses immunochemical staining can assess healing, remodelling, and osteoclastic activity (Baharuddin et al., 2015; Prieto-Potin et al., 2015).

The change in SB pattern after stimulation, with an increased number of osteoblasts along the trabeculae and the presence of non-organized tissue along the trabeculae, suggests bone remodelling. Ethanol injection in the femoral head has been proved to induce trabecular resorption and appositional bone formation (Manggold et al., 2002). Moreover, load impact of the SB has been recognized to induce a significant increase in the number of osteoblasts (Lahm et al., 2006). We could hypothesize that the osteoblasts are responsible for the production of the less organized layer of bone visible under polarized light microscopy, meaning an activation of bone modelling or remodelling. Moreover, the high number of TUNEL positive cells in the SB of 5 of 9 impact-stimulated limbs, suggests apoptosis of osteocytes that is known to activate bone remodelling (Herman et al., 2010).

These histological changes seem also to be responsible for the changes observed at micro-CT.

Changes of subchondral micro-architecture after stimulation showed that the increase in apparent bone density at 4 weeks was associated to changes in trabecular thickness, trabecular separation, trabecular number, specific surface of bone, degree of anisotropy and structure model index. The significant decrease in specific surface (BS/BV) at this time-point for both type of stimulation also reflects the change in structure thickness and complexity, while the decrease in anisotropy and structure model index reflects the changes in architecture. The increase in trabecular thickness and bone volume fraction is a feature of SB in OA in man (Kamibayashi et al., 1995). Changes in the trabecular thickness (from 161µm for control SB to 259µm for stimulated SB) was in the range of what has been described in man (from 146 µm for human control SB to 243 µm for OA human SB), whereas the changes in bone volume fraction (from 39% for control SB to 56% for stimulated SB) were slightly lower (from 29% for control SB to 54% for stimulated SB) (Kamibayashi et al., 1995), Our control values of bone volume fraction and trabecular thickness were consistent with previously reported values (Orth et al., 2012; Chevrier et al., 2014). All these micro-architectural changes in trabecular thickness and bone volume fraction after stimulation suggest that the sheep could mimic SB changes during OA in human.

Changes in SB micro-architecture and histology could be responsible for further changes in cartilage. SB is known to distribute mechanical loads in the joint (Li et al., 2013). Alteration of SB micro-architecture has been proved to be associated with changes in mechanical properties (Goldstein et al., 1993; Day et al., 2001), leading to secondary cartilage damages

(Goldring and Goldring, 2010). In our study, the SB changes were not statistically correlated to histological scoring for cartilage assessment. However, it is possible that the time-frames of SB changes and cartilage changes are different, explaining the absence of statistical correlation, even though the sample size for each time-point was small. Besides these observations, some histological outcomes correlated with each other. Toluidine blue scoring assesses the proteoglycan content of cartilage (Little et al., 2010), as Red Color Index does (Mickievicius et al., 2015). However, Toluidine blue scores increases when proteoglycan content decreases (Little et al., 2010), whereas Red Color Index decreases with loss of proteoglycans (Mickievicius et al., 2015). This explains the negative correlation coefficient between Toluidine blue scores and Red Color Indexes we found. The correlation between Toluidine blue scores and total score for cartilage assessment ($r = 0.5470$; $P=0.00015$) suggests that most of the change in total score was attributed to Toluidine blue score changes.

Histologic assessment also showed a different evolution of histological scores for ethanol- and impact-stimulated limbs. For ethanol-stimulated limbs, the decrease in Red Color Index and Picrosirius red score associated with an increase in total score for cartilage assessment reflected increasing damage of cartilage overtime, with loss of proteoglycans (decrease in Red Color Index) and a loss of tissue organization (decrease in Picrosirius red score). This suggests that ethanol-stimulation of SB is detrimental for cartilage, as previously seen in models of osteonecrosis of the femoral head (Manggold et al., 2002; Zhu et al., 2011). The impact stimulation of the SB showed opposite effects, with decrease in total score for cartilage assessment and an increase in Picrosirius red score and Red Color Index in Safranin O-Fast Green sections. This interestingly suggests a positive effect of SB impact.

Finally, in our study, we did not highlight macroscopic changes of cartilage at all time-points. The absence of change in cartilage appearance at macroscopy even 8 weeks after ethanol injection is consistent with previous report in sheep and goats (Manggold et al., 2002; Zhu et al., 2011). In goats, although cartilage surface was intact at 8 weeks post-injection of 10 ml of absolute alcohol, local loss of lustre was visible in 5 of 6 articular surface of the femoral heads 12 weeks after injection, and cartilage defects were observed at 25 weeks post-injection (Zhu et al., 2011). The absence of macroscopic changes in cartilage, even in presence of microscopic structural damages, could be explained by the potential induction of cartilage damages during histological processing. Indeed, histological process includes fixation, decalcification, paraffin embedding (with dehydration of the tissue), softening of the tissue block, slicing, drying, deparaffinization and staining. Some of these steps can be responsible for artefacts such as disruption, folds, tearing, holes, wrinkling (Hacker et al., 1997; Melrose et al., 2004; Bindhu et al., 2013; Chatterjee, 2014). All of these steps could enhance pre-existing structural micro-damages of cartilage (not visible at macroscopic assessment) and lead to enhanced cartilage changes at microscopic examination. This could partially explain the absence of macroscopic changes even when microscopic structural damages are present.

Our study had several limitations. Firstly, this study is characterized by a small sample size and a relative short observation delay. It could be argued that we would probably get more significant results and greater cartilage changes with higher sample size and longer follow-up, since studies about osteonecrosis of the femoral head showed visible cartilage alterations at later time-points than 8 weeks of follow-up. However, this study aimed at describing early changes after SB stimulation. The aim was not to develop major bone or cartilage necrosis. This also justified the relatively small volume (2ml) of ethanol we used, injected in the medial femoral condyle compared to study injecting ethanol in the femoral head (8-10ml) to induce

osteonecrosis of the femoral head in sheep and goats (Manggold et al., 2002; Zhu et al., 2011).

Secondly, the problems encountered with immunohistochemistry (i.e. cross reactivity) could be attributed to the use of formic acid as a decalcifying solution. Strong acids (i.e. hydrochloric acid) are not suitable for osteochondral samples decalcification since they induce hydrolysis of cartilage matrix (Melrose et al., 2004) and subsequent loss of stain and problem of interpretation of Toluidine blue score for example. Slow-acting chelating agent (namely, ethylene-diaminetetracetic acid: EDTA) is known to preserve fine cell structures and antigenic epitopes (Callis and Sterchi, 1998). However, prolonged stay in EDTA has been proved to induce proteoglycan loss in cartilage (Campo and Betz, 1987; Callis and Sterchi, 1998; Melrose et al., 2004). In our case, decalcification of ovine osteo-chondral samples required up to 10 weeks decalcification in EDTA (data not shown, preliminary tests on 10 osteochondral samples) with concurrent loss in stain intake. Organic acid decalcification (formic acid) was therefore preferred to limit proteoglycan loss during decalcification. Moreover, the formic acid decalcification has already been done on ovine osteochondral samples with adequate stain intake of the cartilage (Melrose et al., 2004). Bad results with immunohistochemistry (non-specific staining; no staining) could be related to decalcification protocol, but also to other processing steps such as antigen retrieval or use of an inadequate primary antibody (not crossing with ovine collagen, or not specific of particular type of collagen).

Finally, this study also emphasized that stimulation of the subchondral bone leads to a low score of lameness (score 1) after ethanol or impact stimulation. This low score of lameness is consistent with other referenced paper for injection of ethanol to mimic osteonecrosis of the femoral head (Manggold et al., 2002; Zhu et al., 2011) and to impact in dogs (Mrosek et al., 2006). This suggests that pain management was adequate, even if the lameness was present. Pain management could have included anti-inflammatory drugs to reduce lameness (Manggold et al., 2002). However, this would have change the potential reaction to stimulation of the SB and biased the study. Moreover, as we were studying the SB stimulation as a primum movens of cartilage changes in the process of osteoarthritis, recognized as an inflammatory disease (Berenbaum, 2013), use of anti-inflammatory drugs was therefore prohibited.

6.5 Conclusion

Extra-articular stimulation of the SB either mechanically (impact) or chemically (ethanol injection) induced micro-architectural changes, that have been previously associated to OA. This stimulation tended to induce microscopic alterations of cartilage that seemed to be different in ethanol-stimulated (deterioration), in impact-stimulated limbs (healing), overtime.

7. Can MRI T2 mapping and compositional CT be used to identify those early structural or compositional changes ?

7. Can MRI T2 mapping and compositional CT be used to identify those early structural or compositional changes ?

Mechanical or chemical extra-articular stimulation of the SB induces detectable alterations of SB and cartilage assessed either by micro-computed tomography or by histology and by biochemistry. Increase in bone volume fraction (or bone apparent density), and trabecular thickness were significant 4-weeks after stimulation. These changes have been described in the course of OA (Radin, 1986; De bri et al., 1995; Bobinac et al., 2003; Burr, 2004; Hayami et al., 2006) and suggested to promote cartilage damages. In this series of 18 sheep, cartilage showed a progressive alteration after ethanol stimulation, with an increase in total OARSI score for cartilage assessment, a decrease in Red Color Index and a decrease in Picrosirius red score. Biochemistry also showed a decrease in water and GAG content.

These invasive assessments are not feasible in clinical practice or in longitudinal studies in living animal because they require excision of tissue that would be detrimental for the joint. Therefore, it is crucial to detect these changes noninvasively, using for example, imaging techniques.

7.1 Material and methods

Imaging the ovine knee

The eighteen ewes were imaged at several time points. We performed pre-stimulation imaging and post-stimulation imaging (at time-point corresponding to the euthanasia of animals, namely: Day 0, 2, 4, 6 and 8 weeks post-stimulation). The protocol included a T2 mapping, a TSE sequence, a blank-CT (CT without contrast medium), and a contrast-enhanced CT.

For T2 mapping and TSE sequence, both knees (left and right) were scanned using high-field 3 Tesla (3T) MR (Verio, Siemens, Erlangen, Germany). The sheep was placed in sternal recumbence, hindlimbs were extended caudally, toward the magnet. A 15-channel-knee coil (Siemens) was used and the targeted limb was maintained in extension with a 5-kg load. The acquisition was performed in 2D, in the sagittal plane. Field of view extended from the base of the patella to 4 cm below the tibial plateau. The sequence parameters were: repetition time: 1420 ms, average number: 2, flip angle: 180, echo number: 5, space between slices: 4.4, slice thickness: 4.0mm, pixel size was: 0.2x 0.2 mm, matrix 512 x 512. The six echo times to perform the T2 mapping were: 15.7 ms, 31.4 ms, 47.1 ms, 62.8 ms, 78.5ms 94.2 ms. The TSE sequence was acquired with the following parameters: repetition time: 3300 ms, echo time: 48 ms, average number: 1, flip angle: 150, space between slices: 4.4, slice thickness: 4.0mm, pixel size was: 0.2x 0.2 mm, matrix 512 x 512. The total length of the sequences was 25 minutes.

After T2 mapping, the sheep was transferred to the CT room. Both knees were imaged with an Emotion 6 scan (Siemens, Erlangen, Germany). The targeted limb was extended caudally and maintained with a 5-kg load, while the other limb was extended cranially and maintained with a roller bandage. This position allowed the knee to lay down in the centre of the gantry. Acquisition parameters were: 130 kVp, 80 mAs, helicoidal/sequential acquisition, pitch factor: 0.4, collimation of 0.63mm, revolution time: 0.6s. Field of view was similar to T2 mapping field of view. The transverse resolution was 0.20 x 0.20 mm. Slices of 0.63 mm were reconstructed with an increment of 0.3 mm resulting in an overlap between the different slices and a resultant longitudinal resolution of 0.3 mm without gap. The voxel size was 0.2x0.2x0.3mm. Images were then transferred on a medical digital imaging system (PACS, Télémis, Louvain-La-Neuve, Belgium). Images were reconstructed using bone algorithm and stored until analysis.

For contrast CT, the parameters were the same as those used for blank images. The CTA injection was performed in the femoropatellar compartment of the stifle, using the retropatellar technique. Synovial fluid was collected, if present. Twenty millilitres of a mixture of 6 ml contrast medium Ultravist 370 mg (Iopromide 768.86 mg/ml, equivalent iode 370 mg/ml, Bayer NV, Diegem, Belgium) and 14 ml of NaCl 0.9% (Viaflo, Baxter, Lessines, Belgium) was subsequently injected. The joint was flexed and extended 100 times to ensure a good spreading of the contrast medium. Finally, the limb was imaged with the same acquisition parameters as the blank CT.

Image analysis

MRI images were transferred to the workstation and processed to extract T2 values (OsiriX). These images were assessed on a diagnostic workstation (Telemis HE Viewer 4.3). For T2 mapping analysis, the colour scale was set up with a window level of 60, and window width of 120. With these settings, the colour scale ranged from blue (shorter T2 relaxation time) to red (longer T2 relaxation time). Automatic calculation of T2 values (mean +/- standard deviation) of cartilage was performed by drawing polygonal regions of interest. These regions of interest were centered on the middle part of the medial femoral condyle (FCM2), on the two successive images (4 mm-thick) abaxially to the insertion of the posterior cruciate ligament. The TSE sequence was used as a control to ensure that only cartilage was included in the region of interest. T2 values (mean+/-standard deviation) were recorded for further analysis.

Contrast-enhanced and blank CT images were also transferred to the workstation for further reconstruction. Slices of 0.63 mm were reconstructed with an increment of 0.3 mm resulting in an overlap between the different slices and a resultant longitudinal resolution of 0.3 mm without gap. Voxel dimensions were 0.20 x 0.20 x 0.30 mm. Image analysis was performed on the diagnostic workstation (Telemis HE Viewer 4.3). Automatic calculation of cartilage attenuation (mean +/- standard deviation) was performed by drawing polygonal regions of interest on the middle third of the medial femoral condyle. The post-contrast images and the pre-contrast images were compared, side-by-side, to find a similar assessment plan (same sagittal plan) (Figure 30). A similar region of interest was drawn on the pre-contrast image (AC_{Blank}) and on the post-contrast image ($AC_{Contrast}$), to get the mean attenuation of cartilage. The mean attenuation of cartilage on the pre-contrast image was substracted to the mean attenuation of cartilage on the post-contrast image ($AC_{Contrast} - AC_{Blank}$). A polygonal region of interest was also drawn on the contrast fluid filling the synovial cavity of the post-contrast

injection image (CF) to provide a normalized attenuation ratio between the calculated attenuation of cartilage and the attenuation of the injected contrast fluid (= ($AC_{Contrast}$ - AC_{Blank}) / CF) (Kokkonen et al., 2012). A direct cartilage:contrast attenuation ratio was also calculated for post-contrast images (= $AC_{Contrast}$ /CF). The calculation of both outcomes (normalized attenuation ratio and direct cartilage:contrast attenuation ratio) was performed on three images and the mean of this three assessments was used for statistics analysis.

Statistics

All data were tested for normality (Shapiro-Wilk normality test and D'Agostino & Pearson normality test). Multiple comparisons among groups were performed with ANOVA, or Kruskal-Wallis test provided non-normality of the data distribution be detected. Comparison between two groups were performed with unpaired t-test, or Mann-Whitney test provided non-normality of the data distribution was detected. Correlation between invasive outcomes for cartilage (histology, biochemistry, gross anatomy) and imaging outcomes (T2 mapping, CECT) were assessed by Spearman or Pearson correlation coefficient, depending on the normality distribution of the data. Statistical analysis was computed with GraphPad Prism 7.04 for Windows (GraphPad Software, La Jolla California USA, www.graphpad.com).

7.2 Results

T2 values of cartilage ranged between 54 ms and 105 ms for ethanol-stimulated limbs, between 46 ms and 88 ms for impact-stimulated limbs, between 39.5 ms and 51 ms for control limbs.

For CECT (Figure 30), the normalized attenuation ratio (= ($AC_{Contrast}$ - AC_{Blank}) / CF) values ranged between 0.040 and 0.072 for ethanol-stimulated limbs, between 0.014 and 0.087 for impact-stimulated limbs, between 0.057 and 0.174 for control limbs. The direct cartilage:contrast fluid attenuation ratio ($AC_{Contrast}$ / CF) ranged between 0.078 and 0.128 for ethanol-stimulated limbs, between 0.092 and 0.197 for impact-stimulated limbs, between 0.097 and 0.243 for control limbs.

No significant differences were found between groups and/or between time-points, neither for T2 values, nor for CECT values.

Correlation between T2 values and invasive outcomes (histological scores and biochemical composition assessment of cartilage) showed only two weak correlations between T2 values and Toluidine blue scores ($r = -0.4193$; $P = 0.0369$); T2 values and water content ($r = 0.2240$; $P = 0.0241$) (Figure 31).

T2 mapping clearly showed a zonal increase in T2 value in the caudal part of the femoral condyle (Figure 33), corresponding to magic angle artefact. This artefact is associated with organized connective tissues such as tendons, ligaments and cartilage (Stadler et al., 2007). It is represented as a progressive increase in T2 value, when collagen fibres are oriented +/- 55° to the main magnetic field. The magic angle was mainly visible on the caudal third of the femoral condyle (Figure 32). In our study, it was visible on both control and contralateral stimulated limb.

Moreover, the slice thickness (4 mm) was responsible of volume averaging in some of the T2 images (Figure 33).

Oedema was visible around the drill track on the anatomical views (Figure 33), for all the drilled limbs at 2 and 4 weeks post-stimulation, half of the limbs 6 weeks after stimulation, and only the two ethanol-stimulated limbs at 8 weeks post-stimulation.

Figure 30. Example of CECT images and CECT regions of interest drawn for calculations. Pre-contrast injection (A) and post-contrast injection (B) images were assessed side-by-side. The section landmarks were set to be similar in both images. Sagittal plan was assessed. A first region of interest was drawn in the post-contrast injection image (B), at the cartilage level of the middle third of the medial femoral condyle, to compute the mean attenuation of cartilage in Hounsfield unit ($AC_{Contrast}$). A similar region of interest was drawn in the pre-contrast injection image (AC_{Blank}). A region of interest was also drawn on the contrast fluid of the post-contrast injection image (B) to normalize the X-ray attenuation (CF). The values were recorded, the normalized attenuation of cartilage was calculated (= ($AC_{Contrast}$ - AC_{Blank}) / CF), as well as the direct cartilage:contrast attenuation ratio (= $AC_{Contrast}$ / CF)

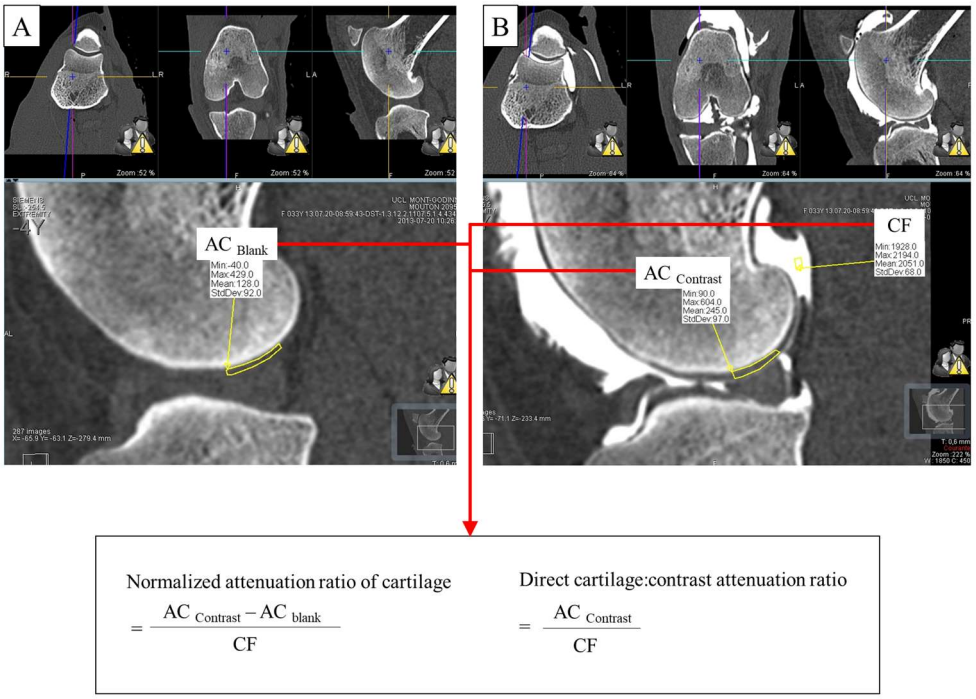

Figure 31. Correlation graphs between T2 values and Toluidine blue scores (A); and water content (B). Although significant, the correlation between T2 values and invasive outcomes is weak.

(A) Increase in Toluidine blue scores (reflecting loss of proteoglycan) was weakly correlated to T2 relaxation time values for cartilage (r = - 0.4193; P = 0.0369). The negative correlation suggests that the loss of proteoglycans (increase in Toluidine blue score was associated to a decrease in T2 value, potentially associated to loss of water.

(B) The correlation between water content and T2 relaxation time values for cartilage was weak, as well (r = 0.2240; P = 0.0241). The positive correlation indicated that the increase in water content was associated with an increase in T2 relaxation time value.

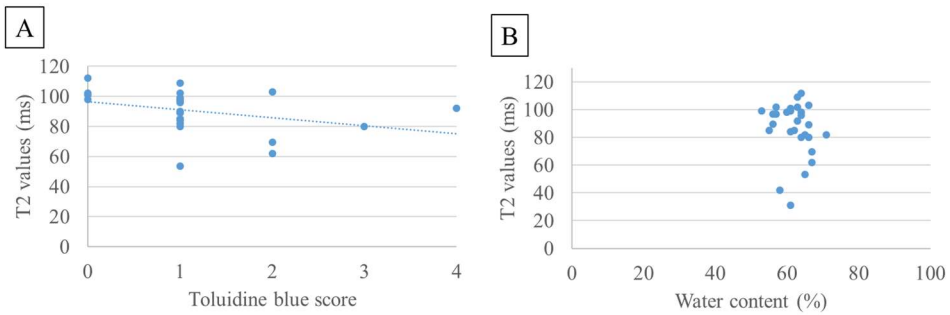

Figure 32. Schematic representation of the magic angle artefact. (A) The sheep was in sternal recumbence. The hindlimbs were caudally extended, the forelimbs were pushed forward. Distal extremities were covered with gloves to avoid contamination of the environment. (B) Representation of the limb, inside the magnet, extended caudally. The limb was maintained in extension by a load. (C) The direction of the main magnetic field is represented (B_0 direction). The magic angle artefact is known to be maximal when fibres are aligned at 55° to the main magnetic field. This angle (red) is not limited to a particular plan, and is therefore present in the different planes (multiple red angle). The perimeter of each disc represents the area of maximal magic angle artefact occurring in the space. (D, E) In the knee, the magic angle can occur in the femur, for example, at the level of the femoral condyles. The coronal (D) and sagittal (E) plane are exampled here. The position of the limb, in caudal extension with a load, shows that the caudal part of the femoral condyle is susceptible to magic angle artefact. In the coronal plane, this artefact can be seen in the more axial part of both femoral condyles.

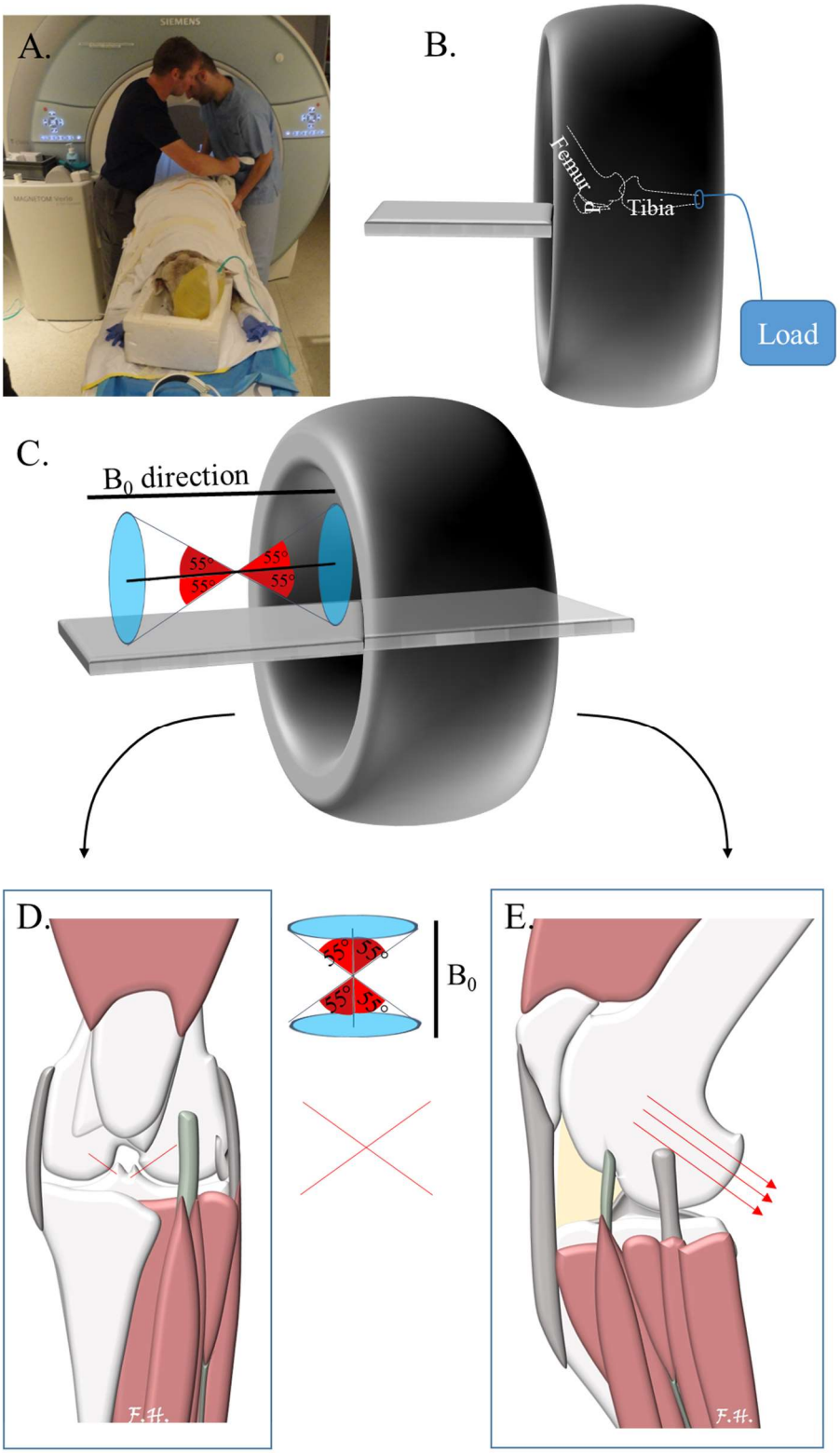
A.
B.
Femur
Tibia
Load
C.
B_0 direction
55°
55°
55°
55°
D.
E.
B_0
F.H.
F.H.

Figure 33. Example of MR images: (A) anatomical view; (B-C) T2 mapping.

(A-B) These images show a volume averaging at the level of the tibial eminence and at the level of the femoral condyle (rectangle). In this area, the signal of each pixel represents a 4mm-depth block, with a mixture of tissues (cartilage, SB, menisci) and therefore an intermediate signal. (A)

In this image, the reaction around the drill track (arrows) is clearly visible.

(C) The cartilage appearance shows an increase in T2 values, represented as a yellow-to-red area (arrows). These areas are aligned along the 55°-axis to the main magnetic field (dotted line). The increase in T2 value in these areas is therefore associated to a magic angle artefact.

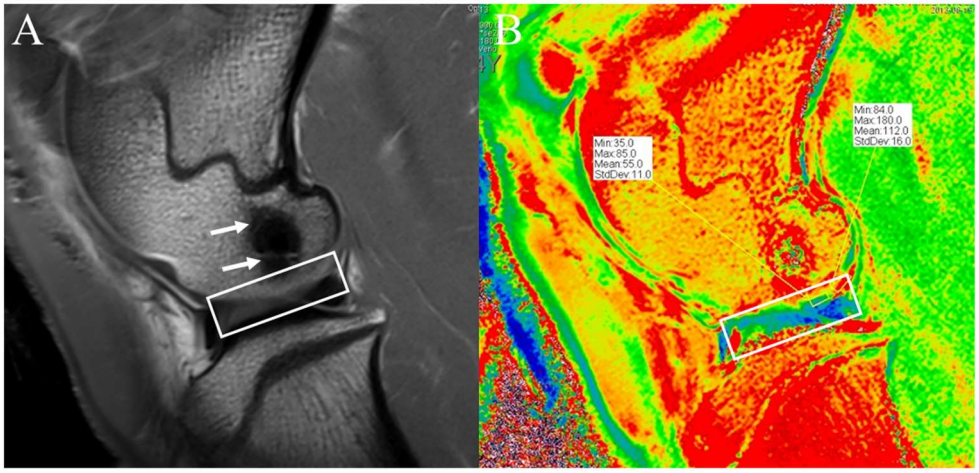

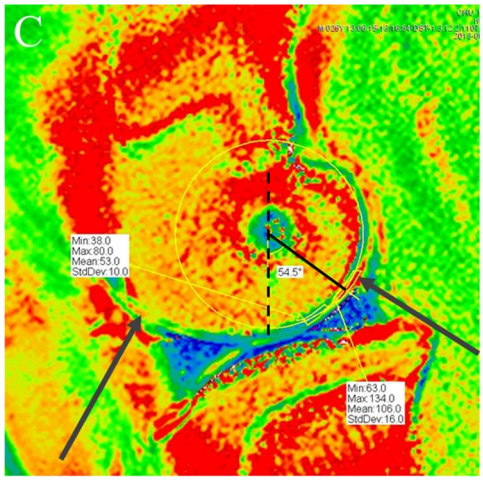

7.3 Discussion

SB has been suggested as one of the primum movens of OA, preceding and promoting cartilage alterations (Blair-Levy et al., 2008; Zhang et al., 2016). In this study, we hypothesized that cartilage changes induced by mechanical or chemical stimulation of the subchondral bone would be visible with T2 or CECT imaging techniques. We also wanted to test the feasibility of T2 mapping *in vivo* in the ovine knee. We found that the T2 mapping and CECT of the ovine knee did not show any significant changes in cartilage at the different time-points, for ethanol- or impact-stimulated limbs. The imaging outcomes (T2 values, CECT attenuation values and CECT cartilage:contrast fluid attenuation ratio) correlated slightly with invasive assessment of cartilage, with unexpected correlations, such as the correlation between T2 values and Toluidine blue score; T2 values and water content, and CECT cartilage:contrast fluid attenuation ratio and Picrosirius red score. These correlations are conflicting with the major description of T2 mapping and CECT imaging.

T2 mapping is known to reflect the hydration, the orientation of collagen fibrils and collagen concentration in cartilage (Lüsse et al., 2000; Watrin et al., 2001; Menezes et al., 2004). T2 mapping has previously been used to monitor cartilage repair (after (osteo-)chondral transplantation, for example) in longitudinal studies in horses (White et al., 2006; Powdner et al., 2011), in sheep (Friske et al., 2012), or in man (Welsch et al., 2010). It has also been used to assess the cartilage maturation process in young to old rats (Watrin et al., 2001). It has been correlated to Picrosirius scores for cartilage organization in horses (White et al., 2006), or to the presence of cartilage defects in man (Apprich et al., 2010). The correlation between water content and T2 mapping has been established in human osteochondral samples of patient scheduled for total knee replacement surgery. In that trial, the T2 values were correlated to water content with an r^2 of 0.51 (for femoral cartilage) to 0.77 (for tibial cartilage) (Lüsse et al., 2000). In our study, the correlation between T2 values and water content was poor ($r = 0.22$). These results could be explained by the limited changes in water content in our study, compared to the changes that could be assessed in very diseased patients scheduled for total knee replacement. In our study, the T2 values were correlated to Toluidine blue scores. This is unexpected. However, we could hypothesize that the proteoglycans loss (increase in Toluidine blue score) could be combined to a loss of water, imaged as decreased T2 values.

For MRI, the lack of correlation with invasive outcomes could also be explained by the image quality. In our study, the T2 mapping of cartilage was acquired with a slice thickness of 4mm. A large slice thickness increases the risk of partial volume artefact (Stadler et al., 2007). This artefact is due to the presence of different tissue in the same voxel. It can occur if the voxel size (the product of the in-plane pixel size by the slice thickness) is relatively high in comparison to the thinness of the structure to image. In our case, the 4-mm slice thickness increases the risk of calculating a T2 value for cartilage and for an additional tissue of the 3-mm thick block, i.e. synovial fluid, SB, or menisci, leading to an artefactual increase (if synovial fluid is enclosed) or decrease (if subchondral bone is enclosed) of T2 value. Although thinner slices would have reduced the risk of partial volume artefact, the increase in acquisition time and the decrease in signal-to-noise ratio would have been detrimental for image analysis (Stadler et al., 2007).

The magic angle artefact is also a concern when imaging organized tissues. It is related to the water relaxation time inside organized collagen fibril network. For example, in the radial zone of cartilage, the collagen fibrils are highly aligned and perpendicular to the SB, restricting water motion. This results in short T2 relaxation time (Mosher et al., 2000; David-Vaudey et al., 2004). However, when the collagen fibrils are oriented 55° relative to the main magnetic field (B_0), this restriction is limited and the relaxation time increases. In the radial zone, T2 relaxation time has been described to increase up to 80% with the direction of the main magnetic field *in vitro* (Xia, 1998) and up to 30% *in vivo* (Mosher et al., 2001). This phenomenon seems to be problematic for cartilage imaging. However, interestingly, the presence of the magic angle artefact at the 55° angle also reflects the presence of highly organized, parallel collagen fibers, while its absence at 55° would suggest lack of collagen fibers organization, and therefore an alteration of cartilage integrity. In our study, the comparison between control limbs and contralateral stimulated limb, showed that the magic angle was present in both limbs, suggesting that the alteration of collagen network described at histology would not be sufficient to change the appearance of cartilage on T2 images.

Noninvasive imaging assessment of GAGs includes dGEMRIC (Bashir et al., 1996; Bashir et al., 1999; Trattnig et al., 1999; Miyata et al., 2006; Xia et al., 2008) and CECT (qCT) (Kallionemi et al., 2007; Aula et al., 2009; Bansal et al., 2010). The dGEMRIC technique requires the injection of gadolinium-based contrast medium that is able to decrease the T1 relaxation time of the accumulating tissue (Bashir et al., 1996; Bashir et al., 1999; Gold et al., 2003; Koulouris, 2006; Gray et al., 2008; Gold et al., 2009). Pre-contrast and post-contrast acquisitions are required, to compare the T1 values before and after (potential) penetration of the contrast medium in the tissue, namely the GAG-depleted cartilage. We did not implement this technique to our protocol since the time-delay is relatively long (60 to 90 minutes) and would require additional anaesthesia of the sheep. We therefore chose the CECT. This technique is faster since it requires a short time-delay (5-10 minutes) between pre-contrast injection acquisition and post-contrast injection acquisition (Siebelt et al., 2011; Stewart et al., 2013). This technique relies upon the penetration of negatively charged contrast medium when GAGs loss has occurred (Cockman et al., 2006; Bansal et al., 2010; Kokkonen et al., 2011). In our case, the CT attenuation values for cartilage did not correlate to biochemically- or histologically-assessed GAGs content.

Our study aimed to use clinical devices (3-T MRI and CT scan) available in clinic to perform imaging assessment of biochemical changes in cartilage. The use of an *in vivo* model, under anaesthesia, limited our possibility to increase duration of MR sequence in order to increase image quality, or to perform multiple acquisitions (i.e. coronal and sagittal plane acquisitions). Moreover, an *in vivo* study limits the possibility for positioning the structure of interest in comparison to an *ex vivo* study on cadaver joints or osteochondral samples, allowing various and repeatable positioning, without dealing with individual particularities, or anatomic characteristics of the hole body. For the ovine knee, we have shown that the presence of the pelvic cavity together with the knee inside the CT gantry affects the CT image quality. The pelvic cavity is crossed by the X-ray beam before reaching the detectors, leading to a signal attenuation (Hontoir et al., 2017). A similar condition occurs when imaging a human patient with large body mass (Yoshimura et al., 2006).

Moreover, it should be remembered that biochemistry or histology assess only one component per analysis, and therefore provide an information about the change of this

particular component, whereas the compositional imaging techniques (T2 mapping or CECT) has been proved to correlate to more than one component. For example, T2 mapping has been correlated to water content, collagen content, but also collagen organization (Lüsse et al., 2000; Watrin et al., 2001; Menezes et al., 2004), while CECT values have been proved to be higher in GAG-rich cartilage, but also in cartilage with higher collagen cross-links (Kokkonen et al., 2011).

To conclude, compositional imaging techniques (T2 mapping and CECT) are feasible in living sheep, although some compromise should be accepted regarding image quality. Nevertheless, the correlation between *in vivo* imaging (reflecting the signal of the tissue itself) and the invasive assessment (representing individual components of the tissue) was not confirmed in this study.

8. Conclusion and perspectives

8. Conclusion and perspectives

OA is a major concern in human and veterinary medicine, with high direct and associated cost for man but also for animals. OA is more and more recognized as an organ disease, with implication of the different components (cartilage, SB and synovium) and potential initiation of the disease in these three tissues. Cartilage has been presented as the critical tissue for OA initiation, but SB and synovium are increasingly suggested as the primum movens for OA, promoting cartilage changes.

Early detection of cartilage changes is crucial since cartilage has limited ability to repair because of its avascularity and the subsequent reduced access for regenerative cells or for chondrocytes to migrate to the damaged area. Imaging techniques, such as radiography, ultrasonography and arthroscopy, are useful to provide assessment of the joint, with depiction of bone, synovium and intra-articular structures. However, these techniques have several limitations. They can be insensitive to early bony or cartilage changes, they provide incomplete assessment of the joint, and, for arthroscopy, they can require invasive access. The use of more advanced and noninvasive techniques, such as MRI and CT is therefore an alternative to detect early cartilage changes. Early changes in cartilage occur at a compositional level before structural changes become visible. MRI and CT compositional imaging would therefore be very useful to identify those changes.

In this context, this thesis aimed at assessing imaging techniques that would identify early and subtle structural and compositional changes of cartilage. To answer the research question, two strategies were chosen. Firstly we assessed CTA and MRI in two models of subtle naturally occurring cartilage defects, i.e. the equine MCP/MTP joint and the ovine stifle.

In this context, this thesis also aimed at assessing whether it was possible to induce, by a chemical or a mechanical insult of the SB, structural and compositional changes of the articular tissues that would be similar to those occurring in OA and that would be identified by noninvasive imaging modalities (CTA, MRI).

Firstly, MRI and CTA were compared in their ability to detect subtle cartilage defects in a series of equine MCP/MTP joint collected at a slaughterhouse and without evidence of articular disease. CTA demonstrated higher sensitivity (82%) and specificity (96%) than MRI (41% and 93%, respectively) to detect cartilage defects in the metacarpo-/metatarso-phalangeal joint. Very good agreement between observers was detected for both CTA (κ= 0.82) and MRI (κ= 0.88). A very recent study, also confirmed that CTA has the best sensitivity to detect cartilage defects in the horse (Suarez et al., 2018). In that study, the cartilage defects were not natural and had been created *ex-vivo*; the limbs were assessed by CTA, MRI, and by MRA. A series of 9 forelimbs (72 defects) were observed. CTA showed the best sensitivity (69.9%) followed by MRA (53.5%) and MRI (33.3%). In the equine carpus, the cartilage is thin, with thickness ranging between 0.17mm and 1.2 mm. The thin cartilage thickness, associated with multiple curvatures of natural cartilage surface of the bones of the carpus was responsible, for volume averaging, potentially explaining the slight difference between the sensitivity reported by those authors and the one we found in our study in the metacarpo-/metatarso-phalangeal joint.

As CTA was found to be an adequate tool to detect subtle cartilage defects (Hontoir et al., 2014; Suarez et al., 2018), we implemented this technique in our animal model: the sheep. We proved that this technique is feasible *ex vivo*, but also *in vivo* with sheep under anaesthesia; and gives an accurate assessment of the cartilage defects in the ovine knee, with high sensitivity (81.8%) and high specificity (95.2%) (Hontoir et al., 2017). This technique was therefore considered as a useful tool to assess cartilage and include only animals with healthy cartilage at baseline in our experimentation in an ovine model.

Secondly, compositional MR and CT have been described as a selective representation of a cartilage component (Kallioniemi et al., 2007) and could therefore be considered as a very promising tool to identify compositional changes before structural changes have developed. However, our review of the literature (Hontoir et al., 2015) revealed the need for validation of these imaging techniques in veterinary medicine, in term of repeatability, intra and inter-agreement, but also acquisition and processing settings, optimization of sequences on clinical devices, and comprehensive assessment of the relation between tissue signal and internal changes. This review nevertheless identified T2 mapping as the technique that would be the more likely to identify compositional changes and the easiest to perform with available MRI units in our experimentation.

Thirdly, we attempted to induce joint changes by stimulation of the SB in an animal model, the ovine knee. We performed either mechanical (impact) or chemical (ethanol injection) stimulation of the subchondral bone and assessed whether changes occurred in SB and cartilage. Several salient findings deserve reporting and discussion. Both stimulation techniques induced an increase in bone apparent density (percent bone fraction) and in trabecular thickness, identified by micro computed tomography. These changes have previously been identified in OA course (Radin, 1986; Matsui et al., 1997; Bobinac et al., 2003). Very interestingly, in our study, histological characteristics tended to be different between both groups (ethanol versus impact).

Ethanol-stimulated limbs showed an increase in structure and total OARSI score for cartilage over time, whereas the Red Color Index and the Picrosirius score of cartilage showed a decrease. These changes are suggesting a progressive alteration of cartilage histological characteristics. This could be explained by the nature of stimulation: ethanol is known to induce tissue dehydration. Bone dehydration has been correlated to change in tissue mechanical properties with increased stiffness (Granke et al., 2015). Change in bone stiffness has been described to promote cartilage alteration (Radin et al., 1986). We could also hypothesize that the chemical stimulation by ethanol induced inflammation and promoted activation of SB cells (osteoblasts, osteoclast).

In impact-stimulated limbs, histological assessment showed the inverse trend, with a decrease in structure and total OARSI score for cartilage, and a concomitant increase in Red Color Index and Picrosirius score, suggesting an improvement of cartilage histological features over time. This might not be so unexpected since drilling bone has been used to stimulate healing. A surgical procedure called osteostixis has been used for example to treat proximal suspensory desmitis, where proximal third metacarpal/tarsal bone was drilled (Launois et al., 2009). It has been suggested that repair would be facilitated, notably by a physical access for cells, through the drill track (Specht & Colahan, 1990; Launois et al., 2003). Another procedure to stimulate cartilage repair is micro-picking where microfracture of the SB is

induced. The basics are to create perforations in the SB, at the cartilage-bone interface ("intra-articular" SB access), after cartilage surgical debridement (Steadman et al., 2001). This technique has been described to enhance quality repair healing by promoting bone marrow element recruitment (Gill et al., 2006). Drilling of subchondral bone can also be performed and has the same goal (promoting cells recruitment for cartilage repair), but the holes are performed with a small drill bit, following an intra-articular route (Chen et al., 2011). SB drilling is followed by less osteocyte lacunae emptiness, with morphologically normal bone matrix surrounding the hole, whereas micro-fracture has been showed to lead to acute fracture and compaction of surrounding bone, with potential sealing of the marrow space access (Chen et al., 2011). In our study, we saw in 5 of the 9 impact-stimulated limbs an accumulation of osteoblasts along the trabeculae on Safranin O-Fast Green sections, and presence of a non-organized collagen layer along the trabeculae on Picrosirius sections observed under polarized-light microscopy, suggesting a potential anabolic stimulation with production of collagen. Our study would suggest that the mechanical stimulation would only stimulate the cells, without inducing catabolic activities (in opposition to traumatic stimulations). There are other examples of mechanical stimulation of the bone such as shock waves. Shock wave therapy has been proved to stimulate bone healing by an increase in osteoblast number and activity, and bone formation (Bulut et al., 2006; Lyon et al., 2013). There are also other examples of drilling techniques to treat SB pathology such as SB cysts. The bone mechanical stimulation is achieved by drilling and insertion of a screw in the SB cyst. This technique has been successfully used to treat SB cysts extra-articularly, without damaging cartilage (Santschi et al., 2015; Roquet et al., 2016; Simon et al., 2017).

Finally, in this thesis, we hypothesized that alterations of cartilage following SB stimulation would be visible by advanced imaging techniques for structural and compositional assessment, CECT and T2 mapping. We showed that these techniques were feasible in living sheep, but we were unable to identify significant differences between groups, or to correlate imaging findings with the histological changes.

This can be due to the limited changes that occurred after stimulation and to the limitations of the imaging modalities. Several limitations were identified, such as the restricted limb positioning in the gantry or inside the coil, the requirement for reduced acquisition time, and the subsequent compromise between short acquisition time and image quality (resolution, signal-to-noise ratio, volume averaging). Most of the compositional imaging techniques have been validated using ultra high field MRI such as 9.4 Tesla or 7 Tesla, on small osteochondral plugs (Kurkijarvi et al., 2004; Kurkijarvi et al., 2008). These plugs are obviously not sensitive to motion artefact, leading to the potentially long-duration scans and higher image quality. In the current study, we suggested that the problem of correlation between T2 mapping and commonly accepted relatives (water content, collagen content or organization) might be due to a problem of partial volume (volume averaging) compelled by limitation of acquisition duration. Moreover, when they are studied on larger structures (hole joint or living patient), CECT and T2 mapping are usually correlated to improvement of cartilage repair after chondral transplant (comparing fibrous tissue to hyaline cartilage-like tissue), or to the disease status assessed by X-ray (Clinical OA versus healthy control) (Li et al., 2007; Dunn et al., 2004), suggesting that the range of difference between the conditions could be higher than what we have encountered in our stimulation model with very and probably too subtle changes.

This PhD thesis highlights several perspectives for research and clinical applications.

We demonstrated what can be expected nowadays with CTA and MRI to detect cartilage changes. The detection of subtle cartilage defects has been proved to be more accurate with CTA than MRI. This accuracy was confirmed *ex vivo* in the metacarpo-/metatarso-phalangeal joint of the horse (Hontoir et al., 2014) and in the equine carpus (Suarez et al., 2018). However, the requirement of general anaesthesia and the associated risks (such as fracture, neuropathy, peri-anaesthetic mortality) (Mee et al., 1998; Wagner, 2009) can limit the use of powerful MRI or CT scans. Moreover, the volume of the body region of interest (i.e. the equine stifle) is also a limiting factor preventing the structure to enter the gantry, where it should lies during scanning periods (Goodrich and Werpy, 2012). Finally, the thickness of the structure of interest, namely the cartilage, is a concern since the image resolution should meet the cartilage thickness requirement. This cartilage thickness has been proved to vary depending on the joint and on the species, i.e. 1.2 mm for the sheep stifle, 2 mm for the equine stifle and 0.2-1.2mm for the equine carpal joint (Appleyard et al., 2003; Frisbie et al., 2006; Suarez et al., 2018). An inadequate resolution would lead to inappropriate cartilage assessment. Moreover, for MRI, some sequences initially developed on ultra-high field (7T and more) are not easy to implement on lower field (3T and lower) keeping a reasonable scanning time and signal-to-noise ratio.

We think also that CTA could be used as a screening tool at baseline to select animals before enrolment for longitudinal research studies. Practically, pre-inclusion assessment of cartilage is rarely performed since it is assumed that young adults, clinically healthy, free of any other disease are suitable for the study (Mrosek et al., 2006; Burger et al., 2007; Kuroki et al., 2011; Schinhan et al., 2012; Moya-Angeler et al., 2016). Even pre-inclusion surgical arthrotomy and joint evaluation, when performed, does not ensure that post-induction assessment will not be biased since surgical observation may miss lesions that are only visible by other imaging modalities. For example, in a study of surgically-induced joint degeneration (Moya-Angeler et al., 2016), the pre-induction assessment of the ovine knee included a common medial parapatellar arthrotomy with a thorough examination of the knee and check for the presence of previous cartilage damages or other abnormalities. However, the final outcome measures included scorings of bone marrow lesions, cysts and articular cartilage, using MRI (Moya-Angeler et al., 2016). MRI was not performed at baseline, maybe because of the difficulty to image the living animal, and conclusions might therefore be biased. This example is not unique, and similar situations are very often found in experimentation with both small and large animal models. We propose that, in the future, the noninvasive assessment of the entire joint should be part of the inclusion criteria. We developed and validated a technique that is feasible *ex vivo* and *in vivo* in an ovine model.

MRI compositional imaging seems much less accessible for clinical application, and must so far be considered as a potential research tool. This study was unable to demonstrate a correlation with the subtle changes we induced in the joint. This might be because the changes were too subtle, or because of the limited capacities of the imaging modalities. In the future, nevertheless, it is important to continue to improve compositional imaging. The idea of trying to identify changes of joint tissue noninvasively and at an early stage is important, and research in that area must be pursued. Based on the findings of the current study, we could consider intensifying the insult of the SB.

The idea of insulting the SB to hopefully induce changes in the cartilage was interesting. The main advantage of our model would be the selective stimulation of the SB. Indeed, the most commonly used techniques to surgically induce OA in the knee are relatively invasive, or induce stimulation of multiple components of the joint. For example, creation of AC defects (Intema et al., 2008; Kaplan et al., 2009; Kuroki et al., 2011) is associated to invasiveness of the joint, with incision of the synovium and risk of localized synovitis, leading to confusing factors regarding the efficacy of the model. Joint destabilizations by anterior cruciate ligament transection or medial meniscectomy (Carney et al., 1984; Brandt et al., 1991; Oakley et al., 2004; Burger et al., 2007; Kuroki et al., 2011; Cake et al., 2013) are also performed with invasiveness and would lead to the same confusing factor. In our study, we specifically stimulated the bone by an extraarticular access and with limited damage to the periarticular tissues.

Unfortunately, our stimuli were probably too light to induce significant changes. We based our protocol on those previously described. However, it not sure to what extent mechanical stimulation should be performed to induce disease. It seems that the action of ethanol was more successful and that this model could be useful for further research. Optimal doses should be found. Nevertheless, the histological differences that we identified between both types of stimulation were interesting since they may be highlighted two different mechanisms, one leading to pathology and the other to repair. This deserves to be investigated further to better understand how disease develops but also how SB stimulation (like drilling, micro-picking, or other) can be useful.

9. References

9. References

Adams ME, Brandt KD. 1991. Hypertrophic repair of canine articular cartilage in osteoarthritis after anterior cruciate ligament transection. Journal of Rheumatololgy 18 (3): 428-35.

Ai T, Zhang W, Priddy NK, Li X. 2012. Diagnostic performance of CUBE MRI sequences of the knee compared with conventional MRI. Clinical Radiology 67: 58-63.

Aigner T, Bertling W, Stob H, Weseloh G, Von Der Mark K. 1993. Independent expression of fibril forming collagen I, II and III in chondrocytes of human osteoarthritic cartilage. The Journal of Clinical Investigation 91: 829-37.

Alazzawi S, Sukeik M, Ibrahim M, Haddad FS. 2016. Management of anterior cruciate ligament injury: pathophysiology and treatment. British Journal of Hospital Medicine (London) 77(4):222-5.

Almonte-Becerril M, Navarro-Garcia F, Gonzalez-Robles A, Vega-Lopez M, Lavalle C, Kouri J. 2010. Cell death of chondrocytes is a combination between apoptosis and autophagy during the pathogenesis of Osteoarthritis within an experimental model. Apoptosis 15: 631–8.

Altman DG, Bland JM. 1994. Diagnostic tests 2: Predictive values. BMJ. 1994: 309:102.

Altman RD, Abramson S, Bruyere O, Clegg D, Herrero-Beaumont G, Maheu E, Moskowitz R, Pavelka K, Reginster JY. 2006. Commentary: osteoarthritis of the knee and glucosamine. Osteoarthritis and cartilage 14(10): 963-6.

Altman RD. 2004. Measurement of structure (disease) modification in osteoarthritis. Osteoarthritis and Cartilage 12: S69-76.

Altman RD, Gold GE. 2007. Atlas of individual radiographic features in osteoarthritis. Osteoarthritis and Cartilage 15 Suppl A:A1-56.

Anderson-MacKenzie JM, Quasnichka HL, Starr RL, Lewis EJ, Billingham ME, Bailey AJ. 2005. Fundamental subchondral bone changes in spontaneous knee osteoarthritis. The international journal of biochemistry & cell biology 37: 224–36.

Andrianakos AA, Kontelis LK, Karamitsos DG, Aslanidis SI, Georgountzos AI, Kaziolas GO, Pantelidou KV, Vafiadou EV, Dantis PC and ESORDIG Study Group. 2006. Prevalence of symptomatic knee, hand, and hip osteoarthritis in Greece. The ESORDIG study. The Journal of Rheumatology 33 (12): 2507-13.

Anetzberger H, Mayer A, Glaser C, Lorenz S, Birkenmaier C, Müller-Gerbl M. 2014. Meniscectomy leads to early changes in the mineralization distribution of subchondral bone plate. Knee Surgery, Sports Traumatolohy, Arthroscopy 22(1):112-9.

Appleyard RC, Burkhardt D, Ghosh P, Read R, Cake M, Swain MV, Murrell GA. 2003. Topographical analysis of the structural, biochemical and dynamic biomechanical properties of cartilage in an ovine model of osteoarthritis. Osteoarthritis and Cartilage 11:65-77.

Apprich S., Welsch GH, Mamisch TC, Szomolanyi, Mayerhoefer M, Pinker K, Trattnig S, 2010. Detection of degenerative cartilage disease: Comparison of high-resolution morphological MR and quantitative T2 mapping at 3.0T. Osteoarthritis and cartilage 18: 1211-7.

Apprich S, Trattnig S, Welsch GH, Noebauer-Huhmann IM, Sokolowski M, Hirschfeld C, Stelzeneder D, Domayer S. 2012. Assessment of articular cartilage repair tissue after matrix-associated autologous chondrocyte transplantation or the microfracture technique in the ankle joint using diffusion-weighted imaging at 3Tesla. Osteoarthritis and cartilage 20: 703-11.

Arøen A, Løken S, Heir S, Alvik E, Ekeland A, Granlund OG, Engebretsen L. 2004. Articular cartilage lesions in 993 consecutive knee arthroscopies. American Journal of Sports Medicine 32: 211–5.

Aula AS, Jurvelin JS, Töyräs J. 2009. Simultaneous computed tomography of articular cartilage and subchondral bone. Osteoarthritis and Cartilage 17: 2583-8.

Aurich M, Squires GR, Reiner A, Mollenhauer JA, Kuettner KE, Poole AR, Cole AA. 2005. Differential matrix degradation and turnover in early cartilage lesions of human knee and ankle joints. Arthritis and Rheumatism 52: 112-9.

Bae WC, Dwek JR, Znamirowski R, Statum SM, Hermida J,C, D'Lima DD, Sah RL, Du J, Chung CB. 2010. Ultrashort echo time MR imaging of osteochondral junction of the knee at 3T: identification of anatomic structures contributing to signal intensity. Radiology 254: 837–45.

Baharuddin NA, Coates DE, Cullinan M, Seymour G, Duncan W. 2015. Localization of RANK, RANKL and osteoprotegerin during healing of surgically created periodontal defects in sheep. Journal of periodontal research 50: 211-9.

Bailey AJ, Sims TJ, Knott L. 2002. Phenotypic expression of osteoblast collagen in osteoarthritic bone: production of type I homotrimer. The international journal of biochemistry & cell biology 34: 176–82.

Bailey AJ, Mansell JP, Sims TJ, Banse X. 2004. Biochemical and mechanical properties of subchondral bone in osteoarthritis. Biorheology 41(3-4): 349-58.

Blagojevic M, Jinks C, Jeffery A, Jordan KP. 2010. Risk factors for onset of osteoarthritis of the knee in older adults: a systematic review and meta-analysis. Osteoarthritis and Cartilage 18(1):24-33.

Baliunas AJ, Hurwitz DE, Ryals AB, Karrar A, Case JP, Block JA, Andriacchi TP. 2002. Increased knee joint loads during walking are present in subjects with knee osteoarthritis. Osteoarthritis Cartilage 10: 573-9.

Bammer R. 2003. Basic principles of diffusion-weighted imaging. European journal of radiology 45: 169-184.

Bank RA, Krikken M, Beekman B, Stoop R, Maroudas A, Lafeber FPJG, Te Koppele JM. 1997. A simplified measurmement of degraded collagne in tissues: application in healthy, fibrillated and osteoarthritic cartilage. Matrix biology 16: 233-43.

Bank RA, Bayliss MT, Lafeber FP, Maroudas A, Tekoppele JM. 1998. Ageing and zonal variation in post-translational modification of collagen in normal human articular cartilage. The age-related increase in non-enzymatic glycation affects biomechanical properties of cartilage. Biochemistry Journal 330(1): 345-51.

Bank RA, Soudry M, Maroudas A, Mizrahi J, TeKoppele JM. 2000. The increased swelling and instantaneous deformation of osteoarthritic cartilage is highly correlated with collagen degradation. Arthritis Rheumatism 43(10): 2202-10.

Bansal PN, Joshi NS, Entezari V, Grinstaff MW, Snyder BD. 2010. Contrast enhanced computed tomography can predict the glycosaminoglycan content and biomechanical properties of articular cartilage. Osteoarthritis and Cartilage 18(2): 184-91.

Bansal PN, Joshi NS, Entezari V, Malone BC, Stewart RC, Snyder BD, Grinstaff MW. 2011. Cationic Contrast Agents Improve Quantification of Glycosaminoglycan (GAG) Content by Contrast Enhanced CT Imaging of Cartilage. Journal of Orthopaedic Research 29: 704-9.

Banse X, Sims TJ, Bailey AJ. 2002. Mechanical properties of adult vertebral cancellous bone: correlation with collagen intermolecular cross-links, Journal of Bone and Mineral Research 17: 1621–8.

Bara JJ, Johnson WE, Caterson B, Roberts S. 2012. Articular cartilage glycosaminoglycans inhibit the adhesion of endothelial cells. Connective Tissue Research 53(3): 220-8.

Barr ED, Pinchbeck GL, Clegg PD, Boyde A, Riggs CM. 2009. Post mortem evaluation of palmar osteochondral disease (traumatic osteochondrosis) of the metacarpo/metatarsophalangeal joint in Thoroughbred racehorses. Equine Veterinary Journal 41: 366-71.

Barrett JF, Keat N. 2004. Artifacts in CT: Recognition and Avoidance. RadioGraphics 24: 1679-91.

Barrett MF, Frisbie DD, McIlwraith CW, Werpy NM. 2012. The arthroscopic and ultrasonographic boundaries of the equine femorotibial joints. Equine Veterinary Journal 44(1): 57-63.

Bashir A, Gray ML, Burstein D. 1996. Gd-DTPA2- as a measure of cartilage degradation. Magnetic Resonance in Medicine 36: 665-73.

Bashir A, Gray ML, Hartke J,Burstein D. 1999. Non-destructive imaging of human cartilage glycosaminoglycan concentration by MRI. Magnetic Resonance Medicine 41: 857-65.

Bassleer C, Henrotin Y, Franchimont P. 1992. In-vitro evaluation of drugs proposed as chondroprotective agents. International Journal Tissue Reaction 14: 231-41.

Bayliss MT, Venn M, Maroudas A, Ali SY. 1983. Structure of proteoglycans from different layers of human articular cartilage. Biochemistry Journal. 209: 387-400.

Bellenger C, Pickles D. 1993. Load-bearing in the ovine medial tibial condyle: effect of meniscectomy. Veterinary and comparative orthopaedics and traumatology 6: 100-4.

Bellido M, Lugo L, Roman-Blas JA, Castaneda S, Caeiro JR, Dapia S, Calvo E, Largo R, Herrero-Beaucmont G, 2010. Subchondral bone microstructural damage by increased remodelling aggravates experimental osteoarthritis preceded by osteoporosis. Arthritis research & therapy 12(4): R152.

Bellido M, Lugo L, Roman-Blas JA, Castaneda S, Calvo E, Largo R, Herrero-Beaumont G. 2011. Improving subchondral bone integrity reduces progression of cartilage damage in experimental osteoarthritis preceded by osteoporosis. Osteoarthritis and Cartilage 19: 1228-36.

Bendele AM, Hulman JF. 1988. Spontaneous cartilage degeneration in guinea pigs. Arthritis and Rheunmatism 31: 561-5.

Berenbaum F. 2013. Osteoarthritis as an inflammatory disease (osteoarthritis is not osteoarthrosis!). Osteoarthritis and cartilage 21(1): 16-21.

Bergman AG, Willen HK, Lindstrand AL, Pettersson HT. 1994. Osteoarthritis of the knee: correlation of subchondral MR signal abnormalities with histopathologic and radiographic features. Skeletal Radiology 23: 445–8.

Bhosale AM, Richardson JB. 2008. Articular cartilage: structure, injuries and review of management. British Medical Bulletin 87: 77-95.

Bidwell LA, Bramlage LR, Rood WA. 2007. Equine perioperative fatalities associated with general anaesthesia at a private practice--a retrospective case series. Veterinary Anaesthesia Analgesia 34(1): 23-30.

Bijlsma JWJ, Berenbaum F, Lafeber FPJG. 2011. Osteoarthritis: an update with relevance for clinical practice. The Lancet 377: 2115-26.

Binch ALA, Cross AK, Le Maitre CL. 2014. The regulation of nerve and blood vessel ingrowth in aneural and avascular intervertebral disc and articular cartilage. OA Arthritis 2(1): 4.

Bindhu Pr, Krishnapillai Rekha, Thomas Priya, Jayanthi P. 2013. Facts in artifacts. Journal of oral and maxillofacial pathology 17(3): 397-401.

Bittersohl B, Hosalkar HS, Hughes T, Kim Y-J, Werlen S, Siebenrock KA, Mamisch TC. 2009. Feasibility of T2* mapping for the evaluation of hip joint cartilage at 1.5 T using a three-dimensional gradient-echo sequence: a prospective study. Magnetic resonance in medicine 62: 896-901.

Bjorkman P, Sandelin J, Harilainen A. 2015. A randomized prospective controlled study with 5-year follow-up of cross-pin femoral fixation versus metal interference screw fixation in anterior cruciate ligament reconstruction. Knee Surgery, Sports Traumatology, Arthroscopy 23(8): 2353–9.

Blair-Levy JM, Watts CE, Fiorentino NM, Dimitriadis EK, Marini JC, Lipsky PE. 2008. A type I collagen defect leads to rapidly progressive osteoarthritis in a mouse model. Arthritis and Rheumatism 58: 1096–106.

Bobinac D, Spankol J, Zoricic S, Maric I. 2003. Changes in articular cartilage and subchondral bone histomorphometry in osteoarthritic knee joints in humans. Bone 32: 284-90.

Boening KJ, 2002. Arthroscopic surgery of the distal and proximal interphalangeal joints. Clinical Techniques in Equine Practice 1(4): 218-25.

Boivin BY, Chavassieux PM, Santora AC, Yates J, Meunier PJ. 2000. Alendronate increases bone strength by increasing the mean degree of mineralization of bone tissue in osteoporotic women. Journal of Bone Mineral Research 27: 687–94.

Bonde HV, Talman ML, Kofoed H. 2005. The area of the tidemark in osteoarthritis—a three-dimensional stereological study in 21 patients. Acta Pathologica, Microbiologica, et Immunologica Scandinavica 113: 349–52.

Borthakur A, Hancu I, Boada FE, Shen GX, Shapiro EM, Reddy R. 1999. *In vivo* triple quantum filtered sodium MRI of human articular cartilage. Journal of Magnetic Resonance 141(2): 286-90.

Borthakur A, Reddy R, 2010. Imaging cartilage physiology. Topics in Magnetic Resonance Imaging 21: 291–6.

Botter SM, van Osch GJ, Clockaerts S, Waarsing JH, Weinans H, van Leeuwen JP. 2011. Osteoarthritis induction leads to early and temporal subchondral plate porosity in the tibial plateau of mice: an *in vivo* microfocal computed tomography study. Arthritis and Rheumatism 63(9): 2690-9.

Bouxsein ML, Boyd SK, Christiansen BA, Guldberg RE, Jepsen KJ, Müller R. 2010. Guidelines for assessment of bone microstructure in rodents using micro-computed tomography. Journal of Bone and mineral research 25(7): 1468-86.

Brama PA, TeKoppele JM, Bank RA, Barneveld A, van Weeren PR. Development of biochemical heterogeneity of articular cartilage: influences of age and exercise. Equine Veterinary Journal 34(3): 265-9.

Brandt KD, Braunstein EM, Visco DM, O'Connor B, Heck D, Albrecht M. 1991. Anterior (cranial) cruciate ligament transection in the dog: a bona fide model of osteoarthritis, not merely of cartilage injury and repair. Journal of Rheumatology 18(3): 436-46.

Braun HJ, Gold GE. 2011. Advanced MRI of articular cartilage. Imaging Medicine 3(5): 541-55.

Braun HJ, Gold GE. 2012. Diagnosis of osteoarthritis: imaging. Bone 51(2): 278-88.

Brennan P, Silman A. 1992. Statistical methods for assessing observer variability in clinical measures. British Medical Journal 304: 1491-4.

Brommer H, van Weeren PR, Brama PA, Barneveld A. 2003. Quantification and age-related distribution of articular cartilage degeneration in the equine fetlock joint. Equine Veterinary Journal 35: 697-701.

Brooks RA, Di Chiro G. 1976. Principles of computer assisted tomography (CAT) in radiographic and radioisotopic imaging. Physics in Medicine and Biology 21(5): 689-732.

Brown RA, Byers PD. 1989. Swelling of cartilage and expansion of the collagen network. Calcified tissue International 45(4): 260-1.

Bruce WJ, Frame K, Burbidge HM, Thompson K, Firth EC. 2002. A comparison of the effects of joint immobilisation, twice-daily passive motion, and voluntary motion on articular cartilage healing in sheep. Veterinary and Comparative Orthopedics and Traumatology 15: 23-9.

Buckwalter JA and Mankin HJ. 1997. Articular cartilage. Part I: tissue design and chondrocyte-matrix interactions. Journal of Bone and Joint Surgery in America 79A: 600-11.

Bullough P. 1981. The geometry of diarthroidal joints, its physiologic maintenance, and the possible significance of age-related changes in geometry-to-load distribution and the development of osteoarthritis. Clinical Orthopaedics 156: 61–6.

Bullough PG, Jagannath A. 1983. The morphology of the calcification front in articular cartilage. Journal of Bone and Joint Surgery 65B: 72–8.

Bulut O, Eroglu M, Ozturk H, Tezeren G, Bulut S, Koptagel E. 2006. Ewtracorporeal shock wave treatment for defective non-union of the radius: a rabbit model. Journal of Orthropaeduc surgery 14(2): 133-7.

Buma P, Verschuren C, Versleyen D, der KP V, Oestreicher AB. 1992. Calcitonin gene-related peptide, substance P and GAP-43/B-50 immunoreactivity in the normal and arthrotic knee joint of the mouse. Histochemistry 98: 327–39.

Burger C, Mueller M, Wlodarczyk P, Goost H, Tolba RH, Rangger C, Kabir K, Weber O. 2007. The sheep as a knee osteoarthritis model: early cartilage changes after meniscus injury and repair. Laboratory animals 41: 420-31.

Burr DB and Schaffler MB. 1997. The involvement of subchondral mineralized tissues in osteoarthrosis. Microscopy Research and Technique 37: 343–57.

Burr DB and Radin EL. 2003. Microfractures and microcracks in subchondral bone: are they relevant to osteoarthrosis? Rheumatic diseases clinics of North America 29(4): 675-85.

Burr DB. 2004. Anatomy and physiology of the mineralized tissues: Role in the pathogenesis of osteoarthrosis. Osteoarthritis and cartilage 12: S20-S30.

Burr DB. 2005. Increased biological activity of subchondral mineralized tissues underlies the progressive deterioration of articular cartilage in osteoarthritis. Journal of Rheumatology 32: 1156–8.

Burr DB, Gallant MA. 2012. Bone remodelling in osteoarthritis. Nature Reviews. Rheumatology 8(11): 665-73.

Burstein D, Gray M,L, Hartman A,L, Gipe R, Foy B,D. 1993. Diffusion of small solutes in cartilage as measured by nuclear magnetic resonance (NMR) spectroscopy and imaging. Journal of Orthopaedic Research 11: 465-78.

Cake MA, Read RA, Corfield G, Daniel A, Burkhardt D, Smith MM, Little CB. 2013. Comparison of gait and pathology outcomes of three meniscal procedures for induction of knee osteoarthritis in sheep. Osteoarthritis Cartilage 21(1): 226-36.

Callis G, Sterchi D. 1998. Decalcification of Bone: Literature Review and Practical Study of Various Decalcifying Agents. Methods, and Their Effects on Bone Histology. Journal of Histotechnology 21(1): 49-58.

Campo RD, Betz RR. 1987. Loss of proteoglycans during decalcification of fresh metaphyses with disodium ethylenediaminetetraacetate (EDTA). Calcified Tissue International 41(1): 52-5.

Carman WJ, Sowers M, Hawthorne VM, Weissfeld LA. 1994. Obesity as a risk factor for osteoarthritis of the hand and wrist: a prospective study. American Journal of Epidemiology 139(2): 119-29.

Carmona L, Ballina J, Gabriel R, Laffon A; EPISER Study Group. 2001. The burden of musculoskeletal diseases in the general population of Spain: results from a national survey. Annals of Rheumatic Diseases 60: 1040-5.

Carney SL, Billingham MEJ, Muir H, Sandy JD. 1984. Demonstration of increased proteoglycan turnover in cartilage explants from dogs with experimental arthritis. Journal of Orthopedic Research 2: 201–6.

Carney SL, Muir H. 1988. The structure and function of cartilage proteoglycans. Physiological reviews 68: 858-910.

Caron JP, Genovese RL. 2003. Principles and practices of joint disease treatment. In: Ross MW, Dyson SJ, eds. Diagnosis and management of lameness in the horse. Philadelphia: Elsevier.

Carrig CB. 1997. Diagnostic imaging of osteoarthritis. Veterinary Clinics of North America. Small Animal Practice 27(4): 777-814.

Carstens A, Kirberger RM, Velleman M, Dahlberg LE, Fletche, L, Lammentausta E. 2013A. Feasibility for mapping cartilage t1 relaxation times in the distal metacarpus3/metatarsus3 of Thoroughbred racehorses using delayed gadolinium-enhanced magnetic resonance imaging of cartilage (dGEMRIC): Normal cadaver study. Veterinary Radiology and Ultrasound 54: 365–72.

Carstens A, Kirberger R,M, Dahlberg L,E, Prozesky L, Fletcher L, Lammentausta E. 2013B. Validation of delayed gadolinium-enhanced imaging of cartilage and T2 mapping for quantifying distal metacarpus/metatarsus cartilage thickness in thoroughbred racehorses. Veterinary Radiology and Ultrasound 54: 139–48.

Castaneda S, Roman-Blas JA, Largo R, Herrero-Beaumont G. 2012. Subchondral bone as a key target for osteoarthritis treatment. Biochemical Pharmacology 83: 315-23.

Chan WP, Huang GS, Hsu SM, Chang YC, Ho WP. 2008. Radiographic joint space narrowing in osteoarthritis of the knee: relationship to meniscal tears and duration of pain. Skeletal Radiology 37(10): 917–22.

Changoor A, Tran-Khanh N, Méthot S, Garon M, Hurtig MB, Shive MS, Buschmann MD. 2011. A polarized light microscopy method for accurate and reliable grading of collagen organization in cartilage repair. Osteoarthritis Cartilage 19(1):126-35.

Charagundla SR Borthakur A, Leigh JS, Reddy R. 2003. Artifacts in $T_{1\rho}$-weighted imaging: correction with a self-compensating spin-locking pulse. Journal of Magnetic Resonance 162: 113-21.

Charagundla SR. 2004. T1ρ weighted magnetic resonance imaging: Principles and diagnostic application. Applied radiology Suppl 33: 32-43.

Chatterjee S. 2014. Artefacts in histopathology. Journal of oral and maxilofacial pathology 18(Suppl 1): 111-6.

Chen H, Hoemann CD, Sun J, Chevrier A, McKee MD, Shive MS, Hurtig M, Buschmann MD. 2011. Depth of subchondral perforation influences the outcome of bone marrow stimulation cartilage repair. Journal of Orthopaedic Research 29(8): 1178-84.

Chevrier A, Kouao AS, Picard G, Hurtig MB, Buschmann MD. 2014. Interspecies Comparison of Subchondral Bone Properties Important for Cartilage Repair. Journal of Orthopaedic Research 33(1): 63-70.

Chiba K, Uetani M, Kido Y, Ito M, Okazaki N, Taguchi K, Shindo H. 2011. Osteoporotic changes of subchondral trabecular bone in osteoarthritis of the knee: a 3-T MRI study. Osteoporosis International 23 (2): 589–97.

Choi K, Kuhn HL, Ciarelli MJ, Goldstein SA. 1990. The elastic moduli of human subchondral, trabecular, and cortical bone tissue and the size-dependency of cortical bone modulus. Journal of Biomechanics 11: 1103–13.

Clark DJ, Jia G, Menendez MI, Choi S, Miller CJ, Sammet S, Flanigan DC, Bertone AL, Knopp MV. 2010. *In vivo* quantification of cartilage regeneration in an equine model at 3T following gene therapy. Proceedings of the International Society for Magnetic Resonance in Medicine 18: 232.

Clark JM. 1990. The structure of vascular channels in the subchondral plate. Journal of Anatomy 171: 105-15.

Clark JM and Huber JD. 1990. The structure of the human subchondral plate. Journal of Bone and Joint Surgery Britain 72(5): 866-73.

Clegg PD, Burke RM, Coughlan AR, Riggs CM, Carter SD. 1997A. Characterisation of equine matrix metalloproteinase 2 and 9 and identification of the cellular sources of these enzymes in joints. Equine Veterinary Journal 29: 335–42.

Cockman MD, Blanton CA, Chmielewski PA, Dong L, Dufresne TE, Hookfin EB, Karb MJ, Liu S, Wehmeyer KR. 2006. Quantitative imaging of proteoglycan in cartilage using a gadolinium probe and microCT. Osteoarthritis and Cartilage. 14(3): 210-4.

Coggon D, Reading I, Croft P, McLaren M, Barrett D, Cooper C. 2001. Knee osteoarthritis and obesity. International journal of Obesity and Related Metabolic Disorders 25(5): 622-7.

Cokelaere S, Malda J, van Weeren R. 2016. Cartilage defect repair in horses: Current strategies and recent developments in regenerative medicine of the equine joint with emphasis on the surgical approach. The Veterinary Journal 214: 61-71.

Couchourel D, Aubry I, Delalandre A, Lavigne M, Martel-Pelletier J, Pelletier JP, Lajeunesse D. Altered mineralization of human osteoarthritic osteoblasts is attributable to abnormal type I collagen production. Arthritis and Rheumatism 60(5): 1438-50.

Crema MD, Nogueira-Barbosa MH, Roemer FW, Marra MD, Niu J, Chagas-Neto FA, Gregio-Junior F, Guermazi A. 2013. Three-dimensional turbo spin-echo magnetic resonance imaging (MRI) and semiquantitative assessment of knee osteoarthritis: comparison with two-dimensional routine MRI. Osteoarthritis and Cartilage 21: 428-33.

Cremer MA, Rosloniec EF, Kang AH. 1998. The cartilage collagens: a review of their structure, organization, and role in the pathogenesis of experimental arthritis in animals and in human rheumatic disease. Journal of Molecular Medicine (Berl) 76(3-4): 275-88.

Crockett R, Grubelnik A, Roos S, Dora C, Born W, Troxler H. 2007. Biochemical composition of the superficial layer of articular cartilage. Journal of biomedical materials research (A) 82: 958-64.

Cui Z, Crane J, Xie H, Jin X, Zhen G, Li C, Xie L, Wang L, Bian Q, Qiu T, Wan M, Xie M, Ding S, Yu B, Cao X. 2016. Halofuginone attenuates osteoarthritis by inhibition of TGF-β activity and H-type vessel formation in subchondral bone. Annals of the Rheumatic Disease 75(9): 1714-21.

Daenen BR, Ferrara MA, Marcelis S, Dondelinger RF. 1998. Evaluation of patellar cartilage surface lesions: comparison of CT arthrography and fat-suppressed FLASH 3D MR imaging. European Radiology 8: 981-85.

Dahaghin S, Bierma-Zeinstra SM, Koes BW, Hazes JM, Pols HA. 2007. Do metabolic factors add to the effect of overweight on hand osteoarthritis? The Rotterdam Study. Annals of the Rheumatic Diseases 66(7): 916-20.

Dahlberg L, Fridén T, Roos H, Lark MW, Lohmander LS. 1994. A longitudinal study of cartilage matrix metabolism in patients with cruciate ligament rupture--synovial fluid concentrations of aggrecan fragments, stromelysin-1 and tissue inhibitor of metalloproteinase-1. British Journal of Rheumatology 33(12): 1107-11.

Damman W, Liu R, Bloem JL, Rosendaal FR, Reijnierse M, Kloppenburg M. 2017. Bone marrow lesions and synovitis on MRI associate with radiographic progression after 2 years in hand osteoarthritis. Annals of the Rheumatic Diseases 76(1): 214–17.

Dattena M, Pilichi S, Rocca S, Mara L, Casu S, Masala G, Manunta L, Manunta A, Passino ES, Pool RR and Cappai P. 2009. Sheep embryonic stem-like cells transplanted in full-thickness cartilage defects. Journal of tissue engineering and regenerative medicine 3: 175-87.

Daubs BM, Markel MD, Manley PA. 2006. Histomorphometric analysis of articular cartilage, zone of calcified cartilage, and subchondral bone plate in femoral heads from clinically normal dogs and dogs with moderate or severe osteoarthritis. American Journal of Veterinary Radiology 67: 1719-24.

Davidson MK, Lindsey JR, Davis JK. 1987. Requirements and selection of an animal model. Israel journal of medical sciences 23: 551-5.

David-Vaudey E, Ghosh S, Ries M, Majumdar S. 2004. T2 relaxation time measurements in osteoarthritis. Magnetic Resonance Imaging 22: 673-82.

Davies-Tuck ML, Wluka AE, Forbes A, Wang Y, English DR, Giles GG, O'Sullivan R, Cicuttini FM. 2010. Development of bone marrow lesions is associated with adverse effects on knee cartilage while resolution is associated with improvement—a potential target for prevention of knee osteoarthritis: a longitudinal study. Arthritis Research and Therapy 12: R10.

Day JD, Manintveld O, Bank RA, Ding M, Sumner DR, Hvid I, van Osch GJVM, Weinans H. 2003.Denatured collagen in osteoarthritic bone, in: 49th Annual Meeting of the Orthopaedic Research Society, New Orleans, LA, 2003.

Day JS, Ding M, van der Linden JC, Hvid I, Sumner DR, Weinans H. 2001. A decreased subchondral trabecular bone tissue elastic modulus is associated with prearthritic cartilage damage. Journal of Orthopaedic Research 19: 914–8.

De Bri E, Reinholt FP, Svensson O. 1995. Primary osteoarthrosis in guinea pigs: A stereological study. Journal of Orthopaedic Research 13: 769–76.

De Filippo M, Bertellini A, Pogliacomi F, Sverzellati N, Corradi D, Garlaschi G, Zompatori M. 2009. Multidetector Computed Tomography Arthrography of the Knee: Diagnostic Accuracy and Indications. European Journal of Radiology 70: 342-51.

de Lange-Brokaar BJ, Ioan-Facsinay A, Yusuf E, Visser AW, Kroon HM, van Osch GJ, Zuurmond AM, Stojanovic-Susulic V, Bloem JL, Nelissen RG, Huizinga TW, Kloppenburg M. 2015. Association of pain in knee osteoarthritis with distinct patterns of synovitis. Arthritis and Rheumatism 67(3): 733-40.

Delgado-Calle J, Sañudo C, Fernández AF, García-Renedo R, Fraga MF, Riancho JA. 2012. Role of DNA methylation in the regulation of the RANKL-OPG system in human bone. Epigenetics 7: 83–91.

Desrochers J, Amrein MW, Matyas JR. 2012. Viscoelasticity of the articular cartilage surface in early osteoarthritis. Osteoarthritis and Cartilage 20: 413-21.

Desrochers J, Amrein MW, Matyas JR. 2013. Microscale surface friction of articular cartilage in early osteoarthritis. Journal of the mechanical behavior of biomedical materials 25: 11-22.

Ding C. 2010. Microarchitectural adaptations in aging an osteoarthrotic subchondral bone issues. Acta orthopaedica suppl 81:1-53.

Disler DG, Recht MP, McCauley TR. 2000. MR imaging of articular cartilage. Skeletal Radiology 29: 367–77.

Domayer SE, Welsch GH, Nehrer S, Chiari C, Dorotka R, Szomolanyi P, Mamisch TC, Yayon A, Trattnig S. 2010. T2 mapping and dGEMRIC after autologous chondrocyte implantation with a fibrin-based scaffold in the knee: preliminary results. European Journal of Radiology 73(3): 636-42.

Dowd G, Gaynor JS, Alvis M, Salman M, Turner AS. 1998. Comparison of transdermal fentanyl and oral phenylbytazone for operative analgesia in sheep. Abstracts of the American College of Veterinary Anesthesiologists Annual Scientific Meeting, October 17th, San Diego, USA.

Du J, Takahashi AM, Chung CB. 2009. Ultrashort TE spectroscopic imaging (UTESI): application to the imaging of short T2 relaxation tissues in the musculoskeletal system. Journal of Magnetic Resonance Imaging 29: 412-21.

Dudhia J. 2005. Aggrecan, aging and assembly in articular cartilage. Cellular and Molecular Life Sciences 62 (19-20): 2241-56.

Duncan H, Jundt J, Riddle JM, Pitchford W, Christopherson T. 1987. The tibial subchondral plate: a scanning electron microscopic study. Journal of Bone and Joint Surgery America 69(8): 1212-20.

Dunn TS, Lu Y, Jin H, Ries MD, Majumdar S. 2004. T2 relaxation time of cartilage at MR imaging: comparison with severity of knee osteoarthritis. Radiology 232: 592-8.

Duvvuri U, Charagundla SR, Kudchodkar SB, Kaufman JH, Kneeland JB, Rizi R, Leigh JS, Reddy R. 2001. Human knee: *in vivo* T1(rho)-weighted MR imaging at 1.5 T--preliminary experience. Radiology 220: 822-6.

Dwyer AJ. 1991. Matchmaking and McNemar in the comparison of diagnostic modalities. Radiology 178: 328-330.

Dyce KM, Wensing CJG.2010. Part I: General anatomy. Chapter 1: Some basic facts and concepts. Textbook of Veterinary Anatomy. 4th edition. 2010. Elsevier.

El-Khoury GY, Alliman KJ, Lundberg HJ, Rudert MJ, Brown TD, Saltzman CL. 2004. Cartilage thickness in cadaveric ankles: measurement with double-contrast multi-detector row CT arthrography versus MR imaging. Radiology 233(3): 768-73.

Elsaid KA, Fleming BC, Oksendahl HL, Machan JT, Fadale PD, Hulstyn MJ, Shalvoy R, Jay GD. 2008. Decreased lubricin concentrations and markers of joint inflammation in the synovial fluid of patients with anterior cruciate ligament injury. Arthritis and Rheumatism 58(6): 1707-15.

Elsaid KA, Jay GD, Warman ML, RheeDK, Chichester CO. 2005. Association of articular cartilage degradation and loss of boundary-lubricating ability of synovial fluid following injury and inflammatory arthritis. Arthritis and Rheumatism 52: 1746–55.

Evans GP, Behiri JC, Vaughan LC, Bonfield W. 1992. The response of equine cortical bone to loading at strain rates experienced *in vivo* by the galloping horse. Equine Veterinary Journal 24: 125-8.

Ewers BJ, Weaver BT, Sevensma ET, Haut RC. 2002. Chronic changes in rabbit retro-patellar cartilage and subchondral bone after blunt impact loading of the patellofemoral joint. Journal of Orthopaedic Research 20(3): 545-50.

Eyre DR, McDevitt CA, Billingham MEJ, Muir H. 1980. Biosynthesis of collagen and other matrix components by articular cartilage in experimental osteoarthritis. Biochemistry Journal 188: 823–37.

Eyre DR, Wu JJ, Apone S. 1987. A growing family of collagens in articular cartilage: identification of 5 genetically distinct types. Journal of Rheumatology S25: 7.

Eyre DR. 1991. The collagens of articular cartilage. Seminars in Arthritis and Rheumatism 21(S2): 2–11.

Farkas TA, Boyd RD, Schaffler MB, Radin EL and Burr DB. 1987. Early vascular changes in rabbit subchondral bone after repetitive impulsive loading. Clinic Orthopaedics 219: 259-67.

Farndale RW, Buttle DJ, Barrett AJ. 1986. Improved quantitation and discrimination of sulphated glycosaminoglycans by use of dimethylmethylene blue. Biochemica et Biophysica Acta 883: 173–7.

Felson DT, Zhang Y, Anthony JM, Naimark A, Anderson JJ. 1992. Weight loss reduces the risk for symptomatic knee osteoarthritis in women. The Framingham Study. Annals of Internal Medicine 116: 535–39.

Felson DT. 1996. Weight and osteoarthritis. American Journal of Clinical Nutrition 63(suppl 3): 430-432.

Felson DT, Zhang Y. 1998. An update on the epidemiology of knee and hip osteoarthritis with a view to prevention. Arthritis and Rheumatism 41(8): 1343-55.

Felson DT, McLaughlin S, Goggins J, LaValley MP, Gale ME, Totterman S, Li W, Hill C, Gale D, 2003. Bone Marrow Edema and Its Relation to Progression of Knee Osteoarthritis. Annals of Internal Medicine 139: 330-7.

Felson DT, Niu J, Guermazi A, Roemer F, Aliabadi P, Clancy M, Torner J, Lewis CE, Nevitt MC. 2007. Correlation of the development of knee pain with enlarging bone marrow lesions on Magnetic Resonance Imaging. Arthritis and Rheumatism 56: 2986–92.

Fife RS, Brandt KD, Braunstein EM, Katz BP, Shelbourne KD, Kalasinski LA, Ryan S. 1991. Relationship between arthroscopic evidence of cartilage damage and radiographic evidence of joint space narrowing in early osteoarthritis of the knee. Arthritis and Rheumatology 34(4): 377-82.

Findlay DM, Kuliwaba JS. 2016. Bone-cartilage crosstalk: a conversation for understanding osteoarthritis. Bone Research 4: 16028.

Flanigan DC, Harris JD, Trinh TQ, Siston RA, Brophy RH. 2010. Prevalence of chondral defects in athletes' knees: a systematic review. Medicine and science in sports and exercise 42: 1795-801.

Foltz WD, Al-Kwifi O., Sussman MS, Stainsby JA, Wright GA. 2003. Optimized spiral imaging for measurement of myocardial T2 relaxation. Magnetic resonance in Medicine 49: 1089-97.

Fox AJ, Bedi A, Rodeo SA. 2009. The Basic Science of Articular Cartilage: Structure, Composition, and Function. Sports Health 1(6): 461-8.

Frank CB. 2004. Ligament structure, physiology and function. Journal of Musculoskeletal and Neuronal Interactions 4(2): 199-201.

Franz T, Hasler EM, Hagg R, Weiler C, Jakob RP, Mainil-Varlet P. 2001. In situ compressive stiffness, biochemical composition, and structural integrity of articular cartilage of the human knee joint. Osteoarthritis and Cartilage 9(6): 582-92.

Franzén A, Inerot S, Hejderup SO, Heinegård D, 1981. Variations in the composition of bovine hip articular cartilage with distance from the articular surface. Biochemistry Journal 195(3): 535–43.

Frazier SB, Roodhouse KA, Hourcade DE, Zhang L. 2008. The quantification of glycosaminoglycans : a comparison of HPLC, Carbazole and Alcian blue methods. Open Glycoscience 1: 31-9.

Friedrich KM, Mamisch TC, Plank C, Langs G, Marlovits S, Salomonowitz E, Trattnig S, Welsch G. 2010. Diffusion weighted imaging for the follow up of patients after matrix associated autologous chondrocyte transplantation. European Journal of Radiology 73: 622–8.

Friedrich KM, Reiter G, Kaiser B, Mayerhöfer M, Deimling M, Jellus V, Horger W, Trattnig S, Schweitzer M, Salomonowitz E. 2011. High-resolution cartilage imaging of the knee at 3T: basic evaluation of modern isotropic 3D MR-sequences. European Journal of Radiology 78: 398-405.

Frisbie DD, Trotter GW, Powers BE, Rodkey WG, Steadman JR, Howard RD, Park RD, McIlwraith CW. 1999. Arthroscopic subchondral bone plate microfracture technique augments healing of large chondral defects in the radial carpal bone and medial femoral condyles of horses. Veterinary Surgery 28: 242-55.

Frisbie DD, Ghivizzani SC, Robbins PD, Evans CH, McIlwraith CW. 2002. Treatment of experimental equine osteoarthritis by *in vivo* delivery of the equine interleukin-1 receptor antagonist gene. Gene Therapy 9: 12-20.

Frisbie DD, Cross MW, McIlwraith CW. 2006. A comparative study of articular cartilage thickness in the stifle of animal species used in human pre-clinical studies compared to articular cartilage thickness in the human knee. Veterinary and Comparative Orthopaedics Traumatology 19: 142–6.

Friske J, Berg A, Wesch GH, Pachowsky M, Myllyharju K, Trattnig S. 2012. High-field high-resolution and microscopic T2-maps of a cartilage repair sheep model on a 7T human scanner: first results. 29th Annual Scientific Meeting, (4-6 october 2012, Lisbon/PT), ESMRMB (European Society of Magnetic Resonance in Medicine and Biology).

Gangi A, Kastler B, Klinkert A, Dietemann JL. 1994. Injection of alcohol into bone metastases under CT guidance. Journal of Computer Assisted Tomography 18(6): 932-5.

Gao S, Du J, Wang F, Bao S. 2013. Magnetic resonance ultrashort echo time spin-echo imaging of the deepest layers of articular cartilage. Science China Life Sciences 56: 672–4.

Garnero P, Peterfy C, Zaim S, Schoenharting M. 2005. Bone marrow abnormalities on magnetic resonance imaging are associated with type II collagen degradation in knee osteoarthritis: a three-month longitudinal study. Arthritis and Rheumatism 52: 2822–9.

Garvican ER, Vaughan-Thomas A, Innes JF,Clegg PD. 2010. Biomarkers of cartilage turnover. Part 1: Markers of collagen degradation and synthesis. The Veterinary Journal 185: 36-42.

Giavaresi G, Fini M, Martini L, Nicoli Aldini N, Rocca M, Torricelli P, Giardino R. 2001. Histomorphometric Characterization of Cancellous and Cortical Bone in an Ovariectomized Sheep Model, Journal of Applied Animal Research, 20:2, 221-232.

Gill TJ, Asnis PD, Berkson EM. 2006. The treatment of articular cartilage defects using the microfracture technique. The Journal of orthopaedic and sports physical therapy 36: 728–38.

Gillis, A., Bashir, A., McKeon, B., Scheller, A., Gray, M.L., Burstein, D., 2001. Magnetic resonance imaging of relative glycosaminoglycan distribution in patients with autologous chondrocyte transplants. Investigative Radiology 36, 743-748.

Gold GE, Chen CA, Koo S, Hargreaves BA, Bangerter NK. 2009. Recent advances in MRI of articular cartilage. American Journal of Roentgenology 193: 628-38.

Gold GE, McCauley TR, Gray ML, Disler DG. 2003. Special focus session - What's new in cartilage? Radiographics 23: 1227-42.

Goldring MB. 2000. The role of the chondrocyte in osteoarthritis. Arthritis and Rheumatism 43: 1916-26.

Goldring MB, Goldring SR. 2007. Osteoarthritis. Journal of cellular Physiology 2013(3): 626-34.

Goldring MB, Marcu KB. 2009. Cartilage homeostasis in health and rheumatic diseases. Arthritis Research Therapy 11(3):224.

Goldring MB and Goldring SR. 2010. Articular cartilage and subchondral bone in the pathogenesis of osteoarthritis. Annals of the New York academy of sciences 1192: 230–7.

Goldring MB, Otero M, Plumb DA, Dragomir C, Favero M, El Hachem K, Hashimoto K, Roach HI, Olivotto E, Borzì RM, Marcu KB. 2011. Roles of inflammatory and anabolic cytokines in cartilage metabolism: signals and multiple effectors converge upon MMP-13 regulation in osteoarthritis. European Cells and Materials 21: 202-20.

Goldring MB, Otero M. 2011. Inflammation in osteoarthritis. Current Opinions in Rheumatology 23(5): 471-8.

Goldring MB, Berenbaum F. 2015. Emerging targets in osteoarthritis therapy. Current Opinion in Pharmacology 22: 51–63.

Goldring MB, Culley KL, Wondimu E, Otero M. 2017. Cartilage and chondrocytes. In: Kelley'sTextbook of Rheumatology (9th ed). Firestein GS, Budd R, Gabriel SE, McInnes IB, O'Fell J. Elsevier Saunders, Philadelphia, USA.

Goldstein SA, Goulet R, McCubbrey D. 1993. Measurement and significance of three-dimensional architecture to the mechanical integrity of trabecular bone. Calcified Tissue International 53 (S1): 127-32.

Goodrich L, Werpy N. 2012. The stifle – scan it or scope it? Proceedings of the Surgical summit of the American College of Veterinary Surgeons, October 31st – November 2nd.

Goodwin DW. 2001. Visualization of the macroscopic structure of hyaline cartilage with MR imaging. Seminar in Musculoskeletal Radiology 5: 305-12.

Graindorge S, Ferrandez W, Ingham E, Jin Z, Twigg P, Fisher J. 2006. The role of the surface amorphous layer of articular cartilage in joint lubrication. Proceedings of the Institution of Mechanical Engineers. Part H, Journal of engineering in medicine 220: 597-607.

Granke M, Does MD, Nyman JS. 2015. The Role of Water Compartments in the Material Properties of Cortical Bone. Calcified Tissue International 97(3): 292-307.

Gray ML, Burstein D, Kim Y-J, Maroudas A. 2008. Magnetic resonance imaging of cartilage glycosaminoglycan: basic principles, imaging technique and clinical applications. Journal of orthopaedic research 26: 281-91.

Grynpas M, Albert B, Katz I, Lieberman I, Pritzker KPH. 1991. Subchondral bone in osteoarthritis. Calcified Tissue International 49: 20–6.

Guerra D, Frizziero L, Losi M, Bacchelli B, Mezzadri G, Pasquali-Ronchetti I. 1996. Ultrastructural identification of a membrane-like structure on the surface of normal articular cartilageJournal of submicroscopic cytology and pathology 28(3): 385-93.

Guilak F, Ratcliffe A, Lane N, Rosenwasser MP, Mow VC. 1994. Mechanical and biochemical changes in the superficial zone of articular cartilage in canine experimental osteoarthritis. Journal of Orthopaedic Research 12(4): 474-84.

Habibzadeh MA, Ay MR, Asl AR, Ghadiri H, Zaidi H. 2012. Impact of miscentering on patient dose and image noise in x-ray CT imaging: phantom and clinical studies. Physica Medica 28: 191-9.

Hacker SA, Healey RM, Yoshioka M, Coutts RD. 1997. A methodology for the quantitative assessment of articular cartilage histomorphometry. Osteoarthritis and Cartilage 5: 343-55.

Hagmann P, Jonasson L, Maeder P, Thiran J-P, Wedeen VJ, Meuli R. 2006. Understanding diffusion MR imaging techniques: from scalar diffusion-weighted imaging to diffusion tensor imaging and beyond. Radiographics. 26 Supplement 1:S205-S223.

Hajian-Tilaki K. 2014. Sample size estimation in diagnostic test studies of biomedical informatics. Journal of Biomedical Informatics 48: 193-204.

Halata Z. 1977. The ultrastructure of the sensory nerve endings in the articular capsule of the knee joint of the domestic cat. Journal of Anatomy 124(3): 717-29.

Halsell RD. 1987. Heating contrast media: role in contemporary angiography. Radiology 164:276-278.

Hani AF, Kumar D, Malik AS, Razak R. 2013. Physiological assessment of *in vivo* human knee articular cartilage using sodium MR imaging at 1.5 T. Magnetic Resonance Imaging 31: 1059–67.

Hardie EM, Simon CR, Martin FR. 2002. Radiographic evidence of degenerative joint disease in geriatric cats: 100 cases (1994–1997). Journal of the American Veterinary Medical Association 220 (5): 628-63.

Hardingham TE, Rayan V, Lewthwaite JC. 1994. Regulation of cartilage matrix synthesis by chondrocytes. Revue du Rhumatisme 61 (Pt2) 93S-98S.

Hashimoto S, Takahashi K, Amiel D, Coutts RD, Lotz M. 1998. Chondrocyte apoptosis and nitric oxide production during experimentally induced osteoarthritis. Arthritis and Rheumatism 41: 1266–74.

Havelak S, Horn V, Spohrová D, Valouch P. 1984. The calcified-non calcified cartilage interface: the tidemark. Acta Biologica Hungary 35: 271-79

Hawezi ZK, Lammentausta E, Svensson J, Dahlberg LE, Tiderius CJ. 2011. *In vivo* transport of Gd-DTPA(2-) in human knee cartilage assessed by depth-wise dGEMRIC analysis. Journal of Magnetic Resonance Imaging 34: 1352-8.

Hayami T, Pickarski M, Zhuo Y, Wesolowski GA, Rodan GA, Duong le T. 2006. Characterization of articular cartilage and subchondral bone changes in the rat anterior cruciate ligament transection and meniscectomized models of osteoarthritis. Bone 38: 234-43.

Haywood L, McWilliams DF, Pearson CI, Gill SE, Ganesan A, Wilson D, Walsh DA. 2003. Inflammation and angiogenesis in osteoarthritis. Arthritis and Rheumatism 48: 2173–7.

Heathfield TF, Onnerfjord P, Dahlberg L, Heinegard D. 2004. Cleavage of fibromodulin in cartilage explants involves removal of the N-terminal tyrosine sulfate-rich region by proteolysis at a site that is sensitive to matrix metalloproteinase-13. Journal of Biological Chemistry 279: 6286–95.

Heir S, Årøen A, Løken S, Sulheim S, Engebretsen L, Reinholt FP. 2010. Intraarticular location predicts cartilage filling and subchondral bone changes in a chondral defect. Acta Orthopaedica 81: 619-27.

Henn RF, Gomoll AH. 2011. A review of the evaluation and management of cartilage defects in the knee. Physics in sports medicine 39: 101-7.

Henrotin Y, Pesesse L, Sanchez C. 2012. Subchondral bone and osteoarthritis: biological and cellular aspects. Osteoporosis International 23(S8): S847-51.

Herman BC, Cardoso L, Majeska RJ, Jepsen KJ, Schaffler MB. 2010. Activation of bone remodeling after fatigue: differential response to linear microcracks and diffuse damage. Bone 47(4): 766-72.

Hette K, Rahal SC, Volpi RS, Ferreira DOL, Teixeira CR. 2008. Arthroscopy of the stifle joint in sheep (artroscopia do joelho de ovinos. Pesquisa Veterinaria Brasileira 28(2): 119-23.

Hjertquist S-O and Lemperg R. 1972. Identification and concentration of the glycosaminoglycans of human articular cartilage in relation to age and osteoarthritis. Calcified Tissues Research 10: 233-37.

Hoa D, Micheau A, Gahide G, Le Bars E, Taourel P. 2008. Chapitre 1 – Résonance magnétique nucléaire (RMN), IN : l'IRM pas à pas, Sauramps Medical, Montpellier, France.

Hoemann CD. 2004. Molecular and biochemical assays of cartilage components. Methods in molecular medicine – Vol 101: Cartilage and osteoarthritis, Vol2: structure and *in vivo* analysis. Ed: De Ceuninck F., Sabatini M., Pastoreau P. – Humnana Press Inc., Springer, Totowa, NJ,.

Hoeman CD, Hurtig M, Rossomacha E, Sun J, Chevrier A, Shive MS, Buschmann MD. 2005 Chitosan-Glycerol Phosphate/Blood Implants improve Hyaline Cartilage Repair in Ovine Microfracture Defects. The Journal Of Bone And Joint Surgery 87 (12): 2671-86.

Hofmann MA, Drury S, Fu C, Qu W, Taguchi A, Lu Y, Avila C, Kambham N, Bierhaus A, Nawroth P, Neurath MF, Slattery T, Beach D, McClary J, Nagashima M, Morser J, Stern D, Schmidt AM. 1999. RAGE mediates a novel proinflammatory axis: a central cell surface receptor for S100/calgranulin polypeptides. Cell 97(7): 889-901.

Holland P, Davies AM, Cassar-Pullicino VN. 1994. Computed tomographic arthrography in the assessment of osteochondritis dissecans of the elbow. Clinical Radiology 49: 231-5.

Holm I, Oiestad BE, Risberg MA, Gunderson R, Aune AK. 2012. No differences in prevalence of osteoarthritis or function after open versus endoscopic technique for anterior cruciate ligament reconstruction: 12-year follow-up report of a randomized controlled trial. American journal of sports medicine 40: 2492–8.

Hontoir F, Nisolle JF, Meurisse H, Simon V, Tallier M, Vanderstricht R, Antoine N, Piret J, Clegg P, Vandeweerd JM. 2014. A comparison of 3-T magnetic resonance imaging and computed tomography arthrography to identify structural cartilage defects of the fetlock joint in the horse. The Veterinary Journal 199(1): 115-22.

Hontoir F, Clegg P, Nisolle JF, Tew S, Vandeweerd JM. 2015. Magnetic resonance compositional imaging of articular cartilage: What can we expect in veterinary medicine? The Veterinary Journal 205(1): 11-20.

Hontoir F, Clegg P, Simon V, Kirschvink N, Nisolle JF, Vandeweerd JM. 2017. Accuracy of computed tomographic arthrography for assessment of articular cartilage defects in the ovine stifle. Veterinary Radiology and Ultrasound 58(5): 512-23.

Hosseininia S, Lindber LR, Dahlberg LE, 2013. Cartilage collagen damage in hip osteoarthritis similar to that seen in knee osteoarthritis; a case-control study of relationship between collagen, glycosaminoglycan and cartilage swelling. BMC Musculoskeletal disorders 9: 14-8.

Huang FS, Simonian PT, Norman AG, Clark JM. 2004. Effects of small incongruities in a sheep model of osteochondral autografting. The American Journal of sports medicine 32: 1842-8.

Hughes PM, Bisset R. 1991. Non-ionic contrast media: a comparison of iodine delivery rates during manual injection angiography. The British Journal of Radiology 64: 417-9.

Hughes T, Welsch GH, Trattnig S, Brandi L, Domayer S, Mamisch TC. 2007. T2-star Relaxation as a means to diffrentiatie Cartilage Repair Tissue after Microfracturing Therapy. Proceedings of the International Society for Magnetic Resonance in Medicine 15: 812.

Hui AY, McCarty WJ, Masuda K, Firestein GS, Sah RL. 2012. A systems biology approach to synovial joint lubrication in health, injury, and disease. Wiley interdisciplinary reviews. Systems biology and medicine 4(1): 15-37.

Hulth A. 1993. Does osteoarthrosis depend on growth of the mineralized layer of cartilage? Clinic Orthopaedics Related Research 287:19–24.

Hunter DJ, Zhang Y, Niu J, Goggins J, Amin S, LaValley MP, Guermazi A, Genant H, Gale D, Felson DT. 2006. Increase in bone marrow lesions associated with cartilage loss: a longitudinal magnetic resonance imaging study of knee osteoarthritis. Arthritis and Rheumatism 54: 1529–35.

Hunter DJ, Lo GH, Gale D, Grainger AJ, Guermazi A, Conaghan PG. 2008. The reliability of a new scoring system for knee osteoarthritis MRI and the validity of bone marrow lesion assessment: BLOKS (Boston Leeds osteoarthritis Knee score). Annals of Rheumatic Disease 67: 206–11.

Hunter DJ, Gerstenfeld L, Bishop G, Davis AD, Mason ZD, Einhorn TA. 2009. Bone marrow lesions from osteoarthritis knees are characterized by sclerotic bone that is less well mineralized. Arthritis Research and Therapy 11(1): R11.

Hunziker EB, Rosenberg LC. 1996. Repair of partial-thickness defects in articular cartilage: cell recruitment from the synovial membrane. The journal of Bone and Joint surgery 78(5): 721-33.

Hurtig MB, Stewart WA, Trout DR, Dobson H, Bahr R, 1995. Magnetic resonance imaging of experimental tendonitis in sheep. Veterinary and Compoarative Orthopaedics and Traumatology 8: 52-57.

Hwang J, Bae WC, Shieu W, Lewis CW, Bugbee WD, Sah RL. 2008. Increased hydraulic conductance of human articular cartilage and subchondral bone plate with progression of osteoarthritis. Arthritis and Rheumatism 58: 3831–42.

Imhof H, Sulzbacher I, Grampp S, Czerny C, Youssefzadeh S, Kainberger F. 2000. Subchondral bone and cartilage disease: a rediscovered functional unit. Investigative Radiology 35: 581–8.

Inoue H. 1981. Alterations in the collagen framework of osteoarthritic cartilage and subchondral bone. International Orthopaedics 5: 47– 52.

Intema F, DeGroot J, Elshof B, Vianen ME, Yocum S, Zuurmond A, Mastbergen SC, Lafeber FP. 2008. The canine bilateral groove model of osteoarthritis. Journal of Orthopaedics Research 26(11): 1471-7.

Intema F, Hazewinkel HAW, Gouwens D, Bijlsma JWJ, Weinans H, Lafeber FPJG, Mastbergen SC. 2010. In early OA, thinning of the subchondral plate is directly related to cartilage damage: results from a canine ACLT-meniscectomy model. Osteoarthritis and Cartilage 18: 691-8.

Iqbal J, Dudhia J, Bird JL, Bayliss MT. 2000. Age-related effects of TGF-beta on proteoglycan synthesis in equine articular cartilage. Biochemical and biophysical research communications 274: 467-71.

Ishiguro N, Ito T, Ito H, Iwata H, Jugessur H, Ionescu M, Poole AR. 1999. Relationship of matrix metalloproteinases and their inhibitors to cartilage proteoglycan and collagen turnover: analyses of synovial fluid from patients with osteoarthritis. Arthritis and Rheumatism 42: 129–36.

Iwanaga T, Shikichi M, Kitamura H, Yanase H, Nozawa-Inoue K. 2000. Morphology and Functional Roles of Synoviocytes in the Joint. Archives of Histology and Cytology 63(1): 17-31.

Jackson DW, Lalor PA, Aberman HM, Simon TM. 2001. Spontaneous repair of full-thickness defects of articular cartialge in a goat model. The journal of bone and joint surgery 83(1): 53-64.

Janssen RP, du Mée AW, van Valkenburg J, Sala HA, Tseng CM. 2013. Anterior cruciate ligament reconstruction with 4-strand hamstring autograft and accelerated rehabilitation: a 10-year prospective study on clinical results, knee osteoarthritis and its predictors. Knee Surgery, Sports Traumatology, Arthroscopy 21:1977–88.

Jay GD, Britt D, Cha CJ. 2000. Lubricin is a product of megakaryocyte stimulating factor (MSF) gene expression by synovial fibroblasts. Journal of Rheumatology 27: 594–600.

Jay JD, Harris DA, Cha CJ. 2001. Boundary lubrication by lubricin is mediated by O-linked β(1-3)Gal-GalNAc oligosaccharides. Glycoconjugate Journal 18: 807–15.

Jeffcott LB, Kold SE. 1982. Stifle lameness in the horse: a survey of 86 referred cases. Euine Veterniary Journal 14: 31-9.

Santschi EM. 2008. Articular fetlock injuries in exercising horses. The Veterinary Clinics of North America. Equine practise 24: 117-32.

Jenkins ZA, van Kogelenberg M, Morgan T, Jeffs A, Fukuzawa R, Pearl E, Thaller C, Hing AV, Porteous ME, Garcia-Miñaur S, Bohring A, Lacombe D, Stewart F, Fiskerstrand T, Bindoff L, Berland S, Adès LC, Tchan M, David A, Wilson LC, Hennekam RC, Donnai D, Mansour S, Cormier-Daire V, Robertson SP. 2009. Germline mutations in WTX cause a sclerosing skeletal dysplasia but do not predispose to tumorigenesis. Nature genetics 41: 95-100.

Jin LH, Choi BH, Kim YJ, Park SR, Jin CZ, Min B-H. 2011. Implantation of bone marrow-derived buffy coat can supplement bone marrow stimulation for articular cartilage repair. Osteoarthritis and Cartilage 19: 1440-8.

Johansen M, Bahrt H, Altman R, Bartels E, Juhl C, Bliddal H, Lund H, Christensen R. 2015. Addressing controversies around intra-articular injections with hyaluronic acid in the treatment of osteoarthritis: meta-regression analyses of randomized trials. Osteoarthritis and cartilage 23: A47.

Johnston GM, Eastment JK, Wood J, Taylor PM. 2002. The confidential enquiry into perioperative equine fatalities (CEPEF): mortality results of Phases 1 and 2. Veterinary Anaesthesia and Analgesia 29(4):159-70.

Joscht M, Martin M, Henin M, Nisolle JF, Kirschvink N, Dugdale A, Godart B, Coulon H, Simon V, Hontoir F, Graffin R, De Raeve Y, Vandeweerd JM. 2016. Angiographic Anatomy of External Iliac Arteries in the Sheep. Anatomia Histologia Embryologia 45(6): 443-9.

Kadri A, Ea HK, Bazille C, Hannouche D, Lioté F, Cohen-Solal ME. 2008. Osteoprotegerin inhibits cartilage degradation through an effect on trabecular bone in murine experimental osteoarthritis. Arthritis and Rheumatism 58(8): 2379-86.

Kalender WA. 2011, Computed tomography. Fundamentals, system technology, image quality, applications. 3rd edition, Dorit Gunia, Publicis publishing, Erlangen, 2011.

Kalke RJ, Di Primio G, Schweitzer ME. 2012. MR and CT Arthrography of the Knee. Seminars in musculoskeletal radiology 16: 57-68.

Kallioniemi AS, Jurvelin JS, Nieminen MT, Lammi MJ, Töyäs J. 2007.Contrast agent enhanced pQCT of articular cartilage. Physics in Medicine and Biology 52: 1209-19.

Kamibayashi L, Wyss UP, Cooke TDV, Zee B. 1995. Trabecular microstructure in the medial condyle of the proximal tibia of patients with knee osteoarthritis. Bone 17: 27–35.

Kang EH, Lee YJ, Kim TK, Chang CB, Chung JH, Shin K, Lee EY, Lee EB, Song YW. 2010. Adiponectin is a potential catabolic mediator in osteoarthritis cartilage. Arthritis Research and Therapy 12(6): R231.

Kaplan LD, Lu Y, Snitzer J, Nemke B, Hao Z, Biro S, Albiero W, Stampfli HF, Markel M, Popkin C, Baum SZ. 2009. The Effect of Early Hyaluronic Acid Delivery on the Development of an Acute Articular Cartilage Lesion in a Sheep Model. American Journal of Sports Medicine 37: 2323-27.

Kapoor M, Martel-Pelletier J, Lajeunesse D, Pelletier JP, Fahmi H. 2010. Role of proinflammatory cytokines in the pathophysiology of osteoarthritis. Nature Review in Rheumatology 7(1):33–42.

Karsdal MA, Madsen SH, Christiansen C, Henrisken K, Fosang AJ, Sondergaard BC. 2008. Cartilage degradation is fully reversible in the presence of aggrecanase but not matrix metalloproteinase activity. Arthritis research and Therapy 10(3): 63.

Karvonen RL, Negendank WG, Fraser SM, Mayes MD, An T, Fernandez-Madrid F. 1990. Articular cartilage defects of the knee: Correlation between magnetic resonance imaging and gross pathology. Annals of Rheumatic Diseases 49: 672–5.

Katta J, Stapleton T, Ingham E, Jin ZM, Fisher J. 2008. The effect of glycosaminoglycan depletion on the friction and deformation of articular cartilage. Proceedings of the Institution of Mechanical Engineers Part H-Journal of Engineering in Medicine 222: 1-11.

Kawcak CE, Norrdin RW, Frisbie DD, Trotter GW, McIlwraith CW. 1998. Effects of osteochondral fragmentation and intra-articular triamcinolone acetonide treatment on subchondral bone in the equine carpus. Equine Veterinary Journal 30(1): 66-71.

Kawcak CE, McIlwraith CW, Norrdin RW, Park RD, James SP. 2001. The role of subchondral bone in joint disease: a review. Equine Veterinary Journal 33(2): 120-6.

Keen HI, Conaghan PG. 2009. Ultrasonography in osteoarthritis. Radiologic clinics of North America 47: 581–94.

Keenan KE, Besier TF, Pauly JM, Han E, Rosenberg J, Smith RL, Delp SL, Beaupre GS, Gold GE. 2011. Prediction of glycosaminoglycan content in human cartilage by age, T1 rho and T2 MRI. Osteoarthritis and Cartilage 19: 171-9.

Kelly BT, Potter HG, Deng X-H, Pearle AD, Turner AS, Warren RF, Rodeo SA. 2006. Meniscal allograft transplantation in the sheep knee: Evaluation of chondroprotective effects. American Journal of Sports Medicine 34: 1464-77.

Kelly BT, Robertson W, Potter HG, Deng XH, Turner AS, Lyman S, Warren RF, Rodeo SA. 2007. Hydrogel meniscal replacement in the sheep knee: Preliminary evaluation of chondroprotective effects. Americna Journal of Sports Medicine 35: 43-52.

Kempson GE. 1982. Relationship between the tensile properties of articular cartilage from the human knee and age. Annals of the Rheumatic Diseases 41: 508-11.

Kiani C, Chen L, Wu YJ, Yee AJ, Yang BB.2002. Structure and function of aggrecan. Cell Research 12(1): 19-32.

Kijowski R, Davis KW, Woods MA, Lindstrom MJ, De Smet AA, Gold GE, Busse RF. 2009. Knee joint: comprehensive assessment with 3D isotropic resolution fast spin-echo MR imaging--diagnostic performance compared with that of conventional MR imaging at 3.0 T. Radiology 252(2): 486-95.

Kijowski R., Blankenbaker DG, Woods M, Munoz Del Rio A., De Smet AA, Reeder SB, 2011. Clinical usefulness of adding 3D cartilage imaging sequences to a routine knee MR protocol. American Journal of Roentgenology 196: 159-67.

Kim KK, Won Y, Kim T-G, B M-H, Choi J., 2015. Comparison of the chemical composition of subchondral trabecular bone of medial femoral condyle between with advanced osteoarthritis and without osteoarthritis. Journal of bone Metabolism 22: 93-7.

Kinns J, Pease A. 2011. Computed tomography (chapter 70) in Section IX diagnosis imaging 979-985. In Equine surgery 4th edition, Auer J, Stick J. Wiley-Blackwell publishing. Kinns J, Pease A, Chapter 70 – Computed Tomography. Equine Surgery, 4th ed. Editors: Auer J, Stick J. Wiley-Blackwell Publishing.

Kirkland, WD. 2011. CT Arthrography. It's not always about the magnet, 63th Annual Midwinter Radiology Conference, February 13th, 2011, by LARS (Los Angeles Radiological Society), Pasadera Convention Center.

Kleeman RU, Schell H, Thompson M, Epari DR, Duda GN, Weiler A. 2007. Mechanical behaviour of articular cartilage after osteochondral autograft transfer in an ovine model. The American journal of sports medicine 35(4): 555-563.

Klein TJ, Chaudhry M, Bae WC, Sah RL. 2007. Depth-dependent biomechanical and biochemical properties of fetal, newborn, and tissue-engineered articular cartilage. Journal of Biomechanics 40(1): 182-90.

Knott L, Whitehead CC, Fleming RH, Bailey AJ. 1995. Biochemical changes in the collagenous matrix of osteoporotic avian bone. Biochemistyr Journal 310(Pt 3): 1045-51.

Knott L, Bailey AJ. 1998. Collagen cross-links in mineralizing tissues: a review of their chemistry, function, and clinical relevance. Bone 22(3): 181-7.

Ko JS, Kim CS, Shin BS, Kim MJ, Lee JH, Kim KH, Lee JH, Kim KH, Do YS. 2011. Changes in pulmonary artery pressures during ethanol sclerotherapy for arteriovenous malformations: identifying the most vulnerable period. Clinical Radiology 66(7): 639-44.

Kokkonen HT, Mäkelä J, Kulmala KA, Rieppo L, Jurvelin JS, Tiitu V, Karjalainen HM, Korhonen RK, Kovanen V, Töyräs J. 2011. Computed tomography detects changes in contrast agent diffusion after

collagen cross-linking typical to natural aging of articular cartilage. Osteoarthritis and Cartilage 19: 1190-8.

Kokkonen HT, Aula AS, Kröger H, Suomalainen JS, Lammentausta E, Mervaala E, Jurvelin JS, Töyräs J. 2012. Delayed Computed Tomography Arthrography of Human Knee Cartilage *In Vivo*. Cartilage 3(4): 334-41.

Komuro H, Olee T, Ku¨hn K, Quach J, Brinson DC, Shikhman A, Valbracht J, Creighton-Achermann L, Lotz M. 2001. The osteoprotegerin/receptor activator of nuclear factor kappaB/receptor activator of nuclear factor kappaB ligand system in cartilage. Arthritis Rheum 44: 2768–76.

Koulouris G. 2006. MRI Evaluation of cartilage. AFL Medical Officers Association Cartilage Injury Forum. Melbourne.

Krenn V, Morawietz L, Burmester GR, Kinne RW, Mueller-Ladner U, Muller B, Haupl T. 2006. Synovitis score: discrimination between chronic low-grade and highgrade synovitis. Histopathology 49:358–64

Krusche-Mandl I, Schmitt B, Zak L, Apprich S, Aldrian S, Juras V, Friedrich KM, Marlovits S, Weber M, Trattnig S. 2012. Long-term results 8 years after autologous osteochondral transplantation: 7T gagCEST and sodium magnetic resonance imaging with morphological and clinical correlation. Osteoarthritis and Cartilage 20: 357-63.

Kulmala KAM, Pulkkinen HJ, Rieppo L, Tiitu V, Kiviranta I, Brünott A., Brommer H., van Weeren R., Brama PAJ, Mikkola MT, Korhonen RK, Jurvelin JS, Töyräs J. 2012. Contrast-enhanced micro-computed tomography in evaluation of spontaneous repair of equine cartilage. Cartilage 3 : 235-44.

Kurkijarvi JE, Nissi MJ, Kiviranta I, Jurvelin JS, Nieminen MT. 2004. Delayed Gadolinium-enhanced MRI of cartilage (dGEMRIC) and T2 characteristics of human knee articular cartilage: Topographical variation and relationships to mechanical properties. Magnetic resonance in medicine 52: 41-6.

Kurkijärvi JE, Nissi MJ, Rieppo J, Töyräs J, Kiviranta I, Nieminen MT, Jurvelin JS . 2008. The zonal architecture of human articular cartilage described by T2 relaxation time in the presence of Gd-DTPA2-. Magnetic Resonance Imaging 26(5): 602-7.

Kuroki K, Cook CR, Cook JL. 2011. Subchondral bone changes in three different canine models of osteoarthritis. Osteoarthritis and Cartilage 19: 1142-9.

Kwack KS, Cho JH, Kim M, Yoon CS, Yoon YS, Choi JW, Kwon JW, Min BH, Sun JS, Kim SY. 2008. Comparison study of intraarticular and intravenous gadolinium-enhanced magnetic resonance imaging of cartilage in a canine model. Acta Radiologica 49: 65–74.

Lacey DL, Timms E, Tan HL, Kelley MJ, Dunstan CR, Burgess T, Elliott R, Colombero A, Elliott G, Scully S, Hsu H, Sullivan J, Hawkins N, Davy E, Capparelli C, Eli A, Qian YX, Kaufman S, Sarosi I, Shalhoub V, Senaldi G, Guo J, Delaney J, Boyle WJ. 1998. Osteoprotegerin ligand is a cytokine that regulates osteoclast differentiation and activation. Cell 93: 165–76.

Lago R, Gomez R, Otero M, Lago F, Gallego R, Dieguez C, Gomez-Reino JJ, Gualillo O. 2008. A new player in cartilage homeostasis: adiponectin induces nitric oxide synthase type II and pro-inflammatory cytokines in chondrocytes. Osteoarthritis Cartilage 16(9): 1101-9.

Lahm A, Uhl M, Erggelet C, Haberstroh J, Mrosek E. 2004. Articular cartilage degeneration after acute subchondral bone damage: an experimental study in dogs with histopathological grading. Acta orthopaedica Scandinavia 75(6): 762-7.

Lahm A, Uhl M, Edlich M, Erggelet C, Kreuz P. 2005. An experimental canine model for subchondral lesions of the knee joint. Knee 12(1): 51–5.

Lahm A, Kreuz PC, Oberst M, Haberstroh J, Uhl M, Maier D. 2006. Subchondral and trabecular bone remodeling in canine experimental osteoarthritis. Archives in Orthopaedic and Trauma Surgery 126: 582-7.

Lai WM, Hou JS, Mow VC. 1991. A triphasic theory for the swelling and deformation behaviors of articular cartilage. Journal of Biomechanical engineering 113(3): 245-58.

Lajeunesse D, Reboul P. 2003. Subchondral bone in osteoarthritis: a biologic link with articular cartilage leading to abnormal remodelling. Current Opinions in Rheumatology 15: 628–33.

Lajeunesse D, 2004. The role of bone in the treatment of osteoarthritis. Osteoarthritis and cartilage 12: S34-S38.

Lakin BA, Grasso DJ, Shah SS, Stewart RC, Bansal PN, Freedman JD, Grinstaff MW, Snyder BD. 2013. Cationic agent contrast-enhanced computed tomography imaging of cartilage correlates with the compressive modulus and coefficient of friction. Osteoarthritis and Cartilage 21: 60-8.

Lakin BA, Patel H, Stok KS, Snyder BD, Grinstaff MW. 2014. Contrast-enhanced computed tomography imaging using a cationic contrast agent correlates with the equilibrium modulus of mouse tibial plateau cartilage. Journal of Orthopaedic Research 34(7) 1130-8.

Lamer TJ. 1999. Lumbar spine pain originating from vertebral osteophytes. Regional Anesthesia and Pain medicine 24: 347–51.

Lammentausta E, Kiviranta P, Töyräs J, Hyttinen MM, Kiviranta I, Nieminen MT, Jurvelin JS. 2007. Quantitative MRI of parallel changes of articular cartilage and underlying trabecular bone in degeneration. Osteoarthritis and Cartilage 15: 1149-57.

Landis JR, Koch GG. 1977. The measurement of observer agreement for categorical data. Biometrics 33: 159–74.

Lane LB, Villacin A, Bullough PG. 1977. The vascularity and remodelling of subchondral bone and calcified cartilage in adult human femoral and humeral heads: An age- and stress-related phenomenon. Journal of Bone and Joint surgery 59-B: 272–8.

Larsson S, Englund M, Struglics A, Lohmander LS. 2015. Interleukin-6 and tumor necrosis factor alpha in synovial fluid are associated with progression of radiographic knee osteoarthritis in subjects with previous meniscectomy. Osteoarthritis and Cartilage 23(11): 1906–14.

Lascelles BDX. 2010. Feline degenerative joint disease. Invited review. Veterinary surgery 39: 2-13.

Launois T, Descrosse F, Perrin R. 2003. Percutanéous osteostixis as treatment for avulsion fractures of the palmar/plantar third metacarpal/metatarsal bone cortex at the origin of the suspensory ligament in 29 cases. Equine Veterinary Education 15(3): 126-138.

Launois TM, Vandeweerd JME, Perrin RAR, Brogniez L, Desbrosse FG, Clegg PD. 2009. Use of computed tomography to diagnose new bone formation associated with desmitis of the proximal aspect of the suspensory ligament in third metacarpal or third metatarsal bones of three horses. Journal of American Veterinary Medicine Association 234: 514-8.

Lawrence RC, Felson DT, Helmick CG, Arnold LM, Choi H, Deyo RA, Gabriel S, Hirsch R, Hochberg MC, Hunder GG, Jordan JM, Katz JN, Kremers HM, Wolfe F. 2008. Estimates of the prevalence of arthritis and other rheumatic conditions in the United States. Part II. Arthritis and Rheumatism 58: 26-35.

Layton MW, Goldstein SA, Goulet RW, Feldkamp LA, Kubinski DJ, Bole GG. 1988. Examination of subchondral bone architecture in experimental osteoarthritis by microscopic computed axial tomography. Arthritis Rheum 31: 1400–5.

Le Pen C, Reygrobellet C, Gérentes I. 2005. Financial cost of osteoarthritis in France. The "COART" France study. Joint Bone Spine 72: 567-570.

Lecouvet F, Dorze B, Dubuc JE, Vande Berg BC, Jamart J, Malghem J. 2007. Cartilage lesions of the gleno-humeral joint: diagnostic effectiveness of multidetector spiral CT arthrography and comparison with arthroscopy. Eur Radiol 17(7): 1763-71.

Li B, Aspden RM. 1997. Composition and mechanical properties of cancellous bone from the femoral head of patients with osteoporosis and osteoarthritis. Journal of Bone and Mineral Research 12: 641–51.

Li G, Yin J, Gao J, Cheng TS, Pavlos NJ, Zhang C, Zheng MH. 2013. Subchondral bone in oteoarthritis: insight into risk factors and microstructural changes. Arthritis research and therapy 15: 223.

Li X, Han ET, Ma CB, Link TM, Newitt DC, Majumdar S. 2005. *In vivo* 3T spiral image based multi-slice T1ρ mapping of knee cartilage in osteoarthritis. Magnetic Resonance in Medicine 54: 929-36.

Li X, Ma B, Link TM, Castillo D-D, Blumenkrantz G, Lozano J, Carballido-Gamio J, Ries M, Majumdar S. 2007. *In vivo* T1rho and T2 mapping of articular cartilage in osteoarthritis of the knee using 3 Tesla MRI. Osteoarthritis Cartilage 15: 789–97.

Liao YY, Lin YM. 2008. McNemar test is preferred for comparison of diagnostic techniques. American Journal of Roentgenology 191: 190.

Liess C, Lüsse S, Karger N, Heller M, Glüer C-C. 2002. Detection of changes in cartilage water content using MRI T2-mapping *in vivo*. Osteoarthritis and cartilage 10: 907-13.

Lill CA, Winterstein E, Eckhardt C., Goldhahn J., Schneider E. 2003. Quantification of histomorphometric and structural bone changes in a sheep model for fracture in osteoporotic bone. Veterinary and Comparative orthopaedics and Traumatology 16: 243-9.

Lindsey CT, Narasimhan A, Adolfo JM, Jin H, Steinbach LS, Link T, Riest M, Majumdar S. 2004. Magnetic resonance evaluation of the interrelationship between articular cartilage and trabecular bone of the osteoarthritic knee. Osteoarthritis and Cartilage 12: 86-96.

Ling W, Regatte RR, Navon G, Jerschow A. 2008. Assessment of glycosaminoglycan concentration *in vivo* by chemical exchange-dependent saturation transfer (gagCEST). PNAS 105: 2266-70.

Little CB, Smith MM. 2008. Animal models of osteoarthritis. Current Rheumatology Reviews 4: 175-82.

Little CB, Smith MM, Cake MA, Read RA, Murphy MJ, Barry FP. 2010. The OARSI histopathology initiative – recommendations for histological assessments of osteoarthritis in sheep and goats. Osteoarthritis and Cartilage 18: S80-S92.

Little JP, Bleedorn JA, Sutherland BJ, Sullivan R, Kalscheur VL, Ramaker MA, Schaefer SL, Hao Z, Muir P. 2014. Arthroscopic assessment of stifle synovitis in dogs with cranial cruciate ligament rupture. PLoS One 9(6): e97329.

Llopis E, Fernandez E, Cerezal L. 2012. MR and CT arthrography of the hip. Seminars in Musculoskeletal Radiology 16: 42-56.

Loeser RF, Shanker G, Carlson CS, Gardin JF, Shelton BJ, Sonntag WE. 2000. Reduction in the chondrocyte response to insulin-like growth factor 1 in aging and osteoarthritis: studies in a non-human primate model of naturally occurring disease. Arthritis and Rheumatism 43:2110-20.

Loeser RF, Goldring SR, Scanzello CR, Goldring MB. 2012. Osteoarthritis: A disease of the joint as an organ. Arthritis and Rheumatism 64 (6): 1697–1707.

Lu XL, Mow VC. 2008. Biomechanics of Articular Cartilage and determination of Material Properties. Medicine and science in sports and exercise 40: 193-9.

Lüsse S, Claassen H, Gehrke T, Hassenpflug J, Schünke M, Heller M, Glüer C-C. 2000. Evaluation of water content by spatially resolved transverse relaxation times of human articular cartilage. Magnetic resonance imaging 18: 423-30.

Lyon R, Liu XC, Kubin M, Schwab J. 2013. Does extracorporeal shock wave therapy enhance healing of osteochondritis dissecans of the rabbit knee? A pilot study. Clinical Orthopaedics and related research 471(4):1159-65.

Lyons TJ, Stoddart RW, McClure SF, McClure J. 2005. The tidemark of the chondro-osseous junction of the normal human knee joint. Journal of Molecular Histology 36: 207–15.

Lyons TJ, McClure SF, Stoddart RW, McClure J. 2006. The normal human chondro-osseous junctional region: evidence for contact of uncalcified cartilage with subchondral bone and marrow spaces. BMC Musculoskeletal Disorders 7:52.

Madelin, G., Babb, J.S., Xia, D., Chang, G., Jerschow, A., Regatte, R.R., 2012. Reproducibility and repeatability of quantitative sodium magnetic resonance imaging *in vivo* in articular cartilage at 3T and 7T. Magnetic resonance in medicine 68, 841-849.

Madry H, van Dijk CN, Mueller-Gerbl M. 2010. The basic science of the subchondral bone. Knee Surgery, Sports Traumatolology. Arthroscopy 18(4): 419-33.

Madry H, Luyten FP, Facchini A. 2012. Biological aspects of early osteoarthritis. Knee Surgery, Sports Traumatolology, Arthroscopy 30(3): 407–22.

Maetzel A, Li LC, Pencharz J, Tomlinson G, Bombardier C; Community Hypertension and Arthritis Project Study Team. 2004. The economic burden associated with osteoarthritis, rheumatoid arthritis, and hypertension: a comparative study. Annals of the rheumatic diseases 63: 395-401.

Malinin T, Ouellette EA. 2000. Articular cartilage nutrition is mediated by subchondral bone: a long-term autograft study in baboons. Osteoarthritis Cartilage 8: 483-91.

Mamisch TC, Menzel MI, Welsch GH, Bittersohl B, Salomonowitz E, Szomolanyi P, Kordelle J, Marlovits S, Trattnig S. 2008. Steady-state diffusion imaging for MR in-vivo evaluation of reparative cartilage after matrix-associated autologous chondrocyte transplantation at 3 tesla—preliminary results. European Journal of Radiology 65: 72–9.

Mamisch TC, Hughes T., Mosche TJ, Mueller C, Trattnig S, Boesch C, Welsch GH, 2012. T2star relaxation times for assessment of articular cartilage at 3T: a feasibility study. Skeletal radiology 41: 287-92.

Manggold J, Sergi C, Becker K, Lukoschek M, Simank HG. 2002. A new animal model of femoral head necrosis induced by intraosseous injection of ethanol. Laboratory Animals 36(2): 173-80.

Mansell JP, Bailey AJ. 1998. Abnormal cancellous bone collagen metabolism in osteoarthritis. Journal of Clinical Investigations 101: 1596-603.

Maroudas A, Bullough P, Swanson SAV, Freeman MAR. 1968. The permeability of articular cartilage. The journal of Boint and Joint Surgery 50B(1): 166-77.

Maroudas A, Muir H, Wingham J. 1969. The correlation of fixed negative charge with glycosaminoglycan content of human articular cartilage. Biochim Biophys Acta 17: 492-500.

Maroudas AI. 1976. Balance between swelling pressure and collagen tension in normal and degenerate cartilage, Nature 260(5554): 808-9.

Marshall WG, Hazewinkel HAW, Mullen D, De Meyer G, Baert K, Carmichael S. 2010. The effect of weight loss on lameness in obese dogs with osteoarthritis. Veterinary Research Communications 34 (3): 241-53.

Martig S, Konar M, Schmökel HG, Rytz U, Spreng D, Scheidegger J, Höhl B, Kircher PR, Boisclair J, Lang J. 2006. Low-field Mri and arthroscopy of meniscal lesions in ten dogs with experimentally induced cranial cruciate ligament insufficiency. Veterinary Radiology and Ultrasound 47(6): 515-22.

Martinez-Calatrava MJ, Prieto-Potín I, Roman-Blas JA, Tardio L, Largo R, Herrero-Beaumont G. 2012. RANKL synthesized by articular chondrocytes contributes to juxta-articular bone loss in chronic arthritis. Arthritis Research and Therapy 14(3):R149.

Mathiessen A, Slatkowsky-Christensen B, Kvien TK, Hammer HB, Haugen IK. 2016. Ultrasound-detected inflammation predicts radiographic progression in hand osteoarthritis after 5 years. Annals of the Rheumatic Diseases 75(5): 825–30.

Mathiessen A, Conaghan PG. 2017. Synovitis in osteoarthritis: current understanding with therapeutic implications. Arthritis Research Therapy 19(1): 18.

Matsui A, Shimizu M, Beale B, Takahashi F, Yamaguchi S. 1997. Assessment of T2 Relaxation Times for Normal Canine Knee Articular Cartilage by T2 Mapping Using 1.5-T Magnetic Resonance Imaging. Veterinary and Comparative Orthopaedics and Traumatology 30(6): 391-7.

Matsuo M, Nishida K, Yoshida A, Murakami T, Inoue H. 2001. Expression of caspase-3 and -9 relevant to cartilage destruction and chondrocyte apoptosis in human osteoarthritic cartilage. Acta Medicine Okayama 55: 333–40.

Mayo-Smith WW, Hara AK, Mahesh M, Sahani DV, Pavlicek W. 2014. How I do it : Managing radiation dose in CT. Radiology 273: 657-72.

McCauley TR, Disler DG. 2001. Magnetic resonance imaging of articular cartilage of the knee. Journal of the American Academy of Orthopaedic Surgeons 9: 2–8.

McCoy AM. 2015. Animal Models of Osteoarthritis Comparisons and Key Considerations Veterinary Pathology 52(5): 803-18.

McGibbon CA, Trahan CA. 2003. Measurement accuracy of focal cartilage defects from MRI and correlation of MRI graded lesions with histology: A preliminary study. Osteoarthritis and Cartilage 11: 483–493.

McIlwraith CW. 1996. General pathobiology of the joint and response to injury. In: Joint Disease in the Horse, Eds: C.W. McIlwraith and G.W. Trotter, W.B. Saunders Co., Philadelphia.

McIlwraith CW, Nixon AJ, Wright IM, Boening J. 2005. Diagnostic and surgical arthroscopy in the horse. 3rd ed. Maryland Heights, MO: Elsevier Mosby.

McIlwraith CW, Frisbie DD, Kawcak CE, Fuller CJ, Hurtig M, Cruz A. 2010. The OARSI histopathology initiative – recommendations for histological assessments of osteoarthritis in the horse. Osteoarthritis and Cartilage 18: S93-105.

McIlwraith CW, Fortier LA, Frisbie DD, Nixon AJ. 2011. Equine model of articular cartilage repair. Cartilage 2(4): 317-26.

McNulty AL, Miller MR, O'Connor SK, Guilak F. 2011. The effects of adipokines on cartilage and meniscus catabolism. Connective Tissue Research 52(6): 523-33.

McQueen FM. 2007. A vital clue to deciphering bone pathology: MRI bone oedema in rheumatoid arthritis and osteoarthritis. Annals of the Rheumatic Diseases 66(12): 1549-52.

Mc Robbie DW, Moore EA, Graves MJ, Prince MR. 2006. Chapter 8 – Getting in tune : resonance and relaxation, IN : MRI : from picture to proton (2nd edition), Cambridge University Press, New York, USA.

Meachim G, Stockwell RA. 1979. The matrix. In Adult Articular Cartilage, 2nd ed., Freeman MAR, pp. 1-67. Tunbridge Wells: Pitman Medical.

Meachim G, Allibone R. 1984. Topographical variation in the calcified zone of upper femoral articular cartilage. Journal of Anatomy 139 (2): 341-52.

Mee AM, Cripps PJ, Jones RS. 1998. A retrospective study of mortality associated with general anaesthesia in horses: elective procedures. Veterinary Record 142(11): 275-6.

Melrose J, Smith S, Ghosh P 2004. Histological and immunological studies on cartilage. In: Methods in molecular medicine – Vol 101: Cartilage and osteoarthritis, Vol2: structure and *in vivo* analysis. Ed: De Ceuninck F., Sabatini M., Pastoreau P. – Humnana Press Inc., Springer, Totowa, NJ.

Mendler M, Eich-Bender SG, Vaughan L, Winterhalter KH, Bruckner P. 1989. Cartilage contains mixed fibrils of collagen types II, IX, and XI. Journal of Cellular Biology 108(1): 191-7.

Menendez MI, Clark DJ, Carlton M, Flanigan DC, Jia G, Sammet S, Weisbrode SE, Knopp MV, Bertone AL. 2011. Delayed human adenoviral BMP-2 or BMP-6 gene therapy for bone and cartilage regeneration in a pony osteochondral model. Osteoarthritis and Cartilage 19, 1066-1075.

Menezes NM, Gray ML, Hartke JR, Burstein D. 2004. T2 and T1ρ MRI in articular cartilage systems. Magnetic resonance medicine 51: 503-9.

Menkes CJ, Lane NE. 2004. Are osteophytes good or bad? Workshop- OsteoArthritis and Cartilage 12: S53–4.

Mente P, Lewis JL. 1994. The elastic modulus of calcified cartilage is an order of magnitude less than that of subchondral bone. Journal of Orthopaedics Research 12: 637–47.

Messai H, Duchossoy Y, Khatib A, Panasyuk A, Mitrovic DR. 2000. Articular chondrocytes from aging rats respond poorly to insulin-like growth factor- 1: an altered signaling pathway. Mechanisms of ageing and development 115: 21-37.

Meuffels DE, Favejee MM, Vissers MM, Heijboer MP, Reijman M, Verhaar JA. 2009. Ten year follow-up study comparing conservative versus operative treatment of anterior cruciate ligament ruptures. A matched-pair analysis of high level athletes. British Journal of Sports Medicine 43(5): 347-51.

Meunier PJ, Boivin G. 1997. Bone mineral density reflects bone mass but also the degree of mineralization of bone: therapeutic implications. Bone 21: 373–7.

Mickevicius T, Pockevicius A, Kucinskas A, Gudas R, Maciulaitis J, Noreikaite A, Usas A. 2015. Impact of storage conditions on electromechanical, histological and histochemical properties of osteochondral allografts. BMC Musculoskeletal Disorders 16: 314.

Miles CA, Sims TJ, Camacho NP, Bailey AJ. 2002. The role of the alpha2 chain in the stabilization of the collagen type I heterotrimer: a study of the type I homotrimer in oim mouse tissues. Journal of Molecular Biology 321: 797–805.

Mink JH, Deutsch AL. 1989. Occult cartilage and bone injuries of the knee: detection, classification and assessment with MR imaging. Radiology 170: 823.

Miyata S, Homma K, Numano T, Furukawa K, Tateishi T, Ushida T. 2006. Assessment of fixed charge density in regenerated cartilage by Gd-DTPA-enhanced MRI. Magnetic Resonance Medicine Sciences 5(2):73-8.

Mlynarik V, Sulzbacher I, Bittsansky M, Fuiko R, Trattnig S. 2003. Investigation of apparent diffusion constant as an indicator of early degenerative disease in articular cartilage. Journal of Magnetic Resonance Imaging 17: 440-4.

Mobasheri A, Henrotin Y. 2010. Identification, validation and quantification of biomarkers for osteoarthritis in human and companion animals: Mission for the next decade. The Veterinary Journal 185: 95-7.

Modesto RB, Mansmann KA, Schaer TP. 2014. Arthroscopy of the normal cadaveric ovine femorotibial joint: a systemic approach to the cranial and caudal compartments. Veterinary and Comparative Orthopaedic and Traumatology 27: 387-94.

Moores AP, Benigni L, Lam CR. 2008. Computed tomography versus arthroscopy for detection of canine elbow dysplasia lesions. Veterinary surgery 34 (4): 390-8.

Moses MA, Wiederschain D, Wu I, Fernandez CA, Ghazizadeh V, Lane WS, Flynn E, Sytkowski A, Tao T, Langer R. 1999. Troponin I is present in human cartilage and inhibits angiogenesis. Proceedings of the National Academy of Sciences of the United States of America 96(6): 2645-50.

Mosher TJ, Dardzinski BJ, Smith MB. 2000. Human articular cartilage: influence of aging and early symptomatic degeneration on the spatial variation of T2- preliminary findings at 3 T. Radiology 214(1): 259-66.

Mosher TJ, Smith H, Dardzinski BJ, Schmithorst VJ, Smith MB, 2001. MR imaging and T2 mapping of femoral cartilage: *in vivo* determination of the magical angle effect. American Journal Of Reontgenology 177: 665-9.

Mosher, T.J., 2006. Musculoskeletal imaging at 3T: Current techniques and future applications. Magnetic Resonance Imaging Clinics of North America 14: 63–76.

Mosher TJ, Liu Y, Torok CM, 2010. Functional cartilage MRI T2 mapping: Evaluating the effect of age and training on knee cartilage response to running. Osteoarthritis and cartilage 18: 358-64.

Moskowitz R. 1999. Bone remodeling in osteoarthritis: subchondral and osteophytic responses. Osteoarthritis Cartilage 7: 323–4.

Mow VC, Kuei SC, Lai WM, Armstrong CG. 1980. Biphasic creep and stress relaxation of articular cartilage in compression? Theory and experiments. Journal of Biomechanical Engineering 102(1): 73-84.

Moya-Angeler J., Gonzalez-Nieto J., Sanchez Monforte J, Altonaga JR, Vaquero J, Forriol F. 2016. Surgical induced models of joint degeneration in the ovine stifle: Magnetic resonance imaging and histological assessment. The knee 23: 214-20.

Mrosek EH, Lahm A, Erggelet C, Uhl M, Kurz H, Eissner B, Schagemann JC. 2006. Subchondral bone trauma causes cartilage matrix degeneration: an immunohistochemical analysis in a canine model. Osteoarthritis and Cartilage 14: 171-8.

Muir H, Bullough P, Maroudas A. 1970. The distribution of collagen in human articular cartilage with some of its physiological implications. Journal of Bone nd Joint Surgery Britain 52(3): 554-63.

Muir H. 1995. The chondrocyte, architect of cartilage: biomechanics, structure, function and molecular-biology of cartilage matrix macromolecules. Bioessays 17: 1039–48.

Muller R, Hahn M, Vogel M, Delling G, Ruegsegger P. 1996. Morphometric analysis of noninvasively assessed bone biopsies: comparison of high-resolution computed tomography and histologic sections. Bone 18(3): 215-20.

Muller-Gerbl M, Dalstra M, Ding M, Linsenmeier U, Putz R, Hvid I. 1998. Distribution of strength and mineralization in the subchondral bone plate of human tibial heads. Journal of Biomechanics 31(Suppl 1):123 Proceedings of the 11th conference of the European Society of Biomechanics.

Muraoka T, Hagino H, Okano T, Enokida M, Teshima R. 2007. Role of subchondral bone in osteoarthritis development: a comparative study of two strains of guinea pigs with and without spontaneously occurring osteoarthritis. Arthritis and Rheumatism 56(10): 3366-74.

Naredo E, Cabero F, Palop MJ, Collado P, Cruz A, Crespo M. 2005. Ultrasonographic findings in knee osteoarthritis: a comparative study with clinical and radiographic assessment. Osteoarthritis and Cartilage 13: 568–74.

Nelson BB, Kawcak CE, Barrett MF, McIlwraith CW, Grinstaff MW, Goodrich LR. 2018. Recent advances in articular cartilage evaluation using computed tomography and magnetic resonance imaging. Equine Veterinary Journal. doi: 10.1111/evj.12808.

Neogi T, Felson D, Niu J, Lynch J, Nevitt M, Guermazi A, Roemer F, Lewis CE, Wallace B, Zhang Y. 2009. Cartilage loss occurs in the same subregions as subchondral bone attrition: a within-knee subregion-matched approach from the multicentre osteoarthritis study. Arthritis and rheumatism (Arthritis cate and research) 61 (11): 1539-44.

Neu CP, Reddi AH, Komvopoulos K, Schmid TM, Di Cesare PE. 2010. Increased friction coefficient and superficial zone protein expression in patients with advanced osteoarthritis. Arthritis and Rheumatism 62(9): 2680–7.

Neuhold LA, Killar L, Zhao W, Sung ML, Warner L, Kulik J, Turner J, Wu W, Billinghurst C, Meijers T, Poole AR, Babij P, DeGennaro LJ. 2001. Postnatal expression in hyaline cartilage of constitutively active human collagenase-3 (MMP-13) induces osteoarthritis in mice. Journal of Clinical Investigations 107: 35-44.

Neuman P, Kostogiannis I, Friden T, Roos H, Dahlberg LE, Englund M. 2009. Patellofemoral osteoarthritis 15 years after anterior cruciate ligament injury – a prospective cohort study. Osteoarthritis Cartilage 17: 284–90.

Neundorf RH, Lowerison MB, Cruz AM, Thomason JJ, McEwen BJ, Hurtig MB. 2010. Determination of the prevalence and severity of metacarpophalangeal joint osteoarthritis in Thoroughbred racehorses via quantitative macroscopic evaluation. American Journal of Veterinary Research 71: 1284-93.

Neve A, Corrado A, Cantatore FP. 2011. Osteoblast physiology in normal and pathological conditions. Cell and Tissue Research 343: 289-302.

Newbould RD, Miller SR, Upadhyay N, Rao AW, Swann P, Gold GE, Strachan RK, Matthews PM, Taylor PC, Brown AP. 2013. T1-weighted sodium MRI of the articulator cartilage in osteoarthritis: A cross sectional and longitudinal study. PLoS ONE 8: e73067.

Nickmanesh R, Stewart R, Snyder B, Grinstaff M, Wilson D. 2015. Contrast-Enhanced Computed Tomography (CECT) Reflects Stiffness of Intact Articular Cartilage. IWOAI 8th International Workshop on osteoarthritis imaging. September 11-14, 2015, Pacific Grove, CA, USA.

Nieminen MT, Töyräs J, Laasanen MS, Silvennoinen J, Helminen HJ, Jurvelin JS. 2004. Prediction of biomechanical properties of articular cartilage with quantitative magnetic resonance imaging. Journal of Biomechanics 37: 321–8.

Nissi MJ, Rieppo J, Töyräs J, Laasanen MS, Kiviranta I, Jurvelin JS, Nieminen MT. 2006. T2 relaxation time mapping reveals age- and species-related diversity of collagen network architecture in articular cartilage. Osteoarthritis and cartilage 14: 1265-71.

Nixon AJ, Cummings JF. 1994. Substance P immunohistochemical study of the sensory innervation of normal subchondral bone in the equine metacarpophalangeal joint. American journal of Veterinary Research 55: 28–33.

Norrdin RW, Kawcak CE, Capwell BA, McIlwraith CW. 1999. Calcified cartilage morphometry and its relation to subchondral bone remodeling in equine arthrosis. Bone 24(2): 109-14.

O'Brien T, Baker TA, Brounts SH, Sample SJ, Markel MD, Scollay MC, Marquis P, Muir P. 2011. Detection of articular pathology of the distal aspect of the third metacarpal bone in thoroughbred racehorses: comparison of radiography, computed tomography and magnetic resonance imaging. Veterinary Surgery 40: 942-51.

O'Brien MP, Penmatsa M, Palukuru U, West P, Yang X, Bostrom MP, Freeman T, Pleshko N. 2015. Monitoring the Progression of Spontaneous Articular Cartilage Healing with Infrared Spectroscopy. Cartilage 6(3): 174-84.

Oakley SP, Lassere MN, Portek I, Szomor Z, Ghosh P, Kirkham BW, Murrell GA, Wulf S, Appleyard RC. 2004. Biomechanical, histologic and macroscopic assessment of articular cartilage in a sheep model of osteoarthritis. Osteoarthritis Cartilage 12: 667-79.

Oakley SP, Portek I, Szomor Z, Appleyard RC, Ghosh P, Kirkham BW, Murrell GA, Lassere MN. 2005. Arthroscopy -- a potential "gold standard" for the diagnosis of the chondropathy of early osteoarthritis. Osteoarthritis and Cartilage 13(5): 368-78.

Oegema TR, Carpenter RJ, Hofmeister F, Thompson RC. 1997. The interaction of the Zone of Calcified Cartilage and Subchondral Bone in Osteoarthritis. Microscopy research and techniques 37: 324-32.

Ogino S, Sasho T, Nakagawa K, Suzuki M, Yamaguchi S, Higaski M, Takahashi K, Moriya H. 2009. Detection of pain-related molecules in the subchondral bone of osteoarthritic knees. Clinical Rheumatology 28: 1395-1402

Olive J, D'Anjou MA, Girard C, Laverty S, Theoret C. 2010A. Fat-suppressed spoiled gradient-recalled imaging of equine metacarpophalangeal articular cartilage. Veterinary Radiology Ultrasound 51(2):107-15.

Olive J, D'Anjou MA, Alexander K, Laverty S, Theoret C. 2010B. Comparison of magnetic resonance imaging, computed tomography, and radiography for assessment of non-cartilaginous changes in equine metacarpophalangeal osteoarthritis. Veterinary Radiology and Ultrasound 51: 267-79.

Oliveria SA, Felson DT, Reed JI, Cirillo PA, Walker AM. 1995. Incidence of symptomatic hand, hip, and knee osteoarthritis among patients in a health maintenance organization. Arthritis and Rheumatism 38(8):1134-41.

Omouri P., Vande berg B.C., Lecouvet F.E., 2011. Value of CT Arthrography in the assessment of cartilage pathology, in : Cartilage imaging : significance, techniques, and new developments, Springer Sciences, Ed. Thomas M. Link, New York, USA.

Omoumi P, Rubini A, Dubuc JE, Vande Berg BC, Lecouvet FE. 2015. Diagnostic performance of CT-arthrography and 1.5T MR-arthrography for the assessment of glenohumeral joint cartilage: a comparative study with arthroscopic correlation. European Journal of Radiology 25: 961-9.

Oni OO, Boyd I. 1998. The origin of the periarticular osteophytes of osteoarthritic knee joints. African Journal of Medical Sciences 27: 23–5.

Orth P, Goebel L, Wolfram U, Ong MF, Gräber S, Kohn D, Cucchiarini M, Ignatius A, Pape D, Madry H. 2012. Effect of Subchondral Drilling on the Microarchitecture of Subchondral Bone. The American Journal of Sports Medicine 40(4): 828-36.

Osterhoff G, Löffler S, Steinke H, Feja C, Josten C, Hepp P. 2011. Comparative anatomical measurements of osseous structures in the ovine and human knee. The Knee 18: 98–103.

Pacchiana PD, Gilley RS, Wallace LJ, Hayden DW, Feeney DA, Jessen CR, Aird B. 2004. Absolute and relative cell counts for synovial fluid from clinically normal shoulder and stifle joints in cats. Journal of American Veterinary Medicine Association 225(12): 1866-70.

Palmer AW, Guldberg RE, Levenston ME. 2006. Analysis of cartilage matrix fixed charge density and three-dimensional morphology via contrast-enhanced microcomputed tomography. Proceedings of the National Academy of Sciences of the United States of America 103: 19255-60.

Pan J, Zhou X, Li W, Novotny JE, Doty SB, Wang L. 2009. In situ measurement of transport between subchondral bone and articular cartilage. Journal of Orthopaedics Research 27(10):1347-52.

Panagides J, Tao N. 1978. Breakdown of articular cartilage proteoglycans by lymphokine-activated macrophages. Inflammation 3: 195-201.

Park YS, Lim SW, Lee IH, Lee TJ, Kim JS, Han JS. 2007. Intra-articular injection of a nutritive mixture solution protects articular cartilage from osteoarthritic progression induced by anterior cruciate ligament transection in mature rabbits: a randomized controlled trial. Arthritis research & therapy 9: R8.

Pastoureau PC, Chomel AC, Bonnet J. 1999. Evidence of early subchondral bone changes in the meniscectomized guinea pig. A densitometric study using dual-energy X-ray absorptiometry subregional analysis. Osteoarthritis and Cartilage 7: 466-73.

Pearce GL, Frisbie DD. 2010. Statistical evaluation of biomedical studies. Osteoarthritis and Cartilage 18, S117-122.

Pearle AD, Warren RF, Rodeo SA. 2005. Basic science of articular cartilage and osteoarthritis. Clinics in Sports Medicine 24: 1-12.

Pelletier J-P, Jovanovic DV, Lascau-Coman V, Fernandes JC, Manning PT, Connor JR, Currie MG, Di Battista JA, Martel-Pelletier J. 2000. Selective inhibition of inducible nitric oxide synthase reduces progression of experimental osteoarthritis *in vivo*: Possible link with the reduction in chondrocyte apoptosis and caspase 3 level. Arthritis and Rheumatism 43: 1290–9.

Pfander D, Cramer T, Deuerling D, Weseloh G, Swoboda B. 2000. Expression of thrombospondin-1 and its receptor CD36 in human osteoarthritic cartilage. Annals of the Rheumatic Diseases 59(6): 448-54.

Pickard JE, Fisher J, Ingham E, Egan J. 1998. Investigation into the effects of proteins and lipids on the frictional properties of articular cartilage. Biomaterials 19(19): 1807-12.

Pierson A, Kirschvink N, Muylkens B, Hontoir F, Raes M, Clegg P, Nisolle JF, Béduin JM, Antoine N, Piret J, Gustin P, Vandeweerd JM. 2012. Prevalebce if naturally occurring cartilage defects in the ovine stifle (knee). Osteoarthritis and Cartilage 20: S73-S74.

Pineda C, Hernandez-Diaz C, Pena A, Villasenor-Ovies P. 2011. The place of ultrasonography in knee joint osteoarthritis: an update. International Journal of Clinical Rheumatology 6(6): 635–42.

Pirson R, Matagne A, Nisolle JF, Hontoir F, Meirlaen P, Gustin P, Kirschvink N, Clegg P, Vandeweerd JM. 2014. What does multiplication of tidemarks mean in the ovine femoro-tibial joint? In: Proceedings of the WCO (World Congress on Osteoarthritis and Osteoporosis), Sevilla, Spain.

Piscaer TM , Waarsing JH , Kops N, Pavljasevic P, Verhaar JA , Van Osch GJ ,Weinans H. 2008. *In vivo* imaging of cartilage degeneration using microCT-arthrography. Osteoarthritis Cartilage 16: 1011-7.

Poole AR, Pidoux I, Reiner A, Choi H, Rosenberg LC. 1984. Association of an extracellular protein (chondrocalcin) with the calcification of cartilage in endochondral bone formation. Journal of Cellular Biology 98(1): 54-65.

Poole CA, Gilbert RT, Herbage D, Hartmann D. 1997. Immunolocalisation of type IX collagen in normal and osteoarthritic canine tibial cartilage and isolated chondrons. Osteoarthritis and Cartilage 5(3): 191-204.

Pottenger LA, Phillips FM, Draganich LF. 1990. The effect of marginal osteophytes on reduction of varus-valgus instability in osteoarthritic knees. Arthritis and Rheumatism 33: 853–8.

Pownder, S., Koff, M.F., Fortier, L., Castiglione, E., Saska, R., Bradica, G., Novakofski, K., Potter, H.G., 2011. Quantitative and morphologic evaluation of cartilage repair in an equine model. Proceedings of the International Society for Magnetic Resonance in Medicine 19: 499.

Pretzel D, Pohlers D, Weinert S, Kinne RW. 2009. *In vitro* model for the analysis of synovial fibroblast-mediated degradation of intact cartilage. Arthritis Research and Therapy 11: R25.

Priam S, Bougault C, Houard X, Gosset M, Salvat C, Berenbaum F, Jacques C. 2013. Identification of soluble 14-3-3 as a novel subchondral bone mediator involved in cartilage degradation in osteoarthritis. Arthritis and Rheuatisms 65: 1831–1842

Prieto-Potin I, Largo R, Roman-Blas JA, Herrero-Beaumont G, Walsh DA. 2015. Characterization of multinucleated giant cells in synovium and subchondral bone in knee osteoarthritis and rheumatoid arthritis. BMC Musculoskeletal Disorders 16: 226.

Pugh JW, Rose RM, Radin EL. 1973 Elastic and viscoelastic properties of trabecular bone: dependence on structure. Journal of Biomechanics 6: 475–85.

Qvistgaard E, Kristoffersen H, Terslev L, Danneskiold-Samsøe B, Torp-Pedersen S, Bliddal H. 2001. Guidance by ultrasound of intra-articular injections in the knee and hip joints. Osteoarthritis and Cartilage 9(6): 512-7.

Radin EL, Paul IL. 1970. Does cartilage compliance reduce skeletal impact loads? The relative force-attenuating properties of articular cartilage, synovial fluid, periarticular soft tissues and bone. Arthritis and Rheumatism 13: 139-44.

Radin EL, Martin RB, Burr DB, Caterson B, Boyd RD, Goodwin C. 1984. Effects of mechanical loading on the tissues of the rabbit knee. Journal of Orthopaedics Research 2: 221-34.

Radin EL, Rose RM. 1986. Role of subchondral bone in the initiation and progression of cartilage damage. Clinical orthopaedics and related research 213: 34–40.

Radin EL, Schaffler M, Gibson G, Tashman S. 1995. Osteoarthrosis as the result of repetitive trauma. In: Osteoarthritic Disorders, Eds: K.E. Kuettner and V.M. Goldberg, American Academy of Orthopaedic Surgeons, Rosemont. pp 197-204.

Ralphs JR, Benjamin M. 1994. The joint capsule: structure, composition, ageing and disease. Journal of Anatomy 184: 503-9.

Rasheed Z, Akhtar N, Haqqi TM. 2011. Advanced glycation end products induce the expression of interleukin-6 and interleukin-8 by receptor for advanced glycation end product-mediated activation of mitogen-activated protein kinases and nuclear factor-{kappa}B in human osteoarthritis chondrocytes. Rheumatology (Oxford) 50: 838–51.

Recht MP, Goodwin DW, Winalski CS, White LM. 2005. MRI of articular cartilage: revisiting current status and future directions. American Journal of Roentgenology 185(4): 899-914.

Redlich K, Hayer S, Ricci R, David JP, Tohidast-Akrad M, Kollias G, Steiner G, Smolen JS, Wagner EF, Schett G. 2002. Osteoclasts are essential for TNF-alpha-mediated joint destruction. Journal of Clinical investigations 110: 1419–27.

Regatte RR, Akella SV, Lonner JH, Kneeland JB, Reddy R. 2006. T1rho relaxation mapping in human osteoarthritis (OA) cartilage: comparison of T1rho with T2. Journal of Magnetic Resonance Imaging 23: 547-53.

Reginster JY. 2002. The prevalence and burden of arthritis. Rheumatology 41 (S1): 3-6.

Riggs CM,Whitehouse GH, Boyde A. 1999. Pathology of the distal condyles of the third metacarpal and third metatarsal bones of the horse. Equine Veterinary Journal 31: 140–8.

Roemer FW, Forbell R, Hunter DJ, Crema MD, Fischer W, Bohndorf K, Guermazi A. 2009. MRI-detected subchondral bone marrow signal alterations of the knee joint: terminology, imaging appearance, relevance and radiological differential diagnosis. Osteoarthritis and Cartilage 17: 115-31.

Roemer FW, Felson DT, Wang K, Crema MD, Marra MD, Nevitt MC, Zhang Y, Torner J, Lewis CE, Guermazi A. 2011. Focal cartilage damage of the knee joint and risk for subsequent cartilage loss: an MRI-Based analysis from the MOST study. In: Proceedings of the 5th international workshop on osteoarthritis imaging, Salzburg.

Roemer FW, Guermazi A. 2012. Osteoarthritis year 2012 in review: imaging. Osteoarthritis Cartilage 20: 1440-6.

Ropes MW, Rossmeisl EC, Bauer W. 1940. The origin and nature of normal human synovial fluid. Journal of clinical investigations 19(6): 795-9.

Roquet I, Lane Easter J, Coomer RPC, Ezquerra LJ, Marsh CA, Trostle SS, Santschi EM. 2017. Treatment of subchondral lucencies in the medial proximal radius with a bone screw in 8 horses. Veterinary Surgery 46(4): 478-85.

Rosset A, Spadola L, Ratib O. 2004. OsiriX: an open-source software for navigating in multidimensional DICOM images. Journal of Digital Imaging 17: 205-16.

Roth R, Akin M, Deligonul U, Kern MJ. 1991. Influence of radiographic contrast media viscosity to flow through coronary angiographic catheters. Catheterization and Cardiovascular Diagnosis 22: 290-4.

Rubin DA, Palmer WE. 2005. Imaging of the knee. In Musculoskeletal diseases - diagnostic imaging and interventional techniques. Holder J, von Shulthess GK, Zollikofer Ch L, 2005 (37th international diagnostic course in Davos, April 2-8, 2005. Springer-Verlag Italia.

Ruegsegger P, Koller B, Muller R. 1996. A microtomographic system for the nondestructive evaluation of bone architecture. Calcified Tissue International 58(1): 24-9.

Ryd L, Brittberg M, Eriksson K, Jurvelin JS, Lindahl A, Marlovits S, Moller P, Richardson JB, Steinwachs M, Zenobi-Wong M. 2015. Pre-osteoarthritis: definition and diagnosis of an elusive clinical entity. Cartilage 6(3): 156–65.

Saadat E, Jobke B, Chu B, Lu Y, Cheng J, Li X, Ries MD, Majumdar S, Link TM. 2008. Diagnostic performance of *in vivo* 3-T MRI for articular cartilage abnormalities in human osteoarthritic knees using histology as standard of reference. European Journal of Radiology 18: 2292–302.

Saito M, Sasho T, Yamaguchi S, Ikegawa N, Akagi R, Muramatsu Y, Mukoyama S, Ochiai N, Nakamura J, Nakagawa K, Nakajima A, Takahashi K. 2012. Angiogenic activity of subchondral bone during the progression of osteoarthritis in a rabbit anterior cruciate ligament transection model. Osteoarthritis and Cartilage 20(12): 1574-82.

Sanchez C, Deberg M, Piccardi N, Msika P, Reginster J, Henrotin Y. 2005A. Osteoblasts from the sclerotic subchondral bone downregulate aggrecan but upregulate metalloproteinases expression by chondrocytes. Osteoarthritis Cartilage 13: 979–87.

Sanchez C, Deberg M, Piccardi N, Msika P, Reginster J, Henrotin Y. 2005B. Subchondral bone osteoblasts induce phenotypic changes in human osteoarthritic chondrocytes. Osteoarthritis Cartilage 13: 988.

Sandy JD, Verscharen C. 2001. Analysis of aggrecan in human knee cartilage and synovial fluid indicates that aggrecanase (ADAMTS) activity is responsible for the catabolic turnover and loss of whole aggrecan whereas other protease activity is required for C-terminal processing in ivivo. Biochemistry Journal 358 (Pt3) 615-26.

Santschi EM, Williams JM, Morgan JW, Johnson CR, Bertone AL, Juzwiak JS. 2015. Preliminary investigation of the treatment of equine medial femoral condylar subchondral cystic lesions with a transcondylar screw. Veterinary Surgery 44(3):281-8.

Sarmanova A, Hall M, Moses J, Doherty M, Zhang W. 2016. Synovial changes detected by ultrasound in people with knee osteoarthritis—a meta-analysis of observational studies. Osteoarthritis and Cartilage 24(8): 1376–83.

Scanzello CR, Goldring SR. 2012. The role of synovitis in osteoarthritis pathogenesis. Bone 51: 249-57.

Scanzello CR, McKeon B, Swaim BH, DiCarlo E, Asomugha EU, Kanda V, Nair A, Lee DM, Richmond JC, Katz JN, Crow MK, Goldring SR. 2011. Synovial inflammation in patients undergoing arthroscopic meniscectomy: molecular characterization and relationship with symptoms. Arthritis and Rheumatism 63(2): 391–400.

Schinhan M, Gruber M, Vavken P, Dorotka R, Samouh L, Chiari C, Gruebl-Barbaras R, Nehrer S. 2012. Critical-size defect induces unicompartmental osteoarthritis in a stable ovine knee. Journal of Orthopaedic Research 30: 214–20.

Schlueter AE, Orth MW. 2004. Equine osteoarthritis: a brief review of the disease and its causes. Equine and Comparative Exercise Physiology 1(4): 221-31.

Schmid MR, Pfirrmann CWA, Hodler J, Vienne P, Zanetti M. 2003. Cartilage Lesions in the Ankle Joint: Comparison of MR Arthrography and CT Arthrography. Skeletal Radiology 32: 259-265.

Schmidt TA, Gastelum NS, Nguyen QT, Schumacher BL, Sah RL. 2007. Boundary lubrication of articular cartilage: role of synovial fluid constituents. Arthritis and Rheumatism 56(3): 882-91.

Schmitt B, Zbyn S, Stelzeneder D, Jellu V, Paul D, Lauer L, Bachert P, Trattnig S. 2011. Cartilage quality assessment by using glycosaminoglycan chemical exchange saturation transfer and 23Na MR imaging at 7T. Radiology 260: 257-264.

Schmitz N, Laverty S, Kraus VB, Aigner T. 2010. Basic methods in histopathology of joint tissues. Osteoarthritis and cartilage 18: S113-116.

Schwarz IM1, Hills BA. 1998. Surface-active phospholipid as the lubricating component of lubricin. British Journal of Rheumatology 37(1):21-6.

Seibold R, Betz A, Eitel F. 1989. Application of an Internal Fixateur to the Femur and Tibia. Veterinary and Comparative ORthropaedics and Traumatology 2: 85-90.

Sellam J, Berenbaum F. 2010. The role of synovitis in pathophysiology and clinical symptoms of osteoarthritis. Nature Reviews Rhumatology 6: 625-35.

Sellam J, Berenbaum F. 2013. Is osteoarthritis ametabolic disease ? Joint Bone Spine 80: 568-573.

Setton LA, Mow VC, Muller FJ, Pita JC, Howell DS. 1993. Altered structure-function relationships for articular cartilage in human osteoarthritis and an experimental canine model. Agents Actions Suppl39: 27-48.

Shafford HL, Hellyer PW, Turner AS. 2004. Intra-articular lidocaine plus bupivacaine in sheep undergoing stifle arthrotomy. Veterinary Anaesthesia and Analgesia 31(1):20-6.

Shahabpour M, Kichouh M, Laridon E, Gielen JL, De Mey J, 2008. The effectiveness of diagnostic imaging methods for the assessment of soft tissue and articular disorders of the shoulder and elbow. European Journal of Radiology 65: 194-200.

Shapiro EM, Borthakur A, Gougoutas AJ, Reddy R2002. 23Na MRI accurately measures FCD in articular cartilage. Magnetic Resonance in Medicine 47: 284-91.

Shapiro F, Koide S, Glimcher MJ. 1993. Cell origin and differentiation in the repair of full-thickness defects of articular cartilage. Journal of Bone and Joint surgery (America): 75(4): 532-53.

Sharma AR, Jagga S, Lee SS, Nam JS. 2013. Interplay between cartilage and subchondral bone contributing to pathogenesis of osteoarthritis. International Journal of Molecular Sciences 14: 19805-830.

Siebelt M, van Tiel J, Waarsing JH, Piscaer TM, van Straten M, Booij R, Dijkshoorn ML, Kleinrensink GJ, Verhaar JA, Krestin GP, Weinans H, Oei EH. 2011. Clinically applied CT arthrotgraphy to measure the sulphated glycosaminoglycan content of cartilage. Osteoarthritis and cartilage 19 1183-89.

Silvast TS, Jurvelin JS, Lammi MJ, Töyräs J. 2009A. pQCT study on diffusion and equilibrium distribution of iodinated anionic contrast agent in human articular cartilage – associations to matrix composition and integrity. Osteoarthritis and cartilage 17: 26-32.

Silvast TS, Jurvelin JS, Aula AS, Lammi MJ, Töyräs J. 2009B. Contrast agent-enhanced computed tomography of articular cartilage: association with tissue composition and properties. Acta Radiol 50: 78-85.

Silvast TS, Jurvelin JS, Tiitu V, Quin TM, Töyräs J. 2013. Bath Concentration of Anionic Contrast Agents Does Not Affect Their Diffusion and Distribution in Articular Cartilage *In Vitro*. Cartilage 4: 42-51.

Simmons EJ, Bertone AL, Weisbrode SE. 1999. Instability-induced osteoarthritis in the metacarpophalangeal joint of horses. American Journal of Veterinary Research 60: 7-13.

Simon O, Meulyzer M, Palmers K, Corraretti G. 2017. Treatment of equine subchondral cystic-like lesions in various anatomical locations with a translesional screw inserted in lag faschion. Scientific Presentation Abstracts: ACVS Surgery Summit October 12-14, Indianapolis, Indiana, Veterinary Surgery 46(7): E12.

Simonet WS, Lacey DL, Dunstan CR, Kelley M, Chang MS, Lüthy R, Nguyen HQ, Wooden S, Bennett L, Boone T, Shimamoto G, DeRose M, Elliott R, Colombero A, Tan HL, Trail G, Sullivan J, Davy E, Bucay N, Renshaw-Gegg L, Hughes TM, Hill D, Pattison W, Campbell P, Sander S, Van G, Tarpley J, Derby P, Lee R, Boyle WJ. 1997. Osteoprotegerin: a novel secreted protein involved in the regulation of bone density. Cell 89: 309–19.

Singh, A., Haris, M., Cai, K., Kassey, V.B., Kogan, F., Reddy, D., Hariharan, H., Reddy, R., 2012. Chemical exchange saturation transfer magnetic resonance imaging of human knee cartilage at 3 T and 7 T. Magnetic Resonance in Medicine 68: 588-94.

Slingerland LI, Hazewinkel HAW, Meij BP, Picavet Ph, Voorhout G. 2011. Cross-sectional study of the prevalence and clinical features of osteoarthritis in 100 cats. The Veterinary Journal 187(3): 304–9.

Smith RL, Thomas KD, Schurman DJ, Carter DR, Wong M, van der Muelen MC. 1992. Rabbit knee immobilization: Bone remodeling precedes cartilage degradation. Journal of Orthopaedics Reearch 10 (1): 88–95.

Smith HE, Mosher TJ, Dardzinski BJ, Collins BG, Collins CM, Yang QX, Schmithorst VJ, Smith MB. 2001. Spatial variation in cartilage T2 of the knee. J Magnetic Resonance Imaging 14: 50-5.

Smith G Jr, Myers SL, Brandt KD, Mickler EA, Albrecht ME. 2005. Effect of intra-articular hyaluronan injection on vertical ground reaction force and progression of osteoarthritis after anterior cruciate ligament transection. Journal of Rheumatology 32: 325-34.

Smith MA, Dyson SJ, Murray RC. 2012. Reliability of high- and low-field magnetic resonance imaging systems for detection of cartilage and bone lesions in the equine cadaver fetlock. Equine Veterinary Journal 44: 684-91.

Smith MD. 2011. The Normal Synovium. Open Rheumatology 5: 100–6.

Sokolove J, Lepus CM. 2013. Role of inflammation in the pathogenesis of osteoarthritis: latest findings and interpretations. Therapeutic advances in musculoskeletal disease 5(2): 77–94.

Song IH, Althoff CE, Hermann KG, Scheel AK, Knetsch T, Schoenharting M, Werner C, Burmester GR, Backhaus M. 2008. Knee osteoarthritis. Efficacy of a new method of contrast-enhanced musculoskeletal ultrasonography in detection of synovitis in patients with knee osteoarthritis in comparison with magnetic resonance imaging. Annals of the Rheumatic Diseases 67(1): 19-25.

Specht TE, Colahan PT. 1990. Osteostixis for incomplete cortical fracture of the third metacarpal bone. Results in 11 horses. Veterinary Surgery 19(1): 34-40.

Stadler A, Schima W, Ba-Ssalamah A, Kettenbach J, Eisenhuber E. 2007. Artifacts in body MR imaging: their appearance and how to eliminate them. European Journal of Radiology 17: 1242-55.

Stahl R, Luke A, Li X, Carballido-Gamio J, Ma CB, Majumdar S, Link TM. 2009. T1rho, T2 and focal knee cartilage abnormalities in physically active and sedentary healthy subjects versus early OA patients - A 3.0-Tesla MRI study. European Journal of Radiology 19: 132-43.

Stanescu R, Knyszynski A, Muriel M P, Stanescu V. 1993. Early lesions of the articular surface in a strain of mice with very high incidence of spontaneous osteoarthritic-like lesions. Journal of Rheumatology 20: 102-10.

Steadman JR1, Rodkey WG, Rodrigo JJ. 2001. Microfracture: surgical technique and rehabilitation to treat chondral defects. Clinical orthopaedics and related research 391 (Suppl):S 362-9.

Stehling C, Liebl H, Krug R, Lane NE, Nevitt MC, Lynch J, McCulloch CE, Link TM. 2010. Patellar cartilage: T2 values and morphologic abnormalities at 3.0-T MR imaging in relation to physical activity in asymptomatic subjects from the osteoarthritis initiative. Radiology 254: 509-20.

Stewart RC, Bansal PN, Entezari V, Lusic H, Nazarian RM, Snyder BD, Grinstaff MW. 2013. Contrast-enhanced CT with a high-affinity cationic contrast agent for imaging *ex vivo* bovine, intact *ex vivo* rabbit, and *in vivo* rabbit cartilage. Radiology 266(1): 141-50.

Stolz M, Gottardi R, Raiteri R, Miot S, Martin I, Imer R, Staufer U, Raducanu A, Düggelin M, Baschong W, Daniels AU, Friederich NF, Aszodi A, Aebi U. 2009. Early detection of aging cartilage and osteoarthritis in mice and patient samples using atomic force microscopy. Nature Nanotechnology 4(3): 186-92.

Stover SM. 2003. The epidemiology of Thoroughbred racehorse injuries. Clinical Techniques in Equine Practice 2: 312–22.

Struewer J, Ziring E, Frangen TM, Efe T, Meissner S, Buecking B, Bliemel C, Ishaque B. 2013. Clinical outcome and prevalence of osteoarthritis after isolated anterior cruciate ligament reconstruction using hamstring graft: follow-up after two and ten years. International Orthopaedics 37: 271–7.

Stubendorff JJ, Lammentausta E, Struglics A, Lindberg L, Heinegård D, Dahlberg LE. 2012. Is cartilage sGAG content related to early changes in cartilage disease? Implications for interpretation of dGEMRIC. Osteoarthritis Cartilage 20(5): 396-404.

Suarez Sanchez-Andrade J, Richter H, Kuhn K, Bischofberger AS, Kircher PR, Hoey S. 2018. Comparison between magnetic resonance imaging, computed tomography, and arthrography to identify artificially induced cartilage defects of the equine carpal joints. Veterinary Radiology and Ultrasound 59(3): 312-25.

Suri S, Gill SE, Massena de Camin S, Wilson D, McWilliams DF, Walsh DA. 2007. Neurovascular invasion at the osteochondral junction and in osteophytes in osteoarthritis. Annals of the Rheumatic Diseases 66: 1423–8.

Sutton S, Clutterbuck A, Harris P, Gent T, Freeman S, Foster N, Barrett-Jolley R, Mobasheri A. 2009. The contribution of the synovium, synovial derived inflammatory cytokines and neuropeptides to the pathogenesis of osteoarthritis. The Veterinary Journal 179(1): 10-24.

Swann DA, Sotman S, Dixon M, Brooks C. 1977. The isolation and partial characterization of the major glycoprotein (LGP-1) from the articular lubricating fraction from bovine synovial fluid. Biochemistry journal 161: 473–85.

Sward P, Fridén T, Boegård T, Kostogiannis I, Neuman P, Roos H. 2013. Association between varus alignment and post-traumatic osteoarthritis after anterior cruciate ligament injury. Knee Surgery, Sports Traumatology, Arthroscopy 21: 2040–47.

Taljanovic MS, Graham AR, Benjamin JB, Gmitro AF, Krupinski EA, Schwartz SA, Hunter TB, Resnick DL. 2008. Bone marrow edema pattern in advanced hip osteoarthritis: quantitative assessment with magnetic resonance imaging and correlationwith clinical examination, radiographic findings, and histopathology. Skeletal Radiology 37: 423– 31.

Taylor C, Carballido-Gamio J, Majumdar S, Li X. 2008. Comparison of quantitative imaging of cartilage for osteoarthritis: T2, T1ρ, dGEMRIC and contrast-enhanced computed tomography. Magnetic Resonance Imaging 27: 779-84.

Taylor P. 1991. Anesthesia in sheep and goats. In Practice 13: 31-6.

Taylor WR, Poepplau BM, Konig C, Ehrig RM, Zachow S, Duda GN, Heller MO. 2011. The medial-lateral force distribution in the ovine stifle joint during walking. Journal of Oarhopaedic Resesrach 29: 567-71.

Tchetverikov I, Lohmander LS, Verzijl N, Huizinga TW, TeKoppele JM, Hanemaaijer R, DeGroot J. 2005. MMP protein and activity levels in synovial fluid from patients with joint injury, inflammatory arthritis, and osteoarthritis. Annals of Rheumatic Diseases 64: 694–8.

Teeple E, Elsaid KA, Fleming BC, Jay GD, Aslani K, Crisco JJ, Mechrefe AP. 2007. Coefficients of friction, lubricin, and cartilage damage in the anterior cruciate ligament-deficient guinea pig knee. Journal of Orthopaedic Research 26:231–237.

Terajima M, Damle S, Penmatsa M, West P, Bostrom M, Hidaka C, Yamauchi M, Pleshko N. 2012. Temporal changes in collagen cross-links in spontaneous articular cartialge repair. Cartilage 3(3): 278-87.

Thomas CM, Fuller CJ, Whittles CE, Sharif M. 2007. Chondrocyte death by apoptosis is associated with cartilage matrix degradation. Osteoarthritis and Cartilage 15: 27–34.

Thomas RH, Resnick D, Alazraki NP, Daniel D, Greenfield R. 1975. Compartmental evaluation of osteoarthritis of the knee: a comparative study of available diagnostic modalities. Radiology 116: 585-94.

Thompson RC Jr, Oegema TR Jr, Lewis JL, Wallace L. 1991. Osteoarthrotic changes after acute transarticular load. An animal model. Journal of Bone and Joint Surgery America 73: 990-1001.

Tiderius CJ, Svensson J, Leander P, Ola T, Dahlberg L, 2004. dGEMRIC (Delayed Gadolinium-Enhanced MRI of Cartilage) indicates adaptive capacity of human knee cartilage. Magnatic Resonance Medicine 51: 286-90.

Tivers MS, Mahoney P, Corr SA. 2008. Canine stifle positive contrast computed tomography arthrography for assessment of caudal horn meniscal injury: a cadaver study. Veterinary Surgery 37: 269-77.

Tong KM, Chen CP, Huang KC, Shieh DC, Cheng HC, Tzeng CY, Chen KH, Chiu YC, Tang CH. 2011. Adiponectin increases MMP-3 expression in human chondrocytes through AdipoR1 signaling pathway. Journal of Cell Biochemistry 112(5): 1431-40.

Torres L, Dunlop DD, Peterfy C, Guermazi A, Prasad P, Hayes KW, Song J, Cahue S, Chang A, Marshall M, Sharma L. 2006. The relationship between specific tissue lesions and pain severity in persons with knee osteoarthritis. Osteoarthritis and Cartilage 14: 1033–40.

Toth T, Ge Z, Daly MP. 2007The influence of patient centering on CT dose and image noise. Medical Physics 34: 3093-101.

Tran-Khanh N, Hoemann CD, McKee MD, Henderson JE, Buschmann MD. 2005. Aged bovine chondrocytes display a diminished capacity to produce a collagen-rich, mechanically functional cartilage extracellular matrix. Journal of Orthopaedics Research 23: 1354-62.

Trattnig S, Mamisch TC, Welsch G, Glaser C, Szomolanyi P, Gebetsroither S, Stastny O, Horger W, Millington S, Marlovits S. 2007a. Quantitative T2 mapping of matrix-associated autologous chondrocyte transplantation at 3T: an *in vivo* cross-sectional study. Investigative Radiology 42: 442-8.

Trattnig S, Marlovits S, Gebetsroither S, Szomolanyi P, Welsch GH, Salomonowitz E, Watanabe A, Deimling M, Mamisch TC. 2007b. Three-dimensional delayed gadolinium-enhanced MRI of cartilage (dGEMRIC) for *in vivo* evaluation of reparative cartilage after matrix-associated autologous chondrocyte transplantation at 3.0T: Preliminary results. Journal of Magnetic Resonance Imaging 26: 974-82.

Trattnig S, Mlynarik V, Breitenseher M, Huber M, Zembsch A, Rand T, Imhof H. 1999. MRI vizualisation of proteoglycan depletion in articular cartilage via intravenous administration of Gd-DTPA. Magnetic resonance imaging 17: 577-83.

Trattnig S, Welsch GH, Juras V, Szomolanyi P, Mayerhoefer ME, Stelzeneder D, Mamisch TC, Bieri O, Scheffler K, Zbyn S. 2010. ^{23}Na MR imaging at 7T after knee matrix-associated autologous chondrocyte transplantation: Preliminary results. Radiology 257: 175-84.

Tucker RL, Sampson SN. 2007. Magnetic Resonance Imaging Protocols for the Horse. Clinical Technique in Equine Practise 6: 2-15.

Turunen MJ, Töyräs J, Lammi MJ, Jurvelin JS, Korhonen RK. 2012. Hyperosmolaric contrast agents in cartilage tomography may expose cartilage to overload-induced cell death. Journal of Biomechanics 45(3): 497-503.

Urban J. 1994. The chondrocyte: a cell under pressure. The British Journal of Rheumatology 33: 901–8.

Upton AR, Holding CA, Dharmapatni AA, Haynes DR. 2012. The expression of RANKL and OPG in the various grades of osteoarthritic cartilage. Rheumatology international 32(2): 535-40.

Van Den Boom R, Van Der Harst MR, Brommer H, Brama PAJ, Barneveld A, Van Weeren PR, Degroot J. 2005. Relationship between synovial fluid levels of glycosaminoglycans, hydroxyproline and general MMP activity and the presence and severity of articular cartilage change on the proximal articular surface of P1. Equine Veterinary Journal 37: 19-25.

van der Harst MR, Brama PAJ, van de Lest CHA, Kiers GH, DeGroot J, van Weeren PR. 2004. An integral biochemical analysis of the main constituents of articular cartilage, subchondral and trabecular bone. Osteoarthritis and Cartilage 12: 752-61.

van der Harst MR, DeGroot J., Kiers GH, Brama PAJ, van de Lest CHA, van Weeren PR. 2005. Biochemical analysis of the articular cartilage and subchondral and trabecular bone of the metacarpophalangeal joint of horses with early osteoarthritis. American Journal of Verterinary Radiology 66(7): 1238-46.

van der Kraan PM, van de Berg WB. 2007. Osteophytes: relevance and biology. Osteoarthritis and Cartilage 15: 237-44.

van Meurs JBJ, Van Lent PLEM, Holthuysen AEM, Singer II, Bayne EK, Van Den Berg WB. 2001. Kinetics of aggrecanase- and metalloproteinase-induced neoepitopes in various stages of cartilage destruction in murine arthritis. Arthritism and Rheumatism 42(6): 1128-39.

van Tiel J, Siebelt M, Waarsing JH, Piscaer TM, van Straten M, Booij R, Dijkshoorn ML, Kleinrensink GJ, Verhaar JA, Krestin GP, Weinans H, Oei EH. 2012. CT arthrography of the human knee to measure cartilage quality with low radiation dose. Osteoarthritis and cartilage 20: 678-85.

van Tiel J, Siebelt M, Reijman M, Bos PK, Waarsing JH, Zuurmond AM, Nasserinejad K, van Osch GJ, Verhaar JA, Krestin GP, Weinans H, Oei EH. 2016. Quantitative in vivo CT arthrography of the human osteoarthritic knee to estimate cartilage sulphated glycosaminoglycan content: correlation with ex-vivo reference standards. Osteoarthritis and Cartilage 24(6):1012-20.

van Turnhout MC, Schipper H, Engel B, Buist W, Kranenbarg S, Van Leeuwen JL. 2010. Postnatal development of collagen structure in ovine articular cartilage. BMC Developmental Biology 10: 108.

Vande Berg BC, Lecouvet FE, Poilvache P, Jamart J, Materne R, Lengele B, Maldague B, Malghem J. 2002. Assessment of the knee cartilage in cadavers with dual-detector spiral CT arthrography and MR imaging. Radiology 222 (2): 430-6.

Vanderperren K, Martens A, Haers H, Duchateau L, Saunders JH. 2009. Arthroscopic visualisation of the third metacarpal and metatarsal condyles in the horse.Equine Veterinary Journal 41(6): 526-33.

Vandeweerd JM, Kirschvink N, Muylkens B, Depiereux E, Clegg P, Herteman N, Lamberts M, Bonnet P, Nisolle JF. 2012. A study of the anatomy and injection techniques of the ovine stifle by positive contrast

arthrography, computed tomography arthrography and gross anatomical dissection. The Veterinary Journal 193(2): 426-32.

Vandeweerd JM, Hontoir F, Kirschvink N, Clegg P, Nisolle JF, Antoine N, Gustin P. 2013. Prevalence of naturally occurring cartilage defects in the ovine knee. Osteoarthritis Cartilage 21(8): 1125-31.

Vandeweerd JM, Vermeylen A, Goossens M, Sternon N, Hontoir F, Nisolle JF, Dugdale A. 2014. Anesthésie chez le mouton de laboratoire. Sciences et Techniques de l'Animal de Laboratoire 40(4): 15-9.

Vandeweerd JM, Zhao Y, Nisolle JF, Zhang W, Zhihong L, Clegg P, Gustin P. 2015. Effect of corticosteroids on articular cartilage: have animal studies said everything? Fundam Clin Pharmacol. 29: 427-38.

Vecchio P, Thomas R, Hills BA. 1999. Surfactant treatment for osteoarthritis. Rheumatology (Oxford) 38(10): 1020-1.

Vellet AD, Marks PH, Fowler PJ, Munro TG. 1991. Occult posttraumatic osteochondral lesions of the knee: prevalence, classification, and short-term sequelae evaluated with MR imaging. Radiology 178 (1): 271-6.

Vener MJ, Thompson RC Jr, Lewis JL, Oegema TR Jr. 1992. Subchondral damage after acute transarticular loading: an in vitro model of joint injury. Journal of Orthopaedics Research 10(6): 759-65.

Venkatesan N, Barre L, Magdalou J, Mainard D, Netter P, Fournel-Gigleux S, Ouzzine M. 2009. Modulation of xylosyltransferase I expression provides a mechanism regulating glycosaminoglycan chain synthesis during cartilage destruction and repair. FASEB journal: official publication of the Federation of American Societies for Experimental Biology 23: 813-822.

Venn M, Maroudas A. 1977. Chemical composition and swelling of normal and osteoarthritic femoral head cartilage. I. Chemical composition. Annals of the Rheumatic diseases 36(2): 121-9.

Verborgt O, Gibson GJ, Schaffler MB. 2000. Loss of osteocyte integrity in association with microdamage and bone remodeling after fatigue *in vivo*. Journal of Bone and Mineral Research 15(1): 60-7.

Verbrugge LM. 1995. Women, Men, and osteoarthritis. Arthritis care and research 8(4): 212-220.

Verzijl N, DeGroot J, Thorpe SR, Bank RA, Shaw JN, Lyons TJ, Bijlsma JW, Lafeber FP, Baynes JW, TeKoppele JM. 2000. Effect of collagen turnover on the accumulation of advanced glycation end products. Journal of Biological Chemistry 275: 39027-31.

von der Mark K, Kirsch T, Nerlich A, Kuss A, Weseloh G, Glückert K, Stöss H. 1992. Type X collagen synthesis in human osteoarthritic cartilage. Indication of chondrocyte hypertrophy. Arthritis and Rheumatism 35(7): 806-11.

Von Engelhardt LV, Lahner M, Klussmann A, Bouillon B, David A, Haage P, Lichtinger TK. 2010. Arthroscopy vs. MRI for a detailed assessment of cartilage disease in osteoarthritis: diagnostic value of MRI in clinical practice. BioMed Central Musculoskeletal Disorders 11: 75.

Wachsmuth L, Engelke K. 2004. High-resolution imaging of osteoarthritis using microcomputed tomography. From: Methods in molecular medicine – Vol 101: Cartilage and osteoarthritis, Vol2: structure and *in vivo* analysis. Ed: De Ceuninck F., Sabatini M., Pastoreau P. – Humnana Press Inc., Springer, Totowa, NJ.

Wagner AE. 2009. Complications in equine anesthesia. Veterinary Clinics of North America. Equine Practice 24: 735-752.

Waldt S, Bruegel M, Ganter K, Kuhn V, Link TM, Rummeny EJ, Woetler K. 2005. Comparison of multislice CT arthrography and MR arthrography for the detection of articular cartilage lesions of the elbow. European Journal of Radiology 15: 784-91.

Walsh DA, McWilliams DF, Turley MJ, Dixon MR, Fransès RE, Mapp PI, Wilson D. 2010. Angiogenesis and nerve growth factor at the osteochondral junction in rheumatoid arthritis and osteoarthritis. Rheumatology 49: 1852–61.

Wancket LM, Baragi V, Bove S, Kilgore K, Korytko PJ, Guzman RE. 2005. Anatomical localization of cartilage degradation markers in a surgically induced rat osteoarthritis model. Toxicology and Pathology 33: 484-9.

Wang L, Wu Y, Chang G, Oesingmann N, Schweitzer ME, Jerschow A, Regatte RR. 2009. Rapid isotropic 3D-sodium MRI of the knee joint *in vivo* at 7T. Journal of Magnetic Resonance Imaging 30: 606-14.

Wang Q, Rozelle AL, Lepus CM, Scanzello CR, Song JJ, Larsen DM, Crish JF, Bebek G, Ritter SY, Lindstrom TM, Hwang I, Wong HH, Punzi L, Encarnacion A, Shamloo M, Goodman SB, Wyss-Coray T, Goldring SR, Banda NK, Thurman JM, Gobezie R, Crow MK, Holers VM, Lee DM, Robinson WH. 2011. Identification of a central role for complement in osteoarthritis. Nature Medicine 17(12): 1674-9.

Wang Y, Wei L, Zeng L, He D, Wei X. 2013 Nutrition and degeneration of articular cartilage. Knee surgery, sports traumatology, arthroscopy 21: 1751-62.

Ward KM, Aletras AH, Balaban RS. 2000. A new class of contrast agents for MRI based on proton chemical exchange dependent saturation transfer (CEST). Journal of Magnetic Resonance 143: 79-87.

Watanabe A, Wada Y, Obata T, Ueda T, Tamura M, Ikehira H, Moriya H. 2006. Delayed gadolinium-enhanced MR to determine glycosaminoglycan concentration in reparative cartilage after autologous chondrocyte implantation: Preliminary results. Radiology 239: 201-208.

Watanabe Y, Takeuchi K, Onaga SH, Sato M, Tsujita M, Abe M, Natsume R, Li MQ, Furuichi T, Saeki M, Izumikawa T, Hasegawa A, Yokoyama M, Ikegawa S, Sakimura K, Amizuka N, Kitagawa H, Igarashi M. 2010. Chondroitin sulfate N-acetylgalactosaminyltransferase-1 is required for normal cartilage development. Biochemical Journal 432, 47-55.

Watrin A, Ruaud JPB, Olivier PTA, Guigamp NC, Gonord PD, Netter PA, Blum AG, Guillot GM, Gillet PM, Loeuille DH. 2001. T2 mapping of rat cartilage. Radiology 219: 395-402.

Watson PJ, Carpenter TA, Hall LD, Tyler JA. 1996. Cartilage swelling and loss in a spontaneous model of osteoarthritis visualized by magnetic resonance imaging. Osteoarthritis and Cartilage 4: 197–207.

Webb GR, Westacott CI, Elson CJ. 1998. Osteoarthritic synovial fluid and synovium supernatants up-regulate tumor necrosis factor receptors on human articular chondrocytes. Osteoarthritis Cartilage 6: 167–76.

Welsch GH, Trattnig S, Scheffler K, Quirbach S, Marlovits S, Domayer S, Bieri O, Mamisch TC. 2008A. Magnetization transfer contrast and T2 mapping in the evaluation of cartilage repair tissue with 3T MRI. Journal of magnetic resonance imaging 28: 979-86.

Welsch GH, Mamisch TC, Hughes T, Zilkens C, Quirbach S, Scheffer K, Kraff O, Schweitzer ME, Szomolanyi P, Trattnig S. 2008B. *In vivo* biochemical 7.0 Tesla magnetic resonance: Preliminary results of dGEMRIC, zonal T2, and T2* mapping of articular cartilage. Investigative Radiology 43: 619-626.

Welsch GH, Trattnig S, Hughes T, Quirbach S, Olk A, Blanke M, Marlovits S, Mamisch TC. 2010. T2 and T2* mapping in patients after matrix-associated autologous chondrocyte transplantation: initial results on clinical use with 3.0Tesla MRI. European Radiology 20: 1515-23.

Welsch GH, Apprich S, Zbyn S, Mamisch TC, Mlynarik V, Scheffler K, Bieri O, Trattnig S. 2011. Biochemical T2, T2* and magnetization transfer ratio MRI of the knee cartilage: feasibility at ultra-high field (7T) compared with high field (3T) strength. European Journal of Radiology 21: 1136-43.

Werpy N. 2012. MRI-The thrill of victory and the agony of defeat. 2012 American College of Veterinary Surgeons (ACVS) – The surgical summit- 1-3 November 2012. National Harbor, Maryland, USA.

Westacott CI, Webb GR, Warnock MG, Sims JV, Elson CJ. 1997. Alteration of cartilage metabolism by cells from osteoarthritic bone. Arthritis and Rheumatism 40: 1282–91.

Wheaton AJ, Borthakur A, Dodge GR, Kneeland JB, Schumacher HR, Reddy R. 2004. Sodium magnetic resonance imaging of proteoglycan depletion in an *in vivo* model of osteoarthritis. Academic Radiology 11: 21-8.

Wheaton AJ, Dodge GR, Borthakur A., Kneeland JB, Schumacher HR, Reddy R. 2005. Detection of changes in articular cartilage proteoglycan by T1ρ magnetic resonance imaging. Journal of Orthopaedics Research 23: 102-8.

White LM, Sussman MS, Hurtig M, Probyn L, Tomlinson G, Kandel R. 2006. Cartilage T2 assessment: Differentiation of normal hyaline cartilage and reparative tissue after arthroscopic cartilage repair in equine subjects. Radiology 241: 407-14.

Wiewiorski M, Miska M, Kretzschmar M, Studler U, Bieri O, Valderrabano V. 2013. Delayed gadolinium-enhanced MRI of cartilage of the ankle joint: Results after autologous matrix-induced chondrogenesis (AMIC)-aided reconstruction of osteochondral lesions of the talus. Clinical Radiology 68 (10): 1031-8.

Wilke MM, Nydam DV, Nixon AJ. 2001. Enhanced early chondrogenesis in articular defects following arthroscopic mesenchymal stem cell implantation in an equine model. Journal of Orthopaedic Research 25(7): 913-25.

Williams A, Qian Y, Bear D, Chu CR. 2010. Assessing degeneration of human articular cartilage with ultra-short echo time (UTE) T2* mapping. Osteoarthritis and Cartilage 18: 539–46.

Williams JM, Rayan V, Sumner DR, Thonar EJ. 2003. The use of intra-articular Na-hyaluronate as a potential chondroprotective device in experimentally induced acute articular cartilage injury and repair in rabbits. Journal of Orthopaedics Research 21(2): 305-11.

Williamson AK, Chen AC, Sah RL. 2001. Compressive properties and function-composition relationship of developing bovine articular cartilage. Journal of Orthopaedic Research 19: 113-21.

Williamson AK, Chen SC, Masuda K, Thonar EJMA, Sah RL. 2003. Tensile mechanical properties of bovine articular cartilage: variations with growth and relationships to collagen network components. Journal of Orthopaedic Research 21: 872-80.

Witherspoon JW, Smirnova IV, McIff TE. 2014. Neuroanatomical distribution of mechanoreceptors in the human cadaveric shoulder capsule and labrum. Journal of Anatomy 225(3): 337-45.

Witschey WR, Borthakur A, Fenty M, Kneeland BJ, Lonner JH, McArdle EL, Sochor M, Reddy R. 2010. T1rho MRI quantification of arthroscopically confirmed cartilage degeneration. Magnetic Resonance in Medicine 63(5): 1376-82.

Wojtys EM, Beaman DN, Glover RA, Janda D. 1990. Innervation of the human knee joint by substance-P fibers. Arthroscopy 6(4): 254-63.

Wotton SF, Duance VC. 1994. Type III collagen in normal human articular cartilage. Histochemistry Journal 26(5): 412-6.

Wright KC, Loh G, Wallace S, Stephens LC. 1990. Experimental evaluation of ethanol- ethiodiol for transcatheter renal embolization. Cardiovascular and interventional radiology 13(5): 309-13.

Wucherer KL, Ober CP, Conzemius MG. 2012. The use of delayed gadolinium enhanced magnetic resonance imaging of cartilage and T2 mapping to evaluate articular cartilage in the normal canine elbow. Veterinary Radiology and Ultrasound 53: 57-63.

Wyler A, Bousson V, Bergot C, Polivka M, Leveque E, Vicaut E, Laredo JD. 2009. Comparison of MR-arthrography and CT-arthrography in hyaline cartilage-thickness measurement in radiographically normal cadaver hips with anatomy as gold standard. Osteoarthritis and Cartilage 17(1): 19-25.

Wyler A, Bousson V, Bergot C, Polivka M, Leveque E, Vicaut E, Laredo JD.2007. Hyaline cartilage thickness in radiographically normal cadaveric hips: comparison of spiral CT arthrographic and macroscopic measurements.Radiology 242(2): 441-9.

Xia Y, Farquhar T, Burton-Wuster N, Vernier-Singer M, Lust G, Jelinski L. 1995. Self-diffusion monitors degraded cartilage. Archives of Biochemistry and Biophysics 10: 323-28.

Xia Y. 1998. Relaxation anisotropy in cartilage by NMR microscopy (μMRI) at 14-μm resolution. Magnetic Resonance in Medicine 39: 941-9.

Xia Y, Moody JB, Burton-Wurster N, Lust G. 2001. Quantitative in situ correlation between microscopic MRI and polarized light microscopy studies of articular cartilage. Osteoarthritis and cartilage 9: 393-406.

Xia Y, Zheng S, Bidthanapally A. 2008. Depth-dependent profiles of glycosaminoglycans in articular cartilage by microMRI and histochemistry. Journal of Magnetic Resonance Imaging 28: 151-7.

Xie L, Tintani F, Wang X, Li F, Zhen G, Qiu T, Wan M, Crane J, Chen Q, Cao X. 2016. Systemic neutralization of TGF-β attenuates osteoarthritis. Annals of the New York Academy of Sciences 1376(1): 53-64.

Xu J, Reh DD and Carey JP, Mahesh M, Siewerden JH. 2012. Technical assessment of a cone-beam CT scanner for oto-laryngology imaging: image quality, dose, and technique protocols. Medical physics 39: 4932-42.

Yamada K, Healey R, Amiel D, Lotz M, Coutts R. 2002. Subchondral bone of the human knee joint in aging and osteoarthritis. Osteoarthritis and cartilage 10: 360-9.

Yanagisawa H, Hoshi K, Asawa Y, Ejiri S, Sato K, Ozawa H. 2012. Matrix remodeling and cytological changes during spontaneous cartilage repair. Journal of Electron Microscopy 61(4): 237–48.

Yoo HJ, Hong SH, Choi JY, Lee IJ, Kim SJ, Choi JA, Kang HS. 2011. Contrast-enhanced CT of articular cartilage: experimental study for quantification of glycosaminoglycan content in articular cartilage. Radiology 261(3): 805-12.

Yoshimura N, Sabir A, Kubo T, Lin PJ, Clouse ME, Hatabu H. 2006. Correlation between image noise and body weight in coronary CTA with 16-row MDCT. Academic Radiology 13(3): 324-8.

Young AA, Smith MM, Smith SM, Cake MA, Ghosh P, Read RA, Melrose J, Sonnabend DH, Roughley PJ, Little CB. 2005. Regional assessment of articular cartilage gene expression and small proteoglycan metabolism in an animal model of osteoarthritis. Arthritis Research and Therapy 7(4): R852-61.

Yusuf E, Nelissen RG, Ioan-Facsinay A, Stojanovic-Susulic V, DeGroot J, van Osch G, Middeldorp S, Huizinga TW, Kloppenburg M. 2010. Association between weight or body mass index and hand osteoarthritis: a systematic review. Annals of Rheumatic Diseases 69(4): 761-5.

Zamli Z, Adams MA, Tarlton JF, Sharif M. 2013. Increased Chondrocyte Apoptosis Is Associated with Progression of Osteoarthritis in Spontaneous Guinea Pig Models of the Disease. Internatinal Journal of Molecular Sciences 14:17729-17743.

Zamli Z, Robson Brown K, Sharif M. 2016. Subchondral Bone Plate Changes More Rapidly than Trabecular Bone in Osteoarthritis. International journal of molecular sciences 17: 1496.

Zanetti M, Bruder E, Romero J, Hodler J. 2000. Bone marrow edema pattern in osteoarthritic knees: correlation between MR imaging and histologic findings. Radiology 215: 835–40.

Zaruby JF, Hurtig MB, Finlay JB, Valliant AE. 1995. Studies on the external fixator pin-bone interface: The effect of pin design and pin cooling in an *in vivo* sheep tibia model. Veterainry and Comparative Orthopaedics and Traumatology 8: 20-31.

Zhang Y, Fukui N, Yahata M, Katsuragawa Y, Tashiro T, Ikegawa S, Lee MT. 2016. Identification of DNA methylation changes associated with disease progression in subchondral bone with site-matched cartilage in knee osteoarthritis. Scientific Reports 30(6): 34460.

Zhen G, Wen C, Jia X, Li Y, Crane JL, Mears SC, Askin FB, Frassica FJ, Chang W, Yao J, Carrino JA, Cosgarea A, Artemov D, Chen Q, Zhao Z, Zhou X, Riley L, Sponseller P, Wan M, Lu WW, Cao X. 2013. Inhibition of TGF-β signaling in mesenchymal stem cells of subchondral bone attenuates osteoarthritis. Nature Medicine 19: 704–12.

Zhou J, van Zijl PCM. 2006. Chemical exchange saturation transfer imaging and spectroscopy. Progress in Nuclear Magnetic Resonance Spectroscopy 48: 109-36.

Zhu ZH, Gao YS, Luo SH, Zeng BF, Zhang CQ. 2011. An animal model of femoral head osteonecrosis induced by a single injection of absolute alcohol: an experimental study. Medical science monitor : international medical journal of experimental and clinical research 17(4): BR97-102.

Zhuo Q, Yang W, Chen J, Wang Y. 2012. Metabolic syndrome meets osteoarthritis. Nature Reviews in Rheumatology 8(12): 729-37

Zscharnak M, Hepp P, Richter R, Aigner T, Schultz R, Somerson J, Josten C, Bader A, Marquass B. 2010. Repair of chronic osteochondral defects using predifferentiated mesenchymal stem cells in an ovine model. American Journal of Sports Medicine 38: 1857-69.

Aknowledgements

I want to warmly acknowledge all the people who crossed my road during this thesis project.

Some just crossed my road, others are still walking beside me, and I am grateful for that.

Specially, I want to thank:

My husband, who's not really my "husband". I am not the one who get married: I'd rather be free to stay with you all my life. I love you.

My son, my only one. You're my sunshine. I love the way we say to each other, every morning, before leaving: "Have fun !"

My mum, for trying to understand what I am doing; my dad, for not trying.

You, Jean-Michel, you're the promotor, the catalyser, you're like an "air traffic control tower". Sorry, it is not sexy, but look at the idea: You help people to choose the right direction, to spread their wings and fly… and then you're still there when they need to land. Thank you for choosing me when I applied ;-) It was the beginning of everything!

Peter, who welcomed me in his lab, who is reassuring. You always seem to have a plan for every project, for every question, for every problem.

All the people who helped me at the University of Liverpool: Simon, Rob, Yalda, Ben, Gemma, George.

The amazing imaging team of Mont-Godinne: Lucie, Renaud, Max, Florent, Nicolas, Quentin, who are always enjoying our new projects, and obviously: Jean-François, who is always there when I need an advice, or when I bring some desert ;-)

All the people who supported me at the University of Namur, in our unit: Benoit, Yves, Hélène, Robert, Isabelle, Nathalie, Laeti, but also in the LabCeTi: Charles, Daniel, Benoit, Johanna, and Colette from the Geology department.

All the people who helped me to fight for my life during 2014… 2015… and who are still with me now. Some are just called "Doctor", others are called "friends".

To this "shit" diagnosed in 2014. I hated you, and then I discovered that, without you, I would probably never know what I really want in my life.
You forced me to stop, you forced me to question myself, you helped me to find my way, my way through life, my way to other people: Noémie, Caro, Vanessa, Annabel, Camille, Sophie. Thank you for all the moments we share together. I love you!

To all people I did not mention here, because I forgot to do… Thank you.

"You meet your destiny on the road you take to avoid it…"

Jean de La Fontaine

July 2014

Force, Courage et Sérénité

Addendum: Published papers

Hontoir F, Nisolle JF, Meurisse H, Simon V, Tallier M, Vanderstricht R, Antoine N, Piret J, Clegg P, Vandeweerd JM. 2014. A comparison of 3-T magnetic resonance imaging and computed tomography arthrography to identify structural cartilage defects of the fetlock joint in the horse. The Veterinary Journal 199(1):115-122.

Hontoir F, Clegg P, Simon V, Kirschvink N, Nisolle JF, Vandeweerd JM. 2017. Accuracy of computed tomographic arthrography for assessment of articular cartilage defects in the ovine stifle. Veterinary Radiology and Ultrasound 58 (5): 512-523.

Hontoir F, Clegg P, Nisolle JF, Tew S, Vandeweerd JM. 2015. Magnetic resonance compositional imaging of articular cartilage: what can we expect in veterinary medicine? The Veterinary Journal 205(1): 11-20.

Vandeweerd JM, **Hontoir F**, Kirschvink N, Clegg P, Nisolle JF, Antoine N, Gustin P. 2013. Prevalence of naturally occurring cartilage defects in the ovine knee. Osteoarthritis Cartilage 21 (8):1125-31.

Vandeweerd JM, Vermeylen A, Goossens M, Sternon N, **Hontoir F**, Nisolle JF, Dugdale A. 2014. Anesthésie chez le mouton de laboratoire. Sciences et Techniques de l'Animal de Laboratoire 40 (4) : 15-19.